REPURPOSING THE HUMAN IMMUNODEFICIENCY VIRUS (HIV) INTEGRASE INHIBITOR RALTEGRAVIR FOR THE TREATMENT OF FELID ALPHAHERPESVIRUS 1 (FHV-1) OCULAR INFECTION

A Dissertation

Presented to the Faculty of the Graduate School

of Cornell University

In Partial Fulfillment of the Requirements for the Degree of

Doctor of Philosophy

by

Matthew Robert Pennington

August 2018

REPURPOSING THE HUMAN IMMUNODEFICIENCY VIRUS (HIV) INTEGRASE INHIBITOR RALTEGRAVIR FOR THE TREATMENT OF FELID ALPHAHERPESVIRUS 1 (FHV-1) OCULAR INFECTION

Matthew Robert Pennington, Ph.D.

Cornell University 2018

Herpesviruses infect many species, inducing a wide range of diseases. Herpesvirus-induced ocular disease, which may lead to blindness, commonly occurs in humans, dogs, and cats, and is caused by human alphaherpesvirus 1 (HHV-1), canid alphaherpesvirus (CHV-1), and felid alphaherpesvirus 1 (FHV-1), respectively. Rapid and effective antiviral therapy is of the utmost importance to control infection in order to preserve the vision of infected people or animals. However, current treatment options are suboptimal, in large part due to the difficulty and cost of *de novo* drug development and the lack of effective models to bridge work in *in vitro* cell cultures and *in vivo*. Repurposing currently approved drugs for viral infections is one strategy to more rapidly identify new therapeutics. Furthermore, studying ocular herpesviruses in cats is of particular importance, as this condition is a frequent disease manifestation in these animals and FHV-1 infection of the cat is increasingly being recognized as a valuable natural-host model of herpesvirus-induced ocular infection

First, the current models to study ocular herpesvirus infections were reviewed. Next, the efficacy of raltegravir was evaluated using a novel corneal explant model. Raltegravir is a human immunodeficiency virus (HIV) integrase inhibitor that was recently shown to poses antiviral activity against human herpesviruses. Then, electric cell-substrate impedance sensing (ECIS)

was evaluated as a novel methodology to study the replication kinetics of herpesviruses. It was also used to characterize a fluorescently labeled FHV-1, created using CRISPR/Cas9 genome. Next, it was found that raltegravir inhibits both viral DNA synthesis initiation and late gene expression, a mechanism consistent with inhibition of viral ICP8. Finally, RNA sequencing was used to explore the indirect effects of raltegravir on the host. It was found that raltegravir treatment promoted the expression of anti-angiogenic factors and altered the metabolism of the host cells, both of which may be beneficial therapeutically.

These results, combined with a recent *in vivo* study in experimentally infected cats, demonstrates that raltegravir is a viable treatment option for FHV-1 and warrants further investigations into its clinical potential against other herpesviruses.

BIOGRAPHICAL SKETCH

Matthew Pennington was born in Shawnee, KS, where he grew up. He first attended St. Joseph's Catholic School and Good Shepherd Catholic School for grade school and then Rockhurst High School (Kansas City, MO). Matthew pursued his baccalaureate degree at Seton Hall University in South Orange, NJ. At Seton Hall, Matthew majored in Biological Sciences, minored in Chemistry, and participated in the both the Biological Sciences and the University Honors Programs. While there, he began research as a freshman studying the effects of the P-TEFb inhibitor flavopiridol on human gammaherpesvirus 8 transcription and replication, leading to his interest in antiviral drug development. During his undergraduate studies, Matthew studied adolescent elephant behavior at the Pongal Game Reserve (KwaZulu-Natal, South Africa), their ecological impacts on their habitat, and methods of population management for his senior theses, driving his interest in animal biology. He graduated in 2013, *Summa cum laude*, and was awarded the Biology Department Honors Citation by the College of Arts and Sciences and the Charles F. and Hannah Chelius Stark Prize by the University Honors Program Faculty. Matthew then enrolled at Cornell University as a graduate student in Immunology and Infectious Diseases to pursue is interest in study the pathology and treatment of animal viruses. He joined the lab of Dr. Gerlinde Van de Walle in the summer of 2014 to study animal herpesviruses, including felid alphaherpesvirus 1 and equid gammaherpesviruses 2 and 5. Following completion of his graduate studies, Matthew accepted a Post-Doctoral Fellowship at Massachusetts Eye and Ear Infirmary (Massachusetts General Hospital, Harvard Medical School) in the lab of Dr. James Chodosh. There he will study the immunopathogenesis of human ocular adenovirus infection.

ACKNOWLEDGEMENTS

There are many people who have helped me throughout my time at Cornell University and without whom I would not have been able to complete this degree. First and foremost, I would like to thank my mentor, Dr. Gerlinde Van de Walle, who allowed me to explore and to take this research in the direction I found interesting, as well as providing the opportunities to dive into other, unrelated, projects. She has provided me with unwavering support over the years and has always been there to provide help and advice. I also owe a special thanks to my special committee, Drs. Colin Parrish, Bettina Wagner, and Eric Ledbetter, for their support, collaborations, enthusiasm, and useful insights to my work.

All of the members of our lab, both past and present, including Melissa Ledet, Becky Harman, Gat Rauner, Joy Tomlinson, Lauren Tofano, Mike Fort, and other members, visiting researchers, and undergraduate students, have made this time an enjoyable and intellectually stimulating experience. In particular, I have to thank Becky for always happily answering my myriad of questions on everything from help with western blots and flow cytometry to opinions on where I should go hiking. Another special thanks is due to Heather Callaway for her help with protein expression, revising papers and grants, random side projects and ideas that never led anywhere, and more. Thanks to Jen Grenier of the Cornell University RNAseq core for patiently teaching me the basics of RNA sequencing and helping me to analyze and reanalyze my data. Additionally, thanks to Don Millar for help designing cloning constructs, Ashley Roloson and Liberty Research for tissue collection, and the staff of Applied BioPhysics for their assistance optimizing the ECIS assays and analyzing the data. Additionally, I owe a debt of gratitude to the Cornell University Feline Health Center for its continued funding of me and our studies over the duration of my Ph.D.

Lastly, I would like to thank all of my friends and family for their support on this journey. I have enjoyed our hikes, dog play-dates, brewery and winery trips, knitting nights, and more immensely. You all have made my time at Cornell more enjoyable and rewarding. I will always be grateful to these friends and future colleagues for their help and support during my time at Cornell University.

TABLE OF CONTENTS

BIOGRAPHICAL SKETCH iii

ACKNOWLEDGEMENTS iv

TABLE OF CONTENTS vi

LIST OF FIGURES x

LIST OF TABLES xiii

LIST OF ABBREVIATIONS xiv

CHAPTER ONE: AN INTRODUCTION TO OCULAR HERPESVIRUS INFECTION AND THE CHALLENGES OF ANTIVIRAL DRUG DEVELOPMENT

1.1. Herpesvirus-associated ocular disease 2

1.2. Current vaccines and therapies for human and animal patients with ocular herpes 7

1.2.1. Humans 7

1.2.2. Dogs 8

1.2.3. Cats 9

1.3. Strategies to accelerate antiviral drug development 11

1.4. Repurposing raltegravir as a therapy for ocular herpesvirus infection 15

1.5. References 17

CHAPTER TWO: NEW PARADIGMS FOR THE STUDY OF OCULAR ALPHAHERPESVIRUS INFECTIONS: INSIGHTS INTO THE USE OF NON-TRADITIONAL HOST MODEL SYSTEMS

2.1. Summary 26

2.2. Introduction 27

2.3. *In vitro* 2D cell culture systems 30

2.3.1. Immortalized cell lines 30

2.3.2. Primary corneal epithelial cells 31

2.3.3. Limitations of 2D cell culture systems 33

2.4. *In vitro* 3D cell culture/explant systems 34

2.4.1. Corneal facsimiles 34
2.4.2. Explants 35
2.4.3. Limitations of 3D cell culture/explant systems 39
2.5. *In vivo* systems 41
2.5.1. Mice 41
2.5.2. Rabbits 42
2.5.3. Dogs 43
2.5.4. Cats 49
2.5.5. Limitations of non-traditional *in vivo* models 51
2.6. Conclusions and future prospects 53
2.7. References 55

CHAPTER THREE: A NOVEL CORNEA EXPLANT MODEL SYSTEM TO EVALUATE ANTIVIRALS AGAINST FELID ALPHAHERPESVIRUS TYPE 1 (FHV-1)

3.1. Summary 75
3.2. Introduction 76
3.3. Results 78
3.4. Discussion 89
3.5. Methods 94
3.6. References 100

CHAPTER FOUR: ELECTRIC CELL-SUBSTRATE IMPEDANCE SENSING (ECIS) TO MONITOR VIRAL GROWTH AND STUDY CELLULAR RESPONSES TO INFECTION WITH ALPHAHERPESVIRUSES IN REAL-TIME

4.1. Summary 105
4.2. Introduction 107
4.3. Results 109
4.4. Discussion 120
4.5. Methods 123
4.6. References 130

CHAPTER FIVE: THE HIV INTEGRASE INHIBITOR RALTEGRAVIR INHIBITS FELID ALPHAHERPESVIRUS 1 (FHV-1) REPLICATION BY TARGETING BOTH DNA REPLICATION AND LATE GENE EXPRESSION

5.1. Summary 135
5.2. Introduction 137
5.3. Results 139
5.4. Discussion 153
5.5. Methods 157
5.6. References 167

CHAPTER SIX: TRANSCRIPTOME PROFILING OF ALPHAHERPESVIRUS-INFECTED CELLS TREATED WITH THE HIV-INTEGRASE INHIBITOR RALTEGRAVIR REVEALS PRFOUND AND SPECIFIC ALTERATIONS IN HOST TRANSCRIPTION

6.1. Summary 176
6.2. Introduction 177
6.3. Results 179
6.4. Discussion 197
6.5. Methods 202
6.6. References 212

CHAPTER SEVEN: DISCUSSION: SUMMARY AND IMPLICATIONS FOR FUTURE ANTIVIRAL DEVELOPMENT

7.1. Summary of Findings 220
7.2. Prospects for raltegravir as a therapy for herpesvirus infections 221
7.2.1. Evaluation of raltegravir *in vivo* 221
7.2.2. Comparison of raltegravir to current FHV-1 therapies 223
7.2.3. Considerations for the practical implementation of oral and topical raltegravir therapy 225
7.2.4. Intellectual property and cost considerations 226
7.3. Application of new techniques in the evaluation of antiviral drugs 228

7.4. The cat as a natural host model of ocular herpesvirus disease 233
7.5. Conclusions 236
7.6. References 237

APPENDIX: List of all protein-coding stringent-DEGs following raltegravir treatment of FHV-1-infected cells. 243

LIST OF FIGURES

Figure 1.1:	Simplified model of the alphaherpesvirus lytic replication cycle.	4
Figure 1.2:	Simplified overview of the innate and adaptive immune responses to ocular herpesvirus infection.	5
Figure 1.3:	Generalized strategy of antiviral drug discovery.	12
Figure 2.1:	Canine corneal epithelial cells (CCECs) support the growth of CHV-1.	32
Figure 2.2:	General progression of lytic herpesvirus infection in cornea explant models.	37
Figure 2.3:	Timeline of the development and validation of the recurrent experimental ocular CHV-1 infection model in dogs.	45
Figure 2.4:	Clinical presentation of experimental and clinical infection of ocular herpesviruses in dogs and cats.	46
Figure 2.5:	In vivo confocal microscopy of canine corneas.	53
Figure 3.1:	The whole feline corneal explant model is susceptible for felid alphaherpesvirus 1 infection.	79
Figure 3.2:	Incubation of FHV-1-infected corneas with cidofovir or acyclovir reduces FHV-1 viral load and epithelial damage (n=3).	81
Figure 3.3:	Raltegravir is not toxic to feline kidney (CRFK) cells and inhibits FHV-1 replication in this cell line (n=3).	84
Figure 3.4:	Raltegravir is effective against FHV-1, but is not toxic by itself for feline corneas.	86
Figure 3.5:	Incubation of FHV1-infected corneas with raltegravir reduces FHV-1 viral load and epithelial damage (n=3).	88
Figure 4.1:	Additional validation data of ECIS as a tool to monitor alphaherpesvirus infections.	110
Figure 4.2:	ECIS easily distinguishes between wells of cells infected with different amounts of FHV-1.	111
Figure 4.3:	FHV-1 infection induces dose-dependent changes in resistance and capacitance.	113

Figure 4.4:	Creation, using CRISPR/Cas9 genome engineering, and characterization of FHV-1-gD-DsRed.	115
Figure 4.5:	ECIS identifies the growth impairments of a recombinant FHV-1.	116
Figure 4.6:	ECIS accurately determines the half maximal effective concentration (EC50) of the antiviral cidofovir.	118
Figure 4.7:	Evaluation of cidofovir cytotoxicity.	119
Figure 5.1:	Generation of mutant felid alphaherpesvirus 1 (FeHV-1) under continuous drug treatment.	140
Figure 5.2:	Growth kinetics of FeHV-1 following raltegravir treatment. (A) Single-step growth kinetics.	143
Figure 5.3:	Raltegravir does not block terminase-mediated genome cleavage.	145
Figure 5.4:	Raltegravir is similarly effective against the FeHV-1 strains FH2CS and C-27.	147
Figure 5.5:	Raltegravir inhibits early stage DNA replication, consistent with ICP8 inhibition.	148
Figure 5.6:	Raltegravir specifically inhibits late gene expression, consistent with ICP8 inhibition.	151
Figure 6.1:	Selection of multiplicity of infection (MOI) for RNAseq of FHV-1-infected cells.	179
Figure 6.2:	Validation of experimental conditions for RNAseq of FHV-1-infected cells.	180
Figure 6.3:	Raltegravir treatment of FHV-1-infected cells alters several related biological processes.	183
Figure 6.4:	Determination of PAA dose.	185
Figure 6.5:	Raltegravir treatment of FHV-1-infected cells promotes the expression of anti-angiogenic genes and inhibits cell stress-associated gene expression.	186
Figure 6.6:	Heatmaps of additional functional families upregulated following raltegravir treatment of FHV-1-infected cells.	188
Figure 6.7:	Raltegravir induces metabolic changes in FHV-1-infected FCECs.	189
Figure 6.8:	Raltegravir induces few transcriptional changes in uninfected FCECs.	193

Figure 6.9:	Electric cell-substrate impedance sensing to evaluate the effects of raltegravir treatment on migration rate of mock-infected cells.	196
Figure 6.10:	FHV-1 infection induces global disruption of host transcription.	201
Figure 7.1:	Evaluation of raltegravir in experimentally FHV-1-infected cats.	222
Figure 7.2:	Evaluation of PVP-I based compounds against FHV-1.	229
Figure 7.3:	Pipeline for antiviral drug discovery and validation using the tools developed in this thesis.	232

LIST OF TABLES

Table 2.1:	Overview of herpesviruses reported in literature to frequently cause ocular disease.	28
Table 3.1:	Primers used in this study for quantitative PCR (qPCR).	99
Table 4.1:	Primers used in this study to create guide RNAs, donor plasmid, and qPCR plasmid standard.	127
Table 5.1:	Non-synonymous mutations in protein coding genes associated with drug selection of FeHV-1.	142
Table 5.2:	Primer sequences used for qRT-PCR in this study.	165
Table 6.1:	Numbers of Illumina sequencing reads per replicate sample in FHV-1-infected cells.	181
Table 6.2:	Top 20 protein-coding differentially expressed genes (DEGs) following raltegravir treatment of FHV-1-infected cells.	184
Table 6.3:	Numbers of Illumina sequencing reads per replicate sample in uninfected cells.	192
Table 6.4:	List of protein-coding differentially expressed genes (DEGs) following raltegravir treatment of uninfected cells.	194
Table 6.5:	Primers targeting *Felis catus* genes utilized in this study for quantitative RT-PCR.	208
Table 7.1:	Antigens and cross-reacting antibodies currently available to identify feline immune cells.	235

LIST OF ABBREVIATIONS

$2^{-\Delta\Delta Ct}$	Comparative Ct method
7AAD	7-aminoactinomycin-D
ABCD	European Advisory Board for Cat Diseases
AlHV-1	Alcelaphine gammaherpesvirus 1
AMP	Adenosine monophosphate
ANOVA	Analysis of variation
APCs	Antigen-presenting cells
Ara-C	Cytosine arabinoside
ATCC	American Type Culture Collection
ATF3	Activating transcript factor 3
ATP	Adenosine triphosphate
Avg	Average
B2M	Beta-2 microglobulin
BCA	Bicinchoninic acid
BoHV-1	Bovine alphaherpesvirus 1
BoHV-4	Bovine gammaherpesvirus 4
BrdU	5-bromo-2'-deoxyuridine
BSA	Bovine serum albumin
C	Capacitance
C'	Normalized capacitance
C’50	Half maximal normalized capacitance
CC_{50}	Half maximal cellular cytotoxicity
CCECs	Canine corneal epithelial cells
cDNA	Complementary DNA
CECs	Corneal epithelial cells
Chk2	Checkpoint kinase 2
CHV-1	Canid alphaherpesvirus 1
CHX	Cycloheximide

Cm	Membrane capacitance
CPE	Cytopathic effect
CPM	Counts per million mapped reads
CRFK	Crandell Rees feline kidney cells
DAPI	4’,6-diamidino-2-phenylindole
DCs	Dendritic cells
DDE	Aspartic acid-aspartic acid-glutamic acid domain
DEGs	Differentially expressed genes
DMEM	Dulbecco’s Modified Eagle Medium
DMSO	Dimethyl sulfoxide
DNA	Deoxyribonucleic acid
dTMP	Deoxythymidine monophosphate
DTT	Dithiothreitol
dTTP	Deoxythymidine triphosphate
EC_{50}	Half maximal effective concentration
ECAR	Extracellular acidification rate
ECIS	Electric cell-substrate impedance sensing
ECM	Extracellular matrix
EDTA	Ethylenediaminetetraacetic acid
EHV-1	Equid alphaherpesvirus 1
EHV-2	Equid gammaherpesvirus 2
ELISAs	Enzyme-linked immunosorbent assays
FBS	Fetal bovine serum
FCECs	Feline corneal epithelial cells
FDA	Food and Drug Administration
FHV-1	Felid alphaherpesvirus 1
FITC	Fluorescein isothiocyanate
FIV	Feline immunodeficiency virus
FPKM	Fragment per kilobase per million mapped reads
gB	Glycoprotein B
gC	Glycoprotein C

gD	Glycoprotein D
gE	Glycoprotein E
gDNA	Genomic DNA
gH	Glycoprotein H
gI	Glycoprotein I
gL	Glycoprotein L
GM-CSF	Granulocyte-macrophage colony-stimulating factor
GO	Gene ontology
h	Hours
H&E	Hematoxylin-eosin
HAS2	Hyaluronan synthetase 2
HCECs	Human corneal epithelial cells
HEC	Hydroxyethyl cellulose
hhp	Hours post plating
HHV-1	Human alphaherpesvirus 1 (also known as herpes simplex virus 1, HSV-1)
HHV-2	Human alphaherpesvirus 2 (also known as herpes simplex virus 2, HSV-2)
HHV-3	Human alphaherpesvirus 3 (also known as varicella-zoster virus, VZV)
HHV-4	Human gammaherpesvirus 4 (also known as Epstein-Barr virus, EBV)
HHV-5	Human betaherpesvirus 5 (also known as human cytomegalovirus, CMV)
HHV-6	Human betaherpesvirus 6
HHV-8	Human gammaherpesvirus 8 (also known as Kaposi's sarcoma-associated herpesvirus, KSHV)
HIV	Human immunodeficiency virus
HO-1	Heme oxygenase 1
hpi	Hours post infection
HSD	Honest significant difference
HSK	Herpes stromal keratitis
hTERT	Human telomerase reverse transcriptase
HVEM	Herpes virus entry mediator
IAV	Influenza A virus
ICP4	Infected cell polypeptide 4

ICP8	Infected cell polypeptide 8
ICP27	Infected cell polypeptide 27
IF	Immunofluorescence
IFN	Interferon
IL	Interleukin
IPTG	Isopropyl β-D-1-thiogalactopyranoside
kHz	Kilohertz
LATs	Latency associated transcripts
LN	Lymph nodes
MDCK	Madin Darby canine kidney cells
MEM	Minimal essential media
min	Minutes
MMPs	Matrix metalloproteinases
MOI	Multiplicity of infection
mRNA	Messenger RNA
MTT	3-(4,5-dimethylthiazol-2-yl)-2,5-diphenyltetrazolium bromide
NADPH	Nicotinamide adenine dinucleotide phosphate
NCBI	National Center of Biotechnology Information
OCR	Oxygen consumption rate
OvHV-2	Ovine gammaherpesvirus 2
PAA	Phosphonoacetic acid
PAGE	Polyacrylamide gel electrophoresis
PAMPs	Pathogen associated molecular patterns
PBMCs	Peripheral blood mononuclear cells
PBS	Phosphate buffered saline
PCR	Polymerase chain reaction
PFU	Plaque forming units
pi	Post infection
PPRs	Pattern recognition receptors
PVP-I	Povidone-iodine
qPCR	Quantitative polymerase chain reaction

qRT-PCR	Quantitative reverse transcription polymerase chain reaction
R	Resistance
R'	Normalized resistance
R’50	Half maximal normalized resistance
Rb	Barrier resistance
RFP	Red fluorescent protein
RNA	Ribonucleic acid
RNAseq	RNA deep sequencing
RPL17	Ribosomal protein L17
RSV	Respiratory syncytial virus
RT	Room temperature
SD	Standard deviation
SHEM	Supplemented hormonal epithelium medium
SNPs	Single nucleotide polymorphisms
SNV	Sin nombre virus
SPF	Specific pathogen free
ssDNA	Single stranded DNA
TCID50	Half maximal tissue culture infectious dose
TG	Trigeminal ganglion
TLR	Toll-like receptor
TNFα	Tumor necrosis factor alpha
TSP-1	Thrombospondin 1
TUNEL	Terminal deoxynucleotidyl transferase dUTP nick end labeling
URI	Upper respiratory infection
UTR	Untranslated region
UV	Ultraviolet
VEGF	Vascular endothelial growth factor
vhs	Virion host shutoff
WT	Wild type
Z	Impedance
Z'	Normalized impedance

Z’50	Half maximal normalized impedance

CHAPTER ONE

AN INTRODUCTION TO OCULAR HERPESVIRUS INFECTION AND THE CHALLENGES OF ANTIVIRAL DRUG DEVELOPMENT

1.1. Herpesvirus-associated ocular disease

Herpesviruses are among the oldest viruses that are still prevalent today, having emerged approximately 400 million years ago and closely co-evolving with their hosts thereafter (1, 2). Well over a hundred species of herpesviruses have been described, which infect a wide range of vertebrate and non-vertebrate animals (3). The hallmark of these large, complex, double-stranded DNA viruses is their ability to establish a lifelong, latent infection that can reactivate to cause repeated bouts of disease (4). These viruses are divided into three families broadly based on the size and organization of their genomes, the host tissues in which they replicate and establish latency, and the diseases induced by infection. Alphaherpesviruses, such as human alphaherpesvirus 1 (HHV-1, also known as human herpes simplex virus 1, HSV-1), as well as various viruses of importance in animals, such as bovine alphaherpesvirus type 1 (BoHV-1), canid alphaherpesvirus 1 (CHV-1), equid alphaherpesvirus type 1 (EHV-1), and felid alphaherpesvirus 1 (FHV-1), all have short replicative cycles (hours), primarily replicate in mucosal and epithelial surfaces leading to lysis of host cells, and primarily establish latency in sensory neurons. This family can cause a wide range of diseases, including respiratory disease, tissue ulceration, cold sores, and neurological disease. Betaherpesviruses, in contrast, have long replication cycles (days), replicate in a variety of cell types, including epithelial, immune, and endothelial cells, and establish latency in lymphocytes. Human betaherpesvirus 5 (HHV-5, also known as human cytomegalovirus, CMV), the prototypical virus of this subfamily, is typically asymptomatic, but can cause congenital infection in newborns and cancer and other symptoms in immunocompromised individuals, all of which can be fatal. Gammaherpesviruses have a variable replication rate and typically replicate in epithelial cells and lymphoid cells. Latency is

usually established in the latter, resulting in cell proliferation and the development of cancers (5–8).

In addition to the infection-induced diseases mentioned above, some alphaherpesviruses, including HHV-1, CHV-1 and FHV-1, are also capable of causing severe ocular infection, which can progress to blindness. Due to the similarities in viral replication and disease progression compared to humans, studies in dogs and cats are increasingly being considered to be excellent natural host systems in which to study ocular herpesvirus infection (reviewed in Chapter 2). The underlying biology of the ocular infection is similar among these viruses. They all spread via the oral-facial route, leading to corneal and/or conjunctival infection. While herpesvirus-associated conjunctivitis may frequently occur, corneal infection arguably causes more severe ocular damage, which may lead to blindness or necessitate corneal transplantation without proper treatment (9). Dendritic and global ulceration of the epithelial surface occurs as a direct result of viral replication in the corneal epithelial cells, resulting in cell lysis. The general lytic replication cycle of these viruses is summarized in Fig. 1.1. During acute infection, the alphaherpesviruses can travel via retrograde axonal transport to the trigeminal ganglion and establish latency. Reactivation by physiological, chemical, and environmental triggers, causes the virus to travel back down the neuron via antero-retrograde transport to again replicate at any site innervated by the ganglion, including the cornea, oral mucosa, lips, and fingertips to undergo another cycle of lytic replication (4, 10, 11).

The severe herpesvirus-induced eye diseases as seen in humans, dogs, and cats usually occur following reactivation and are a direct result of strong pro-inflammatory immune responses, compounded by secondary virus replication-associated damage. This results in a range of corneal diseases, including neurotrophic keratopathy, characterized by puntate

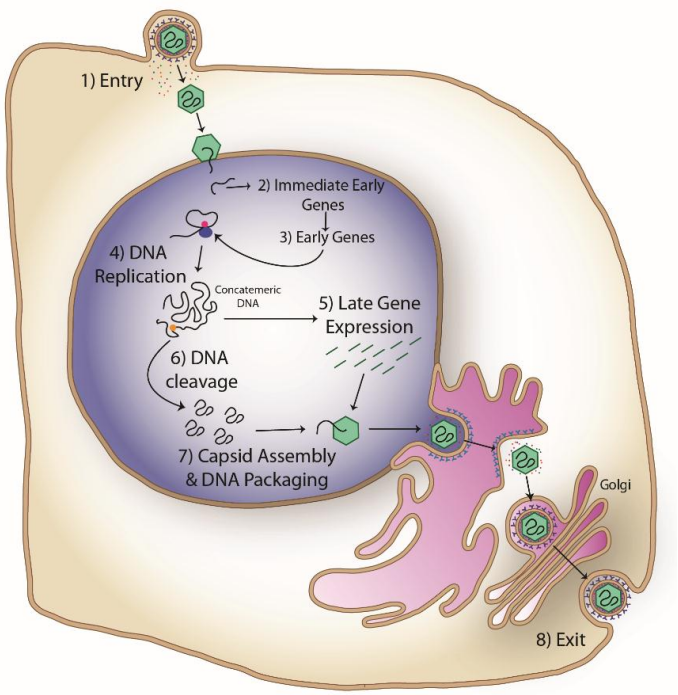

Figure 1.1: Simplified model of the alphaherpesvirus lytic replication cycle. Life cycle diagram is based on the replication cycle of HHV-1, reviewed previously (4, 10, 11). (1) Herpesviral glycoproteins B (gB) and C (gC) bind to extracellular glycoproteins on the target cell (typically heparin sulfate or other glycosaminoglycans) while glycoprotein D (gD) binds to a secondary cell surface receptor (nectin-1, nectin-2, herpes virus entry mediator (HVEM), or 3-*O*-sulfated heparan sulfate), leading to viral/plasma membrane fusion mediated by gD, gB, glycoprotein H (gH), and glycoprotein L (gL). Tegument proteins facilitate take-over of host cell machinery while the nucleocapsid is transported to a nuclear pore, where it injects the genomic DNA. (2) The tegument proteins stimulate expression of the immediate early genes, which (3) mediate the expression of the early genes. (4) Early gene products facilitate replication of the viral DNA using a rolling circle mechanism, resulting in concatemeric DNA synthesis. (5) Expression of late genes increases dramatically following DNA replication and produce the glycoproteins, capsid proteins, tegument proteins, and other products. (6) Terminase (UL15) cleaves concatemeric DNA into individual genome segments. (7) Nucleocapsids assemble and package single copies of the viral DNA. (8) Nucleocapsids bud off of the inner nuclear envelope into the perinuclear lumen, acquiring an immature tegument layer and envelope. Virions are trafficked via the Golgi, where they undergo maturation, before exiting the cell by either exocytosis or cell lysis.

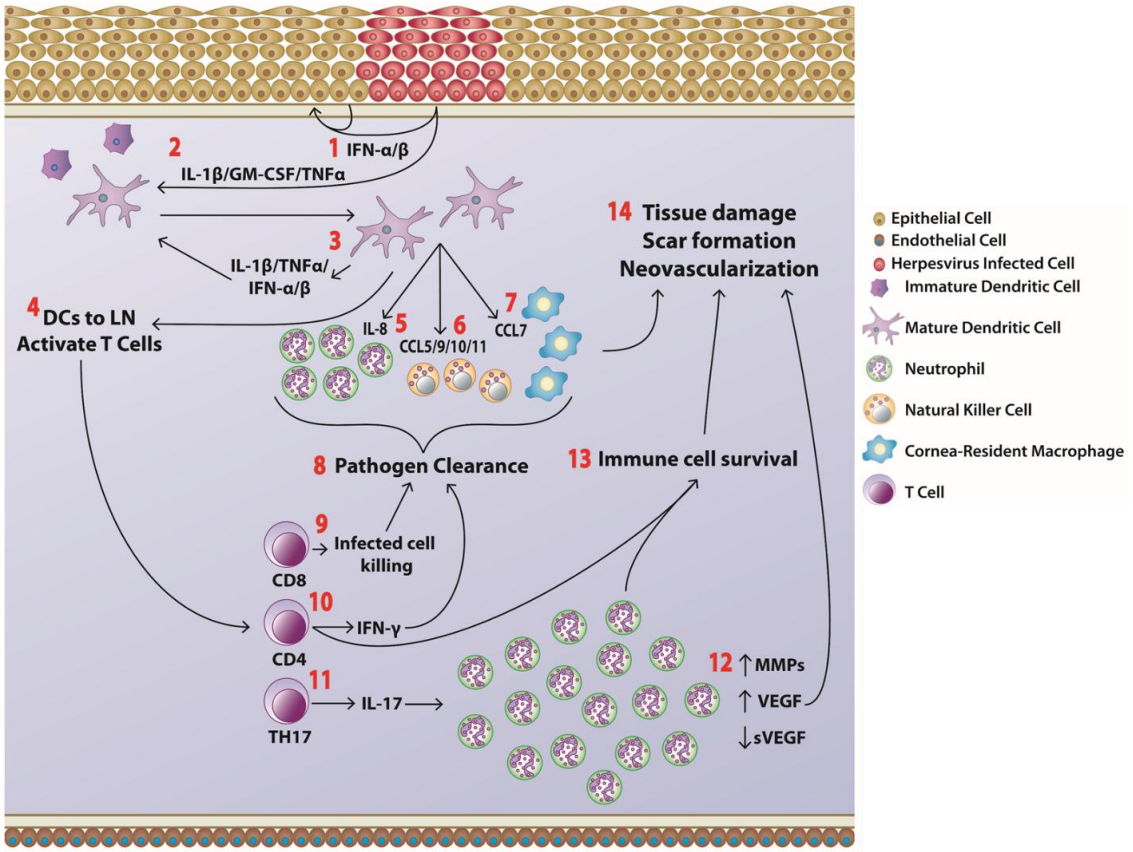

Figure 1.2: Simplified overview of the innate and adaptive immune responses to ocular herpesvirus infection. Immune response diagram is primarily based on studies of HHV-1 infection in mice and rabbits (12–16). Responses in the natural hosts may vary, but this has yet to be explored in detail. (1) Pathogen associated molecular patterns (PAMPs) from the herpesvirus stimulate pattern recognition receptors (PPRs), including toll like receptor (TLR) 3, TLR7, TLR9, and cytoplasmic IFI-16, leading to the release of type 1 interferons (IFN) to establish an antiviral state to limit viral spread. (2) Infected cells secrete cytokines (e.g. interleukin (IL)-1β, granulocyte-macrophage colony-stimulating factor (GM-CSF), and tumor necrosis factor alpha (TNFα) leading to the development of a pro-inflammatory state and recruitment, activation, and maturation of corneal resident dendritic cells (DCs) to the site of infection. (3) Recruited DCs secrete cytokines that further promote DC recruitment and establish a pro-inflammatory environment. Recruited DCs then secrete more IL-1β, TNFα, and IFN to promote further inflammation and DC recruitment and activation. Several immune responses then proceed concurrently. (4) DCs uptake viral antigens and migrate to regional lymph nodes (LN) to stimulate the adaptive immune response, principally T cells.

Figure 1.2 continued. DCs also secrete (5) IL-8 to drive the first major influx of neutrophils, (6) CCL5, 9, 10, and 11 to recruit natural killer cells, which lyse and kill infected epithelial cells, as well as secrete IFN-ɣ, and (7) CCL7 to recruit macrophages, which are activated to adopt the Type 1 phenotype by IFN-ɣ. (8) The combined activities of these innate immune cells largely mediate pathogen clearance. After approximately 7 days, antigen-specific T cells are recruited to the cornea. (9) CD8+ T cells lyse infected cells and (10) Th1 skewed CD4+ T cells secrete IFN-ɣ and other cytokines to maintain the cellular response, further contributing to pathogen clearance. Continued stimulation of the CD4+ cells in the absence of viral replication leads to aberrant cytokine production, principally IL-6, leading to (11) the recruitment of Th17 cells. These cells secrete IL-17 to initiate a second neutrophil influx and monocyte recruitment. (12) Neutrophils upregulate expression of matrix metalloproteinases (MMPs), leading to extracellular matrix remodeling. Additionally, vascular endothelial growth factor (VEGF) expression is upregulated while soluble VEGF is downregulated, leading to angiogenesis and lymphangiogenesis. (13) Cytokines expressed by T cells and neutrophils prolong cellular survival and cytokine production, resulting in (14) tissue damage, scar formation, and neovascularization, all characteristics of stromal keratitis.

epithelial erosions and neurotrophic ulcers, stromal keratitis, divided into necrotizing (due to replicating virus) and immune-stromal (due to immune reaction), endotheliitis, and corneal neovascularization. Of these, stromal keratitis is perhaps the most common, affecting 20-60% of human patients with recurrent ocular herpesvirus disease and primarily results from an inflammatory CD4+ T cell response to herpesviral antigens, which produces a pro-inflammatory cytokine storm. The immune response to ocular herpesvirus infection and the development of stromal keratitis has been reviewed extensively in the literature and is schematically summarized in Fig. 1.2 (12–16). This immune response leads to damage of the ocular tissue and scar formation. During subsequent bouts of reactivation, the adaptive immune system can respond much more quickly than during primary infection, resulting in the accumulation of tissue damage, which, over time, can lead to blindness. In order to limit stromal keratitis and the other

immune-mediated manifestations of ocular disease, corticosteroids are used to suppress the immune response, mainly by inhibiting production of cytokines by the CD4+ T cells (13, 17, 18). However, current treatment guidelines recommend that one or more direct-acting anti-herpesviral drugs be given during any stage of ocular herpesvirus therapy.

1.2. Current vaccines and therapies for human and animal patients with ocular herpes

1.2.1. Humans

As mentioned above, direct-acting antiviral drugs are a critical component for successful management of herpesvirus ocular infection. A wide variety of anti-herpesviral therapies, most using nucleoside analogues to inhibit DNA synthesis, have been developed and many are quite effective at treating HHV-1 infection in humans. However, if corneal infection develops, treatment remains challenging in many cases. Trifluridine is the most commonly prescribed anti-HHV-1 therapeutic in the United States, but it has poor bioavailability and, as a result, can cause ocular surface toxicity (19). Oral valacyclovir and acyclovir and topical ganciclovir are also commonly prescribed, but must be taken several times per day and, therefore, can result in poor patient compliance (19, 20). These drugs, and the second-line therapies foscarnet and cidofovir, are also occasionally associated with ocular toxicity, nausea, vomiting, and other side effects (21). Furthermore, prolonged treatment with these antivirals can result in the selection of drug resistant viruses, particularly in immunocompromised individuals (22–24) and a small percentage of patients with recurrent ocular herpes do not respond to treatment for unknown reasons (13). Since therapies are only partially effective, there has been an intense search for preventative and therapeutic vaccines for both HHV-1 and human alphaherpesvirus 2 (HHV-2, also known as herpes simplex virus 2, HSV-2). However, and despite a number of promising

candidates in various phases of development and clinical evaluation, there are currently still no approved vaccines for HHV-1 or HHV-2 (25).

1.2.2. Dogs

No drugs have ever been developed to specifically target CHV-1 infection in dogs. Instead, the same nucleoside analogues used to treat HHV-1 are given, although it should not be automatically assumed that these compounds will have similar efficacy and toxicity in the dog. Currently, no formal guidelines exist for treatment of CHV-1 infection in adult dogs. Studies focused on evaluating antiviral efficacy against CHV-1 *in vitro* are rare (26). However, three drugs, originally developed to treat HHV-1 infection, have been evaluated *in vivo* against CHV-1. Topical cidofovir was effective at lowering ocular viral shedding, but was associated with higher clinical ocular disease scores and higher conjunctival and cornea leukocyte infiltration than vehicle-treated animals, and, therefore, future studies are needed to determine an effective, yet clinically tolerable formulation and dosage regimen (27). Topical trifluridine and ganciclovir, in contrast, were both well tolerated and effective at lowering both viral shedding and clinical scores. However, both of these compounds required frequent administration—trifluridine was applied 6 times daily for 2 days and then 4 times daily for 12 days while ganciclovir was applied 5 times daily for 7 days and then 3 times daily for 7 days (28, 29). Such frequent treatment may result in poor owner compliance, and therefore sub-standard antiviral efficacy.

One subunit vaccine (Eurican Herpes 205, Merial, Lyon, France) is used in some countries to immunize seronegative pregnant dams and has been experimentally shown to prevent or reduce morbidity and mortality in their puppies with induced CHV-1 infection (30, 31). However, a therapeutic vaccination is likely to be more useful in dogs than a preventative one due to the young age at which dogs become infected. Recently, it was shown that the

Eurican Herpes 205 vaccine could reduce clinical ocular disease scores in the short-term, and induce long term CHV-1-specific immunity in the long term when given to latently infected and experimentally reactivated mature dogs. However, it was noted that vaccination did not prevent the development of ocular disease, viral shedding, or reactivation (32).

It is thought that the incidence and clinical importance of ocular CHV-1 infections is likely to increase, based on the increasingly longer lifespans of dogs which coincide with an increase in chronic immunomodulatory systemic diseases that may require immunosuppressive therapeutics (33). Therefore, a renewed interest in the development of new CHV-1 vaccines and therapeutics can be expected in the coming years.

1.2.3. Cats

Treating FHV-1 infection of cats has similar challenges as treating HHV-1 and CHV-1. No antiviral has been developed to specifically treat FHV-1 infection, and, similar to CHV-1 in dogs, affected cats are treated with antivirals developed for HHV-1 infection. The European Advisory Board for Cat Diseases (ABCD) recommends trifluridine for the treatment of ocular FHV-1, though ganciclovir, cidofovir, and idoxuridine, are also suggested (34, 35). However, no placebo-controlled clinical trials have been performed to demonstrate the efficacy of trifluridine, ganciclovir, and idoxuridine in cats (35–37). Additionally, and similar to the compounds tested against CHV-1, these may require frequent administration. For example, topical trifluridine is recommended to be given every 1-2 hours initially, followed by every 4-12 hours thereafter (34). It was recently shown that twice-daily topical cidofovir can reduce clinical disease and viral shedding in experimentally infected cats (38), though there are concerns that long term cidofovir treatment may induce nasolacrimal cicatrization (37). Acyclovir is not recommended as it appears to have low bioavailability and a poor inhibitory effect against FHV-1 (39),

hypothesized to be due to an altered viral thymidine kinase substrate recognition site relative to HHV-1 (40) and/or a reduced ability of feline cellular kinases to catalyze the second and third phosphorylation steps to produce acyclovir triphosphate, the active form of the compound (41). Additionally, its oral prodrug, valacyclovir, should never be used as it has been shown to induce fatal hepatic and renal necrosis and bone marrow suppression in cats (42). Famciclovir, the oral prodrug of penciclovir, was also recently shown to be effective at reducing clinical disease and viral shedding in a masked, placebo-controlled experimental infection trial (43). It has since become more widely used, though an appropriate dosage schedule has not been agreed upon by veterinarians due to the complex and nonlinear pharmacokinetics of this drug in cats (37).

Two other compounds have been investigated, perhaps more thoroughly than any of the nucleoside analogues described above, for their therapeutic effects against FHV-1, though their efficacy remains contradictory. L-lysine is thought to antagonize arginine availability to or utilization by HHV-1 during protein synthesis and thus inhibits viral replication due to a higher arginine-to-lysine ratio in host proteins compared to viral proteins (37). An initial *in vitro* study with FHV-1 demonstrated that lysine supplementation did reduce viral replication (44). This lead to several *in vivo* studies, with two experimental infection studies demonstrating the efficacy of oral lysine supplementation to reduce viral shedding and clinical disease scores during primary infection (45, 46). However, three studies utilizing either shelter cats or cats with enzootic upper respiratory tract infection found no benefit to oral lysine in reducing disease frequency or severity. A more recent *in vitro* study reassessing the effects of lysine in FHV-1-infected CRFK cells found no evidence of inhibition of viral reduction (50), further questioning lysine as a viable treatment option. Interferon (IFN) treatment, consisting of the exogenous application of these cytokines to induce an antiviral state in uninfected cells, has a similar history. IFN-α and

IFN-ω were both shown to be effective at inhibiting viral replication in CRFK cultures (51–53). Four *in vivo* studies have evaluated using either feline IFN-ω or human IFN-α2b infection, but produced only a minimal benefit at best (54–57). Thus, there is also no strong evidence to justify the use of interferon treatment *in vivo*. However, these trials not only demonstrate the strong interest in identifying new treatments for FHV-1, but also show that many therapies with demonstrated activity *in vitro* do not necessarily translate and retain efficacy *in vivo*.

In contrast to humans and dogs, prophylactic FHV-1 vaccination has been a common component of the recommended core vaccines for cats for many years. Both modified-live and inactivated vaccines are commercially available, all based on the same serotype (36). These are most commonly compounded with vaccines against other feline pathogens, including feline calicivirus, feline panleukopenia virus, *Chlamydia psittaci,* and feline leukemia virus. These vaccines also vary in their vaccination schedule and the mode of delivery, with both subcutaneous and intranasal vaccines available. Despite their widespread use, these vaccines are only effective at reducing clinical scores. They do not prevent infection, virus shedding, establishment of latency, or the appearance of clinical signs (12, 14). Therefore, anti-herpesviral therapies will continue to be necessary to treat FHV-1 infections even in vaccinated cats. More generally, new anti-herpesviral therapies, particularly those with FHV-1 (or CHV-1) specific experimental evidence to support their use, are needed to treat or supplement the current drug regimens for ocular infections.

1.3. Strategies to accelerate antiviral drug development

This relative lack of effective antivirals to treat ocular herpesvirus infection, and in particular CHV-1 and FHV-1, largely stems from the difficulty and expense of developing new

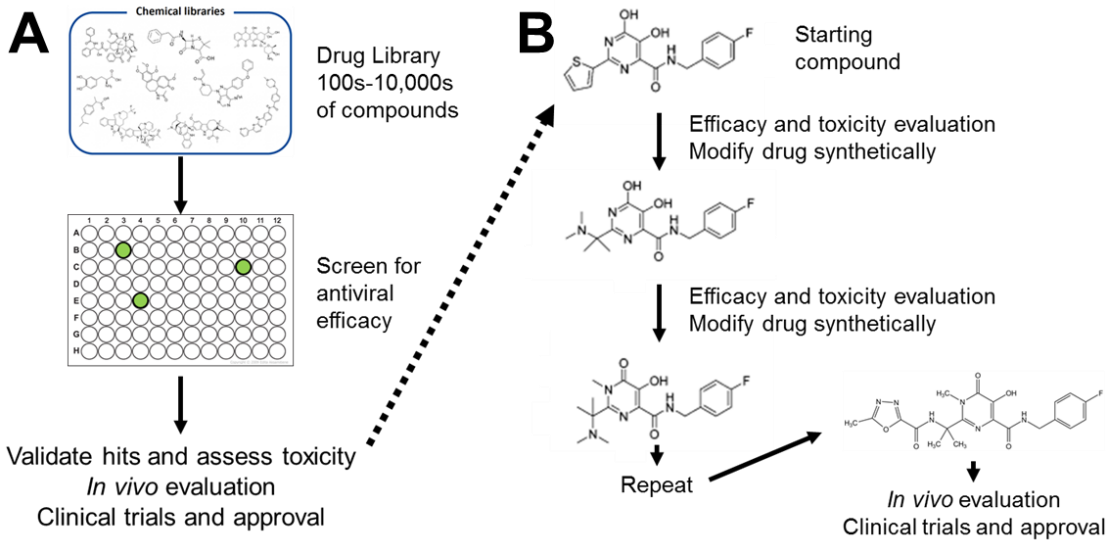

Figure 1.3: Generalized strategy of antiviral drug discovery. (A) Large chemical libraries are screened for antiviral efficacy against target virus and for toxicity to the host cell. Those with antiviral efficacy at acceptably low toxicity must then undergo *in vivo* evaluation and clinical trials. **(B)** Drugs discovered by screens or other methods may additionally undergo rational drug design to increase their efficacy and reduce toxicity. Shown here are the initial modifications leading to the creation of raltegravir (final compound), from Summa, *et al.* 2008 (77).

therapies. A 2009 study estimated 1 in 5,000 odds of successfully obtaining approval for a new therapy and estimated the cost between $1.3-1.7 billion in the United States (58). Since then, costs have only risen and are likely still rising, with a 2014 study putting the cost at that time at $2.6-2.8 billon (59). This cost largely stems from the initial identification of compounds with antiviral effects and the evaluation of the efficacy and toxicity of these compounds *in vivo*.

Historically, identification of putative antiviral compounds has been accomplished by screens of large chemical libraries and/or rational drug design (Fig. 1.3). A variety of methods exist to screen hundreds to hundreds of thousands of chemicals for antiviral activity, and this approach was used to identify nearly all of the currently approved anti-herpesviral drugs (60). Typically, a monolayer of cells is infected with the virus and treated with the compounds. The

cells are then assessed for cytopathic effect and toxicity by any of a number of standard assays, though newly developed platforms may also aid in screening (see Chapter 4). Compounds that inhibit viral replication at suitably low toxicity are then selected for further validation and/or mechanistic studies (61–63). Alternatively, screening approaches may use either biochemical assays to identify inhibitors of specific catalytic enzymes or other biological functions or the identification of inhibitors that alter the host immune response to promote viral clearance, rather than directly inhibiting viral replication (60). Promising compounds identified by these screens or developed by other methods may then undergo rational drug design, chemically modifying the compounds to enhance their efficacy and specificity based on their known target and/or to reduce their toxicity to the host (64). While this method has been extensively used and has proven effective at developing novel inhibitors of human immunodeficiency virus (HIV) (65), it requires a precise knowledge of the molecular target of the drug. Therefore, it can require a great deal of time and money to successfully accomplish.

Repurposing drugs designed for other applications is another strategy that has been historically used to develop new antiviral therapies. For example, acyclovir was originally designed as an adjuvant therapy to potentiate the anticancer activity of the nucleoside analogue, cytosine arabinoside (Ara-C), an inhibitor of adenosine deaminase, but was found to have anti-HHV-1 activity by a drug screen in HHV-1-infected cells (60, 66). Repurposing approved drugs to treat new conditions can accelerate drug development and reduce associated costs, as the safety and pharmacokinetic profiles of these drugs are already known for their on-label uses (67, 68). This strategy has been more widely adopted in recent years, in large part due to the development of novel bioinformatic techniques that allow for the *in silico* prediction of drug-protein interactions and cross-reactivity. For example, both drug-library based screens and

screens of unique panels of drugs with known interactions in cellular pathways involved in viral infection have been used to identify therapeutics that, in addition to their approved use, also inhibit replication of recent emerging viruses such as ebolavirus, coronaviruses, and chikungunya virus (69–71).

Once an antiviral compound has been identified, it must then be evaluated for efficacy and toxicity *in vivo.* This is typically first performed in a small animal model, usually mice, before proceeding to large-scale clinical trials in the target animal or humans. As mentioned, if this was done by repurposing an existing drug, this safety information is likely already known and, therefore, only efficacy testing is needed. Nevertheless, most of the compounds that show efficacy in cell culture are ineffective or toxic *in vivo*, for example feline IFN-ω and oral lysine, as discussed above. Explants, or *ex vivo* organ, organotypic, or organoid cultures, are one strategy to address this discrepancy and can be used to better predict *in vivo* outcomes. These cultures maintain normal three-dimensional structures and cell-to-cell contacts similar to *in vivo* tissues, whereas traditional cell culture disrupts them. As they involve more than one cell type, explants are also considered to be more physiologically relevant than cell culture systems (72). They can, therefore, serve as stepping stones between *in vitro* and *in vivo* models to validate cell culture results, taking advantage of discarded materials to reduce costs. Additionally, they can limit the amount of animal experimentation needed and thus satisfying the 3 R's of animal research, i.e. replacement, reduction, and refinement (73). Such systems have already aided in drug discovery efforts targeting a variety of tissues, including intestines (74), skin (75), and the central nervous system (76). A more elaborate description on ocular explants is given in Chapter 2.

1.4. Repurposing raltegravir as a therapy for ocular herpesvirus infections

New tools, models, and strategies are needed to evaluate novel compounds to treat ocular herpesvirus infections. Repurposing existing drugs and the use of appropriate models of infection may lead to the more rapid identification of effective therapies than *de novo* drug discovery. One compound that warrants evaluation as an anti-herpesviral drug is raltegravir, an HIV integrase inhibitor that was approved by the United States Food and Drug Administration (FDA) in 2007 (77). Raltegravir remains widely used in humans to treat HIV due to its low toxicity, high efficacy against that virus, low propensity for drug-drug interactions, and its efficacy in both treatment-naïve and treatment-experienced patients, regardless of age, sex, or race (78–80). It specifically functions by binding to an aspartic acid-aspartic acid-glutamic acid (DDE) domain in the catalytic core of HIV integrase, which is structurally homologous to the RNase H domain of eukaryotic recombinases and transposases, to prevent the strand transfer reaction that joins the 3'-processed viral DNA ends to the host genomic DNA, thus preventing HIV cDNA integration (81, 82). Interestingly, structural characterization of the nuclease domain of the terminase protein (UL89) of HHV-5 demonstrated that terminase and HIV integrase share significant structural homology, including the RNase H domain. This group demonstrated that raltegravir can inhibit the nuclease function of HHV-5 terminase *in vitro*, suggesting it may inhibit concatemeric viral genome cleavage during infection (83). Subsequently, raltegravir was shown to also be an effective inhibitor of HHV-1. However, it was demonstrated to target HHV-1 UL42, the DNA polymerase accessory factor, instead inhibiting viral DNA replication (84).

The primary objective of this thesis was to evaluate raltegravir as a therapy for ocular FHV-1 herpesvirus infection, both as a natural host model of this infection and for the benefit of feline health. FHV-1 was chosen because (1) its ocular manifestations are more common in adult

animals than CHV-1, (2) this virus is well-suited to culture and study in the laboratory, (3) it has been studied more extensively than CHV-1, leading to the availability of useful laboratory reagents, and (4) oral raltegravir has already been shown to be non-toxic to cats (85), allaying toxicity concerns that are common in treating cats. A secondary objective of this thesis was to develop new tools and methodologies to explore the efficacy and mechanisms of antivirals, both specific to FHV-1 and more broadly to other viruses. Current models available to study ocular herpesvirus infection and the value of natural host models are reviewed in Chapter 2. Chapter 3 describes the evaluation of the anti-FHV-1 efficacy of raltegravir *in vitro* and in a newly established corneal explant model. These results subsequently allowed for the evaluation of raltegravir *in vivo* using a feline acute infection model, demonstrating that raltegravir reduced both clinical scores and virus shedding duration in FHV-1 infected cats (86) (Discussed in Chapter 7). Chapter 4 describes the optimization of electric cell-substrate impedance sensing (ECIS) as a methodology to study several aspects of herpesvirus biology, including antiviral efficacy and toxicity. Chapter 5 describes results that indicate that raltegravir directly inhibits FHV-1 DNA replication initiation and late gene expression as two separate events, consistent with inhibition of the early protein ICP8. Chapter 6 describes results that indicate that raltegravir, in addition to its direct-acting effect, also boosts the expression of anti-angiogenic genes and modulates host metabolism, returning it to a homeostatic state. Taken together, this thesis demonstrates that raltegravir, and integrase inhibitors in general, is a viable antiviral for the treatment of FHV-1 and establishes new tools and methodologies to aid in the evaluation of antivirals (Chapter 7).

1.5. References

1. McGeoch DJ, Dolan A, Ralph AC. 2000. Toward a comprehensive phylogeny for mammalian and avian herpesviruses. J Virol 74:10401–6.
2. Grose C. 2012. Pangaea and the out-of-Africa model of varicella-zoster virus evolution and phylogeography. J Virol 86:9558–65.
3. Riddell A, Jeffery-Smith A, Tong CYW. 2017. Herpesviruses. Medicine (Baltimore) 45:767–771.
4. Flint S, Enquist L, Racaniello V, Skalka A. 2009. Principles of Virology. Third Edit. ASM Press, Washington DC.
5. Whitley RJ. 1996. Herpesviruses. Medical Microbiology. University of Texas Medical Branch at Galveston.
6. Jenkins FJ, Hoffman LJ. 2000. Overview of Herpesviruses 33–49.
7. Arvin A, Campadelli-Fiume G, Mocarski E, Moore PS, Roizman B, Whitley R, Yamanishi K. 2007. Human Herpesviruses. Human Herpesviruses: Biology, Therapy, and Immunoprophylaxis. Cambridge University Press.
8. Davison AJ, Eberle R, Ehlers B, Hayward GS, McGeoch DJ, Minson AC, Pellett PE, Roizman B, Studdert MJ, Thiry E. 2009. The order Herpesvirales. Arch Virol 154:171–7.
9. Pennington M, Ledbetter E, Van de Walle G. 2017. New paradigms for the study of ocular alphaherpesvirus infections: insights into the use of non-traditional host model systems. Viruses 9:349.
10. Zhu L, Zhu H. 2014. Ocular herpes: the pathophysiology, management and treatment of herpetic eye diseases. Virol Sin 29:327–342.
11. Kukhanova MK, Korovina AN, Kochetkov SN. 2014. Human herpes simplex virus: Life cycle and development of inhibitors. Biochem 79:1635–1652.
12. Gaskell R, Dawson S, Radford A, Thiry E. 2007. Feline herpesvirus. Vet Res 38:337–54.
13. Al-Dujaili LJ, Clerkin PP, Clement C, McFerrin HE, Bhattacharjee PS, Varnell ED, Kaufman HE, Hill JM. 2011. Ocular herpes simplex virus: how are latency, reactivation, recurrent disease and therapy interrelated? Future Microbiol 6:877–907.
14. Maes R. 2012. Felid herpesvirus type 1 infection in cats: a natural host model for alphaherpesvirus pathogenesis. ISRN Vet Sci 2012:495830.
15. Rowe AM, St Leger AJ, Jeon S, Dhaliwal DK, Knickelbein JE, Hendricks RL. 2013.

Herpes keratitis. Prog Retin Eye Res 32:88–101.

16. Giménez F, Suryawanshi A, Rouse BT. 2013. Pathogenesis of herpes stromal keratitis--a focus on corneal neovascularization. Prog Retin Eye Res 33:1–9.
17. Wiederrecht G, Lam E, Hung S, Martin M, Sigal N. 1993. The mechanism of action of FK-506 and cyclosporin A. Ann N Y Acad Sci 696:9–19.
18. Knickelbein JE, Hendricks RL, Charukamnoetkanok P. 2009. Management of herpes simplex virus stromal keratitis: an evidence-based review. Surv Ophthalmol 54:226–234.
19. Austin A, Lietman T, Rose-Nussbaumer J. 2017. Update on the management of infectious keratitis. Ophthalmology 124:1678–1689.
20. Tsatsos M, MacGregor C, Athanasiadis I, Moschos MM, Hossain P, Anderson D. 2016. Herpes simplex virus keratitis: an update of the pathogenesis and current treatment with oral and topical antiviral agents. Clin Experiment Ophthalmol 4:824–837.
21. Azher TN, Yin X-T, Tajfirouz D, Huang AJ, Stuart PM. 2017. Herpes simplex keratitis: challenges in diagnosis and clinical management. Clin Ophthalmol 11:185–191.
22. Choong K, Walker NJ, Apel AJ, Whitby M. 2010. Aciclovir resistant herpes keratitis. Clin Experiment Ophthalmol 38:309–13.
23. Andrei G, Snoeck R. 2013. Herpes simplex virus drug-resistance. Curr Opin Infect Dis 26:551–560.
24. Piret J, Boivin G. 2016. Antiviral resistance in herpes simplex virus and varicella-zoster virus infections. Curr Opin Infect Dis 29:654–662.
25. Johnston C, Gottlieb SL, Wald A. 2016. Status of vaccine research and development of vaccines for herpes simplex virus. Vaccine 34:2948–2952.
26. Tanaka T, Nakatani S, Xuan X, Kumura H, Igarashi I, Shimazaki K ichi. 2003. Antiviral activity of lactoferrin against canine herpesvirus. Antiviral Res 60:193–9.
27. Ledbetter EC, Spertus CB, Pennington MR, Van de Walle GR, Judd BE, Mohammed HO. 2015. In vitro and in vivo evaluation of cidofovir as a topical ophthalmic antiviral for ocular canine herpesvirus-1 infections in dogs. J Ocul Pharmacol Ther 31:642–649.
28. Spertus CB, Mohammed HO, Ledbetter EC. 2016. Effects of topical ocular application of 1% trifluridine ophthalmic solution in dogs with experimentally induced recurrent ocular canine herpesvirus-1 infection. Am J Vet Res 77:1140–1147.
29. Ledbetter EC, Nicklin AM, Spertus CB, Pennington MR, Van de Walle GR, Mohammed

HO. 2017. Evaluation of topical ophthalmic ganciclovir gel in the treatment of experimentally induced ocular canine herpesvirus-1 infection. Am J Vet Res.

30. Poulet H, Guigal PM, Soulier M, Leroy V, Fayet G, Minke J, Chappuis Merial G. 2001. Protection of puppies against canine herpesvirus by vaccination of the dams. Vet Rec 148:691–5.
31. Chabchoub A, Kallel F, Haddad S, Landolsi F, Rmili M, Van Gool F. 2006. Canine herpes virus infection : evaluation of vaccine efficiency (inactive vaccine) in reproductive bitches with 2 different protocols, field trial. Rev Med Vet (Toulouse) 12:573–578.
32. Ledbetter EC, Kim K, Dubovi EJ, Mohammed HO, Felippe MJB. 2016. Clinical and immunological assessment of therapeutic immunization with a subunit vaccine for recurrent ocular canine herpesvirus-1 infection in dogs. Vet Microbiol 197:102–110.
33. Ledbetter EC. 2013. Canine herpesvirus-1 ocular diseases of mature dogs. N Z Vet J 61:193–201.
34. Thiry E, Addie D, Belák S, Boucraut-Baralon C, Egberink H, Frymus T, Gruffydd-Jones T, Hartmann K, Hosie MJ, Lloret A, Lutz H, Marsilio F, Pennisi MG, Radford AD, Truyen U, Horzinek MC. 2009. Feline herpesvirus infection: ABCD guidelines on prevention and management. J Feline Med Surg 11:547–555.
35. Horzinek MC, Addie D, Belák S, Boucraut-Baralon C, Egberink H, Frymus T, Gruffydd-Jones T, Hartmann K, Hosie MJ, Lloret A, Lutz H, Marsilio F, Möstl K, Pennisi MG, Radford AD, Thiry E, Truyen U. 2013. ABCD: Update of the 2009 guidelines on prevention and management of feline infectious diseases. J Feline Med Surg 15:530–539.
36. Gould D. 2011. Feline Herpesvirus-1. Ocular manifestations, diagnosis and treatment options. J Feline Med Surg 13:333–346.
37. Thomasy SM, Maggs DJ. 2016. A review of antiviral drugs and other compounds with activity against feline herpesvirus type 1. Vet Ophthalmol 19:119–130.
38. Fontenelle JP, Powell CC, Veir JK, Radecki S, Lappin MR. 2008. Effect of topical ophthalmic application of cidofovir on experimentally induced primary ocular feline herpesvirus-1 infection in cats. Am J Vet Res 69:289–293.
39. Nasisse MP, Guy JS, Davidson MG, Sussman W, De Clercq E. 1989. In vitro susceptibility of feline herpesvirus-1 to vidarabine, idoxuridine, trifluridine, acyclovir, or bromovinyldeoxyuridine. Am J Vet Res 50:158–60.

40. Solaroli N, Johansson M, Persoons L, Balzarini J, Karlsson A. 2008. Substrate specificity of feline and canine herpesvirus thymidine kinase. Antiviral Res 79:128–132.
41. Maggs DJ. 2010. Antiviral therapy for feline herpesvirus infections. Vet Clin North Am - Small Anim Pract 40:1055–1062.
42. Nasisse MP, Dorman DC, Jamison KC, Weigler BJ, Hawkins EC, Stevens JB. 1997. Effects of valacyclovir in cats infected with feline herpesvirus 1. Am J Vet Res 58:1141–4.
43. Thomasy SM, Lim CC, Reilly CM, Kass PH, Lappin MR, Maggs DJ. 2011. Evaluation of orally administered famciclovir in cats experimentally infected with feline herpesvirus type-1. Am J Vet Res 72:85–95.
44. Maggs DJ, Collins BK, Thorne JG, Nasisse MP. 2000. Effects of L-lysine and L-arginine on in vitro replication of feline herpesvirus type-1. Am J Vet Res 61:1474–8.
45. Maggs DJ, Nasisse MP, Kass PH. 2003. Efficacy of oral supplementation with L-lysine in cats latently infected with feline herpesvirus. Am J Vet Res 64:37–42.
46. Stiles J, Townsend WM, Rogers QR, Krohne SG. 2002. Effect of oral administration of L-lysine on conjunctivitis caused by feline herpesvirus in cats. Am J Vet Res 63:99–103.
47. Maggs D, Sykes J, Clarke H, Yoo S, Kass P, Lappin M, Robers Q, Waldron M, Fascetti A. 2007. Effects of dietary lysine supplementation in cats with enzootic upper respiratory disease. J Feline Med Surg 9:97–108.
48. Rees TM, Lubinski JL. 2008. Oral supplementation with l-lysine did not prevent upper respiratory infection in a shelter population of cats. J Feline Med Surg 10:510–513.
49. Drazenovich TL, Fascetti AJ, Westermeyer HD, Sykes JE, Bannasch MJ, Kass PH, Hurley KF, Maggs DJ. 2009. Effects of dietary lysine supplementation on upper respiratory and ocular disease and detection of infectious organisms in cats within an animal shelter. Am J Vet Res 70:1391–1400.
50. Cave NJ, Dennis K, Gopakumar G, Dunowska M. 2014. Effects of physiologic concentrations of l-lysine on in vitro replication of feline herpesvirus 1. Am J Vet Res 75:572–80.
51. Fulton RW, Burge LJ. 1985. Susceptibility of feline herpesvirus 1 and a feline calicivirus to feline interferon and recombinant human leukocyte interferons. Antimicrob Agents Chemother 28:698–9.

52. Sandmeyer LS, Keller CB, Bienzle D. 2005. Effects of interferon-alpha on cytopathic changes and titers for feline herpesvirus-1 in primary cultures of feline corneal epithelial cells. Am J Vet Res 66:210–6.
53. Siebeck N, Hurley DJ, Garcia M, Greene CE, Köstlin RG, Moore PA, Dietrich UM. 2006. Effects of human recombinant alpha-2b interferon and feline recombinant omega interferon on in vitro replication of feline herpesvirus-1. Am J Vet Res 67:1406–11.
54. Haid C, Kaps S, Gönczi E, Hässig M, Metzler A, Spiess BM, Richter M. 2007. Pretreatment with feline interferon omega and the course of subsequent infection with feline herpesvirus in cats. Vet Ophthalmol 10:278–284.
55. Gil S, Leal RO, Duarte A, McGahie D, Sepúlveda N, Siborro I, Cravo J, Cartaxeiro C, Tavares LM. 2013. Relevance of feline interferon omega for clinical improvement and reduction of concurrent viral excretion in retrovirus infected cats from a rescue shelter. Res Vet Sci 94:753–763.
56. Ballin AC, Schulz B, Helps C, Sauter-Louis C, Mueller RS, Hartmann K. 2014. Limited efficacy of topical recombinant feline interferon-omega for treatment of cats with acute upper respiratory viral disease. Vet J 202:466–470.
57. Fenimore A, Carter K, Fankhauser J, Hawley JR, Lappin MR. 2016. Evaluation of intranasal vaccine administration and high-dose interferon- α2b therapy for treatment of chronic upper respiratory tract infections in shelter cats. J Feline Med Surg 18:603–611.
58. Collier R. 2009. Drug development cost estimates hard to swallow. CMAJ 180:279–80.
59. DiMasi JA, Grabowski HG, Hansen RW. 2016. Innovation in the pharmaceutical industry: New estimates of R&D costs. J Health Econ 47:20–33.
60. Biron KK. 2007. Candidate anti-herpesviral drugs; mechanisms of action and resistanceHuman Herpesviruses: Biology, Therapy, and Immunoprophylaxis. Cambridge University Press.
61. Li Q, Maddox C, Rasmussen L, Hobrath J V, White LE. 2009. Assay development and high-throughput antiviral drug screening against Bluetongue virus. Antiviral Res 83:267–73.
62. Atkins C, Evans CW, White EL, Noah JW. 2012. Screening methods for influenza antiviral drug discovery. Expert Opin Drug Discov 7:429–438.
63. Matza-Porges S, Eisen K, Ibrahim H, Haberman A, Fridlender B, Joseph G. 2014. A new

antiviral screening method that simultaneously detects viral replication, cell viability, and cell toxicity. J Virol Methods 208:138–143.

64. Öberg B. 2006. Rational design of polymerase inhibitors as antiviral drugs. Antiviral Res 71:90–95.

65. Wlodawer A. 2002. Rational approach to AIDS drug design through structural biology. Annu Rev Med 53:595–614.

66. Elion GB, Furman PA, Fyfe JA, de Miranda P, Beauchamp L, Schaeffer HJ. 1977. Selectivity of action of an antiherpetic agent, 9-(2-hydroxyethoxymethyl) guanine. Proc Natl Acad Sci U S A 74:5716–20.

67. Law GL, Tisoncik-Go J, Korth MJ, Katze MG. 2013. Drug repurposing: a better approach for infectious disease drug discovery? Curr Opin Immunol 25:588–592.

68. Mounce BC, Cesaro T, Moratorio G, Hooikaas PJ, Yakovleva A, Werneke SW, Smith EC, Poirier EZ, Simon-Loriere E, Prot M, Tamietti C, Vitry S, Volle R, Khou C, Frenkiel M-P, Sakuntabhai A, Delpeyroux F, Pardigon N, Flamand M, Barba-Spaeth G, Lafon M, Denison MR, Albert ML, Vignuzzi M. 2016. Inhibition of polyamine biosynthesis is a broad-spectrum strategy against RNA viruses. J Virol 90:9683–9692.

69. Johansen LM, Brannan JM, Delos SE, Shoemaker CJ, Stossel A, Lear C, Hoffstrom BG, Dewald LE, Schornberg KL, Scully C, Lehár J, Hensley LE, White JM, Olinger GG. 2013. FDA-approved selective estrogen receptor modulators inhibit Ebola virus infection. Sci Transl Med 5:190ra79.

70. Dyall J, Coleman CM, Hart BJ, Venkataraman T, Holbrook MR, Kindrachuk J, Johnson RF, Olinger GG, Jahrling PB, Laidlaw M, Johansen LM, Lear-Rooney CM, Glass PJ, Hensley LE, Frieman MB. 2014. Repurposing of clinically developed drugs for treatment of Middle East respiratory syndrome coronavirus infection. Antimicrob Agents Chemother 58:4885–4893.

71. Albulescu IC, van Hoolwerff M, Wolters LA, Bottaro E, Nastruzzi C, Yang SC, Tsay S-C, Hwu JR, Snijder EJ, van Hemert MJ. 2015. Suramin inhibits chikungunya virus replication through multiple mechanisms. Antiviral Res 121:39–46.

72. Resau JH, Sakamoto K, Cottrell JR, Hudson EA, Meltzer SJ. 1991. Explant organ culture: A review. Cytotechnology 7:137–149.

73. Russell WM., Burch RL. 1959. The principles of humane experimental technique.

Methuen, London.

74. Leushacke M, Barker N. 2014. Ex vivo culture of the intestinal epithelium: strategies and applications. Gut 63:1345–54.
75. Mathes SH, Ruffner H, Graf-Hausner U. 2014. The use of skin models in drug development. Adv Drug Deliv Rev 69–70:81–102.
76. Daviaud N, Garbayo E, Schiller PC, Perez-Pinzon M, Montero-Menei CN. 2013. Organotypic cultures as tools for optimizing central nervous system cell therapies. Exp Neurol 248:429–40.
77. Summa V, Petrocchi A, Bonelli F, Crescenzi B, Donghi M, Ferrara M, Fiore F, Gardelli C, Gonzalez Paz O, Hazuda DJ, Jones P, Kinzel O, Laufer R, Monteagudo E, Muraglia E, Nizi E, Orvieto F, Pace P, Pescatore G, Scarpelli R, Stillmock K, Witmer M V., Rowley M. 2008. Discovery of raltegravir, a potent, selective orally bioavailable HIV-integrase inhibitor for the treatment of HIV-AIDS infection. J Med Chem 51:5843–5855.
78. Hughes CA, Robinson L, Tseng A, MacArthur RD. 2009. New antiretroviral drugs: a review of the efficacy, safety, pharmacokinetics, and resistance profile of tipranavir, darunavir, etravirine, rilpivirine, maraviroc, and raltegravir. Expert Opin Pharmacother 10:2445–2466.
79. Nguyen B-YT, Isaacs RD, Teppler H, Leavitt RY, Sklar P, Iwamoto M, Wenning LA, Miller MD, Chen J, Kemp R, Xu W, Fromtling RA, Vacca JP, Young SD, Rowley M, Lower MW, Gottesdiener KM, Hazuda DJ. 2011. Raltegravir: the first HIV-1 integrase strand transfer inhibitor in the HIV armamentarium. Ann N Y Acad Sci 1222:83–89.
80. Liedtke M, Tomlin C, Miller M, Lockhart S, Rathbun RC. 2014. Long-term efficacy and safety of raltegravir in the management of HIV infection. Infect Drug Resist 7:73.
81. Mouscadet JF, Tchertanov L. 2009. Raltegravir: molecular basis of its mechanism of action. Eur J Med Res 14 Suppl 3:5–16.
82. McColl DJ, Chen X. 2010. Strand transfer inhibitors of HIV-1 integrase: Bringing IN a new era of antiretroviral therapy. Antiviral Res 85:101–118.
83. Nadal M, Mas PJ, Mas PJ, Blanco AG, Arnan C, Solà M, Hart DJ, Coll M. 2010. Structure and inhibition of herpesvirus DNA packaging terminase nuclease domain. Proc Natl Acad Sci U S A 107:16078–83.
84. Zhou B, Yang K, Wills E, Tang L, Baines JD. 2014. A mutation in the DNA polymerase

accessory factor of herpes simplex virus 1 restores viral DNA replication in the presence of raltegravir. J Virol 88:11121–11129.

85. Boesch A, Cattori V, Riond B, Willi B, Meli ML, Rentsch KM, Hosie MJ, Hofmann-Lehmann R, Lutz H. 2015. Evaluation of the effect of short-term treatment with the integrase inhibitor raltegravir (Isentress™) on the course of progressive feline leukemia virus infection. Vet Microbiol 175:167–178.

86. Spertus CB, Pennington MR, Van de Walle GR, Badanes ZI, Judd BE, Mohammed HO, Ledbetter EC. 2018. Effects of oral raltegravir in cats with experimentally-induced ocular and respiratory feline herpesvirus-1 infection. Am J Vet Res. Under Review.

CHAPTER TWO

NEW PARADIGMS FOR THE STUDY OF OCULAR ALPHAHERPESVIRUS INFECTIONS: INSIGHTS INTO THE USE OF NON-TRADITIONAL HOST MODEL SYSTEMS

*Manuscript from: Matthew R. Pennington, Eric C. Ledbetter, and Gerlinde R. Van de Walle 2017. New paradigms for the study of ocular alphaherpesvirus infections: insights into the use of non-traditional host model systems. *Viruses* 9(11), 349.

2.1. Summary

Ocular herpesviruses, most notably human alphaherpesvirus 1 (HHV-1), canid alphaherpesvirus 1 (CHV-1), and felid alphaherpesvirus 1 (FHV-1), infect and cause severe disease that may lead to blindness. CHV-1 and FHV-1 have a pathogenesis and induce clinical disease in their hosts that is similar to HHV-1 ocular infections in humans, suggesting that infection of dogs and cats with CHV-1 and FHV-1, respectively, can be used as a comparative natural host model of herpesvirus-induced ocular disease. In this review, we discuss both strengths and limitations of the various available model systems to study ocular herpesvirus infection, with a focus on the use of these non-traditional, virus-natural host models. Recent work has demonstrated the robustness and reproducibility of experimental ocular herpesvirus infections in dogs and cats, and, therefore, these non-traditional models can provide additional insights into the pathogenesis of ocular herpesvirus infections.

Keywords: herpesvirus; HHV-1; CHV-1; FHV-1; ocular infection; model systems; natural host infection

2.2. Introduction

Herpesviruses commonly infect and can cause ocular disease in a variety of species (Table 2.1). The prevalence of persistent infections that result in the presentation of ocular disease, however, is difficult to determine as it varies dramatically based on the population surveyed and the study methodology. Still, ocular diseases caused by human alphaherpesvirus 1 (HHV-1, also known as herpes simplex virus 1, HSV-1), canid alphaherpesvirus 1 (CHV-1), and felid alphaherpesvirus 1 (FHV-1) are among the most common causes of clinical herpesvirus-associated ocular disease, and can lead to ocular pain, tissue destruction, and blindness in severe cases (1–3). The pathogenesis of these viruses is very similar and has been reviewed extensively (2–6). Briefly, a person or animal becomes infected following contact with the ocular, nasal, or salivary secretions of an actively shedding host via the orofacial route. This leads to infection of epithelial cells of the oral mucosa, the cornea, and/or the conjunctiva. In the case of FHV-1, and to a much lesser extent CHV-1, primary infection can also be established in the mucosae of the nasal septum, turbinate, nasopharynx, upper trachea, tonsils, and mandibular lymph nodes, leading to the development of respiratory disease (5, 7). Following replication in epithelial cells, the virus is able to access the sensory neurons of the peripheral nervous system and travel via retrograde transport to the trigeminal ganglion (TG), where latency is established. Following reactivation, the virus can travel back down the axons and access all sites innervated by the TG, namely the oral cavity and the eye, where the virus will replicate again in epithelial cells of these tissues. This process can happen repeatedly, and so tissue damage and clinical signs

Table 2.1: Overview of herpesviruses reported in literature to frequently cause ocular disease.

Virus	Abbreviations	Subfamily	Associated ocular diseases	Overall prevalence	Herpesvirus-associated ocular disease prevalence	References
Human alphaherpesvirus 1	HHV-1/ HSV-1	Simplexvirus	Corneal lesions, stromal & epithelial keratitis, conjunctivitis	67-90%	12-36/100,000	(3, 136–140)
Canid alphaherpesvirus 1	CHV-1	Varicellovirus	Corneal lesions, stromal & epithelial keratitis, conjunctivitis	21-98%	Unknown	(2, 141–146)
Felid alphaherpesvirus 1	FHV-1	Varicellovirus	Corneal lesions, stromal & epithelial keratitis, conjunctivitis	40-97%	Unknown	(147–151)
Human alphaherpesvirus 3	HHV-3/ VZV	Varicellovirus	Herpes zoster ophthalmicus	>95%	19-31/100,000	(152–154)
Equid alphaherpesvirus 1	EHV-1	Varicellovirus	Chorioretinitis	52%- “endemic”	50-90% of choroidal lesions in experimental infection	(155–158)
Equid gammaherpesvirus 2	EHV-2	Percavirus	Keratoconjunctivitis	51-93%	8-60% of keratoconjunctivitis cases tested	(159–164)
Bovine alphaherpesvirus 1	BoHV-1	Varicellovirus	Keratoconjunctivitis	20-97%	4.95/100	(165–167)
Bovine gammaherpesvirus 4	BoHV-4	Rhadinovirus	Keratoconjunctivitis & ocular discharge	21-35%	Unknown	(168–171)
Alcelpahine gammaherpesvirus 1 & Ovine gammaherpesvirus 2	AlHV-1 OvHV-2	Macavirus	Ocular discharge	29-77%	Typical symptom of malignant catarrhal fever	(172–175)

can be present during both primary infection and following reactivation, leading to recurrent ocular disease. Ocular disease develops as a result of the direct lysis of conjunctival or corneal epithelial cells. However, the most severe clinical signs are observed after the establishment of latency in the TG and subsequent cycles of reactivation. This leads to the formation of herpes stromal keratitis (HSK), which consists of severe corneal lesions, corneal neovascularization, and infiltration of immune cells that contribute to destruction of the cornea, ultimately leading to blindness. Due to the striking similarities in pathogenesis of HHV-1, CHV-1, and FHV-1, studies in dogs and cats are proposed as valuable virus-natural host models to study the pathogenesis of human herpesvirus infections of the eye (2, 5, 8, 9).

In this review, we discuss the strengths and limitations of different model systems available to study ocular herpesvirus infection, with an emphasis on the use of virus-natural host systems, the role of which has been generally underutilized in favor of studies in mice and rabbits (3, 10). The importance of studying infection in the natural host is well recognized for several viruses, particularly emerging zoonotic viruses, as there are often differences in the symptoms of the disease among the natural, transmission, and human and/or animal hosts due to a variety of factors, including anatomical, physiological, metabolic, behavioral, genetic, and immune (11). Indeed, there is an emerging appreciation for (i) the recognition that in some cases, mouse models cannot fully recapitulate the disease presentation and progression as it occurs in the natural host and (ii) the value of studies in natural hosts as comparative models for human diseases. An excellent example is the infection of woodchucks with woodchuck hepatitis virus, which is well recognized as a

comparative model of hepatitis B virus in humans due to the similarities in liver disease developed in both species following infection (12, 13). Since herpesviruses have been coevolving with their hosts over millions of years and are exquisitely adapted to their respective host (14–16), studies of ocular herpesvirus infection in the natural host are, therefore, valuable to better understand how different hosts respond to herpesvirus infection and/or which host factors are important for both establishment and control of infection. Moreover, and importantly, virus-natural hosts models are useful to screen novel vaccines and antivirals based on better predictive outcomes.

2.3. *In Vitro* 2D Cell Culture Systems

2.3.1. Immortalized Cell Lines

A variety of immortalized cell lines have been used to study replication of herpesviruses capable of infecting the eye, as well as evaluating the efficacy of antiviral drugs. African green monkey kidney epithelial cells (Vero cells) are perhaps the most commonly used immortal cell line to study HHV-1 (17–20), although other cell types like CV-1, an African green monkey kidney fibroblast cell line, or MRC-5, a human lung fibroblast cell line, are also frequently utilized (18, 21). For CHV-1 and FHV-1, Madin-Darby canine kidney cells (MDCK) and Crandell-Reese feline kidney (CRFK) cells, respectively, are almost exclusively used, with a major focus on evaluating antivirals in these cell lines (22–26). The advantages of using immortalized cell lines are their ease of growing and the availability of cell lines from the respective host. However, it has to be noted that these cell lines are not

derived from ocular tissues and, therefore, do not represent the cells that the virus encounters at the primary site of infection.

2.3.2. Primary Corneal Epithelial Cells

Work in recent years has recognized that primary corneal epithelial cells (CECs), the primary ocular site of replication of HHV-1, FHV-1, and CHV-1, can be used to overcome some of the limitations of immortalized cells, and have been successfully isolated from humans (HCECs), dogs (CCECs), and cats (FCECs) (27–29). Isolation of primary corneal cells is accomplished either by outgrowth from a corneal explant, or via mechanical and enzymatic separation of corneal tissue. HCECs and FCECs have been described to support infection of HHV-1 and FHV-1, respectively (28, 30, 31). Likewise, we have successfully isolated CCECs and confirmed that they can be infected with CHV-1 (Fig. 2.1). FCECs and CCECs have the advantage in that they can be isolated from herpesvirus-free, healthy animals from commercial research breeding colonies (see 2.3.3). A disadvantage, however, is their limited lifespan. For example, FCECs are described to undergo senescence by passage 45, with gradual changes in morphology observable from passages 20-45 onwards (28). In our experience, however, morphological transformation of FCECs to a fibroblastoid phenotype can occur as early as passage 10, quickly followed by extensive cell death in subsequent passages (data not shown). One possibility to circumvent this is to immortalize CECs. Several such lines have been described, including the hTCEpi line, a human telomerase reverse transcriptase (hTERT) expressing HCEC line shown to maintain normal karyotype and cell cycle kinetics to at least passage 240 (32), and a SV40-adenovirus vector

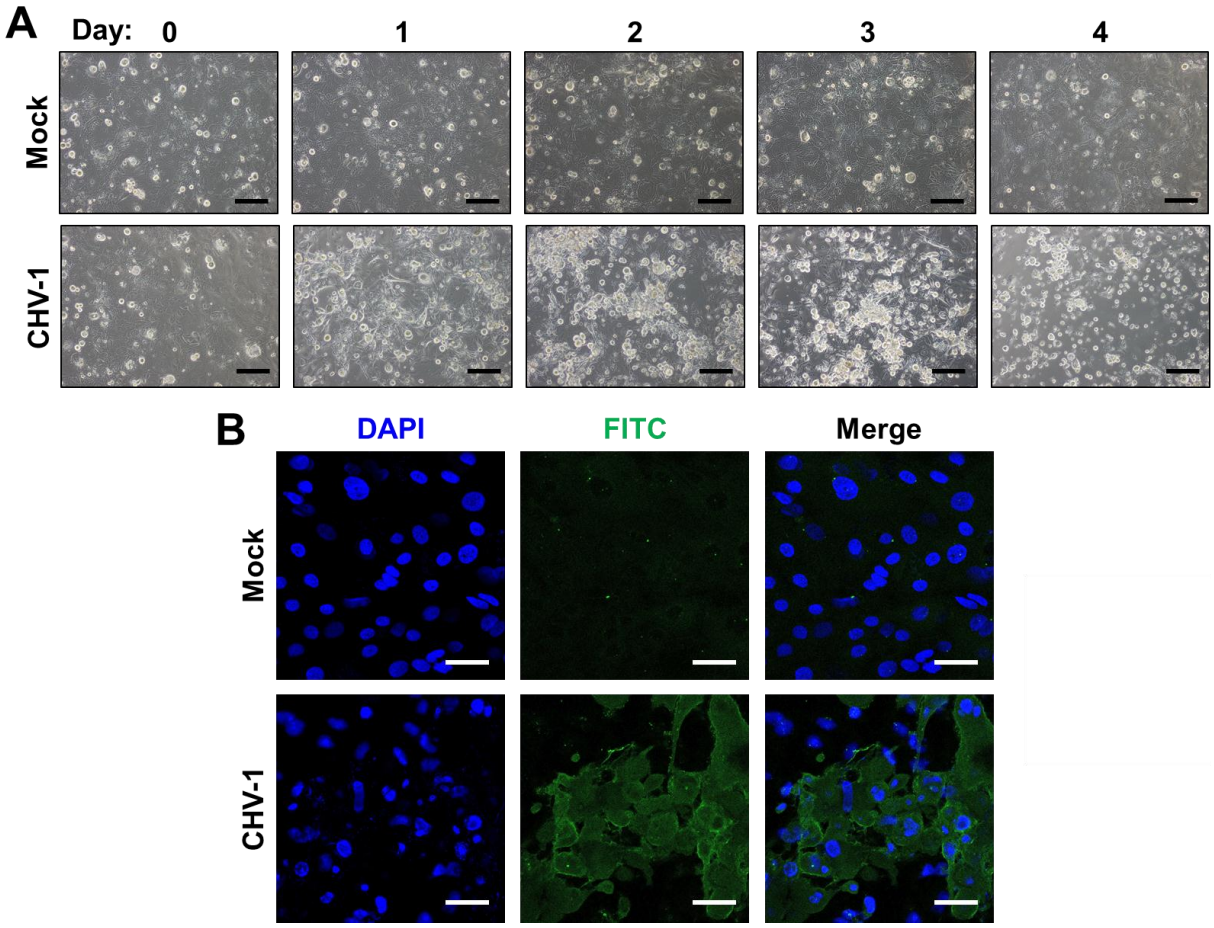

Figure 2.1: Canine corneal epithelial cells (CCECs) support the growth of CHV-1. CCECs were either mock-infected or infected at an MOI=1 with the CHV-1 strain Duk. **(A)** Representative light micrographs of the course of the infection. Scale bar, 100 µm. **(B)** At 4 days post infection, CCECs were fixed in acetone and stained according to the manufacturer's directions with a commercially available FITC-conjugated anti-CHV-1 antibody (VMRD, Pullman, WA; Cat#C5-F-CHV). Representative mock- and CHV-1-infected fields are shown. Scale bar, 100 µm

transformed HCEC cell line that displayed a normal growth phenotype for more than 400 generations (33). Many HCEC lines immortalized via telomerase, SV-40, and/or Rous sarcoma virus are commercially available via biological material resource centers such as American Type Culture Collection (ATCC).

2.3.3. Limitations of 2D cell culture systems

One of the major limitations of 2D cell cultures is the absence of other cells and components of the ocular system, including the immune defense system. While 2D cell cultures can recapitulate the innate immune responses of epithelial cells to the virus, e.g. interferon production, they are unable to model more complex innate immune responses as well as the adaptive immune response that are the primary drivers of HSK (34). Additionally, neovascularization, i.e. the ingrowth of blood vessels into the cornea, is a common component of HSK (35), and the breaking of corneal angiogenic privilege cannot be fully modeled in traditional 2D cell culture systems, though the growth patterns of endothelial cells can be analyzed individually in culture.

Additionally, it is well recognized that antiviral activity observed in 2D cell culture systems does not always translate into antiviral activity *in vivo*, and potential drug toxicity is seldom accurately recapitulated in these simplified model systems (36). Several examples of this exist in the search for effective antivirals against FHV-1. For instance, the nucleoside analogue idoxuridine was found to inhibit the replication of FHV-1 in CRFK at a half maximal effective concentration (EC_{50}) ranging between 4.3-6.8 µM (22, 37). However, when evaluating its efficacy to treat cats presenting to the clinic with naturally acquired FHV-1-associated ocular disease, it was found that 4 out of 7 idoxuridine-treated FHV-1-infected cats exhibited no improvement or even worsened with therapy (38). Another example is acyclovir, a nucleoside analogue that was shown to be effective at inhibiting FHV-1 replication in CRFK at EC_{50} values ranging between 57.9-66.6 µM (22, 23). When

valacyclovir, a prodrug of acyclovir with better oral bioavailability, was evaluated in cats as a systemic therapy for FHV-1 ocular infections, it was found that all cats in the study develop acute conjunctivitis in addition to exhibiting systemic toxicity (39). However, a study in which topical acyclovir treatment was evaluated in a limited number of client-owned cats did show some moderate improvement in clinical scores after a five time/day acyclovir treatment regimen for 21 days, which was initiated after a 21-day treatment with chlortetracycline due to suspected *Chlamydophila spp*. infection (40). Thus, and despite initially promising results in CRFK, the use of acyclovir as a therapy for FHV-1 infection is still debated. On the other hand, the use of the nucleoside analogue cidofovir is an example where results in 2D cell culture did translate into efficacy of this drug in vivo. Cidofovir showed an EC_{50} of 11.0 μM in CRFK (22), and its antiviral activity and minimal toxicity was then confirmed in FCECs (41). A follow-up study using topical cidofovir in experimentally-infected cats showed that this drug significantly reduced viral shedding and ocular clinical disease (42), and, consequently, cidofovir is currently one of the most commonly used topical antivirals used to treat ocular FHV-1 infection (43).

2.4. *In Vitro* 3D Cell Culture/Explant Systems

2.4.1. Corneal facsimiles

Corneal facsimiles, comprised of cornea cells grown in matrices, have sought to mimic the 3D structure of the cornea and cell-to-cell interactions in a renewable and cost-effective manner. One such model consists of human corneal stromal fibroblasts mixed with type I

collagen in transwell plates overlaid with Matrigel to simulate the corneal stroma and basement membrane, and this model has been used for corneal inflammation and adenovirus infection studies (44). Subsequent improvements consisted of culturing epithelial cells over these stromal cells and the incorporation of an endothelium to create full thickness corneal equivalents (45). Other models have been developed to recapitulate the 3D structure of specific portions of the cornea. For example, hydrogen scaffolds for corneal stromal tissues (46), decellularized human, porcine, or bovine corneas as a scaffold for reconstructing the corneal epithelium, anterior stroma, and/or the endothelium (47–49), and hybrid electrospun poly (lactic-co-glycolide) mats combined with plastic compressed collagen matrices for entire corneas (50) have all been described as potential *in vitro* 3D models of the cornea. However, and to our knowledge, none of these model systems have been used to study herpesvirus infections. Therefore, the use of these models to accurately recreate in vivo herpesvirus infection events remains to be determined.

2.4.2. Explants

Explants, also referred to as *ex vivo* organ, organotypic, or organoid cultures, are highly sophisticated physiological systems that maintain the normal three-dimensional structures and cell-to-cell contacts of the tissue as they are found in vivo, without the disruption required to place such tissues into 2D cell culture. Moreover, since many pathological conditions, including ocular herpesvirus infection, involve more than one cell type, explants are considered to be much more physiologically relevant compared to cell culture systems (51). Therefore, explants are proposed as stepping stones to bridge *in vitro* and *in vivo* models

to validate cell culture results while limiting the amount of animal experimentation needed and thus satisfying the 3 R's of animal research (52). Corneal or, more correctly, corneoscleral explants, were first developed as a means to prolong the time that human corneas could be preserved prior to transplantation (53) as well as to study wound healing in the human eye (54, 55). These explants were then expanded for the purpose of studying ocular herpesvirus infection. The methodology for obtaining and culturing these corneas is similar across species, and consists of removing the eye from the donor and aseptically dissecting the corneoscleral buttons. The cornea is then placed epithelial side down and the endothelial cavity is filled with a 1% agarose solution to mimic the vitreous humor, providing support to maintain the normal 3D structure of the cornea (25). Corneas may or may not be scarified prior to infection with herpesvirus, and are either covered with media and cultured for up to 8 days, or placed in a rocking air-liquid interface and cultured for up to three weeks. Thus far, corneoscleral explants have been described to model HHV-1 infection using human, rabbit, and pig corneas (56–59), CHV-1 infection using canine corneas (8), and FHV-1 infection using feline corneas (25, 60). The infection in these cornea models was shown to be similar across the different viruses and is depicted schematically in Fig. 2.2. Briefly, corneal epithelial cells are the primary site of replication and viral plaques are formed upon cell lysis. The explants are typically infected at a high MOI to ensure infection and, as a result, virus is found uniformly across the epithelium, resulting in damage to the entire epithelium. However, using a porcine cornea explant to model HHV-1 growth, Thakkar et al. showed that dendritic ulcerations form in a virus inoculum-dependent manner, eventually leading to the

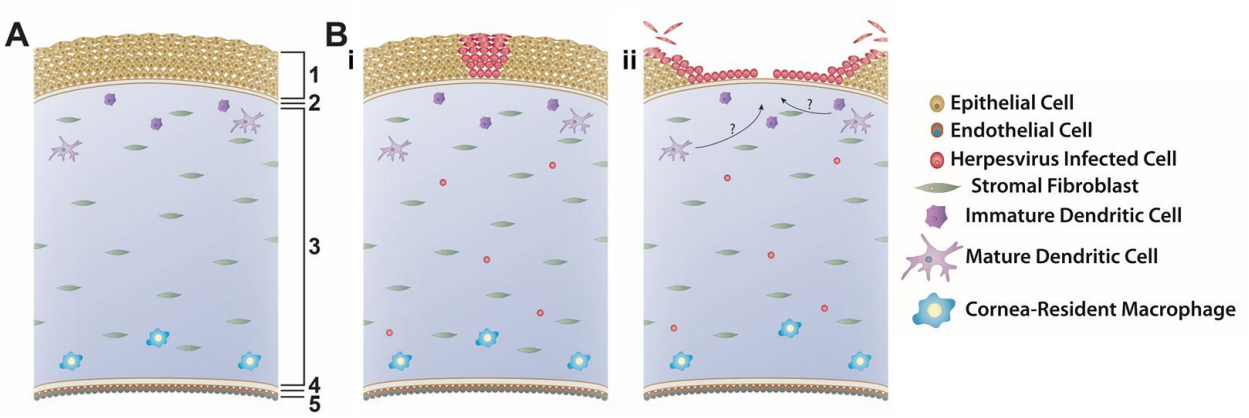

Figure 2.2: General progression of lytic herpesvirus infection in cornea explant models. **(A)** Structure of normal cornea with the five layers indicated: (1) epithelium, (2) Bowman's layer (absent in felines and canines), (3) stroma, populated by stromal fibroblasts and various resident immune cells, (4) Descemet's membrane, and (5) endothelium. **(B)** Following herpesvirus infection of the cornea explant, corneal epithelial cells become infected in a dose-dependent manner, resulting in the formation of plaques and dendrites. Unidentified stromal cells may also become infected (i). Following prolonged incubation, corneal epithelial cells are lysed and slough off into the culture media, leading to complete destruction of the epithelium (ii). The contribution of resident corneal immune cells in the host response to herpesvirus infection has not been formally investigated in explant cultures to date.

formation of larger, geographic ulceration commonly observed in vivo (59). Additionally, some models suggest that cells deeper in the corneal tissue, including endothelial cells and other unidentified cells, may also become infected (8, 58) (Fig. 2.2). Collectively, these data show that the infection patterns in corneal explants closely mimic the pathogenesis of ocular herpesvirus infections in vivo.

Human and rabbit corneal explants have been used to study the inhibition of herpesviral replication using phosphonoacetic acid (PAA) and to demonstrate the role of Checkpoint Kinase 2 (Chk2) in promoting HHV-1 replication in the cornea, suggesting that Chk2

inhibitors could be used to treat HHV-1 ocular infection (56, 57). Our group has used canine corneal explants to assess the local innate immune response and inflammation associated with CHV-1, similar to what has been done for HHV-1 infection of human corneal explants (8, 58). Feline corneal explants have been used by our group to study the efficacy and toxicity of acyclovir, cidofovir, and the anti-human immunodeficiency virus (HIV) integrase inhibitor raltegravir against FHV-1 replication (25). We found that the levels of efficacy of acyclovir and cidofovir in the explant model against FHV-1 were comparable to reported efficacy results *in vivo* (see 2.3.3), with cidofovir being significantly more effective than acyclovir, thus supporting the physiological relevance of this model. Furthermore, we showed that raltegravir is effective against FHV-1 using our feline corneal explant model and is non-toxic for corneal tissues, suggesting that topical raltegravir could prove to be a novel treatment option for FHV-1 ocular infection in cats (25).

Besides the corneal epithelial cells which play an important role as initiators of the innate immune response through a variety of pattern recognition receptors (61, 62), the cornea also harbors a heterogeneous population of resident antigen-presenting cells in both stroma and epithelium (63, 64) (Fig. 2.2). These cells respond to cytokine cues from the epithelial cells and help to orchestrate the response of the systemic immune response that leads to clearance of the virus (65–67). However, to our knowledge, no study has evaluated the presence, activity, or role in controlling the infection of these innate immune cells in corneal explants.

2.4.3. Limitations of 3D Cell Culture/Explant Systems

There are a couple of notable drawbacks using *ex vivo* cultures compared to 2D cell cultures, including higher costs, difficulty of access to donor tissue, and a greater degree of variability between samples (56). The source of the donor tissue could also be a concern. Corneas from human donors available for research are usually those deemed unsuitable for corneal transplantation and often come from older donors or donors with severe medical disorders (8, 58). Indeed, approximately 41% of donated human corneas are discarded from consideration for transplant, primarily because of medical contraindication or poor endothelial quality, and thus become available for experimentation (68). In contrast, canine and feline corneas can be collected from healthy research animals that are euthanized for unrelated reasons, and are even commercially available as fresh grafts for transplantation purposes in these animals, resulting in a much better quality of these tissues.

Contamination with infectious agents is another limitation of using and culturing primary cornea tissues. For example, the presence of bacterial and fungal contamination has been studied in human corneas for transplantation. Overall, it was found that the contamination rate of cornea cultures ranges from 0.53% to 11% (69–76). This contamination can be controlled to some extent by an initial decontamination procedure and subsequent culturing with penicillin, streptomycin, amphotericin B, voriconazole, or similar antibiotics and antimycotics. However, care must be taken to refresh the media periodically as the concentration of these agents can decline by as much as 86% during prolonged culture (77). In addition, and importantly, intra-corneal contamination with herpesviruses itself is a

possibility. While HSK patients do have approximately 100 times more HHV-1 DNA in their corneas than healthy patients, HHV-1 is periodically shed in the tears of HHV-1 seropositive, yet asymptomatic individuals (78). This has led to considerable debate in the field as to if HHV-1 may establish latency in the cornea itself, though latency associated transcripts (LATs) have not been irrefutably detected in corneal tissue, or if such shedding is a result of frequent subclinical replication in the cornea (79, 80). Nevertheless, studies have shown that between 1.8 to 38% of donor corneas for transplantation were contaminated with HHV-1 DNA using PCR (81–85). One study further demonstrated that infectious HHV-1 could be isolated successfully from 7 PCR positive cases, although it was noted that these donors had a history of long-standing or severe illnesses, often in the hospital, that may have contributed to this active viral shedding (86). Likewise, FHV-1 has been detected in the corneas of clinically health cats at a rate of 20% (87), and although the frequency of CHV-1 DNA in clinically healthy dog corneas has not been evaluated to our knowledge, it is most likely similar to FHV-1. It is currently not clear how the presence of herpesviral DNA or even potentially low levels of infectious virus impact experimental outcomes in corneal explants. However, the likelihood of herpesvirus contamination is likely to be low. Furthermore, specific pathogen-free (SPF), including herpesvirus-free, dogs and cats are available commercially from laboratory animal supply companies and so the use of corneas from these animals could, therefore, address the concern of low-level herpesvirus infection of donor corneas. If such animals are not available or human tissue is to be used, negative controls of uninfected matched corneas from the same donor should ideally be included.

2.5. *In Vivo* Systems

Rabbits and mice are commonly used to study HHV-1 ocular infection and this has been reviewed extensively (3, 10). Here, we will give a brief overview of the general pathogenesis of ocular HHV-1 in these traditional models and we will elaborate more on the non-traditional model species such as dogs and cats. The latter two models represent virus-natural host infection models and as such, can complement studies on the pathogenesis of human herpesvirus infections of the eye.

2.5.1. Mice

Studies in mice constitute the majority of our understanding on HHV-1 pathogenesis *in vivo*, including the immune response and latency. Mice are more commonly used than rabbits based on their small size, which reduces the amount of drugs and chemicals required for testing, the cost of boarding, and the ready availability of inbred strains with the same genetic makeup (3). In addition, a large number of knockout and transgenic mice exist that allows for a detailed dissection of pathways and factors involved in ocular herpesvirus infections (10). C57BL/6 strains are most commonly used and are infected in one or both eyes by scarifying the cornea using a needle to induce physical disruption of the corneal epithelial cells to facilitate infection. These mice are then infected with HHV-1 at titers ranging between 10^3 and $2x10^6$ plaque forming units (PFU) per eye. The HHV-1 McKrae strain is most commonly used for animal infections, in part due to the ability of this virus strain to establish higher genome numbers per neuron (88). In addition, the RE and 17Syn+ HHV-1 strains are also frequently used, both of which establish high numbers of genomes per neuron when

compared to other virus strains such as KOS (89–93). However, these virus and mouse-strain dependent responses may also allow for the elucidation of the virus and host factors involved in the development of recurrent ocular herpesvirus-associated keratitis.

Despite the many strengths of using mice, as described above, there are a few limitations. The small size of the cornea makes it difficult to assess corneal lesions and there is a corresponding limited amount of tear film volume making the assessment of viral shedding more challenging. Furthermore, the small size of harvested tissue can potentially limit subsequent analysis. The major limitation of the mouse model, however, is that it is not the ideal model for studying viral reactivation. Indeed, there is controversy as to whether spontaneous reactivation in immunocompetent mice actually occurs. Therefore, reactivation is typically induced by either raising the body temperature of the animal to high levels of 42°C or by directly exposing the cornea to UV light, among other methods (10, 94–96). Even with these methods, only low levels of induced reactivation are observed in mice, albeit with a higher efficiency in the BALB/c compared to C57BL/6 mice (3, 10).

2.5.2. Rabbits

Rabbits are also used to study HHV-1 ocular infection, and they address some of the limitations of the mouse model. Their larger corneal surface can be imaged more easily and quantified by slit-lamp examination. There is also a higher amount of corneal tissue and tear film available for downstream analyses. New Zealand white rabbits are almost exclusively used as their non-pigmented eyes allow for easier examination, though Dutch Belted rabbits are also used due to their smaller size and subsequently cheaper housing and treatment costs.

Less variation in experimental design is also reported in studies using the rabbit model compared to the mouse model. The McKrae strain is typically used to infect the non-scarified eye at a concentration of $2x10^5$ PFU/eye, due to this strain's high reactivation frequency (97–99). However, other strains of HHV-1 (Rodanus, RE, F, KOS, 17Syn+, and E-43) can also spontaneous reactivate and are, therefore, occasionally used (10, 100).

Despite the strength of the rabbit model regarding this spontaneous reactivation, it does have a number of limitations that contribute to its reduced use compared to the mouse model. Inbred rabbit strains are expensive and can be difficult to obtain. Also, fewer transgenic strains exist compared to mice, although some have been used to study ocular herpesvirus infection, such as the humanized HLA-A*0201 transgenic rabbit, which has been used to evaluate the efficacy of a CD8+ T cell epitope-based prophylactic vaccine against ocular HHV-1 infection (101).

2.5.3. Dogs

Ocular CHV-1 infection in dogs is a good representation of ocular infections in humans due to similar pathogenesis and clinical presentation of the disease (2, 102). Whereas prior work focused on the fatal hemorrhagic form of CHV-1 by infecting newborn puppies, Wright and Cornwell described in 1969 the experimental infections of six-week old puppies with 10^5 $TCID_{50}$ of a CHV-1 field strain via different routes, including the intraconjunctival route. They found that one out of the five puppies infected via this route developed ocular discharge from the infected eye at day 3 post infection (pi), shed virus, and showed infiltration of lymphocytes and macrophages into the infected conjunctiva, as well as necrosis of the

epithelial cells (103). Decades later, Ledbetter et al. developed and optimized a CHV-1 reactivation model using a single colony of experimentally infected dogs (104) and a schematic timeline for these studies is shown in Fig. 2.3. Briefly, the right eyes of 18-month old SPF beagles were infected with $2x10^5$ $TCID_{50}$ of CHV-1-Duk, a CHV-1 field strain isolated from a dog presenting with dendritic ulcerative keratitis, either without scarification or using the microtrephination technique, a mild form of scarification (Fig 2.3, blue color). This resulted in all 8 CHV-1-infected dogs shedding CHV-1, with viral loads peaking at 5 days pi and then steadily declining until no virus could be recovered from ocular swabs by 15 days pi. Clinical scores peaked at approximately 7-10 days pi, after which they gradually declined until clinical signs were no longer present, around day 30 pi (104). No spontaneous reactivation was observed in these dogs until the end of the study, which was 8 months pi (or day 224 pi). A mild to moderate conjunctivitis, characterized by intermittent blepharospasm, conjunctival hyperemia, chemosis, and mucoid to mucopurulent ocular discharge, was typically observed in these experimentally infected dogs during primary infection (Fig. 2.4A). The development of corneal ulcerations, however, was not as frequent in experimentally infected dogs when compared to natural CHV-1 infections, where this is a common clinical sign (Fig. 2.4A).

Following the 8-month recovery period, reactivation was induced in six dogs from the aforementioned primary infection study (Fig. 2.3, green color), confirmed to be clinically healthy and not shedding virus, with 3.0 mg/kg of the immunosuppressant prednisolone given orally every day for 7 days. Peak viral shedding was observed at 10 days post reactivation

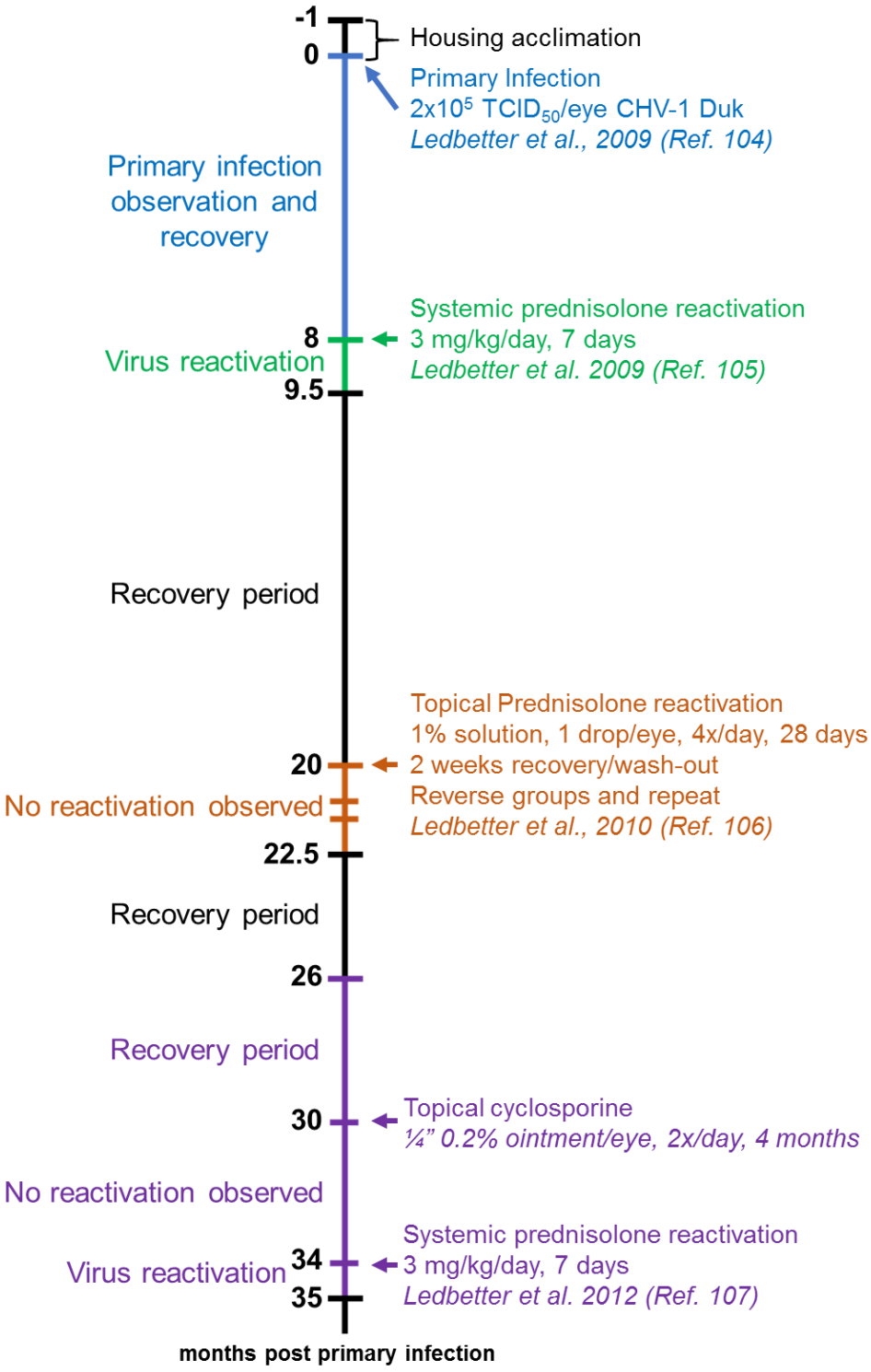

Figure 2.3: Timeline of the development and validation of the recurrent experimental ocular CHV-1 infection model in dogs. Dogs were initially infected with $2x10^5$ TCID50/eye CHV-1 Duk strain. Virus reactivation was then attempted using different methods in the same colonies of dogs at various times post infection. Different infection or reactivation studies are indicated with different colors.

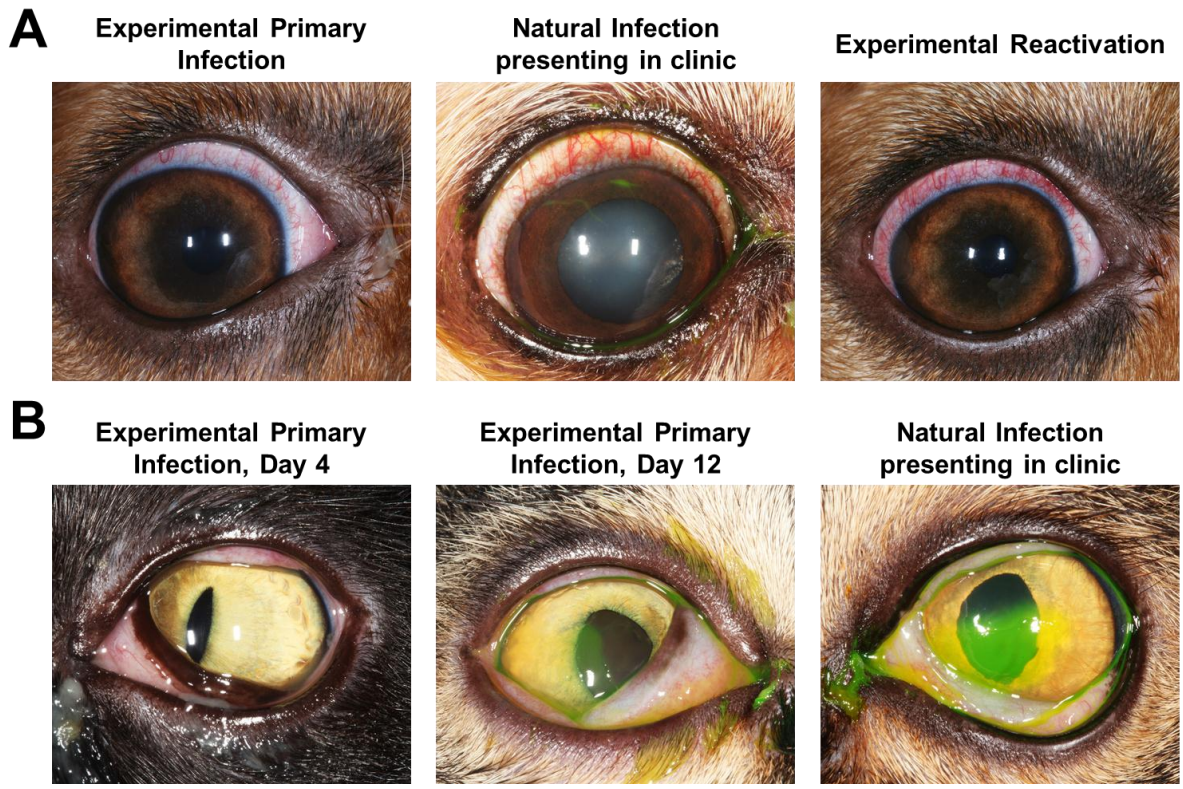

Figure 2.4: Clinical presentation of experimental and clinical infection of ocular herpesviruses in dogs and cats. (A) Representative CHV-1-associated ocular disease in dogs at day 10 post primary experimental infection, natural infection presenting to the clinic, or at day 7 post reactivation with systemic prednisolone. Experimentally infected dog eyes were stained with lissamine green, although no retention in either dog was observed. Naturally infected dog eyes were stained with fluorescein dye to visualize corneal ulcers **(B)** Representative FHV-1-associated ocular disease in cats following primary experimental infection at day 4 post infection, with conjunctivitis only, and at day 12 post infection, with both corneal ulceration and conjunctivitis, or natural infection presenting to the clinic with both corneal ulceration and conjunctivitis. Cat eyes were stained with fluorescein dye to visualize corneal ulcers.

and 5 out of the 6 dogs developed bilateral conjunctivitis or ulcerative keratitis (only 1 dog developed corneal ulcers) between 3 and 18 days post reactivation (105). This observed clinical disease presentation was similar to the primary experimental infection (Fig. 2.4A).

Following a second 10-month recovery period, these animals were used to evaluate the ability of topical prednisolone to induce reactivation when delivered as a 1% ophthalmic solution with 1 drop per eye four times per day for 28 days (Fig. 2.3, orange color). Following a 2-week steroid wash-out period, the groups were reversed and the treatments were repeated. This treatment, however, did not result in virus shedding and clinical disease beyond some mild conjunctivitis in some dogs that was not believed to be virus-related (106). Six months later, or 26 months following primary infection, the same animals were given a topical treatment with the immunosuppressant cyclosporine (1/4 inch strip of 0.2% ointment, twice daily in both eyes) and, likewise, no reactivation was observed (107) (Fig. 2.3, purple color). It should be noted, however, that reactivation could be induced again in these animals when subjected to systemic prednisolone treatment at 33-36 weeks following cyclosporine treatment (107) (Fig. 2.3, purple color). An additional study in a separate colony of dogs indicated that the immunosuppressant cyclophosphamide (200 mg/m^2 intravenous) could not induce reactivation, however, systemic prednisolone was again used to successfully induce reactivation in these animals at 6 months post cyclophosphamide treatment (108). These results indicate that colonies of latently infected dogs can be maintained and used for both primary infection as well as repeated reactivation studies. Finally, an additional study demonstrated that strontium-90 beta radiotherapy (36.7 cGy/s),which is frequently used as an adjuvant treatment for a variety of ocular surface, adnexal neoplasms, and inflammatory conditions in dogs, was not capable of inducing reactivation, (109), indicating that this therapy is associated with a low risk of recurrent ocular herpes disease.

The systemic prednisolone reactivation model was also used to evaluate the abilities of topical cidofovir, trifluridine, and ganciclovir to either control or prevent CHV-1-associated ocular disease, as well as to evaluate the efficacy of a subunit vaccine (24, 26, 110, 111). The experimental design of these studies was similar and consisted of a minimum 12-week acclimation period following acquisition of the dogs, infecting the dogs as described above, a 12-month recovery period to allow for the establishment of latent infection, and then reactivation using oral prednisolone for 7 days beginning on study day 1. All dogs reactivated successfully using systemic prednisolone therapy, with virus shedding peaking around day 9 post reactivation and clinical scores peaking on days 7-10 post reactivation. Topical antiviral therapy was initiated at various days for different lengths of time. Cidofovir was found to be effective at reducing viral shedding, but was associated with increased conjunctival and corneal leukocyte infiltration as quantified with in vivo confocal microscopy and exacerbation of ocular disease as detected by clinical ophthalmic examination (24). In contrast, trifluridine was highly effective to control the course of clinical disease and reduce viral shedding (110). For the subunit vaccine study, dogs were vaccinated twice at 57 and 15 days prior to the administration of oral prednisolone to latently infected dogs. The vaccinations did not prevent the development of ocular disease or viral shedding. However, they did reduce the clinical ocular disease scores in the post-vaccinal period short-term and increased CHV-1 specific immunity long-term (111).

Collectively, the data from the experimental ocular CHV-1 dog model showed that (i) CHV-1 can be readily and reproducibly reactivated in CHV-1 latently infected animals using

systemic prednisolone with a high rate of reactivation, demonstrating the robustness of this model, and (ii) CHV-1 either does not reactivate spontaneously in immunocompetent adult dogs or reactivation occurs at a level below the detection limit of the assays utilized in these studies.

2.5.4. Cats

Ocular herpesvirus infections in cats is also proposed to be a good representation of ocular infections in humans due to similar pathogenesis and clinical presentation of the disease (5). Experimental ocular FHV-1 infection models in cats have been used primarily to study the efficacy of antiviral therapies. One of the first experimental *in vivo* studies used SPF cats that were infected with 10^5 PFU per eye of different FHV-1 strains, followed by scarification of the cornea. With this approach, conjunctival epithelial cell infection was apparent by day 4 pi and corneal epithelium infection by day 8 pi (112). Other experimental models applied between 1.5 and $3x10^6$ PFU per eye of various field strains to the non-scarified eye and this reliably resulted in peak viral titers at approximately 3 days pi and ocular clinical scores around day 7-8 pi, after which they declined over the following 14-21 days (39, 42, 113, 114). Experimental primary FHV-1 infection is characterized by the development of conjunctivitis, dendritic or geographic ulcerative keratitis, and blepharitis (Fig. 2.4B). Cats may also exhibit varying degrees of blepharospasm, conjunctival hyperemia, chemosis, and ocular discharge, which may appear serious or mucopurulent. Typically, no major differences in the clinical signs of experimentally versus naturally infected cats are observed (Fig. 2.4B)

In contrast to HHV-1 infection studies in mice and rabbits, the FHV-1 strain used to inoculate cats is not of critical importance. Evidence for that was first provided by the study of Nasisse et al., where they observed no difference in the presentation and course of the disease following infection with five different strains of FHV-1, including 4 field strains (112). Moreover, and in general, FHV-1 is accepted to have little strain variation based on the observations that all strains belong to one serotype antigenically and isolates are relatively homogeneous by restriction enzyme digestion (4, 115). Finally, it was recently shown that the genomes of 24 clinical strains of FHV-1, collected over a period of 40 years, showed remarkably low levels of diversity and no potential genetic determinants of virulence could be identified (116).

In addition to the acute models of ocular FHV-1 infection, a preliminary latency-reactivation model has also been described (117). For this, 14 SPF cats were infected with $7x10^4$ PFU of an unspecified plaque-purified field strain of FHV-1. All cats showed clinical signs consistent with primary FHV-1 infection, recovered without treatment, and no indication of disease was observed in the 5-month follow-up period. Reactivation of FHV-1 was induced at 5.5 months pi, using a single dose of methylprednisolone acetate (5 mg/kg) intramuscularly, and 3 out of 14 cats (21%) developed bilateral conjunctivitis. However, the authors noted that 12 out of 14 cats (86%) had FHV-1 detectable in ocular swabs by PCR just prior to corticosteroid administration. Since they had recently rehoused the cats from group housing to individual cages in order to conduct the reactivation study, it was hypothesized that this event induced the high rate of virus shedding. While no clinical disease was noted

prior to methylprednisolone injection, viral shedding before rehousing was not determined. Therefore, while corticosteroid injection did appear to induce clinical disease in a small percentage of cats, it is not clear whether the reactivation was due to the treatment or the rehousing event. Additionally, it is possible that viral shedding was not controlled after primary infection, although the cats recovered from clinical disease during the 5-month recovery period. Still, this study illustrates that reactivation can potentially be induced in cats using immunosuppression similar to what has been demonstrated for the dog model, although additional studies are needed to further validate this reactivation model.

2.5.5. Limitations of non-traditional in vivo models

Despite the unique and important strength of fully recapitulating the pathogenesis of ocular herpesvirus infections in a natural host setting, the use of cats and dogs as comparative models for HHV-1 infection has certain limitations. Cats and dogs are much more expensive to buy and maintain compared to mice and rabbits, and specific housing is required. Additionally, there are important ethical and public-perception considerations associated with the use of companion animals as experimental animal models (118, 119). Moreover, no transgenic cats and dogs exist yet that could be useful for ocular herpesvirus infection studies, although transgenic red fluorescent protein-expressing cats and dogs have been described (120, 121). The development of transgenic cats and dogs to assist in the study or treatment of various diseases requires successful *in vitro* fertilization approaches, which have been described in cats since the early 1990s and in dogs only recently (122, 123).

Also, and in contrast to rodent models, molecular tools to study the hosts' immune reactions in response to FHV-1 and CHV-1 infections are largely lacking, although several groups are actively working on expanding this tool kit for virology and other studies. For example, a TaqMan-based qPCR assay targeting 12 genes has been described to study the innate immune response of feline embryonic fibroblasts to infection with feline leukemia virus in culture (124), and our group has utilized a canine microarray to evaluate the local immune response in response to ocular CHV-1 infection in the air-liquid canine corneal organ culture model (8). Furthermore, as both the dog and cat genomes have been sequenced and at least partially annotated, transcriptome profiling is possible. RNA sequencing has been used to assess the transcriptome profiles of canine-derived tumors (125, 126) and to study the immunological response of canine dermal fibroblasts to burdock extract treatment (127), among other studies. However, to our knowledge, no study has used RNA sequencing of virus-infected canine cells. In contrast, RNA sequencing has been used to profile virus infection of feline cells. For example, it has been used to assess the transcriptome profile of feline immunodeficiency virus (FIV) infected feline T-lymphocytes (128), and we recently performed RNA sequencing of FHV-1-infected FCECs (129). In addition, many antibody companies are expanding their repertoires beyond mouse and human, and new antibodies that are either specific for or cross-react with canine and feline immune cell epitopes are being developed. Furthermore, and a possible way to circumvent the lack of antibodies against immune cells is to use in vivo confocal microscopic examination, which is routinely used in ophthalmology clinics to assess leukocyte infiltrations in real time in the cornea and

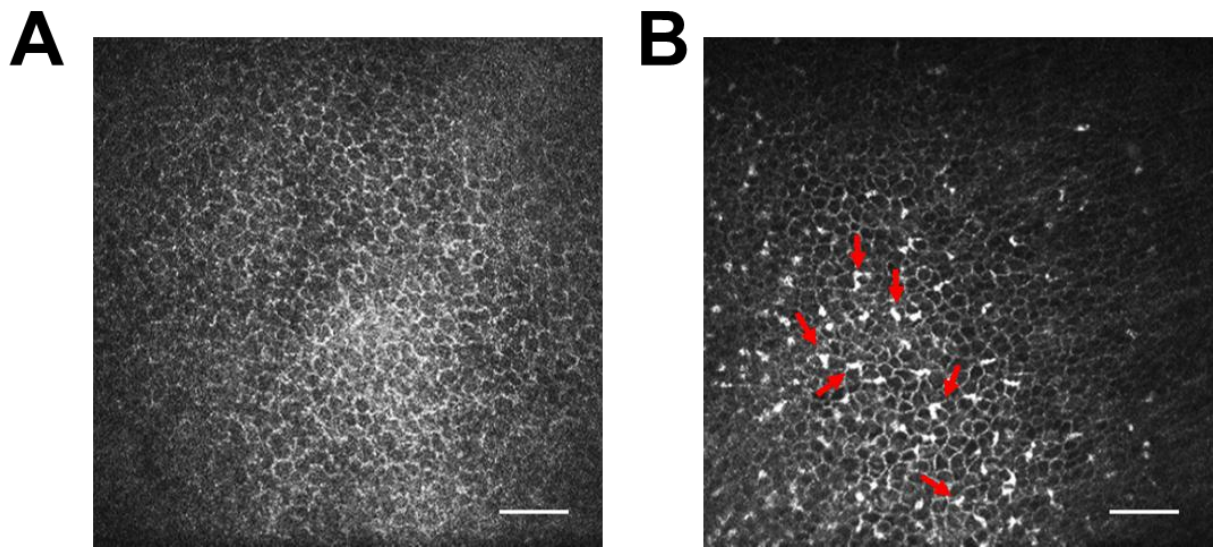

Figure 2.5: *In vivo* confocal microscopy of canine corneas. Representative confocal photomicrographs of the cornea of an uninfected dog **(A)** and following ocular CHV-1 infection at day 10 post infection **(B).** Note the corneal infiltration with leukocytes following virus infection, which appear as highly reflective, irregularly shaped white cells within the corneal epithelium (see arrows) *In vivo* confocal microscopy of cats yields similar photomicrographs. Scale bar, 50 µm.

conjunctiva of dogs (Fig 2.5) and cats. For example, *in vivo* confocal microscopy was used to demonstrate that topical cidofovir treatment induced increased leukocyte infiltration into the cornea and conjunctiva of CHV-1-infected dogs, an undesired side effect that contributed to the ocular toxicity of this drug (24). *In vivo* confocal microscopy has been used to define the structure of the normal cat cornea (130, 131), and was recently used by our group to assess leukocyte infiltrates in cats with experimental ocular FHV-1 infection (132).

2.6. Conclusion and Future Prospects

Various models to study ocular herpesviruses exist, ranging from 2D *in vitro* cell culture over 3D *ex vivo* organ cultures to *in vivo* experimental eye infection models. While mice and

rabbits have been used traditionally for *in vivo* studies using HHV-1, recent work with CHV-1 and FHV-1 in dogs and cats, respectively, has shown the robustness and reproducibility of these virus-natural host models to study ocular herpesvirus infections and disease. Many studies have shown that a successful translation of research from *in vitro* cell culture to *in vivo* experiments, and from mouse or rabbit work to human applications, is not always guaranteed. Therefore, the choice of an appropriate model system is of the utmost importance. An ideal model system should (i) be a natural host for the given virus (5, 133), (ii) recapitulate the tissues of relevant importance with the appropriate cytoarchitecture (134), (iii) recreate the characteristics of the disease, including relevant immune responses (67, 135), and (iv) be renewable or reusable (52). The importance of each criterion varies based on the experiment at hand. Despite the limitations in working with non-traditional animal models, either as explants or *in vivo*, we believe in their value to complement results obtained with the existing traditional models, especially with an expansion of the tools to study these species and their increasing acceptance in the research field. Indeed, dogs and cats, amongst other domesticated veterinary species, are naturally infected with various pathogens that are closely related to pathogens that infect humans, making these animals a translational valuable model for viral pathogenesis studies. Moreover, veterinary viruses are frequently used as surrogates of human viruses in the discovery and development of novel antiviral drugs and vaccines against human pathogens, and, as highlighted in this review, these types of studies are also applicable for ocular herpesviruses. Such studies may provide new insights into how different hosts respond to infection and/or which host factors are important for the

establishment and control of infection, ultimately leading to the benefit of both human and animal health.

Acknowledgments: We apologize to authors whose work was not cited due to space limitations. We would like to acknowledge the Cornell Feline Health Center for the continuous support of our studies.

2.7. References

1. Gould D. 2011. Feline Herpesvirus-1. Ocular manifestations, diagnosis and treatment options. J Feline Med Surg 13:333–346.
2. Ledbetter EC. 2013. Canine herpesvirus-1 ocular diseases of mature dogs. N Z Vet J 61:193–201.
3. Rowe AM, St Leger AJ, Jeon S, Dhaliwal DK, Knickelbein JE, Hendricks RL. 2013. Herpes keratitis. Prog Retin Eye Res 32:88–101.
4. Gaskell R, Dawson S, Radford A, Thiry E. 2007. Feline herpesvirus. Vet Res 38:337–54.
5. Maes R. 2012. Felid herpesvirus type 1 infection in cats: a natural host model for alphaherpesvirus pathogenesis. ISRN Vet Sci 2012:495830.
6. Zhu L, Zhu H. 2014. Ocular herpes: the pathophysiology, management and treatment of herpetic eye diseases. Virol Sin 29:327–342.
7. Kawakami K, Ogawa H, Maeda K, Imai A, Ohashi E, Matsunaga S, Tohya Y, Ohshima T, Mochizuki M. 2010. Nosocomial outbreak of serious canine infectious tracheobronchitis (kennel cough) caused by canine herpesvirus infection. J Clin Microbiol 48:1176–1181.
8. Harman RM, Bussche L, Ledbetter EC, Van de Walle GR. 2014. Establishment and characterization of an air-liquid canine corneal organ culture model to study acute herpes

keratitis. J Virol 88:13669–77.

9. Pennington MR, Van de Walle GR. 2017. Electric cell-substrate impedance sensing to monitor viral growth and study cellular responses to infection with alphaherpesviruses in real time. mSphere 2:e00039-17.
10. Webre JM, Hill JM, Nolan NM, Clement C, McFerrin HE, Bhattacharjee PS, Hsia V, Neumann DM, Foster TP, Lukiw WJ, Thompson HW. 2012. Rabbit and mouse models of HSV-1 latency, reactivation, and recurrent eye diseases. J Biomed Biotechnol 2012:612316.
11. Bean AGD, Baker ML, Stewart CR, Cowled C, Deffrasnes C, Wang L-F, Lowenthal JW. 2013. Studying immunity to zoonotic diseases in the natural host - keeping it real. Nat Rev Immunol 13:851–61.
12. Menne S, Cote PJ. 2007. The woodchuck as an animal model for pathogenesis and therapy of chronic hepatitis B virus infection. World J Gastroenterol 13:104–24.
13. Kulkarni K, Jacobson IM, Tennant BC. 2007. The role of the woodchuck model in the treatment of hepatitis B virus infection. Clin Liver Dis 11:707–725.
14. Domingo E, Parrish CR, Holland JJ. 2008. Origin and evolution of viruses. Elsevier Academic Press.
15. White DW, Suzanne Beard R, Barton ES. 2012. Immune modulation during latent herpesvirus infection. Immunol Rev 245:189–208.
16. Wertheim JO, Smith MD, Smith DM, Scheffler K, Kosakovsky Pond SL. 2014. Evolutionary origins of human herpes simplex viruses 1 and 2. Mol Biol Evol 31:2356–2364.
17. Field HJ, Huang M-L, Lay EM, Mickleburgh I, Zimmermann H, Birkmann A. 2013. Baseline sensitivity of HSV-1 and HSV-2 clinical isolates and defined acyclovir-resistant strains to the helicase–primase inhibitor pritelivir. Antiviral Res 100:297–299.
18. Piret J, Boivin G. 2014. Antiviral drug resistance in herpesviruses other than cytomegalovirus. Rev Med Virol 24:186–218.
19. Kongyingyoes B, Priengprom T, Pientong C, Aromdee C, Suebsasana S, Ekalaksananan

T. 2016. 3,19-isopropylideneandrographolide suppresses early gene expression of drug-resistant and wild type herpes simplex viruses. Antiviral Res 132:281–286.

20. Novoa B, Romero A, Álvarez ÁL, Moreira R, Pereiro P, Costa MM, Dios S, Estepa A, Parra F, Figueras A. 2016. Antiviral activity of myticin C peptide from mussel: an ancient defense against herpesviruses. J Virol 90:7692–7702.
21. Zhou B, Yang K, Wills E, Tang L, Baines JD. 2014. A mutation in the DNA polymerase accessory factor of herpes simplex virus 1 restores viral DNA replication in the presence of raltegravir. J Virol 88:11121–11129.
22. Maggs DJ, Clarke HE. 2004. In vitro efficacy of ganciclovir, cidofovir, penciclovir, foscarnet, idoxuridine, and acyclovir against feline herpesvirus type-1. Am J Vet Res 65:399–403.
23. van der Meulen K, Garré B, Croubels S, Nauwynck H. 2006. In vitro comparison of antiviral drugs against feline herpesvirus 1. BMC Vet Res 2:13.
24. Ledbetter EC, Spertus CB, Pennington MR, Van de Walle GR, Judd BE, Mohammed HO. 2015. In vitro and in vivo evaluation of cidofovir as a topical ophthalmic antiviral for ocular canine herpesvirus-1 infections in dogs. J Ocul Pharmacol Ther 31:642–649.
25. Pennington MR, Fort MW, Ledbetter EC, Van de Walle GR. 2016. A novel corneal explant model system to evaluate antiviral drugs against feline herpesvirus type 1 (FHV-1). J Gen Virol 97:1414–1425.
26. Ledbetter EC, Nicklin AM, Spertus CB, Pennington MR, Van de Walle GR, Mohammed HO. 2017. Evaluation of topical ophthalmic ganciclovir gel in the treatment of experimentally induced ocular canine herpesvirus-1 infection. Am J Vet Res.
27. Kim H-S, Jun Song X, de Paiva CS, Chen Z, Pflugfelder SC, Li D-Q. 2004. Phenotypic characterization of human corneal epithelial cells expanded ex vivo from limbal explant and single cell cultures. Exp Eye Res 79:41–49.
28. Sandmeyer LS, Keller CB, Bienzle D. 2005. Culture of feline corneal epithelial cells and infection with feline herpesvirus-1 as an investigative tool. Am J Vet Res 66:205–9.

29. Werner A, Braun M, Kietzmann M. 2008. Isolation and cultivation of canine corneal cells for in vitro studies on the anti-inflammatory effects of dexamethasone. Vet Ophthalmol 11:67–74.

30. Shah A, Farooq A, Tiwari V, Kim MJ, Shukla D. 2010. HSV-1 infection of human corneal epithelial cells: receptor-mediated entry and trends of re-infection. Mol Vis 16:2476–86.

31. García-Posadas L, Arranz-Valsero I, López-García A, Soriano-Romaní L, Diebold Y. 2013. A new human primary epithelial cell culture model to study conjunctival inflammation. Invest Ophthalmol Vis Sci 54:7143–52.

32. Robertson DM, Li L, Fisher S, Pearce VP, Shay JW, Wright WE, Cavanagh HD, Jester J V. 2005. Characterization of growth and differentiation in a telomerase-immortalized human corneal epithelial cell line. Investig Opthalmology Vis Sci 46:470.

33. Araki-Sasaki K, Ohashi Y, Sasabe T, Hayashi K, Watanabe H, Tano Y, Handa H. 1995. An SV40-immortalized human corneal epithelial cell line and its characterization. Invest Ophthalmol Vis Sci 36:614–21.

34. Rolinski J, Hus I. 2014. Immunological aspects of acute and recurrent herpes simplex keratitis. J Immunol Res 2014:513560.

35. Giménez F, Suryawanshi A, Rouse BT. 2013. Pathogenesis of herpes stromal keratitis--a focus on corneal neovascularization. Prog Retin Eye Res 33:1–9.

36. Astashkina A, Mann B, Grainger DW. 2012. A critical evaluation of in vitro cell culture models for high-throughput drug screening and toxicity. Pharmacol Ther 134:82–106.

37. Nasisse MP, Guy JS, Davidson MG, Sussman W, De Clercq E. 1989. In vitro susceptibility of feline herpesvirus-1 to vidarabine, idoxuridine, trifluridine, acyclovir, or bromovinyldeoxyuridine. Am J Vet Res 50:158–60.

38. Stiles J. 1995. Treatment of cats with ocular disease attributable to herpesvirus infection: 17 cases (1983-1993). J Am Vet Med Assoc 207:599–603.

39. Nasisse MP, Dorman DC, Jamison KC, Weigler BJ, Hawkins EC, Stevens JB. 1997. Effects of valacyclovir in cats infected with feline herpesvirus 1. Am J Vet Res 58:1141–

4.

40. Williams DL, Robinson JC, Lay E, Field H. 2005. Efficacy of topical aciclovir for the treatment of feline herpetic keratitis: results of a prospective clinical trial and data from in vitro investigations. Vet Rec 157:254–7.

41. Sandmeyer LS, Keller CB, Bienzle D. 2005. Effects of cidofovir on cell death and replication of feline herpesvirus-1 in cultured feline corneal epithelial cells. Am J Vet Res 66:217–22.

42. Fontenelle JP, Powell CC, Veir JK, Radecki S, Lappin MR. 2008. Effect of topical ophthalmic application of cidofovir on experimentally induced primary ocular feline herpesvirus-1 infection in cats. Am J Vet Res 69:289–293.

43. Thiry E, Addie D, Belák S, Boucraut-Baralon C, Egberink H, Frymus T, Gruffydd-Jones T, Hartmann K, Hosie MJ, Lloret A, Lutz H, Marsilio F, Pennisi MG, Radford AD, Truyen U, Horzinek MC. 2009. Feline herpesvirus infection ABCD guidelines on prevention and management. J Feline Med Surg 11:547–555.

44. Rajaiya J, Zhou X, Barequet I, Gilmore MS, Chodosh J. 2015. Novel model of innate immunity in corneal infection. Vitr Cell Dev Biol - Anim 51:827–834.

45. Ghezzi CE, Rnjak-Kovacina J, Kaplan DL. 2015. Corneal tissue engineering: recent advances and future perspectives. Tissue Eng Part B Rev 21:278–87.

46. Lai J-Y, Li Y-T, Cho C-H, Yu T-C. 2012. Nanoscale modification of porous gelatin scaffolds with chondroitin sulfate for corneal stromal tissue engineering. Int J Nanomedicine 7:1101.

47. Shafiq MA, Gemeinhart RA, Yue BYJT, Djalilian AR. 2012. Decellularized human cornea for reconstructing the corneal epithelium and anterior stroma. Tissue Eng Part C Methods 18:340–348.

48. Hashimoto Y, Funamoto S, Sasaki S, Honda T, Hattori S, Nam K, Kimura T, Mochizuki M, Fujisato T, Kobayashi H, Kishida A. 2010. Preparation and characterization of decellularized cornea using high-hydrostatic pressurization for corneal tissue engineering. Biomaterials 31:3941–3948.

49. Bayyoud T, Thaler S, Hofmann J, Maurus C, Spitzer MS, Bartz-Schmidt K-U, Szurman P, Yoeruek E. 2012. Decellularized bovine corneal posterior lamellae as carrier matrix for cultivated human corneal endothelial cells. Curr Eye Res 37:179–186.

50. Kong B, Sun W, Chen G, Tang S, Li M, Shao Z, Mi S. 2017. Tissue-engineered cornea constructed with compressed collagen and laser-perforated electrospun mat. Sci Rep 7:970.

51. Resau JH, Sakamoto K, Cottrell JR, Hudson EA, Meltzer SJ. 1991. Explant organ culture: A review. Cytotechnology 7:137–149.

52. Russell WM., Burch RL. 1959. The principles of humane experimental technique. Methuen, London.

53. Armitage WJ. 2011. Preservation of human cornea. Transfus Med Hemother 38:143–147.

54. Richard NR, Anderson JA, Weiss JL, Binder PS. 1991. Air/liquid corneal organ culture: a light microscopic study. Curr Eye Res 10:739–749.

55. Collin HB, Anderson JA, Richard NR, Binder PS. 1995. *In vitro* model for corneal wound healing; organ-cultured human corneas. Curr Eye Res 14:331–339.

56. Alekseev O, Tran AH, Azizkhan-Clifford J. 2012. Ex vivo organotypic corneal model of acute epithelial herpes simplex virus type I infection. J Vis Exp e3631.

57. Alekseev O, Limonnik V, Donovan K, Azizkhan-Clifford J. 2015. Activation of checkpoint kinase 2 is critical for herpes simplex virus type 1 replication in corneal epithelium. Ophthalmic Res 53:55–64.

58. Drevets P, Chucair-Elliott A, Shrestha P, Jinkins J, Karamichos D, Carr DJJ. 2015. The use of human cornea organotypic cultures to study herpes simplex virus type 1 (HSV-1)-induced inflammation. Graefe's Arch Clin Exp Ophthalmol 253:1721–8.

59. Thakkar N, Jaishankar D, Agelidis A, Yadavalli T, Mangano K, Patel S, Tekin SZ, Shukla D. 2017. Cultured corneas show dendritic spread and restrict herpes simplex virus infection that is not observed with cultured corneal cells. Sci Rep 7:42559.

60. Li Y, Van Cleemput J, Qiu Y, Reddy VRAP, Mateusen B, Nauwynck HJ. 2015. Ex vivo

modeling of feline herpesvirus replication in ocular and respiratory mucosae, the primary targets of infection. Virus Res 210:227–231.

61. Rasmussen SB, Jensen SB, Nielsen C, Quartin E, Kato H, Chen ZJ, Silverman RH, Akira S, Paludan SR. 2009. Herpes simplex virus infection is sensed by both Toll-like receptors and retinoic acid-inducible gene- like receptors, which synergize to induce type I interferon production. J Gen Virol 90:74–8.

62. Thompson MR, Kaminski JJ, Kurt-Jones EA, Fitzgerald KA. 2011. Pattern recognition receptors and the innate immune response to viral infection. Viruses 3:920–40.

63. Hamrah P, Huq SO, Liu Y, Zhang Q, Dana MR. 2003. Corneal immunity is mediated by heterogeneous population of antigen-presenting cells. J Leukoc Biol 74:172–178.

64. Carvalho ARR, Naranjo C, Leiva M, Fondevila D, Iborra A, Martinez P, Peña T. 2009. Canine normal corneal epithelium bears a large population of CD45-positive cells. Vet J 179:437–442.

65. Morgan RV, Abrams KL, Kern TJ. 1996. Feline eosinophilic keratitis: a retrospective study of 54 cases: (1989-1994). Vet Comp Ophthalmol.

66. Novak N, Peng WM. 2005. Dancing with the enemy: the interplay of herpes simplex virus with dendritic cells. Clin Exp Immunol 142:405–10.

67. Kaye S, Choudhary A. 2006. Herpes simplex keratitis. Prog Retin Eye Res 25:355–380.

68. Röck T, Hofmann J, Thaler S, Bramkamp M, Bartz-Schmidt KU, Yoeruek E, Röck D. 2016. Factors that influence the suitability of human organ-cultured corneas. Graefe's Arch Clin Exp Ophthalmol 254:135–41.

69. Hagenah M, Böhnke M, Engelmann K, Winter R. 1995. Incidence of bacterial and fungal contamination of donor corneas preserved by organ culture. Cornea 14:423–6.

70. Armitage WJ, Easty DL. 1997. Factors influencing the suitability of organ-cultured corneas for transplantation. Invest Ophthalmol Vis Sci 38:16–24.

71. Gain P, Thuret G, Chiquet C, Vautrin A-C, Carricajo A, Acquart S, Maugery J, Aubert G. 2001. Use of a pair of blood culture bottles for sterility testing of corneal organ culture media. Br J Ophthalmol 85:1158–1162.

72. Pels L. 1997. Organ culture: the method of choice for preservation of human donor corneas. Br J Ophthalmol 81:523–525.
73. Spelsberg H, Reinhard T, Sengler U, Daeubener W, Sundmacher R. 2002. Organ-cultured corneal grafts from septic donors: a retrospective study. Eye 16:622–627.
74. Borderie VM, Laroche L. 1998. Microbiologic study of organ-cultured donor corneas. Transplantation 66:120–3.
75. Röck D, Wude J, Bartz-Schmidt KU, Yoeruek E, Thaler S, Röck T. 2017. Factors influencing the contamination rate of human organ-cultured corneas. Acta Ophthalmol 95:e706–e712.
76. Gruenert AK, Rosenbaum K, Geerling G, Fuchsluger TA. 2017. The influence of donor factors on corneal organ culture contamination. Acta Ophthalmol 95:733–740.
77. Seiler TG, Tschopp M, Zimmerli S, Tappeiner C, Wittwer V V, Frueh BE. 2016. Time course of antibiotic and antifungal concentrations in corneal organ culture. Cornea 35:127–31.
78. Hill JM, Clement C. 2009. Herpes simplex virus type 1 DNA in human corneas: what are the virological and clinical implications? J Infect Dis 200:1–4.
79. Kaufman HE, Azcuy AM, Varnell ED, Sloop GD, Thompson HW, Hill JM. 2005. HSV-1 DNA in tears and saliva of normal adults. Invest Ophthalmol Vis Sci 46:241–7.
80. Farooq A, Shukla D. 2011. Corneal latency and transmission of herpes simplex virus-1. Future Virol 6:101–108.
81. Cleator GM, Klapper PE, Dennett C, Sullivan AL, Bonshek RE, Marcyniuk B, Tullo AB. 1994. Corneal donor infection by herpes simplex virus: herpes simplex virus DNA in donor corneas. Cornea 13:294–304.
82. Openshaw H, McNeill JI, Lin XH, Niland J, Cantin EM. 1995. Herpes simplex virus DNA in normal corneas: persistence without viral shedding from ganglia. J Med Virol 46:75–80.
83. Garweg JG, Boehnke M. 1997. Low rate shedding of HSV-1 DNA, but not of infectious virus from human donor corneae into culture media. J Med Virol 52:320–5.

84. van Gelderen BE, Van der Lelij A, Treffers WF, van der Gaag R. 2000. Detection of herpes simplex virus type 1, 2 and varicella zoster virus DNA in recipient corneal buttons. Br J Ophthalmol 84:1238–43.

85. Broniek G, Langwińska-Wośko E, Sybilska M, Szaflik JP, Przybylski M, Wróblewska M. 2016. Occurrence of viral DNA in paired samples of corneal rim and cornea preservation fluid. J Med Virol.

86. Sengler U, Reinhard T, Adams O, Krempe C, Sundmacher R. 2001. Herpes simplex virus infection in the media of donor corneas during organ culture: frequency and consequences. Eye (Lond) 15:644–7.

87. Stiles J, Pogranichniy R. 2008. Detection of virulent feline herpesvirus-1 in the corneas of clinically normal cats. J Feline Med Surg 10:154–9.

88. Sawtell NM, Poon DK, Tansky CS, Thompson RL. 1998. The latent herpes simplex virus type 1 genome copy number in individual neurons is virus strain specific and correlates with reactivation. J Virol 72:5343–50.

89. Mulik S, Xu J, Reddy PBJ, Rajasagi NK, Gimenez F, Sharma S, Lu PY, Rouse BT. 2012. Role of miR-132 in angiogenesis after ocular infection with herpes simplex virus. Am J Pathol 181:525–534.

90. Matundan H, Mott KR, Ghiasi H. 2014. Role of CD8+ T cells and lymphoid dendritic cells in protection from ocular herpes simplex virus 1 challenge in immunized mice. J Virol 88:8016–27.

91. Chucair-Elliott AJ, Zheng M, Carr DJJ. 2015. Degeneration and regeneration of corneal nerves in response to HSV-1 infection. Invest Ophthalmol Vis Sci 56:1097–107.

92. Jiang Y, Yin X, Stuart PM, Leib DA. 2015. Dendritic cell autophagy contributes to herpes simplex virus-driven stromal keratitis and immunopathology. MBio 6:e01426-15.

93. Royer DJ, Zheng M, Conrady CD, Carr DJJ. 2015. Granulocytes in ocular HSV-1 infection: opposing roles of mast cells and neutrophils. Invest Ophthalmol Vis Sci 56:3763–75.

94. Feldman LT, Ellison AR, Voytek CC, Yang L, Krause P, Margolis TP. 2002. Spontaneous molecular reactivation of herpes simplex virus type 1 latency in mice. Proc Natl Acad Sci U S A 99:978–83.

95. Gebhardt BM, Halford WP. 2005. Evidence that spontaneous reactivation of herpes virus does not occur in mice. Virol J 2:67.

96. Margolis TP, Elfman FL, Leib D, Pakpour N, Apakupakul K, Imai Y, Voytek C. 2007. Spontaneous reactivation of herpes simplex virus type 1 in latently infected murine sensory ganglia. J Virol 81:11069–74.

97. Jester J, Morishige N, BenMohamed L, Brown DJ, Osorio N, Hsiang C, Perng GC, Jones C, Wechsler SL. 2016. Confocal microscopic analysis of a rabbit eye model of high-incidence recurrent herpes stromal keratitis. Cornea 35:81–8.

98. He J, Cosby R, Hill JM, Bazan HEP. 2016. Changes in corneal innervation after HSV-1 latency established with different reactivation phenotypes. Curr Eye Res 1–6.

99. Srivastava R, Dervillez X, Khan AA, Chentoufi AA, Chilukuri S, Shukr N, Fazli Y, Ong NN, Afifi RE, Osorio N, Geertsema R, Nesburn AB, Wechsler SL, BenMohamed L. 2016. The herpes simplex virus latency-associated transcript gene is associated with a broader repertoire of virus-specific exhausted CD8+ T cells retained within the trigeminal ganglia of latently infected HLA transgenic Rabbits. J Virol 90:3913–28.

100. Kollias CM, Huneke RB, Wigdahl B, Jennings SR. 2015. Animal models of herpes simplex virus immunity and pathogenesis. J Neurovirol 21:8–23.

101. Chentoufi AA, Dasgupta G, Christensen ND, Hu J, Choudhury ZS, Azeem A, Jester J V, Nesburn AB, Wechsler SL, BenMohamed L. 2010. A novel HLA (HLA-A*0201) transgenic rabbit model for preclinical evaluation of human CD8+ T cell epitope-based vaccines against ocular herpes. J Immunol 184:2561–71.

102. Evermann JF, Ledbetter EC, Maes RK. 2011. Canine reproductive, respiratory, and ocular diseases due to canine herpesvirus. Vet Clin North Am Small Anim Pract 41:1097–1120.

103. Wright NG, Cornwell HJC. 1969. The susceptibility of six-week old puppies to canine

herpes virus. J Small Anim Pract 10:669–674.

104. Ledbetter EC, Dubovi EJ, Kim SG, Maggs DJ, Bicalho RC. 2009. Experimental primary ocular canine herpesvirus-1 infection in adult dogs. Am J Vet Res 70:513–21.

105. Ledbetter EC, Kim SG, Dubovi EJ, Bicalho RC. 2009. Experimental reactivation of latent canine herpesvirus-1 and induction of recurrent ocular disease in adult dogs. Vet Microbiol 138:98–105.

106. Ledbetter EC, Kice NC, Matusow RB, Dubovi EJ, Kim SG. 2010. The effect of topical ocular corticosteroid administration in dogs with experimentally induced latent canine herpesvirus-1 infection. Exp Eye Res 90:711–7.

107. Ledbetter EC, da Silva EC, Kim SG, Dubovi EJ, Schwark WS. 2012. Frequency of spontaneous canine herpesvirus-1 reactivation and ocular viral shedding in latently infected dogs and canine herpesvirus-1 reactivation and ocular viral shedding induced by topical administration of cyclosporine and systemic administration of corticosteroids. Am J Vet Res 73:1079–1084.

108. Mundy P, da Silva EC, Ledbetter EC. 2012. Effects of cyclophosphamide myelosuppression in adult dogs with latent canine herpesvirus-1 infection. Vet Microbiol 159:230–235.

109. Nicklin AM, McEntee MC, Ledbetter EC. 2014. Effects of ocular surface strontium-90 beta radiotherapy in dogs latently infected with canine herpesvirus-1. Vet Microbiol 174:433–7.

110. Spertus CB, Mohammed HO, Ledbetter EC. 2016. Effects of topical ocular application of 1% trifluridine ophthalmic solution in dogs with experimentally induced recurrent ocular canine herpesvirus-1 infection. Am J Vet Res 77:1140–1147.

111. Ledbetter EC, Kim K, Dubovi EJ, Mohammed HO, Felippe MJB. 2016. Clinical and immunological assessment of therapeutic immunization with a subunit vaccine for recurrent ocular canine herpesvirus-1 infection in dogs. Vet Microbiol 197:102–110.

112. Nasisse MP, Guy JS, Davidson MG, Sussman WA, Fairley NM. 1989. Experimental ocular herpesvirus infection in the cat. Sites of virus replication, clinical features and

effects of corticosteroid administration. Invest Ophthalmol Vis Sci 30:1758–1768.

113. Haid C, Kaps S, Gönczi E, Hässig M, Metzler A, Spiess BM, Richter M. 2007. Pretreatment with feline interferon omega and the course of subsequent infection with feline herpesvirus in cats. Vet Ophthalmol 10:278–284.

114. Thomasy SM, Lim CC, Reilly CM, Kass PH, Lappin MR, Maggs DJ. 2011. Evaluation of orally administered famciclovir in cats experimentally infected with feline herpesvirus type-1. Am J Vet Res 72:85–95.

115. Hamano M, Maeda K, Mizukoshi F, Une Y, Mochizuki M, Tohya Y, Akashi H, Kai K. 2003. Experimental infection of recent field isolates of feline herpesvirus type 1. J Vet Med Sci 65:939–43.

116. Vaz PK, Job N, Horsington J, Ficorilli N, Studdert MJ, Hartley CA, Gilkerson JR, Browning GF, Devlin JM. 2016. Low genetic diversity among historical and contemporary clinical isolates of felid herpesvirus 1. BMC Genomics 17:704.

117. Maggs DJ, Nasisse MP, Kass PH. 2003. Efficacy of oral supplementation with L-lysine in cats latently infected with feline herpesvirus. Am J Vet Res 64:37–42.

118. Driscoll JW. 1995. Attitudes toward animals: species ratings. Soc Anim 3:139–150.

119. Baumans V. 2004. Use of animals in experimental research: an ethical dilemma? Gene Ther 11:S64–S66.

120. Yin XJ, Lee HS, Yu XF, Choi E, Koo BC, Kwon MS, Lee YS, Cho SJ, Jin GZ, Kim LH, Shin HD, Kim T, Kim NH, Kong IK. 2008. Generation of cloned transgenic cats expressing red fluorescence protein. Biol Reprod 78:425–31.

121. Hong SG, Kim MK, Jang G, Oh HJ, Park JE, Kang JT, Koo OJ, Kim T, Kwon MS, Koo BC, Ra JC, Kim DY, Ko C, Lee BC. 2009. Generation of red fluorescent protein transgenic dogs. Genesis 47:314–22.

122. Pope CE, Keller GL, Dresser BL. 1993. In vitro fertilization in domestic and non-domestic cats including sequences of early nuclear events, development in vitro, cryopreservation and successful intra- and interspecies embryo transfer. J Reprod Fertil Suppl 47:189–201.

123. Nagashima JB, Sylvester SR, Nelson JL, Cheong SH, Mukai C, Lambo C, Flanders JA, Meyers-Wallen VN, Songsasen N, Travis AJ. 2015. Live Births from domestic dog (Canis familiaris) embryos produced by in vitro fertilization. PLoS One 10:e0143930.

124. Robert-Tissot C, Rüegger VL, Cattori V, Meli ML, Riond B, Gomes-Keller MA, Vögtlin A, Wittig B, Juhls C, Hofmann-Lehmann R, Lutz H. 2011. The innate antiviral immune system of the cat: molecular tools for the measurement of its state of activation. Vet Immunol Immunopathol 143:269–81.

125. Decker B, Parker HG, Dhawan D, Kwon EM, Karlins E, Davis BW, Ramos-Vara JA, Bonney PL, McNiel EA, Knapp DW, Ostrander EA. 2015. Homologous mutation to human BRAF V600E is common in naturally occurring canine bladder cancer--evidence for a relevant model system and urine-based diagnostic test. Mol Cancer Res 13:993–1002.

126. Brachelente C, Cappelli K, Capomaccio S, Porcellato I, Silvestri S, Bongiovanni L, De Maria R, Verini Supplizi A, Mechelli L, Sforna M. 2017. Transcriptome analysis of canine cutaneous melanoma and melanocytoma reveals a modulation of genes regulating extracellular matrix metabolism and cell cycle. Sci Rep 7:6386.

127. Pomari E, Stefanon B, Colitti M. 2013. Effect of Arctium lappa (burdock) extract on canine dermal fibroblasts. Vet Immunol Immunopathol 156:159–166.

128. Ertl R, Klein D. 2014. Transcriptional profiling of the host cell response to feline immunodeficiency virus infection. Virol J 11:52.

129. Pennington MR, Grenier JK, Van de Walle GR. 2018. Transcriptome profiling of alphaherpesvirus-infected cells treated with the HIV-integrase inhibitor raltegravir reveals profound and specific alterations in host transcription. J Gen Virol. In Press.

130. Kafarnik C, Fritsche J, Reese S. 2007. In vivo confocal microscopy in the normal corneas of cats, dogs and birds. Vet Ophthalmol 10:222–230.

131. Kafarnik C, Fritsche J, Reese S. 2008. Corneal innervation in mesocephalic and brachycephalic dogs and cats: assessment using in vivo confocal microscopy. Vet Ophthalmol 11:363–367.

132. Spertus CB, Pennington MR, Van de Walle GR, Badanes ZI, Judd BE, Mohammed HO, Ledbetter EC. 2018. Effects of oral raltegravir in cats with experimentally-induced ocular and respiratory feline herpesvirus-1 infection. Am J Vet Res. Under Review.
133. Hughes DJ, Kipar A, Sample JT, Stewart JP. 2010. Pathogenesis of a model gammaherpesvirus in a natural host. J Virol 84:3949–3961.
134. McHugh KJ, Saint-Geniez M, Tao SL. 2013. Topographical control of ocular cell types for tissue engineering. J Biomed Mater Res B Appl Biomater 101:1571–84.
135. Taylor AW. 2016. Ocular immune privilege and transplantation. Front Immunol 7:37.
136. Labetoulle M, Auquier P, Conrad H, Crochard A, Daniloski M, Bouée S, El Hasnaoui A, Colin J. 2005. Incidence of herpes simplex virus keratitis in france. Ophthalmology 112:888–895.e1.
137. Xu F, Sternberg MR, Kottiri BJ, McQuillan GM, Lee FK, Nahmias AJ, Berman SM, Markowitz LE. 2006. Trends in herpes simplex virus type 1 and type 2 seroprevalence in the United States. JAMA 296:964.
138. Young RC, Hodge DO, Liesegang TJ, Baratz KH. 2010. Incidence, recurrence, and outcomes of herpes simplex virus eye disease in Olmsted County, Minnesota, 1976-2007: the effect of oral antiviral prophylaxis. Arch Ophthalmol (Chicago, Ill 1960) 128:1178–83.
139. Burcea M, Gheorghe A, Pop M. 2015. Incidence of herpes simplex virus keratitis in HIV/AIDS patients compared with the general population. J Med Life 8:62–3.
140. Looker KJ, Magaret AS, May MT, Turner KME, Vickerman P, Gottlieb SL, Newman LM. 2015. Global and regional estimates of prevalent and incident herpes simplex virus type 1 infections in 2012. PLoS One 10:e0140765.
141. Nöthling JO, Hüssy D, Steckler D, Ackermann M. 2008. Seroprevalence of canine herpesvirus in breeding kennels in the Gauteng Province of South Africa. Theriogenology 69:276–282.
142. Babaei H, Akhtardanesh B, Ghanbarpour R, Namjoo A. 2010. Serological evidence of canine herpesvirus-1 in dogs of Kerman city, south-east of Iran. Transbound Emerg Dis

57:348–51.

143. Ledbetter EC, Kim SG, Dubovi EJ. 2009. Outbreak of ocular disease associated with naturally-acquired canine herpesvirus-1 infection in a closed domestic dog colony. Vet Ophthalmol 12:242–247.

144. Krogenæs A, Rootwelt V, Larsen S, Sjøberg EK, Akselsen B, Skår TM, Myhre SS, Renström LHM, Klingeborn B, Lund A. 2012. A serologic study of canine herpes virus-1 infection in the Norwegian adult dog population. Theriogenology 78:153–158.

145. Krogenæs A, Rootwelt V, Larsen S, Renström L, Farstad W, Lund A. 2014. A serological study of canine herpesvirus-1 infection in a population of breeding bitches in Norway. Acta Vet Scand 56:19.

146. Larsen RW, Kiupel M, Balzer H-J, Agerholm JS. 2015. Prevalence of canid herpesvirus-1 infection in stillborn and dead neonatal puppies in Denmark. Acta Vet Scand 57:1.

147. Maggs DJ, Lappin MR, Nasisse MP. 1999. Detection of feline herpesvirus-specific antibodies and DNA in aqueous humor from cats with or without uveitis. Am J Vet Res 60:932–6.

148. Kang B-T, Park H-M. 2008. Prevalence of feline herpesvirus 1, feline calicivirus and Chlamydophila felis in clinically normal cats at a Korean animal shelter. J Vet Sci 9:207–9.

149. Henzel A, Brum MCS, Lautert C, Martins M, Lovato LT, Weiblen R. 2012. Isolation and identification of feline calicivirus and feline herpesvirus in Southern Brazil. Braz J Microbiol 43:560–8.

150. McManus CM, Levy JK, Andersen LA, McGorray SP, Leutenegger CM, Gray LK, Hilligas J, Tucker SJ. 2014. Prevalence of upper respiratory pathogens in four management models for unowned cats in the Southeast United States. Vet J 201:196–201.

151. Rypuła K, Płoneczka-Janeczko K, Bierowiec K, Kumala A, Sapikowski G. Prevalence of viral infections in cats in southwestern Poland in the years 2006 to 2010. Berliner und Münchener tierärztliche Wochenschrift 127:163–5.

152. Shaikh S, Ta CN. 2002. Evaluation and management of herpes zoster ophthalmicus. Am Fam Physician 66:1723–30.

153. Borkar DS, Tham VM, Esterberg E, Ray KJ, Vinoya AC, Parker J V, Uchida A, Acharya NR. 2013. Incidence of herpes zoster ophthalmicus: results from the Pacific Ocular Inflammation Study. Ophthalmology 120:451–6.

154. Johnson RW, Alvarez-Pasquin M-J, Bijl M, Franco E, Gaillat J, Clara JG, Labetoulle M, Michel J-P, Naldi L, Sanmarti LS, Weinke T. 2015. Herpes zoster epidemiology, management, and disease and economic burden in Europe: a multidisciplinary perspective. Ther Adv Vaccines 3:109–20.

155. Allen GP, Bolin DC, Bryant U, Carter CN, Giles RC, Harrison LR, Hong CB, Jackson CB, Poonacha K, Wharton R, Williams NM. 2008. Prevalence of latent, neuropathogenic equine herpesvirus-1 in the Thoroughbred broodmare population of central Kentucky. Equine Vet J 40:105–110.

156. Lunn DP, Davis-Poynter N, Flaminio MJBF, Horohov DW, Osterrieder K, Pusterla N, Townsend HGG. 2009. Equine herpesvirus-1 consensus statement. J Vet Intern Med 23:450–61.

157. Hussey GS, Goehring LS, Lunn DP, Hussey SB, Huang T, Osterrieder N, Powell C, Hand J, Holz C, Slater J. 2013. Experimental infection with equine herpesvirus type 1 (EHV-1) induces chorioretinal lesions. Vet Res 44:118.

158. Yildirim Y, Yilmaz V, Kirmizigul AH. 2015. Equine herpes virus type 1 (EHV-1) and 4 (EHV-4) infections in horses and donkeys in northeastern Turkey. Iran J Vet Res 16:341–4.

159. Collinson PN, O'Rielly JL, Ficorilli N, Studdert MJ. 1994. Isolation of equine herpesvirus type 2 (equine gammaherpesvirus 2) from foals with keratoconjunctivitis. J Am Vet Med Assoc 205:329–31.

160. Borchers K, Wolfinger U, Goltz M, Broll H, Ludwig H. 1997. Distribution and relevance of equine herpesvirus type 2 (EHV-2) infections. Arch Virol 142:917–928.

161. Borchers K, Frölich K, Ludwig H. 1999. Detection of equine herpesvirus types 2 and 5

(EHV-2 and EHV-5) in Przewalski's wild horses. Arch Virol 144:771–80.

162. Kershaw O, von Oppen T, Glitz F, Deegen E, Ludwig H, Borchers K. 2001. Detection of equine herpesvirus type 2 (EHV-2) in horses with keratoconjunctivitisVirus Research.

163. Craig MI, Barrandeguy ME, Fernández FM. 2005. Equine herpesvirus 2 (EHV-2) infection in thoroughbred horses in Argentina. BMC Vet Res 1:9.

164. Borchers K, Ebert M, Fetsch A, Hammond T, Sterner-Kock A. 2006. Prevalence of equine herpesvirus type 2 (EHV-2) DNA in ocular swabs and its cell tropism in equine conjunctivaVeterinary Microbiology.

165. Webber JJ, Selby LA. 1981. Risk factors related to the prevalence of infectious bovine keratoconjunctivitis. J Am Vet Med Assoc 179:823–6.

166. Nandi S, Kumar M, Manohar M, Chauhan RS. 2009. Bovine herpes virus infections in cattle. Anim Heal Res Rev 10:85–98.

167. Raaperi K, Orro T, Viltrop A. 2014. Epidemiology and control of bovine herpesvirus 1 infection in Europe. Vet J 201:249–256.

168. Bartha A, Juhász M, Liebermann H. 1966. Isolation of a bovine herpesvirus from calves with respiratory disease and keratoconjunctivitis. A preliminary report. Acta Vet Acad Sci Hung 16:357–8.

169. Graham DA, McNeill GJ, Calvert V, Mawhinney K, Curran W, Ball NW, Todd D. 2005. Virological and serological evidence of bovine herpesvirus type 4 in cattle in Northern Ireland. Vet Rec 157:539–43.

170. Aslan ME, Azkur AK, Gazyagci S. 2015. Epidemiology and genetic characterization of BVDV, BHV-1, BHV-4, BHV-5 and Brucella spp. infections in cattle in Turkey. J Vet Med Sci 77:1371–1377.

171. Cvetojević Đ, Savić B, Milićević V, Kureljušić B, Jezdimirović N, Jakić-Dimić D, Pavlović M, Spalević L. 2016. Prevalence of Bovine herpesvirus type 4 in aborting dairy cows. Pol J Vet Sci 19:731–736.

172. Seal BS, Heuschele WP, Klieforth RB. 1989. Prevalence of antibodies to alcelaphine

herpesvirus-1 and nucleic acid hybridization analysis of viruses isolated from captive exotic ruminants. Am J Vet Res 50:1447–53.

173. Russell GC, Stewart JP, Haig DM. 2009. Malignant catarrhal fever: a review. Vet J 179:324–35.

174. Bremer CW. 2010. The prevalence of ovine herpesvirus-2 in 4 sheep breeds from different regions in South Africa. J S Afr Vet Assoc 81:93–6.

175. O'Toole D, Li H. 2014. The pathology of malignant catarrhal fever, with an emphasis on ovine herpesvirus 2. Vet Pathol 51:437–52.

176. Thiry J, Keuser V, Muylkens B, Meurens F, Gogev S, Vanderplasschen A, Thiry E. 2006. Ruminant alphaherpesviruses related to bovine herpesvirus 1. Vet Res 37:169–190.

177. Tryland M, Das Neves CG, Sunde M, Mork T. 2009. Cervid herpesvirus 2, the primary agent in an outbreak of infectious keratoconjunctivitis in semidomesticated reindeer. J Clin Microbiol 47:3707–3713.

178. Evans AL, das Neves CG, Finstad GF, Beckmen KB, Skjerve E, Nymo IH, Tryland M. 2012. Evidence of alphaherpesvirus infections in Alaskan caribou and reindeer. BMC Vet Res 8:5.

179. Squires R, Wilson P, Whelan N, Johnstone A, Ayanegui-Alcérreca M, Castillo-Alcala F, Knight D. 2012. Alpha and gamma herpesvirus detection in two herds of farmed red deer (Cervus elaphus) in New Zealand. N Z Vet J 60:69–75.

180. Rola J, Larska M, Socha W, Rola JG, Materniak M, Urban-Chmiel R, Thiry E, Żmudziński JF. 2017. Seroprevalence of bovine herpesvirus 1 related alphaherpesvirus infections in free-living and captive cervids in Poland. Vet Microbiol 204:77–83.

181. Tryland M, Romano JS, Marcin N, Nymo IH, Josefsen TD, Sørensen KK, Mørk T. 2017. Cervid herpesvirus 2 and not Moraxella bovoculi caused keratoconjunctivitis in experimentally inoculated semi-domesticated Eurasian tundra reindeer. Acta Vet Scand 59:23.

182. Wright EP, Waugh LF, Goldstein T, Freeman KS, Kelly TR, Wheeler EA, Smith BR,

Gulland FMD, Goldstein T. 2015. Evaluation of viruses and their association with ocular lesions in pinnipeds in rehabilitation. Vet Ophthalmol 18:148–159.

CHAPTER THREE

A NOVEL CORNEA EXPLANT MODEL SYSTEM TO EVALUATE ANTIVIRALS AGAINST FELID ALPHAHERPESVIRUS TYPE 1 (FHV-1)

*Manuscript from: Matthew R. Pennington, Michael W. Fort, Eric C. Ledbetter, and Gerlinde R. Van de Walle. 2016. A novel cornea explant model system to evaluate antivirals against feline herpesvirus type 1 (FHV-1). *Journal of General Virology* 97(6):1414-25.

3.1. Summary

Felid alphaherpesvirus 1 (FHV-1) is the most common viral cause of ocular surface disease in cats. Many antiviral drugs are used to treat FHV-1, but require frequent topical application and most lack well-controlled *in vivo* studies to justify their clinical use. Therefore, better validation of current and novel treatment options is urgently needed. Here, we report on the development of a feline whole corneal explant model that supports FHV-1 replication and thus can be used as a novel model system to evaluate the efficacy of antiviral drugs. The anti-herpes nucleoside analogues cidofovir and acyclovir, which are clinically used to treat ocular herpesvirus infection in cats and have previously been evaluated in traditional 2-dimensional feline cell cultures *in vitro*, were evaluated in this explant model. Both drugs suppressed FHV-1 replication when given every 12 h, with cidofovir showing greater efficacy. In addition, the potential efficacy of the retroviral integrase inhibitor raltegravir against FHV-1 was evaluated, both in cell culture as well as in the explant model. Raltegravir was not toxic to feline cells or corneas and most significantly inhibited FHV-1 replication at 500 µM in both systems. Importantly, this drug was effective when given only once every 24 h. Taken together, our data indicate that the whole feline cornea explant model is a useful tool for the evaluation of antiviral drugs and, furthermore, that raltegravir appears a promising novel antiviral drug to treat ocular herpesvirus infection in cats.

Key words: cornea, explant model, FHV-1, ocular herpes, antiviral

3.2. Introduction

Alphaherpesvirinae, a subfamily of *Herpesviridae*, cause disease in many species including humans and animals of veterinary importance. These large DNA viruses are characterized by (i) a short replication cycle, (ii) infection through mucosal and epithelial surfaces, and (iii) induction of lifelong latency, primarily in neurons (1). Felid alphaherpesvirus 1 (FHV-1), a varicellovirus of this subfamily, has an estimated 90-97% seroprevalence in cats (2). Furthermore, about 80% of FHV-1-infected cats remain latently infected for life and 45% of these animals intermittently shed virus (3). Notably, FHV-1 is the most common viral cause of ocular surface disease in cats, primarily inducing acute corneal ulceration and the development of chronic stromal keratitis (4–6).

While several FHV-1 vaccines have widespread use and can reduce clinical signs, they only confer partial protection against infection, viral shedding, and latency load (4). Therefore, many cats still develop FHV-1-associated ocular disease despite vaccination. Treatment requires a multifaceted approach tailored both to the individual patient and to the owner, although all current treatment regimens rely on the use of antiviral drugs. Despite the fact that many antiviral drugs, primarily nucleoside analogues, have been tested *in vitro* for efficacy against FHV-1, no antiviral agent has ever been designed specifically for either FHV-1 or for use in cats (6–8). Moreover, many require frequent topical application and most lack well-controlled *in vivo* studies to justify their clinical use (5). For example, cidofovir is one of the few nucleosides analogues that have been tested in cats under well-controlled experimental conditions and showed a significant reduction in clinical disease scores in FHV-1-infected, cidofovir-treated cats compared to FHV-1-infected, untreated control cats, though no reduction in viral shedding was noted (9). Another nucleoside analogue frequently used to inhibit alphaherpesvirus

replication is acyclovir. Yet, there are contrasting indications for its use to treat ocular FHV-1 infections and the drug's reported half maximal effective concentration (EC_{50}) of 57.9 µM (10) is approximately 50-500x greater than the range of acyclovir of 0.07-0.97 µM against 77 different HSV-1 isolates (11). Additionally, its oral prodrug, valacyclovir, is toxic to cats (12). Thus acyclovir is not generally recommended for use in cats, although topical acyclovir may be useful to treat drug-resistant ulcers (13) and one study reports the successful topical administration of acyclovir, 5 times a day for a period of 21 days, to cats with ocular FHV-1 (14).

Recently, Yan *et al.* (15) reported that small molecule human immunodeficiency virus (HIV) integrase inhibitors were capable of blocking replication of all three families of herpesviruses by targeting viral DNA replication, late gene expression, and viral recombination. Furthermore, it was also recently found that raltegravir, a currently available retroviral integrase inhibitor approved by the United States Food and Drug Administration (FDA) in 2007 (16), was able to interfere with UL42, the DNA polymerase accessory factor of human alphaherpesvirus 1 (HHV-1, also known as herpes simplex virus 1, HSV-1) (17). Based on the fact that (i) the FHV-1-encoded UL42 shares 24% amino acid sequence homology with HSV-1 UL42 (18) and (ii) raltegravir appears safe to administer systemically to cats (19), raltegravir could be an attractive novel antiviral drug to treat ocular herpesvirus infection in cats.

The lack of an effective and standardized antiviral therapy to treat feline ocular herpes infections largely stems from the limitation of the traditional 2-dimensional *in vitro* cell culture system and the logistical complications of working with live cats, such as the high cost of acquiring these animals from approved vendors, the high cost of care, and ethical considerations. Organ explant model systems are valuable tools as they preserve the tissue cytoarchitecture to more accurately reproduce what occurs at the organismal level (20, 21) and, therefore, are a

useful steppingstone to bridge *in vitro* and *in vivo* evaluation of drugs, including antiviral drugs. Indeed, the valuable use of explants in drug discovery has been reported for a variety of organs, including intestines (22), skin (23), and the central nervous system (24). Furthermore, the use of discarded material is less expensive than live animal use and reduces the number of experimental animals needed, as outlined by the 3R concept (25).

Therefore, the aim of the present study was to use a feline whole cornea explant model system to evaluate the efficacy of commonly used and novel promising antiviral drugs against FHV-1 infection. We found that the anti-herpes nucleoside analogues cidofovir and acyclovir, as well as the retroviral integrase inhibitor raltegravir, could significantly inhibit FHV-1 replication. These data provide additional support to the topical use of cidofovir and acyclovir, and suggest that raltegravir could prove a novel effective antiviral to treat FHV-1-induced ocular herpesvirus infection.

3.3. Results

The whole cornea explant model supports FHV-1 infection.

The whole cornea explant model system was established as shown in Fig. 3.1A. In order to optimize the viral growth conditions, corneas were infected with FHV-1 and cultured at either 34ºC or 37ºC. At 24 hours post infection (hpi), viral growth was approximately four-fold higher at 34ºC compared to 37ºC as assessed by qPCR on corneal tissue for viral genome replication and plaque assay of supernatants for extracellular viral titers (Fig. 3.1B). Consequently, all further experiments were done with corneas cultured at 34ºC. In addition, hematoxylin-eosin (H&E) stainings of corneal cross-sections showed that FHV-1-infected corneas exhibited epithelial damage, characterized by epithelial thinning and detachment, while mock-infected

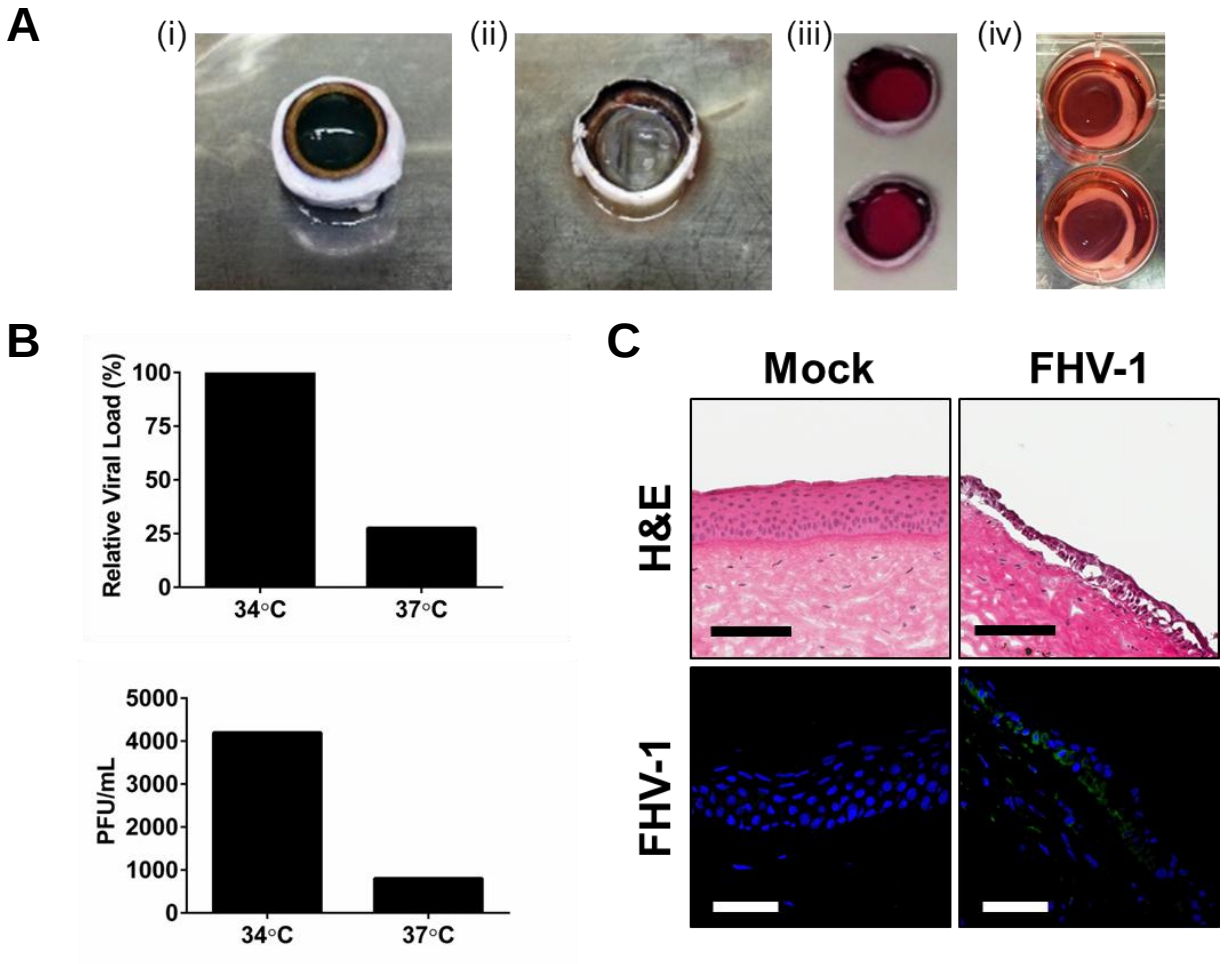

Figure 3.1: The whole feline corneal explant model is susceptible for felid alphaherpesvirus 1 infection. (A) Whole eyes were obtained from cats euthanized for reasons unrelated to this study (i). Corneas were removed from the eye after discarding the lens and iris (ii). The cornea was placed epithelial side down and the inner cavity was filled with 1% low melting point agarose in DMEM (iii). Corneas were placed epithelial side up in 12-well plates and covered with media (iv). **(B)** Paired corneas (n=1) from the same cat were infected with $3x10^5$ PFU FHV-1 and cultured at either 34°C or 37°C for 24 h. Viral load in the cornea at each temperature was assessed by qPCR and normalized to the cornea cultured at 34°C by the ddCt method and set to 100%, and produced infectious virus in the supernatants was assessed by standard plaque assays. **(C)** Mock- or FHV-1-infected corneal cross sections were stained with hematoxylin and eosin (H&E), or with monoclonal anti-FHV-1 antibodies followed by Alexa Fluor 488-conjugated secondary antibodies. Nuclei were stained with DAPI. Scale bars, 100 μm.

corneas displayed a normal, multi-layer stratified squamous epithelium (Fig. 3.1C). Immunofluorescence (IF) of cornea cross-sections using an anti-FHV-1 monoclonal antibody demonstrated the presence of viral antigen primarily in the central region of the epithelium in the epithelium of FHV-1 -infected corneas (Fig. 3.1C), similar to the distribution of FHV-1 in feline corneas *in vivo* (26). In contrast, and as expected, no viral antigen staining was found in mock-infected corneas (Fig. 3.1C). Taken together, these results show that the whole cornea explant model system supports FHV-1 replication and that this replication is more efficient when corneas are cultured at 34ºC.

The anti-herpes nucleoside analogues cidofovir and acyclovir inhibit FHV-1 replication in the whole cornea explant model.

To start evaluating the efficacy of antiviral drugs against FHV-1 in this new explant model system, cidofovir and acyclovir were chosen since these two anti-herpes nucleoside analogues are clinically used to treat ocular herpesvirus infection in cats and have previously been evaluated in traditional 2-dimensional feline cell cultures (10). The EC_{50} of these two antivirals was first determined in FHV-1-infected Crandell-Rees Feline Kidney Cells (CRFKs) to decide on the concentration to be used in the corneal explant model system. An EC_{50} value of 7.1±2.1 µM for cidofovir and an EC_{50} value of 78.6±6.2 µM for acyclovir was found (Fig. 3.2A), similar to what has been reported previously (10). Sets of matched corneas were then infected with $3x10^5$ plaque forming units (PFU) FHV-1 for 2 h, after which one cornea was incubated with the antiviral drug at ~2 times its EC_{50} (i.e. 16.2 µM for cidofovir and 181 µM for acyclovir), while the other cornea was left untreated. Medium with the same concentration of antiviral drug was refreshed every 12 h, broadly based on the *in vivo* half-life of these drugs which is ~2-3 h in adult humans (27, 28), and corneas were collected 2 days later for further analyses. Medium

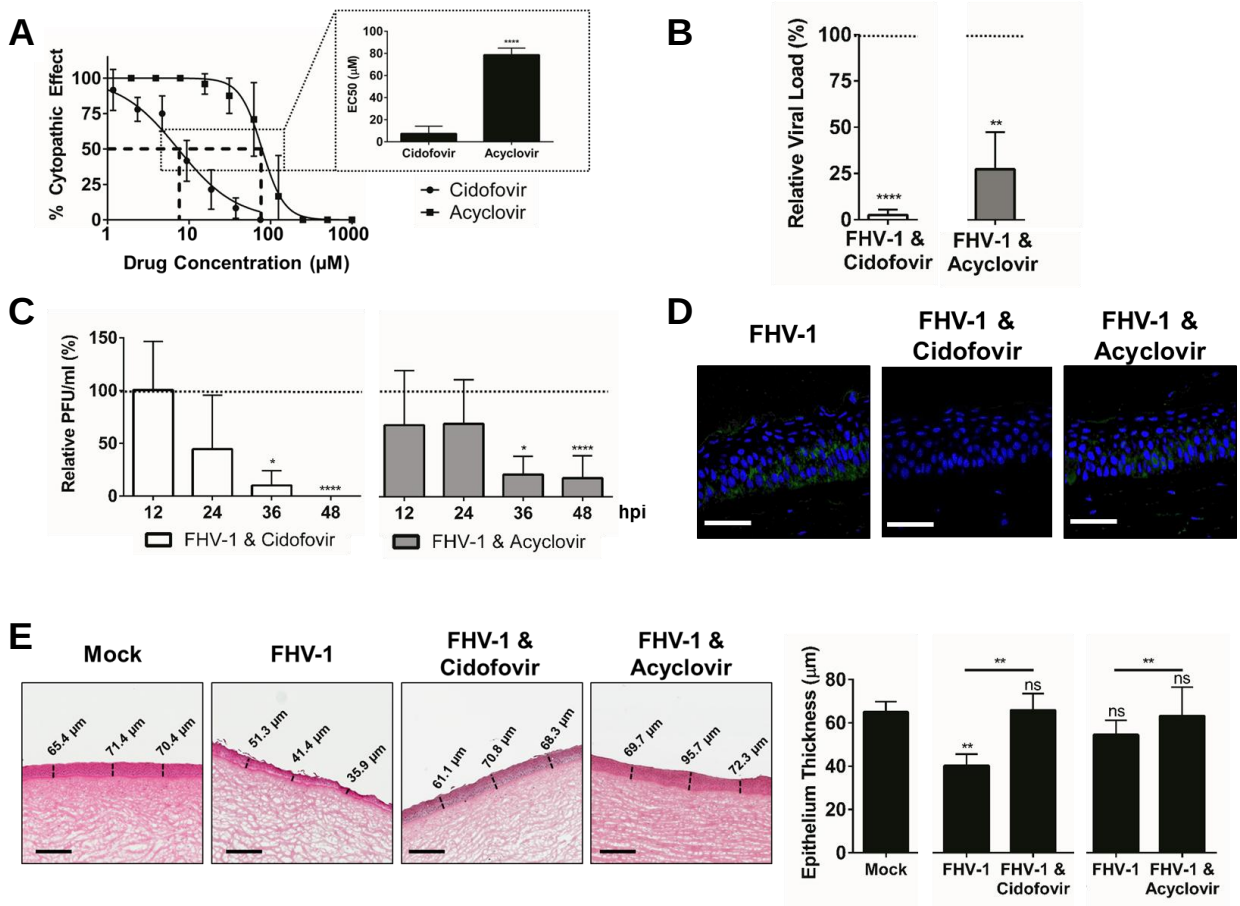

Figure 3.2: Incubation of FHV-1-infected corneas with cidofovir or acyclovir reduces FHV-1 viral load and epithelial damage (n=3). (A) EC_{50} of cidofovir and acyclovir. EC_{50} values were determined to assess the potency of nucleoside analogues to reduce FHV-1-indcued cytopathic effect (CPE) calculated based on the percent of wells showing CPE following treatment of FHV-1-infected CRFK cells with varying concentrations of each drug. **(B, C)** Cidofovir and acyclovir significantly reduce FHV-1 replication in feline corneas. Paired corneas from the same cat were both infected with $3x10^5$ PFU FHV-1 and were either left untreated or treated every 12 h with ~ 2x the EC_{50} concentration of cidofovir (16.2 μM) or acyclovir (181 μM). Viral load in the cornea was assessed by qPCR after 48 h (B) and produced infectious virus in the supernatants was assessed by standard plaque assays every 12 h (C). Dotted line represents FHV-1 infected, untreated matched corneas set to 100%. **(D)** Cidofovir and acyclovir reduce FHV-1 viral antigen-positive staining in feline corneas. Corneal cross sections were stained with monoclonal anti-FHV-1 antibodies followed by Alexa Fluor 488-conjugated secondary antibodies and nuclei were stained with DAPI.

Figure 3.2 continued. Scale bars, 100 μm. **(E)** Cidofovir and acyclovir reduce FHV-1-induced epithelial thinning in feline corneas. Cross sections of mock-infected, FHV-1-infected, and FHV-1-infected and antiviral-treated corneas were stained with hematoxylin and eosin (H&E) and epithelial layer thickness was quantified. Scale bars, 300 μm. The results are presented as mean ± standard deviation. *$p \leq 0.05$; **$p < 0.01$; ****$p < 0.0001$; ns= not significant. (E) Asterisks (significant) or ns (= not significant) above each bar represent comparison to mock-infected corneas. Asterisks above lines represent comparison between treated or untreated FHV-1-infected corneas.

without antiviral drugs was used to refresh control corneas every 12 h. Corneas were collected 48 h later for further analyses.

Upon treatment with cidofovir and acyclovir, FHV-1-infected corneas showed a significant reduction in viral load of 98±3% and 73±20%, respectively, when compared to untreated FHV-1-infected corneas (Fig. 3.2B). Evaluating the extracellular virus production in the supernatants, which were collected every 12 h when media was refreshed, showed that (i) treatment with either antiviral resulted in a significantly reduced virus production starting at 36 h post treatment and (ii) even resulted in the complete absence of extracellular infectious virus at 48 h post treatment with cidofovir (Fig. 3.2C). IF staining of cross-sections from FHV-1-infected, antiviral-treated corneas generally showed an overall reduced viral antigen-positive staining in the epithelium when compared to untreated FHV-1-infected corneas (Fig. 3.2D). FHV-1 infected, untreated control corneas were observed to have significantly thinner epithelial layers than those of the mock-infected, non-matched corneas with the cidofovir, but not the acyclovir experiments (Fig. 3.2E). This inconsistent thinning of the epithelial layer between FHV-1-infected corneas, which is most likely attributed to inter-animal susceptibility to infection, highlights the importance of analyzing drug efficacy data within the matched control. In FHV-1-infected, antiviral-treated corneas, (i) the epithelial layers of antiviral-treated corneas were significantly thicker than those

of the matched FHV-1 infected, untreated control corneas and (ii) no significant difference in epithelial thickness was seen compared to the mock-infected, non-matched corneas (Fig. 3.2E).

Taken together, these results show that both the anti-herpes nucleoside analogues cidofovir and acyclovir can inhibit FHV-1 replication in the whole corneal explant model, with cidofovir having a more pronounced effect compared to acyclovir, and that antiviral drug treatment appears to limit the corneal damage (i.e. reduction of epithelial thickness) observed after FHV-1 infection.

The retroviral integrase inhibitor raltegravir inhibits FHV-1 replication in both Crandell-Rees Feline Kidney (CRFK) cells and the whole cornea explant model.

Based on the recent reports that retroviral integrase inhibitors are also effective against herpesviruses (15, 17), we decided to explore the potential of this class of antiviral drugs against FHV-1 in the whole corneal explant model. To this end, we used the retroviral integrase inhibitor raltegravir as it is currently approved for use in humans for the treatment of human immunodeficiency virus infection (16) and was recently shown to be safe for use in cats (19). Since this drug has never been evaluated for FHV-1, we started with testing its effect on FHV-1 replication in the traditional 2-dimensional cell culture system using CRFK cells. First, cytotoxicity of the drug was assessed by incubating CRFKs with increasing concentrations of raltegravir for 24 h. No effect on viability was observed up to 500 µM (Fig. 3.3A). At higher concentrations, i.e. 1000 and 2000 µM raltegravir, a significant reduction in cell viability of around 15% was found (Fig. 3.3A). No effect on viability was seen when CRFKs were incubated with the volume-matched amounts of DMSO (Fig. 3.3A).

Next, we assessed antiviral activity of raltegravir by determining both plaque numbers and sizes in FHV-1-infected CRFKs treated with this antiviral drug at various concentrations ranging

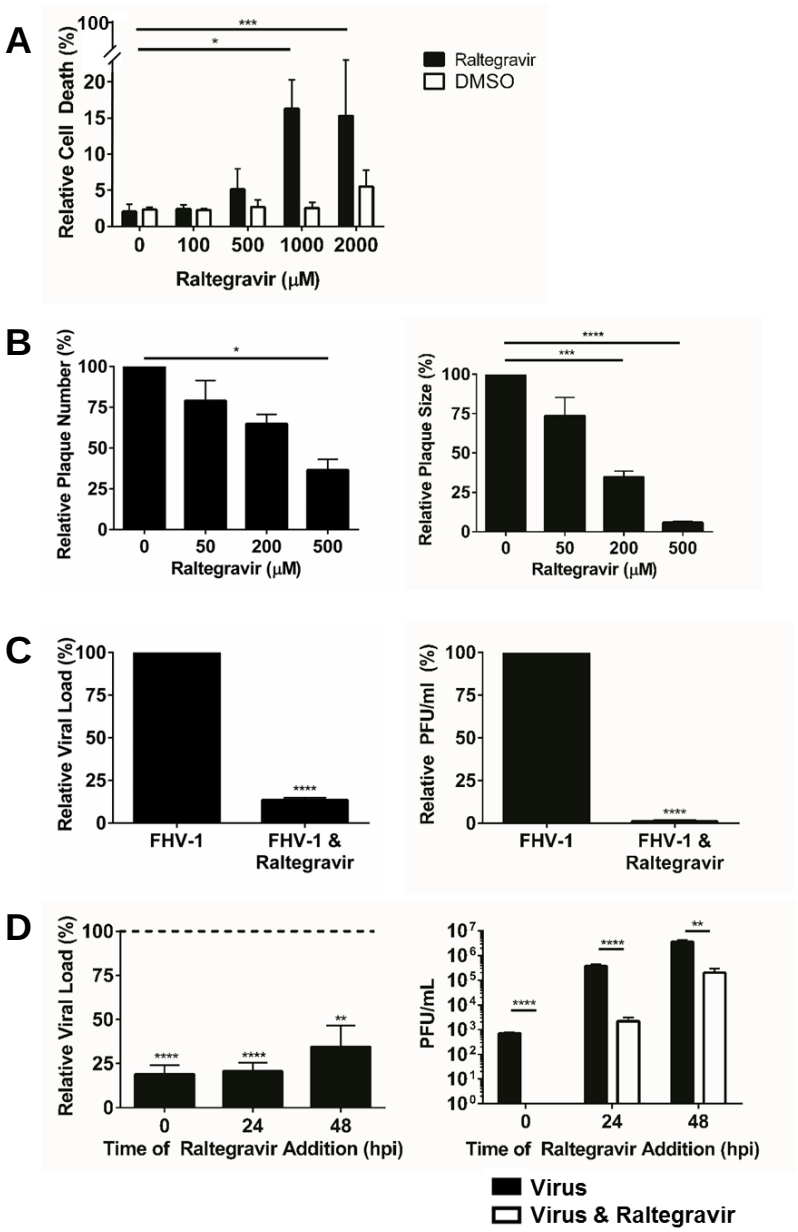

Figure 3.3: Raltegravir is not toxic to feline kidney (CRFK) cells and inhibits FHV-1 replication in this cell line (n=3). (A) Raltegravir is not toxic to CRFK cells. CRFK cells were incubated for 24 h with increasing concentrations of raltegravir or DMSO (control). Cell death was determined by flow cytometry using 7-aminoactinomycin D (7AAD) staining and is expressed relative to paraformaldehyde fixed cells (100% cell death). **(B)** Raltegravir reduces plaque number and size in FHV-1-infected CRFK cells. Relative plaque number and relative plaque size of confluent CRFK cells in 24-well plates infected with 75 PFU/well FHV-1 and treated for 24 h with 0-500 μM of raltegravir.

Figure 3.3 continued. **(C)** Raltegravir significantly reduces FHV-1 replication in CRFK cells when applied directly after infection. CRFK cells in T25 flasks were infected with 200 PFU/flask FHV-1 for 2 h, washed, and subsequently incubated with ~2x the EC_{50} concentration of raltegravir (500 µM) for 24 h. Viral load in CRFK cells was assessed by qPCR and produced infectious virus in the supernatants was assessed by standard plaque assays after 24 h. **(D)** Raltegravir significantly reduces FHV-1 replication when applied later after infection. CRFK cells in T25 flasks were infected with 50 PFU/flask FHV-1 and treated with 500 µM raltegravir at 0, 24, and 48 hpi. Relative viral load in CRFK cells was assessed by qPCR and produced infectious virus in the supernatants was assessed by standard plaque assays following 24 h of drug treatment. Dotted line represents FHV-1 infected, untreated CRFK viral load set to 1.0. Results are presented as mean ± standard deviation. *$p \leq 0.05$; **$p < 0.01$; ***$p < 0.001$; ****$p < 0.0001$.

from 0 µM (control) up to 500 µM. A dose-dependent decrease in relative plaque numbers, indicative of viral infectivity, was observed, which reached significance at 500 µM (Fig. 3.3B) and likewise, a dose-dependent decrease in relative plaque sizes, indicative of cell-to-cell spread, was observed, which reached significance starting at 200 µM (Fig. 3.3B). To further corroborate these findings, we infected CRFKs with FHV-1 for 2 h at 37ºC, washed the cells and treated them with 500 µM raltegravir for 24 h. A significant decrease in both viral genome copies and extracellular infectious virus was found in raltegravir-treated compared to untreated FHV-1-infected CRFK cells after 24 h (Fig. 3.3C). Finally, a time kinetic experiment was also performed to explore the efficacy of 500 µM raltegravir on FHV-1 replication when administered at different time points (0-48 hpi). A significant reduction in both viral genome copies and extracellular infectious virus was found in treated versus untreated, FHV-1-infected CRFKs at all different time points tested (Fig. 3.3D). Taken together, these data collectively show that, in the traditional 2-dimensional cell culture system, raltegravir is effective at inhibiting FHV-1 replication (i) in a dose-dependent manner, with significance at 500 µM, and (ii) even when

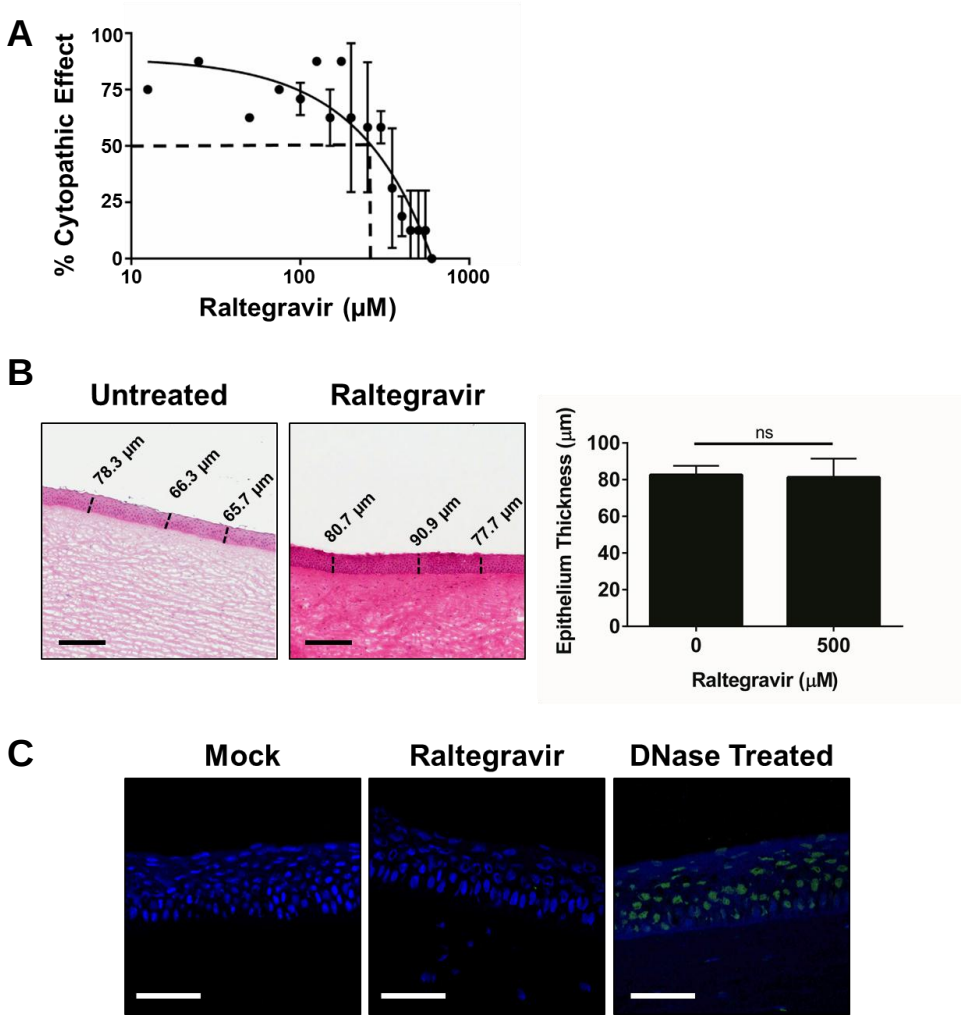

Figure 3.4: Raltegravir is effective against FHV-1, but is not toxic by itself for feline corneas. (A) The EC_{50} of raltegravir (n=3). The EC_{50} value was determined to assess the potency of raltegravir to reduce FHV-1-induced cytopathic effect and was calculated based on the percent of wells showing CPE following treatment of FHV-1-infected CRFK cells with varying concentrations of raltegravir. **(B, C)** Raltegravir does not affect the epithelial layer thickness or viability. Paired corneas from the same cat were treated with ~2x the EC_{50} concentration of raltegravir (500 μM) or left untreated and 24 h later, samples were collected for analyses. Representative pictures of H&E stained untreated and raltegravir-treated feline cornea sections and quantification of epithelial layer thickness. Scale bars, 300 μm. (B). Representative pictures of TUNEL-stained untreated and raltegravir-treated feline corneas. A mock-infected section was treated with DNase as a positive control. Scale bars, 100 μm. (C). Results are presented as mean ± standard deviation. ns= not significant.

applied 48 h after FHV-1 infection.

Because of these promising results observed in CRFK cultures, we next wanted to explore the effects of raltegravir against FHV-1 in the physiologically relevant, whole corneal explant model system. In line with our studies on the efficacy of the anti-herpes nucleoside analogues, the EC_{50} of raltegravir was first determined in order to decide on the concentration to be used in the corneal explant model system. The EC_{50} of raltegravir was found to be 215.6±7.7 µM (Fig. 3.4A) and, consequently, 500 µM was used for experiments in the corneal explant model since this (i) equals ~2 times its EC_{50} and (ii) corresponds with the significant reduction in FHV-1 replication as observed in the CRFK cultures. Next, the cytotoxicity of this concentration of raltegravir was evaluated using matched corneas and no visual histological changes in the epithelial layer, nor any difference in epithelial thickness were observed in H&E-stained cross-sections of raltegravir-treated versus untreated corneas (Fig. 3.4B). Additionally, no TUNEL-positive epithelial cells, indicative of cell death, were detected following raltegravir treatment (Fig. 3.4C). This absence of staining was not due to a technical error as TUNEL-positive cells were readily visible in a control feline cornea that was treated with the enzyme DNase I (Fig. 3.4C).

After confirming that raltegravir was not toxic for the corneal epithelium, its antiviral properties were further studied in the corneal explant model system. To this end, matched FHV-1-infected corneas were treated with 500 µM raltegravir or left untreated (control) every 24 h for 2 days. The interval of treatment of 24 h was broadly based on the *in vivo* half-life of this drug, which is reported to be 7-12 h in humans (29). A significant reduction in both viral genome copies and extracellular infectious virus was found (Fig. 3.5A), and a generally reduced viral antigen-positive staining in corneal cross-sections (Fig. 3.5B), was observed in raltegravir-

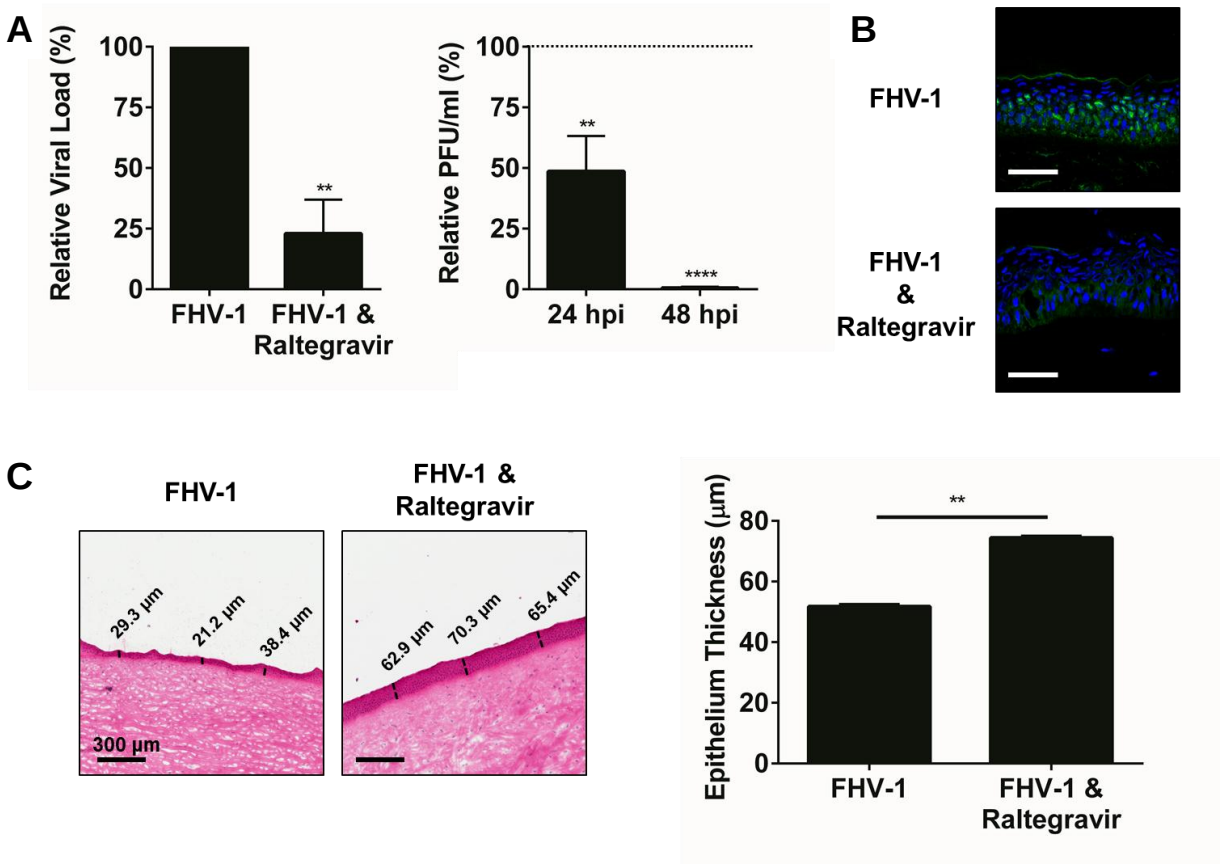

Figure 3.5: Incubation of FHV1-infected corneas with raltegravir reduces FHV-1 viral load and epithelial damage (n=3). Paired corneas from the same cat were both infected with $3x10^5$ PFU FHV-1 and were either left untreated or treated every 24 h with ~2x the EC_{50} concentration of raltegravir (500 µM). **(A)** Raltegravir significantly reduces FHV-1 replication in feline corneas. Viral load in the cornea was assessed by qPCR after 48 h and produced infectious virus in the supernatants was assessed by standard plaque assays every 24 h. Dotted line represents the viral load in supernatants collected from FHV-1 infected, untreated matched corneas, set to 100%. **(B)** Corneal cross sections were stained with monoclonal anti-FHV-1 antibodies followed by Alexa Fluor 488-conjugated secondary antibodies and nuclei were stained with DAPI. Scale bars, 100 µm. **(C)** Raltegravir reduces FHV-1-induced epithelial thinning in feline corneas. Cross sections of FHV-1-infected, untreated and FHV-1-infected, raltegravir-treated corneas were stained with H&E and epithelial layer thickness was quantified. Scale bars, 300 µm. Results are presented as mean ± standard deviation. **p<0.01; ****p<0.0001.

treated versus untreated FHV-1-infected corneas. Moreover, we observed in the H&E-stained corneal cross-sections that the epithelial layers of the corneas following raltegravir treatment were significantly thicker compared to those of the matched FHV-1-infected, untreated controls (Fig. 3.5C). When comparing the results of these FHV-1-infected, untreated corneas, with the non-matched, mock-infected control corneas shown in Fig. 3.2E, a significant reduction in the average thickness of the epithelial layer in FHV-infected corneas was observed (Student's t test, $p=0.03$). In contrast, no significant difference was found between the FHV-1-infected, raltegravir-treated corneas and the non-matched, mock-infected control corneas shown in Fig. 3.2E (Student's t test, $p=0.07$). Taken together, these results demonstrate that in the whole corneal explant model system raltegravir significantly inhibits FHV-1 replication and prevents the FHV-1-induced epithelial thinning.

3.4. Discussion

FHV-1 is the most common viral cause of ocular disease in cats and while several antiviral drugs are used to treat ocular FHV-1, many require frequent topical application and most lack well-controlled *in vivo* studies to justify their clinical use. In the present study, we reported on the development of a feline whole corneal explant model that supports FHV-1 replication and that was used to evaluate the efficacy of antivirals against FHV-1 in a physiologically relevant model.

In general, the development and testing of novel drugs is a complex and expensive process. From 1991-2000, only an 11% success rate in bringing new drugs to the market was reported, with substantial failure occurring during Phase I-III clinical testing. Low efficacy and toxicity are indicated as primary drivers of drug attrition (30) and potential toxicity is seldom recapitulated in

simplified *in vitro* models such as 2-dimensional cell culture (31). Explant models can take advantage of "waste" tissue materials left over from other groups to serve as an intermediary evaluation stage between 2-dimensional cell culture and live animal work. Since explant models consist of different cell types and maintain the 3-dimensional architecture, they are believed to recapitulate the *in vivo*-like cell heterogeneity and architecture much better then 2-dimensional monocultures, and as such, are better predictors of *in vivo* efficacy of drugs (31).

Recently, the development of a partial corneal explant was described to evaluate its use to study FHV-1 replication (32). In these partial explants, the authors only observed virus infection at the borders where the corneal tissue was cut, but not in the center of the cornea. This is in contrast to our findings where FHV-1 replication, as assessed by immunofluorescence stainings, was primarily found in the center of intact corneas. Several explanations can potentially account for this discrepancy. First, the study of Li *et al.* (32) used the C-27 FHV-1 strain, whereas we used another virus strain, namely the strain FH2CS, and they hypothesized that the inability of C-27 to properly infect corneas could be explained by viral attenuation due to prolonged passage. Second, they cultured corneas at 37ºC and the temperature of culturing these explants during infection could also play a critical role. Indeed, when evaluating the effects of temperature on FHV-1 replication in feline corneas, we found that 34ºC supported higher FHV-1 replication than 37ºC. This can be explained by the fact that corneas are directly exposed to the outside environment and thus have a lower temperature than the general body temperature. Indeed, it has been shown that feline corneas have a temperature of approximately 33ºC (33) and consequently, it is reasonable to assume that ocular herpesviruses are specifically adapted to grow at these lower temperatures. Third, the use of a partial corneal explant instead of a whole explant could mask virus infection if virus replication is localized to certain regions of the corneal epithelium. In this regard, we noticed

when scanning corneal cross sections for FHV-1 positive cells that only partial regions throughout the cornea appeared positive instead of a uniform infection of the entire corneal epithelium, (data not shown). Since we infected the corneas epithelial side down, as previously described by Alekseev *et al.* (34), it is possible that this method may have limited access of the virus to the small central part of the cornea that was in contact with the culture plate and could potentially explain why we did not observe a uniform infection of the epithelium. It will be interesting in future experiments to evaluate FHV-1 replication when corneas are infected epithelial side up, and whether this will result in differences compared to infection of corneas epithelial side down.

Another observation we made was that FHV-1 infection generally resulted in a thinner epithelial layer when compared to mock-infected corneas, although this was very unpredictable. A likely explanation for this inconsistency is that these comparisons were made with corneas from different cats, as the matched corneas were used to compare FHV-1 infection in the presence or absence of antiviral drugs, and consequently, emphasizes the importance of using matched corneas from the same cats in order to directly compare an experimental condition with its appropriate control condition.

To validate our novel corneal explant model as a useful tool to evaluate antiviral drugs, we first focused on the anti-herpes nucleoside analogues cidofovir and acyclovir, which are already used clinically and have been evaluated previously in cell culture (5, 10). We found that both antiviral drugs were capable of inhibiting FHV-1 replication in feline corneas, but cidofovir appeared to be more effective (higher reduction) and more consistent (smaller standard deviations) at controlling infection when compared to acyclovir. Overall, and importantly, the results in the whole corneal explant model appear to match what has been observed *in vivo* with these two antivirals. Indeed, cidofovir treatment at a 12 h interval and a dose of ~16 µM was

quite effective at inhibiting FHV-1 replication in the corneal explant model, similarly to its antiviral effects *in vivo* as assessed by a reduction in viral titers in ocular swabs of experimentally infected cats (9). When looking at acyclovir, much higher concentrations, ~180 µM, were needed to efficiently inhibit FHV-1 replication at a similar treatment interval in the feline corneal explant model and a much larger standard deviation was observed. Williams *et al.* (14) evaluated the efficacy of topical acyclovir in 30 client-owned FHV-1-positive cats. These cats were first treated with the antibiotic chlortetracycline for 2-3 weeks and due to the lack of any improvement in ocular disease, received a 5-times/day topical treatment with acyclovir. This resulted in a clinical recovery of ocular disease after 12 days of acyclovir treatment. However, due to the lack of control cats in that study, it is difficult to make strong conclusions regarding the efficacy of topical acyclovir *in vivo*. Additionally, Nasisse *et al.* (12) reported that the oral prodrug of acyclovir, valacyclovir, is toxic to cats. This was likely due to the systemic toxicity of acyclovir itself. If the low bioavailability of acyclovir could be overcome, it would likely have similar toxicity. It is current not clear if long-term topical administration of acyclovir would also be toxic to cats. Our data with the corneal explant model system suggest that acyclovir can indeed be effective to treat FHV-1-induced ocular disease, but due to the high frequency of treatment and high dosage required, as well as its potentially toxic effects, there may be more appropriate antiviral drugs for ocular herpesvirus infection in cats.

Finally, we decided to use our whole corneal explant model system to evaluate an antiviral drug that has not previously been used to treat FHV-1 infection in general, or FHV-1-induced ocular herpesvirus disease in specific. This antiviral drug raltegravir, is an FDA-approved retroviral integrase inhibitor which was recently shown to inhibit replication of human alphaherpesvirus 1 (16, 17). Similar to the anti-herpes nucleoside analogues, raltegravir was also

capable of inhibiting FHV-1 replication in the feline corneal explant system. It is interesting to note is that this effect was observed when raltegravir was added at a 24 h interval, in contrast to the 12 h interval of the nucleoside analogues, and as such, we would like to suggest raltegravir as a novel promising antiviral drug for topical use in cats with less frequent applications. The latter is especially important since patient compliance is a common problem in the treatment of FHV-1 ocular infection and so the use of antiviral drugs that have to be given less frequently may increase the likelihood of compliance (5, 14). Unfortunately, raltegravir was found to have a relatively high EC_{50} value which could limit its practical use against ocular FHV-1, even though we did not observe any direct toxic effects in our corneal explant system at a 500 µM raltegravir, the concentration that significantly inhibited FHV-1 replication. It will be of interest to screen additional integrase inhibitors, like 118-D-24 or XZ45, in our whole corneal explant model system to identify more potent inhibitors of FHV-1 replication with a higher therapeutic index. For example, the integrase inhibitor XZ45 was shown recently to have an EC_{50} of as low as 1 µM against HHV-1 (15) and so it is planned in future experiments to test this integrase inhibitor in our feline corneal explant system also.

Taken together, our current study is the first to report, to our knowledge, on the use of a whole corneal explant system to evaluate antiviral drugs to treat ocular FHV-1 infection, helping to bridge the gap between evaluating drugs in traditional cell culture and animals and highlighting the importance of screening potential compounds in explant models prior to animal studies.

3.5. Methods

Virus, cells and antiviral drugs

The FHV-1 strain FH2CS, isolated from a litter of kittens presenting to the New York State Veterinary College of Cornell University with signs of respiratory infection (35), was used in this study. Crandell-Rees Feline Kidney (CRFK) cells were maintained in cell line media consisting of Dulbecco's Modified Eagle Medium (DMEM) with 1 g/L glucose, L-glutamine & sodium pyruvate, 10% fetal bovine serum (FBS), and penicillin (200 U/ml)/streptomycin (200 μg/ml), at 37°C and 5% CO_2. Acylovir (EMD Millipore) and raltegravir (ChemieTek) were dissolved in dimethyl sulfoxide (DMSO) and stored at -20°C. Cidofovir (Gilead Sciences) was available as an intravenous solution (Vistide®) and stored at room temperature.

Collection of feline eyes

Eyes were obtained from cats euthanized for reasons unrelated to this study (Liberty Research, Waverly, NY). These cats were raised under specific pathogen free conditions and vaccinated against FHV-1, but were never exposed to an active infection. Random serological testing was performed monthly to ensure cats were not exposed to the virus. All cats sampled had not received boosters for at least 4 weeks prior to euthanasia. The eyes were assessed visually for abnormalities such as corneal abrasions or ulcers, anisocoria, ocular discharge, or strabismus by a trained Licensed Veterinary Technician. Cats were sedated with an intramuscular injection of ketamine and euthanized with either Euthasol (Virbac) or Beuthansia-D (Schering-Plough) via intracardiac injection. Whole eyes were removed immediately after euthanasia. Eyes were transported to the laboratory in sterile phosphate buffered saline (PBS) containing a 2% anti-microbial/anti-mycotic solution on ice.

Whole corneal explant model system

Feline corneal explants were established as previously described for canine corneas, with some modifications (36). Clear corneas, including the limbus region and approximately 5 mm of the sclera, were aseptically and non-traumatically removed from the rest of the eye using a scalpel and dissection scissors (Fig. 3.1A, i). The iris and lens were removed and discarded (Fig. 3.1A, ii). Corneas were placed epithelial side down in a sterile ceramic plate (Avogadro's Lab Supply), and the inner cavity formed by the cornea and sclera was filled with a 1% low-melting-point agarose solution in DMEM with 1 g/L glucose, L-glutamine & sodium pyruvate to provide structural support and maintain the normal three-dimensional shape of the cornea (Fig. 3.1A, iii). Corneas were turned epithelial side up, unless indicated otherwise, and further cultured in 12-well plates overlaid with cornea culture medium, consisting of DMEM, 10% FBS, penicillin (200 U/ml)/streptomycin (200 μg/ml), 1% nonessential amino acids, 1% sodium pyruvate, and 300 μg/ml L-glutamine (Fig. 3.1A, iv). Corneas were used immediately for experiments and total time from eye collection to culture was approximately 1.5 hours.

To evaluate the effects of temperature on viral growth, paired corneas from the same cat (n=1) were placed epithelial side down in 12-well culture plates and infected with $3x10^5$ PFU FHV-1 for 2 h at either 34°C or at 37°C, as described by Alekseev *et al.*, (34). Corneas were rinsed with PBS, placed epithelial side up in new 12-well plates containing 2.5 ml cornea culture media, and then cultured for an additional 24 h at either 34°C or at 37°C. Media was then collected and centrifuged at 10,000 xg for 10 minutes to pellet cellular debris and these cell-free supernatants were frozen for viral titrations. The sclera was removed from the cornea and discarded. Corneas, epithelial side up, were bisected evenly in half, and snap-frozen for DNA extraction and PCR evaluation

To evaluate the efficacy of the antiviral drugs cidofovir, acyclovir, and raltegravir, paired corneas from the same cat were placed epithelial side down in 12-well culture plates and infected with $3x10^5$ PFU FHV-1 for 2 h at 34°C. Corneas were rinsed with PBS and then placed epithelial side up in new 12-well plates containing 2.5 ml cornea culture medium with 0 μM (control) or ~2 times the EC_{50} of the drug, as we determined and as we describe below, and cultured for 48 h. Media was collected and replaced with fresh media and drug every 12 or 24 h for the nucleoside analogues or raltegravir, respectively. Collected media were centrifuged as described above. At 48 h, the sclera was removed and discarded. Corneas were placed epithelial side up and bisected evenly in half, and snap-frozen for DNA extraction and PCR or embedded in clear frozen section compound (VWR) for histology and immunofluorescence analyses.

To evaluate the cytotoxicity of raltegravir for feline corneas, paired corneas from the same cat were incubated epithelial side up in 12-well culture plates with 2.5 ml cornea culture medium containing 0 (control) or 500 μM raltegravir for 24 h at 34°C. Corneas were collected and embedded in clear frozen section compound for histology and immunofluorescence (IF).

Traditional 2-dimensional CRFK cell cultures

The EC_{50} concentration of all antiviral drugs used in this study was determined, exactly as previously described, and was calculated based on the percent of wells with cytopathic effect (CPE) at each concentration (37).

To evaluate cytotoxicity of raltegravir for CRFK cells, cells were grown to confluency in T25 flasks. Confluent monolayers were treated in triplicate with media containing increasing concentrations of raltegravir or a volume-matched amount of DMSO (control) and cultured for 24 h. Cells were treated with accutase, stained with 7-AAD (ThermoFisher Scientific) and assessed for viability via flow cytometry using a Gallios flow cytometry (Beckman Coulter)

controlled by Kaluza for Gallios (Version 1.0.14029.14028). Paraformaldehyde fixed cells were included as a positive control for cell death. Data were analyzed using Kaluza Analysis (Version 1.3.14026.13330).

To evaluate the efficacy of raltegravir against FHV-1 replication in CRFK cells, three sets of experiments were performed. First, CRFK cells were plated at a density of 75,000 cells per well in 24-well plates, grown overnight, and infected with 75 PFU FHV-1 for 2 h at 37°C. Virus supernatants were removed and replaced with 0.94% carboxymethyl cellulose in minimal essential medium (MEM), supplemented with 225 mg/ml $NaHCO_3$, 10% FBS, and penicillin/streptomycin containing increasing concentrations of raltegravir. Wells were cultured until viral cytopathic effect (CPE) in the controls was visible (~2 days). Average plaque numbers per well were counted and the average plaque size was measured using ImageJ (Version 1.48). Second, confluent cells were infected for 2 h with 200 PFU FHV-1 in T25 flasks. Supernatant was removed and replaced with media containing 0 (control) or 500 μM raltegravir. Cell-free supernatants and cells were collected 24 h later for plaque assay analysis. Third, confluent CRFKs were infected for 2 h with 50 PFU FHV-1 in T25 flasks, and treated with 500 μM raltegravir at 0, 24, and 48 h post infection (hpi). Twenty-four h post drug treatment, cell-free supernatants and cells were collected for analysis.

Histology

Frozen corneas were cut into twelve 6 μm nonconsecutive sections and mounted on glass slides. Slides were stained with hematoxylin and eosin (H&E) and imaged using the Aperio ScanScope. Average epithelial measurements were quantified using the Aperio ImageScope software (Version 12.1.0.0529) based on measurements taken approximately every 150 μm across the entire section. Representative images showing the average thickness of the epithelium

were then compiled. Three separate, non-matched, mock-infected corneas cultured for 24 hours were also included as controls.

Immunofluorescence (IF)

An In Situ Cell Death Detection Kit (Fluorescein, Roche) was used, according to the manufacturer's instructions, on cornea sections to analyze corneal cell viability (TUNEL assay). To ensure results were not due to technical error, sections of a control cornea, incubated with 1 mg/ml DNase I (Sigma-Aldrich) in 50 mM Tris-HCl, pH 7.5, 10 mM $MgCl_2$ and 1 mg/ml bovine serum albumin (BSA) for 1h at 37°C, were included.

To detect FHV-1 by IF, a mouse monoclonal anti-FHV-1 (clone FHV7-7C; AbD Serotec) or isotype control antibody (Abcam), diluted 1:400 in PBS, was added to 2:3 (v/v) acetone:ethanol-fixed corneal sections for 1 h. An Alexa-Fluor-488-conjugated secondary goat anti-mouse antibody (Jackson ImmunoResearch), diluted 1:100, was then added for 30 min. Nuclei were counterstained with 0.5 μg/ml DAPI (EMD Chemicals Inc) and slides were fixed using Glycergel mounting medium (Dako). Five nonconsecutive cross sections were analyzed. Images were captured using a Zeiss LSM confocal microscope with an attached camera controlled by ZEN imaging software. Separate, non-matched, mock-infected corneal tissues were included as negative controls.

Viral plaque assays

To evaluate the release of infectious virus, extracellular virus titers were determined using standard plaque assays on CRFK cells, as previously described (38). Briefly, five sequential ten-fold dilutions of the cell-free supernatant from either the 2-dimensional or cornea assays were added onto monolayers of CRFK cells in 24-well plates to calculate PFU/mL.

Table 3.1: Primers used in this study for quantitative PCR (qPCR).

Gene	Primer Sequence (5'-3')	Amplicon Length (bp)
FHV-1		
Glycoprotein E (gE)	*F:* GTGTTTCCAATTCTCACACCCG *R:* CTCATGCAGGGTATATATCCCGG	86
Infected Cell Polypeptide 4 (ICP4)	*F:* GGTAGCAGCAGTAGTAGCAGTAG *R:* CTTCAATTCTCGATTCGGTGGTG	132
Cellular		
Beta-2 microglobulin (B2M)	*F:* CATGGACACTCTAGATCCTGAGC *R:* CAAGAGATCCAGCTTCACAGAGG	102
Ribosomal Protein L17 (RPL17)	*F:* AAGAACACACGGGAAACTGC *R:* CTGGGCACACCTACCAACTC	138

F: Forward; R: Reverse.

Quantitative polymerase chain reaction (qPCR)

To evaluate FHV-1 replication in CRFK or corneal cells, viral DNA copies were measured using qPCR. To this end, DNA from CRFK cells pellets or half of the corneas, as described above, was isolated using the DNeasy Blood & Tissue Kit (Qiagen). Primers used to detect viral and reference genes are described in Table 1, and 30 ng DNA was added to triplicate wells of a 96-well reaction plates with SYBR green master mix and 0.3 μM forward and reserve primers. qPCR was performed using an ABI 7500 Fast Real Time PCR System (ThermoFisher Scientific). The comparative C_T method ($2^{-\Delta\Delta Ct}$) was used to quantify gene expression levels. Reference values set to 100 consisted of DNA from either mock-infected or FHV-1-infected, untreated samples, and were used to calculate results as DNA fold change.

Statistical Analysis

Data were statistically evaluated by GraphPad Prism (Version 6.04 for Windows) and are expressed as the mean ± standard deviation of triplicate independent experiments. For all analyses, $p \leq 0.05$ was considered significant.

Acknowledgements

This work was funded by a Cornell University Feline Health Center (FHC) Research Grant. We wish to thank Rebecca Harman and Lauren Tofano for their excellent technical assistance and Colin Parrish for providing us with the FHV-1 strain FH2CS.

3.6. References

1. Davison AJ, Eberle R, Ehlers B, Hayward GS, McGeoch DJ, Minson AC, Pellett PE, Roizman B, Studdert MJ, Thiry E. 2009. The order Herpesvirales. Arch Virol 154:171–7.
2. Maggs DJ, Lappin MR, Nasisse MP. 1999. Detection of feline herpesvirus-specific antibodies and DNA in aqueous humor from cats with or without uveitis. Am J Vet Res 60:932–6.
3. Gaskell RM, Povey RC. 1977. Experimental induction of feline viral rhinotracheitis virus re-excretion in FVR-recovered cats. Vet Rec 100:128–33.
4. Gaskell R, Dawson S, Radford A, Thiry E. 2007. Feline herpesvirus. Vet Res 38:337–54.
5. Gould D. 2011. Feline Herpesvirus-1. Ocular manifestations, diagnosis and treatment options. J Feline Med Surg 13:333–346.
6. Stiles J. 2014. Ocular manifestations of feline viral diseases. Vet J 201:166–173.
7. Galle LE. 2004. Antiviral therapy for ocular viral disease. Vet Clin North Am - Small Anim Pract 34:639–653.
8. Maggs DJ. 2010. Antiviral therapy for feline herpesvirus infections. Vet Clin North Am - Small Anim Pract 40:1055–1062.
9. Fontenelle JP, Powell CC, Veir JK, Radecki S, Lappin MR. 2008. Effect of topical

ophthalmic application of cidofovir on experimentally induced primary ocular feline herpesvirus-1 infection in cats. Am J Vet Res 69:289–293.

10. Maggs DJ, Clarke HE. 2004. In vitro efficacy of ganciclovir, cidofovir, penciclovir, foscarnet, idoxuridine, and acyclovir against feline herpesvirus type-1. Am J Vet Res 65:399–403.
11. Sangdara A, Bhattarakosol P. 2008. Acyclovir susceptibility of herpes simplex virus isolates at King Chulalongkorn Memorial Hospital, Bangkok. J Med Assoc Thai 91:908–12.
12. Nasisse MP, Dorman DC, Jamison KC, Weigler BJ, Hawkins EC, Stevens JB. 1997. Effects of valacyclovir in cats infected with feline herpesvirus 1. Am J Vet Res 58:1141–4.
13. Rand J. 2006. Part 1: Cat with upper respiratory tract signs, p. 9. *In* Problem-based feline medicine. Elsevier Health Sciences, Philadelphia.
14. Williams DL, Robinson JC, Lay E, Field H. 2005. Efficacy of topical aciclovir for the treatment of feline herpetic keratitis: results of a prospective clinical trial and data from in vitro investigations. Vet Rec 157:254–7.
15. Yan Z, Bryant KF, Gregory SM, Angelova M, Dreyfus DH, Zhao XZ, Coen DM, Burke TR, Knipe DM. 2014. HIV integrase inhibitors block replication of alpha-, beta-, and gammaherpesviruses. MBio 5:e01318-14.
16. Summa V, Petrocchi A, Bonelli F, Crescenzi B, Donghi M, Ferrara M, Fiore F, Gardelli C, Gonzalez Paz O, Hazuda DJ, Jones P, Kinzel O, Laufer R, Monteagudo E, Muraglia E, Nizi E, Orvieto F, Pace P, Pescatore G, Scarpelli R, Stillmock K, Witmer M V., Rowley M. 2008. Discovery of raltegravir, a potent, selective orally bioavailable HIV-integrase inhibitor for the treatment of HIV-AIDS infection. J Med Chem 51:5843–5855.
17. Zhou B, Yang K, Wills E, Tang L, Baines JD. 2014. A mutation in the DNA polymerase accessory factor of herpes simplex virus 1 restores viral DNA replication in the presence of raltegravir. J Virol 88:11121–11129.
18. Zhukovskaya NL, Guan H, Saw YL, Nuth M, Ricciardi RP. 2015. The processivity factor complex of feline herpes virus-1 is a new drug target. Antiviral Res 115:17–20.
19. Boesch A, Cattori V, Riond B, Willi B, Meli ML, Rentsch KM, Hosie MJ, Hofmann-Lehmann R, Lutz H. 2015. Evaluation of the effect of short-term treatment with the

integrase inhibitor raltegravir (Isentress™) on the course of progressive feline leukemia virus infection. Vet Microbiol 175:167–178.

20. Resau JH, Sakamoto K, Cottrell JR, Hudson EA, Meltzer SJ. 1991. Explant organ culture: A review. Cytotechnology 7:137–149.
21. Grivel J-C, Margolis L. 2009. Use of human tissue explants to study human infectious agents. Nat Protoc 4:256–269.
22. Leushacke M, Barker N. 2014. Ex vivo culture of the intestinal epithelium: strategies and applications. Gut 63:1345–54.
23. Mathes SH, Ruffner H, Graf-Hausner U. 2014. The use of skin models in drug development. Adv Drug Deliv Rev 69–70:81–102.
24. Daviaud N, Garbayo E, Schiller PC, Perez-Pinzon M, Montero-Menei CN. 2013. Organotypic cultures as tools for optimizing central nervous system cell therapies. Exp Neurol 248:429–40.
25. Russell WM., Burch RL. 1959. The principles of humane experimental technique. Methuen, London.
26. Nasisse MP, Guy JS, Davidson MG, Sussman WA, Fairley NM. 1989. Experimental ocular herpesvirus infection in the cat. Sites of virus replication, clinical features and effects of corticosteroid administration. Invest Ophthalmol Vis Sci 30:1758–1768.
27. Cundy KC, Petty BG, Flaherty J, Fisher PE, Polis MA, Wachsman M, Lietman PS, Lalezari JP, Hitchcock MJ, Jaffe HS. 1995. Clinical pharmacokinetics of cidofovir in human immunodeficiency virus-infected patients. Antimicrob Agents Chemother 39:1247–52.
28. Kimberlin DW, Whitley RJ. 2007. Antiviral therapy of HSV-1 and HSV-2. Hum Herpesviruses Biol Ther Immunoprophyl 1153–74.
29. Hicks C, Gulick RM. 2009. Raltegravir: The first HIV type 1 integrase inhibitor. Clin Infect Dis 48:931–939.
30. Kola I, Landis J. 2004. Opinion: Can the pharmaceutical industry reduce attrition rates? Nat Rev Drug Discov 3:711–716.
31. Astashkina A, Mann B, Grainger DW. 2012. A critical evaluation of in vitro cell culture models for high-throughput drug screening and toxicity. Pharmacol Ther 134:82–106.
32. Li Y, Van Cleemput J, Qiu Y, Reddy VRAP, Mateusen B, Nauwynck HJ. 2015. Ex vivo

modeling of feline herpesvirus replication in ocular and respiratory mucosae, the primary targets of infection. Virus Res 210:227–231.

33. Roh HD, Goldstick TK, Linsenmeier RA. 1990. Spatial variation of the local tissue oxygen diffusion coefficient measured in situ in the cat retina and cornea. Adv Exp Med Biol 277:127–36.
34. Alekseev O, Tran AH, Azizkhan-Clifford J. 2012. Ex vivo organotypic corneal model of acute epithelial herpes simplex virus type I infection. J Vis Exp e3631.
35. Walton TE, Gillespie JH. 1970. Feline viruses. VII. Immunity to the feline herpesvirus in kittens inoculated experimentally by the aerosol method. Cornell Vet 60:232–9.
36. Harman RM, Bussche L, Ledbetter EC, Van de Walle GR. 2014. Establishment and characterization of an air-liquid canine corneal organ culture model to study acute herpes keratitis. J Virol 88:13669–77.
37. Ledbetter EC, Spertus CB, Pennington MR, Van de Walle GR, Judd BE, Mohammed HO. 2015. In vitro and in vivo evaluation of cidofovir as a topical ophthalmic antiviral for ocular canine herpesvirus-1 infections in dogs. J Ocul Pharmacol Ther 31:642–649.
38. Groth AD, Contreras MT, Kado-Fong HK, Nguyen KQ, Thomasy SM, Maggs DJ. 2014. In vitro cytotoxicity and antiviral efficacy against feline herpesvirus type 1 of famciclovir and its metabolites. Vet Ophthalmol 17:268–74.

CHAPTER FOUR

ELECTRIC CELL-SUBSTRATE IMPEDANCE SENSING (ECIS) TO MONITOR VIRAL GROWTH AND STUDY CELLULAR RESPONSES TO INFECTION WITH ALPHAHERPESVIRUSES IN REAL-TIME

*Manuscript from: Matthew R. Pennington and Gerlinde R Van de Walle. 2017. Electric cell-substrate impedance sensing (ECIS) to monitor viral growth and study cellular responses to infection with alphaherpesviruses in real-time. *mSphere* 2(2) e00039-17.

4.1. Summary

Electric cell-substrate impedance sensing (ECIS) measures changes in an electrical circuit formed in a culture dish. As cells grow over a gold electrode, they block the flow of electricity and this is read as an increase in electrical impedance in the circuit. ECIS has previously been used in a variety of applications to study cell growth, migration, and behavior in response to stimuli in real-time and without the need for cellular labels. Here, we demonstrate that ECIS is also a valuable tool to study infection by alphaherpesviruses. To this end, we used ECIS to study the kinetics of cells infected with felid alphaherpesvirus type 1 (FHV-1), a close relative of human alphaherpesviruses 1 and 2 (HHV-1 and HHV-2), and compared the results to those obtained with conventional infectivity assays. First, we demonstrated that ECIS can easily distinguish between wells of cells infected with different amounts of FHV-1 and provides information about the cellular response to infection. Second, we found ECIS useful to identify differences between the replication kinetics of a recombinant DsRed Express2-labeled FHV-1, created via CRISPR/Cas9 genome engineering, and wild type FHV-1. Finally, we demonstrated that ECIS can accurately determine the half maximal effective concentration (EC_{50}) of antivirals. Collectively, our data show that ECIS, in conjunction with current methodologies, is a powerful tool that can be used to monitor viral growth and study the cellular response to alphaherpesvirus infection.

Importance: Alphaherpesviruses, including those that commonly infect humans such as HHV-1 and HHV-2, typically infect and cause cellular damage of epithelial cells at mucosal surfaces, leading to disease. The development of novel technologies to study the cellular responses to infection may allow for a more complete understanding of virus replication and the creation of novel antiviral therapies. This study demonstrates the use of ECIS to study various aspects of

herpesvirus biology, with a specific focus on changes in cellular morphology as a result of infection. We conclude that ECIS represents a valuable new tool to study alphaherpesvirus infections in real time and in an objective and reproducible manner.

Key words: ECIS; FHV-1; growth kinetic; herpesvirus; genome editing; antivirals

4.2. Introduction

Electric cell-substrate impedance sensing (ECIS) is a label-free, impedance-based method to study cellular kinetics in real-time and relies on measuring the changes in electrical impedance of a circuit formed in a tissue culture dish plated with cells. This methodology was first described by Giaever and Keese (1) and is used to quantify morphological changes on a nanoscale range, well beyond the limits of light microscopy. Cells are cultured on small thin film gold electrodes, which are available for use in a variety of patterns and sizes depending on the specific ECIS application. A non-invasive alternating current is then applied through a resistor over the kilohertz (kHz) frequency range and the change in electrical impedance is calculated at predetermined intervals (2). As cells attach to and spread out over the electrodes, the impedance increases due to the insulation of the electrodes by the cell membranes and the formation of tight junctions blocking the electric current flow. Conversely, when cells are stressed and/or dying, the disruption of cell-to-cell junctions due to rounding of membranes and detachment of cells from the well plates allows for a greater passage of the electric current, which is read as a decrease in impedance over time (3).

ECIS is well-established in many fields, such as cancer metastasis, toxicology, wound healing, and other cell biological-related fields (4–6), and, recently, is also becoming increasingly recognized as a useful tool for virologic studies. Thus far, ECIS has been used primarily to study viral growth and cellular responses to infection with RNA viruses, such as respiratory syncytial virus (RSV), influenza A virus (IAV), and Sin Nombre virus (SNV) (7–9). Additionally, one study described the use of ECIS to study the effects of a transient overexpression of the human gammaherpesvirus 8 (HHV-8, also known as Kaposi's sarcoma associated herpesvirus, KSHV) proteins MIR-1 and MIR-2 on the attachment, spreading, and

junction formation of immortalized dermal microvascular endothelial cells (10). However, ECIS has not yet been used to study the cellular responses to infection with herpesviruses in the context of a lytic infection.

Felid alphaherpesvirus 1 (FHV-1), a member of the *alphaherpesvirinae* and a close relative to human alphaherpesvirus 1 (HHV-1, also known as herpes simplex virus 1, HSV-1) and 2 (HHV-2), the causative agents of cold sores and genital herpes, respectively, is an important pathogen of cats worldwide. FHV-1 infection is not only the single most important pathogen contributing to feline upper respiratory infection (URI), but it is also the most common viral pathogen to cause ocular disease in cats (11, 12). FHV-1 replication in the cornea of the eye generally results in conjunctivitis, but other clinical symptoms including corneal ulceration and the development of chronic stromal keratitis are also very common (11–13). Likewise, HHV-1 can cause serious ocular disease in humans, and since FHV-1 ocular infection closely mimic all aspects of the clinical presentation of the disease and the associated immune responses as seen in humans, cats are accepted as an excellent comparative model species for ocular HHV-1 infection (14).

In the present study, we used FHV-1 as proof of concept to evaluate the potential of ECIS to study viral growth of and cellular responses to infection with alphaherpesviruses as a complement to the conventionally used infectivity assays. We found that ECIS could detect dose-dependent changes in impedance due to virus-induced cell death at various multiplicities of infection with FHV-1. Moreover, we showed that ECIS can be used to characterize of the growth of recombinant herpesviruses and is a useful tool to accurately calculate the half maximal effective concentration (EC_{50}) of antivirals.

3.3. Results

ECIS can be used to model kinetic growth curves and to study morphological changes in response to herpesvirus infection

An essential preliminary step when using ECIS to ensure proper analysis and interpretation of the data is to determine the optimal frequencies at which to monitor changes in impedance (Z), resistance (R), and capacitance (C) of the cells, as optimal frequencies can vary depending on cell type. The optimal frequencies are those at which the largest difference between wells that contain cells and wells that do not contain cells (cell-free) is measured. We used the feline kidney cell line CRFK in our studies and determined, using the ECIS software, optimal frequencies for impedance at 16,000 Hz, for resistance at 4,000 Hz, and for capacitance at 64,000 Hz (Fig. 4.1A). These values were in agreement with the suggested defaults, as determined by Applied BioPhysics (Troy, NY), and were used for all subsequent data acquisitions.

Initially, we evaluated whether ECIS could discriminate between wells of cells infected with FHV-1 at various multiplicities of infection (MOI). To this end, CRFK cells were plated on an ECIS polyethylene terephthalate 96-well plate with 10 interdigitated electrode fingers (96W10idfPET) and impedance was monitored at 16,000 Hz for an initial 24 hours (h) to establish baseline impedance levels (Fig. 4.2A). At 24 h post plating (hpp), cells were infected with 10-fold serial dilutions of FHV-1 and impedance was measured until the impedance of all infected wells reached that of the cell-free control wells, which corresponded to 72 h post infection (hpi) or 96 hpp. All wells initially recorded a peak in impedance immediately following addition of virus or control media, most likely as a result of the physical manipulation of the cells, although the height of this peak varied with MOI. Such a peak is commonly observed in ECIS experiments and has been reported previously in the context of IAV infection (8), despite

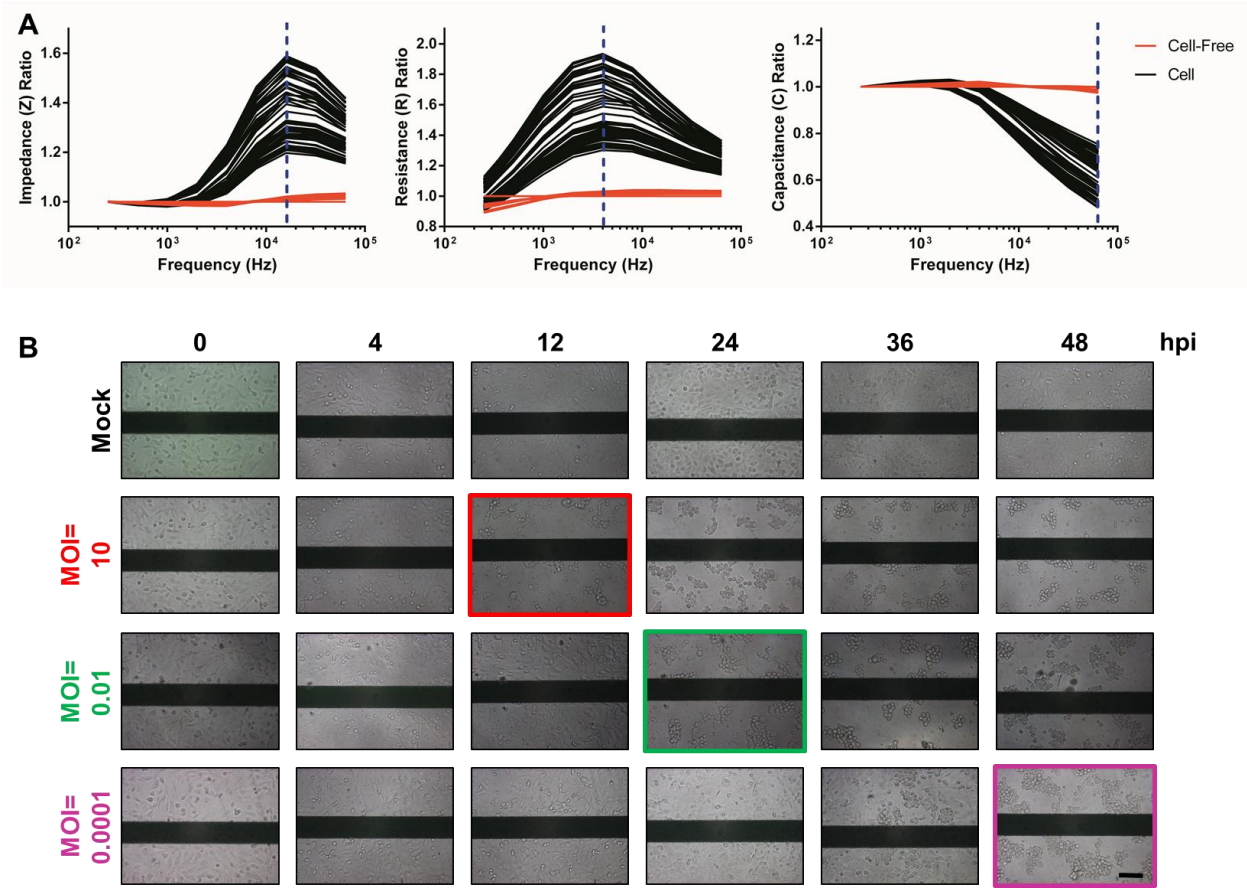

Figure 4.1: Additional validation data of ECIS as a tool to monitor alphaherpesvirus infections. **(A)** Graphs of the ratio of impedance (Z), resistance (R), and capacitance (C) of CRFK-containing wells to cell-free wells at 24 h post plating, calculated and plotted as a function of frequency. Dotted blue lines represent the frequency with the maximal difference between cell-containing and cell-free wells. **(B)** Light microscopy pictures of ECIS wells infected with indicated MOIs of FHV-1 at different time points (0-48 h post infection). Pictures with a colored box represent the time points at which substantial cytopathic effect (CPE) was observed for the different MOIs. The black bars in the images are ECIS electrodes. Scale bar, 25 µm.

morphological changes not being readily observable by light microscopy at this time (data not shown). All wells with FHV-1-infected cells then showed a subsequent decrease in impedance, which occurred at different points post infection, with wells infected with higher MOIs having an earlier decrease compared to wells infected with low MOIs (Fig. 4.2A). These changes in

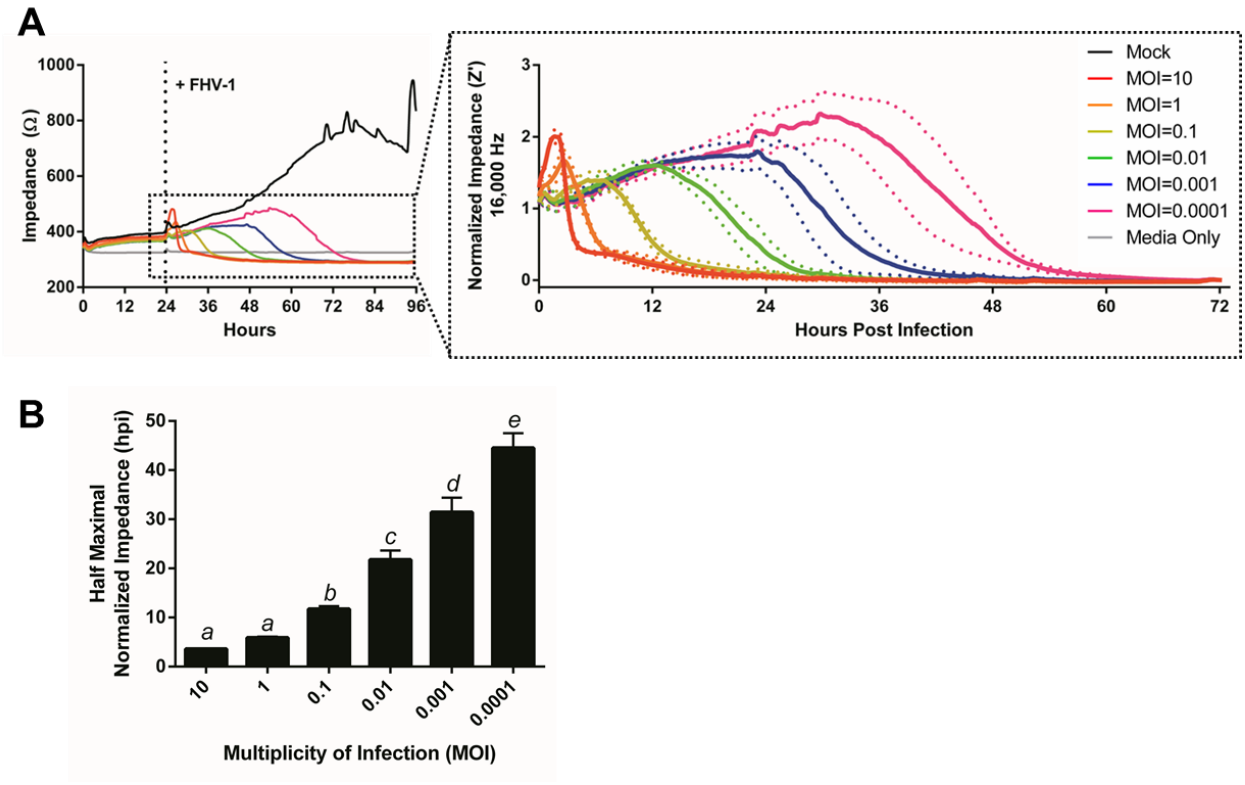

Figure 4.2: ECIS easily distinguishes between wells of cells infected with different amounts of FHV-1. (A) CRFKs were plated in ECIS wells and impedance was monitored for 24 h at 16,000 Hz. Wells were then infected with indicated MOIs of FHV-1. Insert: Normalized impedance values (Z') following FHV-1 infection. **(B)** Half maximal Z' (Z'_{50}) values for impedance curves based on data from panel A. Different letters indicate significantly different Z'_{50} values, as determined by one-way ANOVA.

impedance corresponded to the formation of cytopathic effect (CPE), characterized by rounding of cell membranes and detachment of the cells from the electrodes, as observed by light microscopy performed at specific time points (Fig. 4.1B). In contrast, the impedance of wells with mock-infected cells continued to rise steadily over time, corresponding to the formation of a confluent monolayer. At approximately 72 hpp, impedance in the mock-infected wells began to plateau and oscillate due to micromotion of the wells on the electrode, as has been reported previously in ECIS experiments (Fig. 4.2A) (15). As the impedance at the time of infection varied slightly between replicates due to minor differences in cell numbers, we chose to

normalize the impedance data (Z') for further analysis (Fig. 4.2A, insert). These normalized data were then used to calculate the time point post infection at which each MOI induced a half maximal drop in the normalized impedance, and termed this the Z'_{50} time point. We found no statistical difference in Z'_{50}, expressed in hpi, between MOIs 10 and 1, but all subsequent 10-fold serial dilutions of FHV-1 did show statistically significant differences in Z_{50} values (Fig. 4.2B).

The ECIS ZΘ instrument we utilized in this study calculates complex impedance using the measured resistance and capacitance parameters. Therefore, these values can be also analyzed individually to gain more biological information on how exactly cells respond to manipulation, such as infection with an alphaherpesvirus. Resistance is applied at low frequency, in our study optimally at 4,000 Hz, to induce the electrical current to flow underneath and in the paracellular space between cells, and as such, provides information on the nature of tight junctions and other cell-cell interactions (16). Similar to impedance, we observed an MOI-dependent decrease in resistance in response to infection with FHV-1 (Fig. 4.3A), indicating that herpesvirus infections disrupt cell-cell interactions. This is in agreement with previous work showing that HHV-2 causes down-regulation of gap junctions between infected cells (17). Capacitance, in contrast, is applied at high voltage, in our study optimally at 64,000 Hz, and refers to the ability of the electrode in the well to store electrical charge. The plasma membrane of the cells can act as small capacitors and as cells attach to the electrode, they restrict the ability of the electrode to store a charge. The capacitance of the circuit therefore decreases, as opposed to the increases observed with resistance and impedance, and represents cell attachment to and spreading over a substrate (16). The observed dose-dependent increase in capacitance upon infection with decreasing MOIs of FHV-1 (Fig. 4.3B) indicates that cell detachment from the electrodes takes longer when cells are infected with less virus, as expected. When calculating both the half maximal normalized

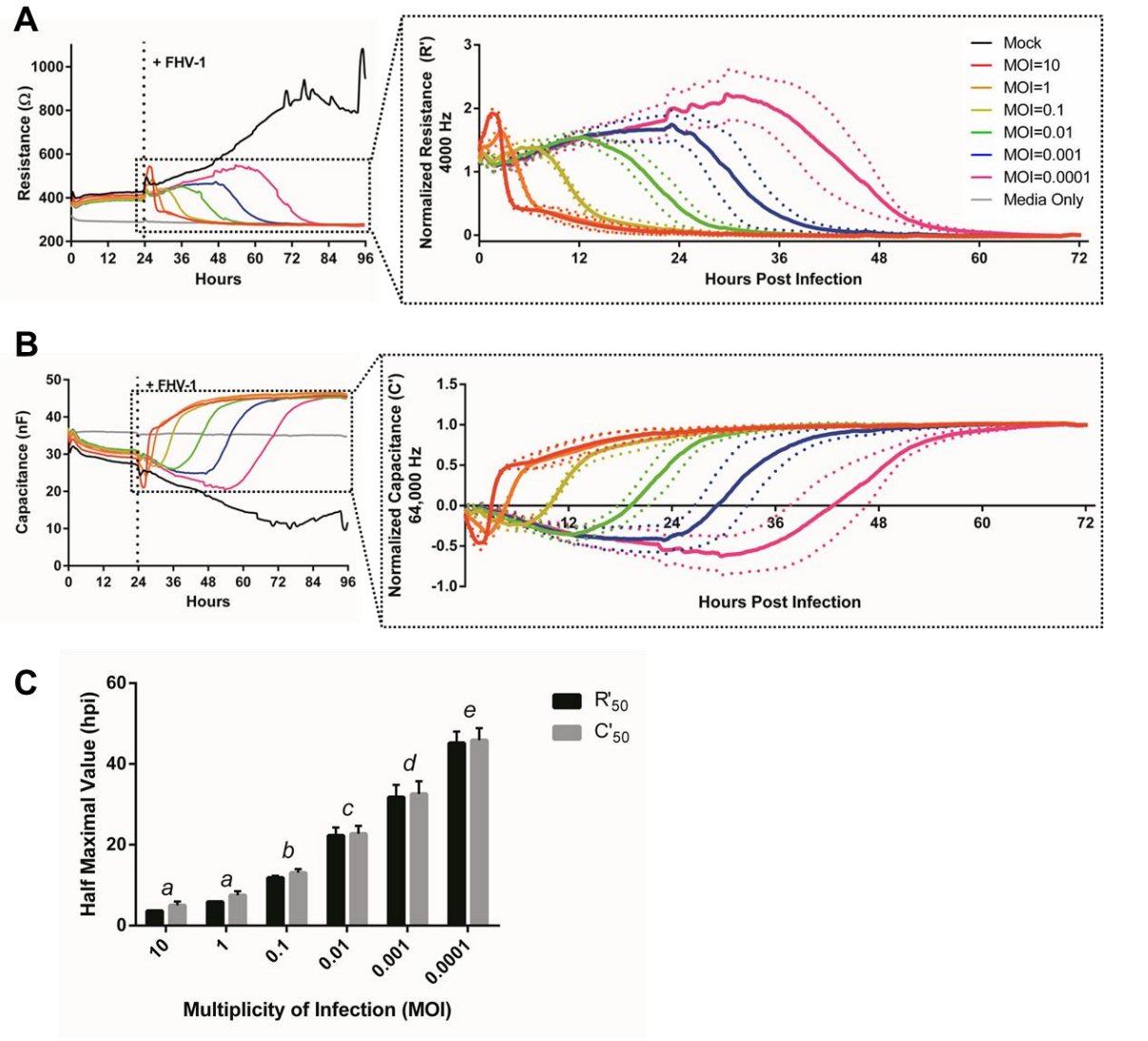

Figure 4.3: FHV-1 infection induces dose-dependent changes in resistance and capacitance. (A-B) Resistance (R) and capacitance (C) measurements, at 4,000 Hz and 64,000 Hz, respectively, following infection of CRFKs with indicated MOIs of FHV-1 at 24 h post plating. Inserts: Normalized resistance (R') and capacitance (C') values following FHV-1 infection. **(C)** Comparison of half maximal R' (R'_{50}) and C' (C'_{50}) values, based on data from panels A and B. Different letters indicate MOI R'_{50} or C'_{50} values that are significantly different, as determined by one-way ANOVA. No significant differences between R'_{50} and C'_{50} values were observed at any MOI, as determined by Student's T Test.

resistance (R'_{50}) and the half maximal normalized capacitance (C'_{50}) for each infectious dose (Fig. 4.3C), we observed the same statistically significant difference in dose-responses to infection as seen with the Z'_{50} (Fig. 4.2B, one-way ANOVA, $p \leq 0.05$). There was no statistically

significant difference between the R'_{50} and C'_{50} values at any MOI (Student's T Test, $p > 0.05$) (Fig. 4.3C), indicating that disruption of cell-cell junctions and detachment of the cells from the electrode in response to FHV-1 infection occurs at approximately the same time rather than sequentially.

Taken together, these results indicate that ECIS can distinguish between wells of cells infected with different amounts of FHV-1 and provides quantitative information about the morphological changes of infected cells in real time, without the need for static sample collection.

ECIS can be used to characterize the growth kinetics of recombinant herpesviruses

We recently decided to create a fluorescently labeled FHV-1 recombinant virus for easy identification of infected cells by immunofluorescence and flow cytometry. To this end, we used CRISPR/Cas9 genome engineering, based on recently described protocols for editing HHV-1 (18–20), and fused the DsRed Express2 protein to the C terminus of glycoprotein (gD), based on a previous study where introduction of monomeric red fluorescent protein (RFP) at this location did not impact herpesvirus growth (21) (Fig. 4.4A-B). We initially confirmed the location of the DsRed insertion by PCR analysis (Fig. 4.4C) and Sanger sequencing. We subsequently characterized the growth of this FHV-1-gD-DsRed recombinant virus using the traditional characterization assays such as viral plaque assays and single- and multi-step growth kinetics, compared to wild type (WT) FHV-1.

When comparing the growth of FHV-1-gD-DsRed to the growth of WT FHV-1, we found no significant differences in intracellular viral genome copies in the single-step growth experiments at all time points tested (Fig. 4.5A(i)). However, we did observe an approximately 1 log reduction in extracellular infectious virus progeny in FHV-1-gD-DsRed-infected cells compared

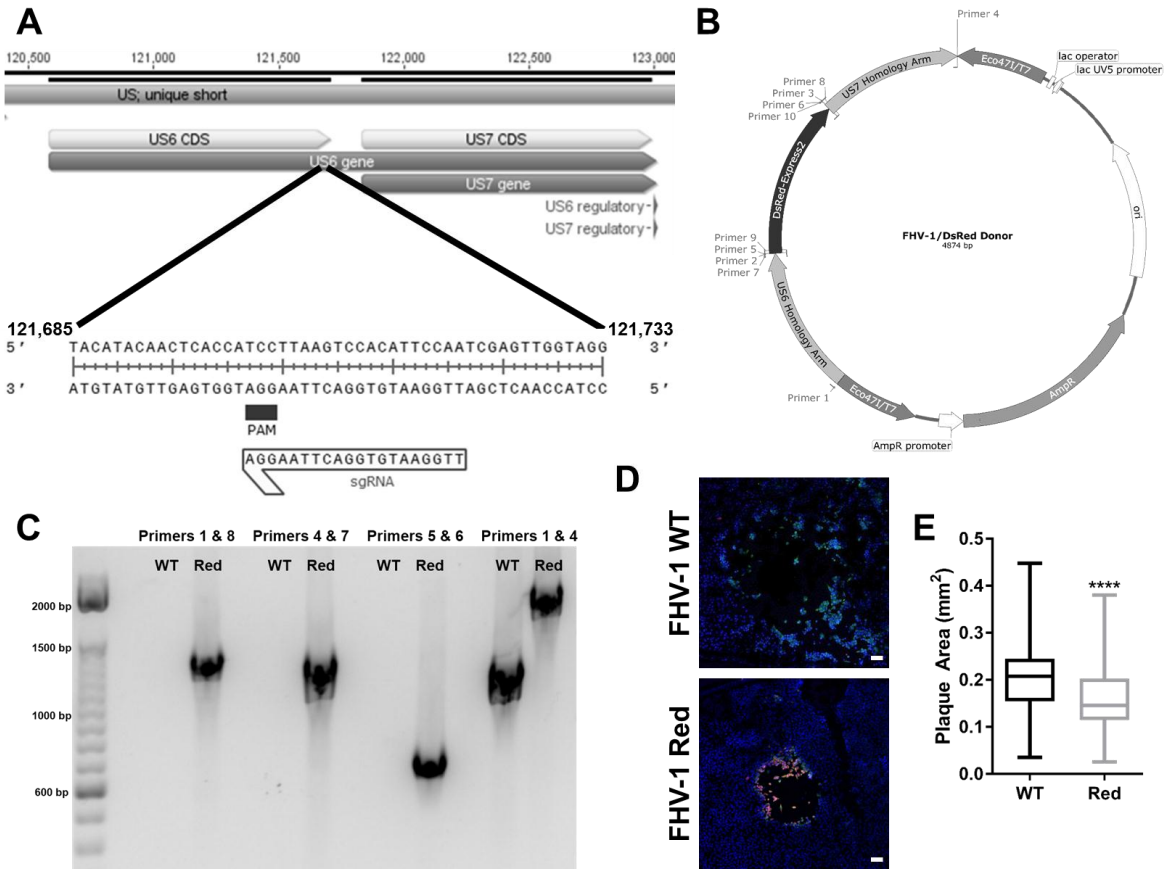

Figure 4.4: Creation, using CRISPR/Cas9 genome engineering, and characterization of FHV-1-gD-DsRed. (A) Schematic representation of the site of introduction for DsRed Express2 at the C terminal end of US6, with the target site and sequence of the guide RNA indicated. **(B)** Schematic map of the pJET1.2-FHV-1-DsRed donor vector showing the FHV-1 homology regions to drive the insertion of DsRed via homology directed repair**. (C)** Confirmation of DsRed Express2 insertion at the targeted location. Four primer sets were used to amplify different regions around the insertion site from WT and edited virus. **(D)** CRFKs were infected with 10 PFU/cover slip with FHV-1-gD-DsRed (red) or WT FHV-1, stained with an anti-FHV-1-antibody (green), and nuclei were counterstained with DAPI (blue). **(E)** Quantification of the area of viral plaques, showing the median value and quartiles. ****, $p<0.0001$.

to WT-infected cells, which started at 8 hpi and remained for the duration of the experiment (Fig. 4.5A(ii)). Similar patterns were also observed in the multi-step growth experiments (Fig. 4.5A(iii) & (iv)). With this growth defective FHV-1-gD-DsRed in hand, we decided to evaluate

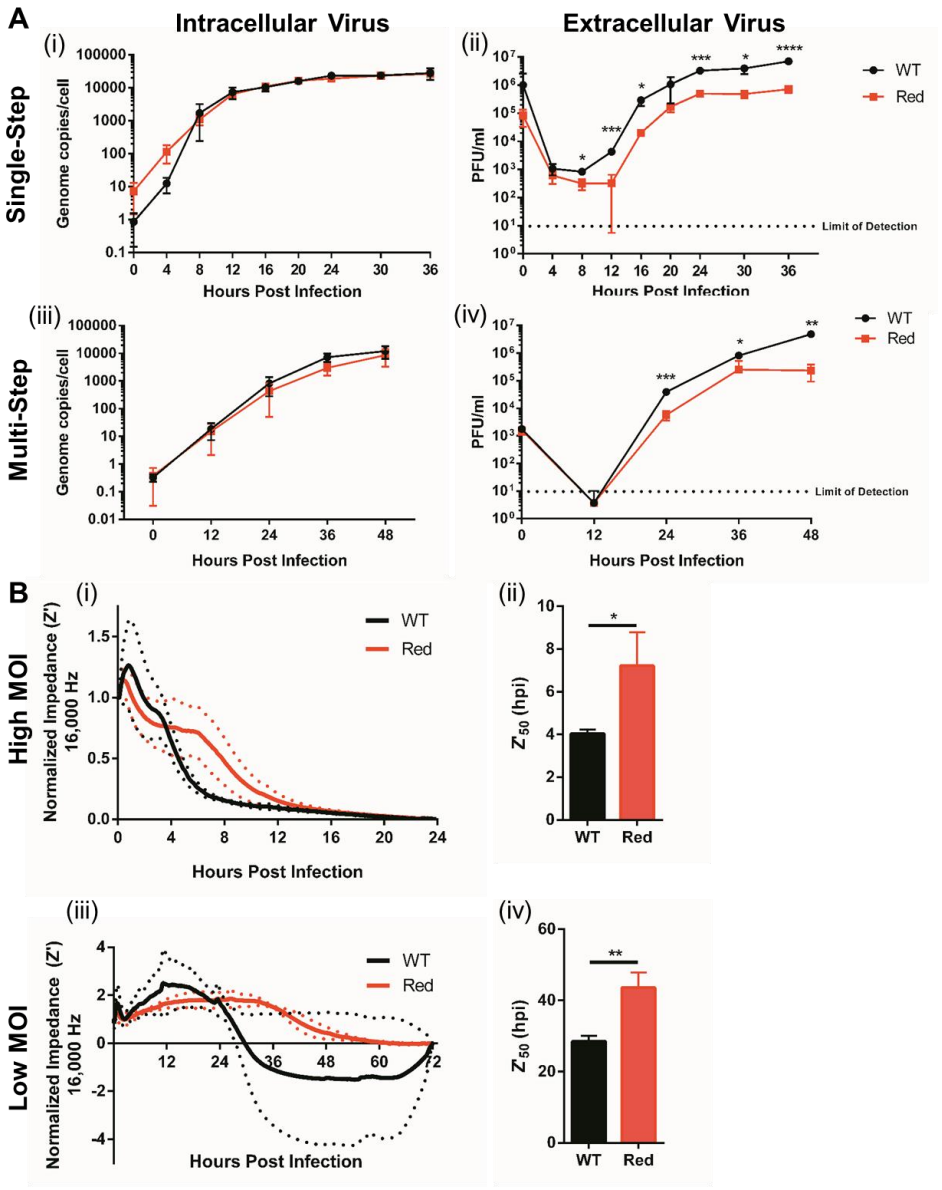

Figure 4.5: ECIS identifies the growth impairments of a recombinant FHV-1. (A) CRFKs were infected with FHV-1-gD-DsRed or WT FHV-1 at an MOI of 3 or 0.01, to measure the single- (i-ii) and multi-step (iii-iv) growth curves, respectively, using conventional viral infectivity assays. qPCR was used to quantify intracellular genomic viral DNA copies and standard plaque assays were used to quantify extracellular virus titers. **(B)** Normalized impedance (Z') values of CRFKs infected with FHV-1-gD-DsRed or WT FHV-1 at a high MOI of 3 (i) or low MOI of 0.01 (iii). Half maximal Z' (Z'_{50}) values for impedance curves based on data from (i) and (iii) were determined (ii and iv, respectively). *, $p < 0.05$; **, $p \leq 0.01$; ***, $p \leq 0.001$; ****, $p \leq 0.0001$.

whether ECIS is capable of detecting similar differences between FHV-1-gD-DsRed and WT FHV-1. To this end, wells with confluent monolayers of CRFK cells were infected with FHV-1 at high (matching the single-step kinetics) and low (matching the multi-step kinetics) MOIs and impedance changes were monitored over time. At both high and low MOIs, a decrease in normalized impedance was observed at earlier time points in WT-infected wells compared to FHV-1-gD-DsRed-infected wells (Fig. 4.5B(i) & (iii)). Z'_{50} values were then calculated to statistically compare the ECIS results obtained with these two viruses and we found significant differences for both high MOI (single-step) experiments, with a half maximal impedance at 4.0 ± 0.2 hpi in WT-infected wells compared to 7.2 ± 1.6 hpi in FHV-1-gD-DsRed-infected wells (Student's T Test, p=0.03) (Fig. 4.5B(ii)), and the low MOI (multi-step) experiments, with a half maximal impedance at 28.5 ± 1.6 hpi compared to 43.6 ± 4.2 hpi (Student's T Test, p=0.004) (Fig. 4.5B (iv)).

However, our current ECIS experiment does not allow us to determine the nature of the growth defect associated with fusion of DsRed to gD. To this end, we conducted conventional plaque size assays. We found that the FHV-1-gD-DsRed produced significantly smaller plaques than WT FHV-1, suggesting that the recombinant virus is impaired in its ability to move from cell-to-cell (Fig. 4.3D-E). DsRed is described to obligatorily tetramerize *in vivo* to form a rather rigid structure (22, 23), likely partially inhibiting the function of gD, to account for this defect.

Taken together, the results from these experiments indicate that ECIS is a useful tool to initially screen and identify differences between the replication kinetics of recombinant and wild type alphaherpesviruses to allow for a more targeted characterization of selected viruses using conventional viral growth assays.

ECIS can be used to calculate the half maximal effective concentration (EC_{50}) of antivirals

Finally, we evaluated if ECIS could be used to calculate the half maximal effective concentration (EC_{50}) of antiviral drugs. We decided to use cidofovir for these experiments, which is a topical nucleoside analogue commonly used to treat FHV-1-induced ocular disease

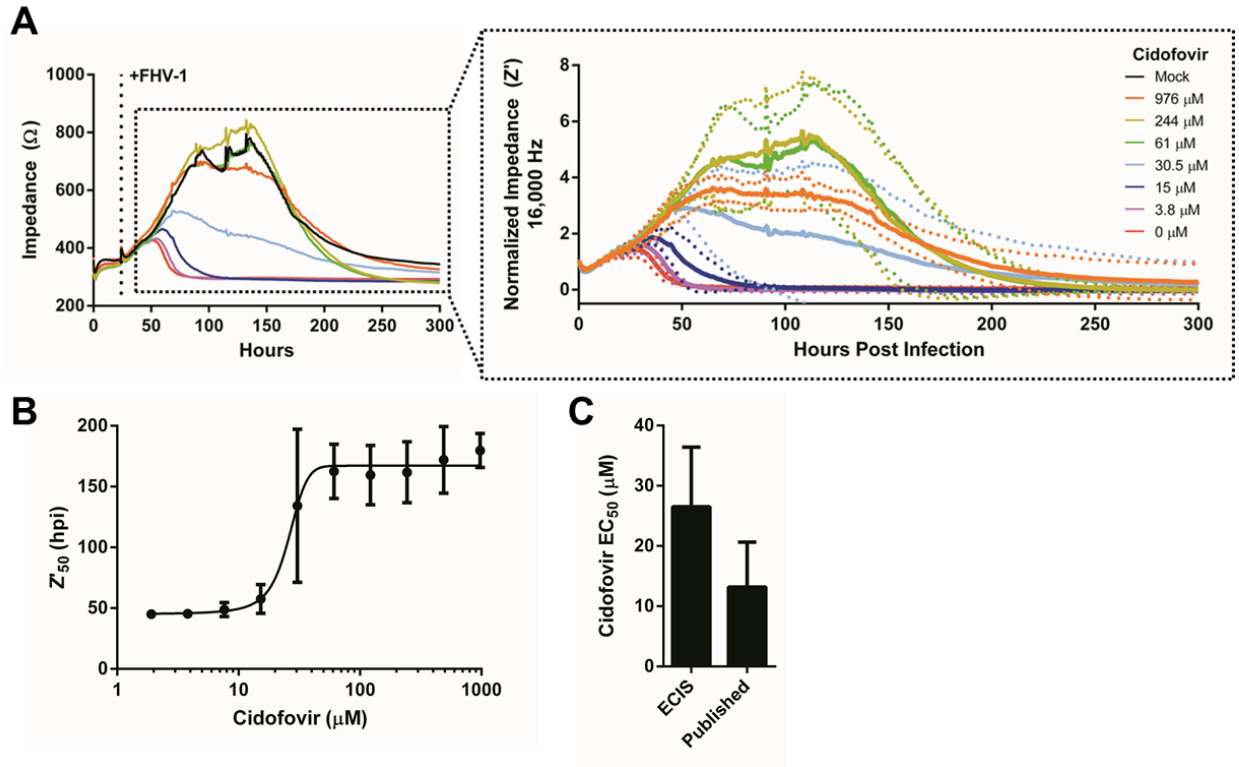

Figure 4.6: ECIS accurately determines the half maximal effective concentration (EC_{50}) of the antiviral cidofovir. (A) CRFKs were infected with MOI=0.01 of FHV-1 and treated with two-fold dilutions of cidofovir (ranging from 976 to 1.9 µM) at 24 h post plating. Non-treated FHV1-infected and mock-infected CRFKs were included as controls. Insert: Normalized impedance values (Z') following FHV-1 infection and cidofovir treatment. For clarity, only Z' for a select set of cidofovir concentrations are shown. **(B)** Dose-response curve of the Z'_{50} value of each cidofovir concentration used to determine the EC_{50} value. **(C)** Comparison of the EC_{50} value of cidofovir as determined by ECIS in the present study to previously published EC_{50} values as determined by standard plaque reduction assays (25–27). No significant difference between ECIS-based and previously published EC_{50} values was observed.

with reported clinical efficacy based on a controlled *in vivo* experimental study (12, 24). We and others have previously determined the EC_{50} of cidofovir against FHV-1 using traditional plaque reduction assays, and found the EC_{50} to range between 7.9 and 21.5 µM (25–27). To determine the EC_{50} using ECIS, CRFKs were infected with FHV-1 at an MOI of 0.01 and treated with decreasing concentrations of cidofovir at the time of infection. Impedance changes were monitored over time until cell death was observed in all wells (Fig. 4.6A). The normalized impedance curves (Fig. 4.6A, insert) were used to calculate the Z'_{50} values for each cidofovir treatment and these values were then used to construct a dose-response curve. The dose-response curve allowed us to compute an EC_{50} value of 26.5±9.9 µM. We found no statistically significant difference between EC_{50} values obtained by ECIS and the conventional plaque reduction assays (Student's T-Test, p=0.13, Fig. 4.6B-C), indicating that ECIS can be used to accurately determine the half maximal effective concentration (EC_{50}) of antivirals. Finally, we determined the half maximal cellular cytotoxicity (CC_{50}) using both ECIS and the conventional 3-(4,5-dimethylthiazol-2-yl)-2,5-diphenyltetrazolium bromide (MTT) cell viability assay. A CC_{50} of 1273±124.7 µM and 1600±97.8 µM was calculated using MTT assays and ECIS, respectively

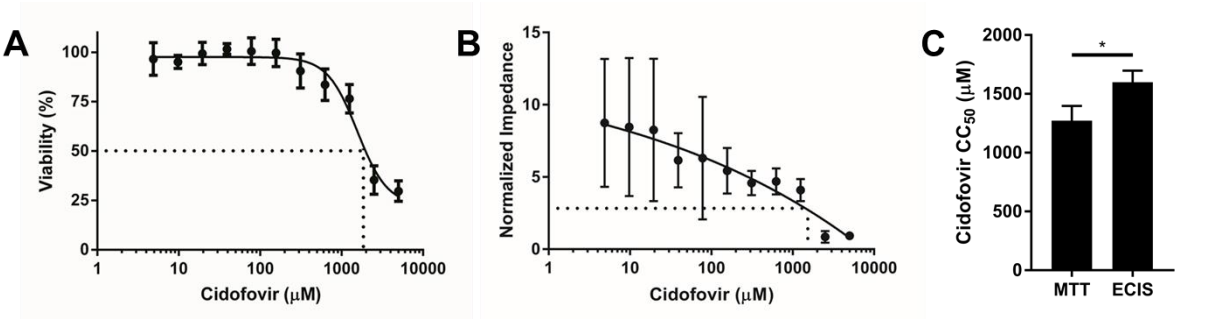

Figure 4.7: Evaluation of cidofovir cytotoxicity. (A) Calculation of cidofovir CC_{50} at 5 days post treatment using MTT cell viability assay. **(B)** Calculation of cidofovir CC_{50} at 3 days post treatment using ECIS. Dotted lines represent the CC_{50} value. **(C)** Comparison of the CC_{50} values determined using both methods.

(Fig. 4.7A&B), and although these numbers were in the same range (between 1000 and 2000 μM), they were found to be statistically significantly different (Fig. 4.7C).

4.4. Discussion

Traditionally, plaque assays or PCR are used to evaluate single- and multi-step growth kinetics of herpesviruses, specifically focusing on factors related to viral entry and cell-to-cell spread, respectively (28). In the present study, we propose electric cell-substrate impedance sensing (ECIS) as a novel tool to study herpesvirus growth kinetics, with the major advantages that ECIS provides an objective quantification in real time, thus avoiding the need for static intermittent sample collection and extensive post-experimental processing. ECIS specifically measures nanoscale changes morphological changes of infected cells, and thus is a more sensitive tool than assessing morphology by light microscopy or by fixing and staining infected cells (1). Here, we demonstrate the utility of ECIS to three specific virological applications. ECIS is likely to be most useful as a supplement to conventional assays or as an initial screening tool before further experimentation. With regards to the latter, ECIS allows for a 96-well plate format, which significantly increases the number of samples that can be run simultaneously when compared to the conventional viral infectivity methodology, and as such, may provide a useful medium-to-high throughput platform for screening purposes related to herpesvirus growth and cellular morphological changes in response infection. Indeed, by our calculation for one 96-well plate, including appropriate controls and replicates, up to 45 individual samples can be run simultaneously.

When taking a closer look at the normalized ECIS data, we consistently observed an early spike in impedance following infection with FHV-1 at different MOIs, and this was also

observed when measuring resistance and capacitance, the latter showing a decreased spike. These fluctuations can partially be explained by the physical manipulation of the cells required to add the virus or control media, which results in temperature and pH changes, as well as the introduction of sheer force. Indeed, a small spike is typically observed following any manipulation of wells in an ECIS experiment and has previously been described in the context of IAV infection (8). However, infection of cells with FHV-1 at high MOIs (i.e. 10 and 1) induced a spike in impedance and resistance, and a drop in capacitance, much larger than the small spike due to manipulation of the wells. To explore the underlying mechanism for these large fluctuations early after infection, we performed several experiments aimed at evaluating changes in (i) cell shape, (ii) movement, and (iii) size of FHV-1-infected cells (data not shown). No dramatic rearrangements of the cytoskeleton of infected cells at early time points post infection could be observed, as assessed by immunofluorescence staining using fluorescently-labeled phalloidin that stains actin, suggesting large scale morphological changes are not the reason for the large spikes. Live cell imaging revealed migration of infected cells starting at several hours post infection, which does not correspond with the time point early after infection when the spikes were recorded by ECIS. Finally, we also evaluated cell size using an established flow cytometry assay (29), based on previous work describing that HSV-1 can induce swelling of infected cells early after infection (30). Using flow cytometry, we did not observe an increase in cell size following infection of cells with high MOIs of FHV-1 in the first four hours of the time course, but in contrast, and to our surprise, we actually observed a decrease in cell size. As ECIS can quantify minute changes in cell shape, size, and movement (1), it is possible that these more conventional methodologies are not sufficiently sensitive to report the changes that we detect via ECIS. Likewise, ECIS analyses of infection with IAV has reported a similar observation

consisting of fluctuations in impedance immediately following infection (8), but without a full understanding of the biological implications underlying this phenomenon, it remains elusive what exactly causes these ECIS changes.

In our current study, we used the ZΘ instrument from Applied BioPhysics, which is a more recent ECIS system that allows for the direct measurement of resistance, representing cell-to-cell interactions, and capacitance, representing cell-to-substrate interactions. Previous models determined impedance using Ohm's Law and were therefore unable to report these values. These individual measurements are valuable as they provide more biological information about the different cellular responses to infection, when compared to impedance analyses alone. In our study with FHV-1, the rates of change between resistance and capacitance were practically identical, indicating that FHV-1 most likely induces structural changes in infected cells, resulting in reduced cell-to-cell contacts and detachment from the culture plate, simultaneous. It will be interesting to evaluate these different parameters in cells infected with other viruses, to get a better idea of the biological relevance of these findings in virus-infected cells beyond the simple formation of CPE. Furthermore, the ZΘ instrument allows for an easy calculation of barrier resistance (Rb), alpha, and membrane capacitance (Cm) values (31). Rb describes the resistivity, an intrinsic property that quantifies how strongly a given material opposes the flow of electric current, of cell-to-cell contacts and, therefore, provides information about the permeability of the monolayer to electrical current flow. Rb is commonly used to assess monolayer integrity of endothelial cells. Alpha is a measure of the constraint on current flow beneath the cells and thus describes changes in the region beneath the cells and Cm represents the average capacitance of the cell plasma membranes (32–34). However, a tight cellular monolayer is essential in order to accurately model these values and since the CRFK cells used in our study did not form a tight

enough monolayer, not even after several days of growth to the point of over-confluency (data not shown), we were unable to model these values. However, other cell lines commonly used for viral infectivity assays, such as Madin Darby Canine Kidney (MDCK) cells, do produce sufficiently tight monolayers to model these values (33). Infecting MDCK with canid alphaherpesvirus 1 (CHV-1), closely related to FHV-1 and also a causative agent of ocular disease similar to HHV-1-induced ocular disease in humans (35), could be used in future ECIS experiments to evaluate these values and determine the biological importance in alphaherpesvirus infections.

We did find a statistically significant difference in the CC_{50} value when calculated by ECIS and the conventional MTT assay. The higher CC_{50} calculated by ECIS is likely due to a difference in the measured variable between the two assays. MTT assays measure the conversion of the substrate to formazan crystals in the mitochondria and thus measures the very early stages of cell death (36, 37). In comparison, ECIS measures morphological changes, more specifically the rounding of cell membranes and detachment from the substrate, which corresponds to later stages of cell death.

Taken together, our data show that ECIS, in conjunction with current methodologies, can be a powerful and valuable complementary tool to monitor viral growth and study the cellular response to alphaherpesvirus infection.

4.5. Methods

Virus, cells and antiviral drug

For this study, the FHV-1 strain FH2CS was used (38). Crandell-Rees Feline Kidney (CRFK) (ATCC) were maintained in cell line media consisting of Dulbecco's Modified Eagle

Medium (DMEM) with 1 g/L glucose, L-glutamine & sodium pyruvate, 10% FBS, and penicillin (200 U/ml)/streptomycin (200 μg/ml), and cultured at 37°C and 5% CO_2. The nucleoside analogue cidofovir, available as a 75 mg/ml intravenous solution (Vistide®; Gilead Sciences, Foster City, CA) was used at concentrations ranging between 1.9 and 976 μM in the EC_{50} experiment and between 4.9 and 5000 μM in the CC_{50} experiment.

Electric cell-substrate impedance sensing (ECIS)

Electric cell-substrate impedance sensing (ECIS) was used to monitor virus- or drug-induced cellular changes as a proxy for cell death in a variety of experiments. To this end, 20,000 CRFKs were plated into triplicate wells of a 96W10idfPET plate (Applied BioPhysics Inc, Troy, NY), which had been pretreated for 15 minutes (min) with 10 mM L-cysteine at room temperature (RT), followed by 30 min with cell line media. Plates were allowed to rest for 30 min at RT prior to incubation and ECIS monitoring, to allow for an even distribution of the cells to the wells. Cells were infected at 24 hpp with FHV-1 at different multiplicities of infection (MOIs), ranging from an MOI of 0.0001 to an MOI of 10, and treated with or without the antiviral cidofovir at different concentrations, depending on the experiment. Mock-infected and cell-free wells were included as controls for all experiments. Capacitance (C) and resistance (R) were measured at the indicated frequencies in a series RC circuit for 24 h using an ECIS Model ZΘ instrument with a 96 well array station (Applied BioPhysics Inc., Troy, NY) and these values were then used to automatically calculate complex impedance (Z). Measurements were taken at the minimal interval time allowed by the plate set up (typically every 5-12 minutes, depending on the number of samples run in an experiment). An additional ECIS 96W10idfPET plate was similarly prepared and images were captured at specified intervals using an Olympus CKX41 microscope

(Center Valley, PA) controlled with Infinity Analyze Version 6.4 software (Lumenera Corporation, Ottawa, Canada) for microscopic analyses.

ECIS Data Analyses

To determine the appropriate frequencies to evaluate impedance (Z), resistance (R), and capacitance (C), the ratio of cell-containing wells to cell-free wells for each parameter was plotted as a function of frequency at 24 hpp, prior to the addition of the virus. The frequency with the greatest difference between the cell-free and sample wells for each parameter was used as the optimal frequency for all further experiments.

Impedance data were normalized (Z') utilizing the following formula:

$$Z' = \frac{Z_x - Z_{end}}{Z_{0\ hpi} - Z_{end}}$$

to normalize the starting impedance at the time of infection ($Z_{0\ hpi}$) to a value of 1 and the final impedance at the end of the experiment (Z_{end}) to a value of 0, scaling the impedance of the intervening time points (Z_x) proportionally. The same formula was also used to normalize resistance (R'). To normalize capacitance (C') following formula was used:

$$C' = \frac{C_x - C_{0\ hpi}}{C_{end} - C_{0\ hpi}}$$

in order to normalize the starting capacitance at the time of infection ($C_{0\ hpi}$) to a value of 0 and the final impedance at the end of the experiment (C_{end}) to a value of 1, scaling the intervening time points (C_x) proportionally. GraphPad Prism (Version 6.04 for Windows) was used to fit the normalized data for each of the three parameters into a sigmoidal, 4 parameter logistic dose-response curve using a least squares fit model and the half maximal normalized impedance (Z'_{50}), resistance (R'_{50}), or capacitance (C'_{50}) were calculated based on this curve. To determine

the EC_{50} of cidofovir, a dose response curve was constructed using the Z'_{50} values and the CC_{50} was calculated similarly.

Creation of DsRed-labeled FHV-1

The FHV-1-gD-DsRed was created using CRISPR/Cas9 genome engineering, based on previously described protocols for editing HSV-1 (18–20). Briefly, the CRISPR plasmid was engineered using the method described by Ran et al (19). The sgRNA forward and sgRNA reverse primers (Table 1) were annealed together and cloned into the pSpCas9(BB)-2A-Puro (PX459) V2.0 vector, a gift from Feng Zhang (Addgene plasmid #62988) (Fig. 4.3A). A donor plasmid was created to drive insertion of the DsRed Express2 gene into the C-terminal end of *US6* by homology directed repair and consisted of a 620 bp virus fragment corresponding to the C-terminus of *US6*, the 675 bp DsRed Express2 gene, and a 605 bp virus fragment corresponding to the *US6* STOP codon, the intergenic region between *US6* and *US7*, and the initial part of the *US7* gene cloned into the pJET1.2 PCR Cloning Vector (ThermoFisher Scientific, Waltham, MA) (Fig. 4.3B). The CRISPR/Cas9 and donor plasmids (1250 ng each) were transfected into confluent CRFK cells using LT1 transfection reagent for 3 days (Mirus Bio LLC, Madison, WI). Transfected cells were selected using 5 µg/ml puromycin in cell line media for 3 days and allowed to recover for 1 week. Next, cells were transfected with an additional 500 ng donor plasmid and simultaneously infected with approximately 6,500 PFU FHV-1. A pure FHV-1-gD-DsRed stock was then obtained by three rounds of limiting dilution assays (28).

Insertion of DsRed into the desired location in FHV-1 was verified by traditional polymerase chain reaction (PCR) and Sanger sequencing at the Cornell University Institute of Biotechnology. Immunofluorescent microscopy was used to verify expression of the DsRed protein in FHV-1-gD-DsRed infected CRFKs, which were counterstained with a mouse

monoclonal anti-FHV-1 (clone FHV7-7C; Bio-Rad, Hercules, CA) and DAPI. WT FHV-infected CRFKs and isotype control antibodies (Abcam, Cambridge, UK) were included as controls. Cells were imaged exactly as previously described (27).

Table 4.1. Primers used in this study to create guide RNAs, donor plasmid, and qPCR plasmid standard.

Primer Name	*Sequence (5'-3')*	*Description*
sgRNA Forward	CACCGTTGGAATGTGGACTTAAGGA	sgRNA to *US6* stop codon
sgRNA Reverse	AAACTCCTTAAGTCCACATTCCAAC	sgRNA to *US6* stop codon
Primer 1	CGGCCCAATTTAATCAAGG	*US6* homology arm, forward
Primer 2	AGGATGGTGAGTTGTATGTA	*US6* homology arm, reverse
Primer 3	GTCCACATTCCAATCGAGTT	*US7* homology arm, forward
Primer 4	AACACCGAAAGGCCAAATAC	*US7* homology arm, reverse
Primer 5	ATGGATAGCACTGAGAACGT	DsRed Express2, forward
Primer 6	TTACTGGAACAGGTGGTGGC	DsRed Express2, reverse
Primer 7	ACTCACCATCCTATGGATAGCACT	*US6*/DsRed overhang, forward
Primer 8	TGGAATGTGGACTTACTGGAACAG	*US7*/DsRed overhang, reverse
Primer 9	AGTGCTATCCATAGGATGGTGAGT	*US6*/DsRed overhang, reverse
Primer 10	CTGTTCCAGTAAGTCCACATTCCA	*US7*/DsRed overhang, forward
US7 Plasmid Standard Forward	CTTTCCGGTCCTGTCTCCAC	qPCR Primer, forward
US7 Plasmid Standard Reverse	GGTTAAATCTTACCCGCAGTGC	qPCR Primer, reverse

Evaluation of FHV-1-gD-DsRed Growth kinetics using conventional viral plaque assays

Viral plaque size assays were performed, exactly as previously described (39), and fifty plaques were captured using an Olympus CKX41 microscope (Center Valley, PA) controlled with Infinity Analyze Version 6.4 software (Lumenera Corporation, Ottawa, Canada). Image J was used to measure the area of each plaque.

Single-step (MOI=3) and multi-step (MOI=0.01) growth kinetic assays were performed, also exactly as previously described (39), except the adsorption period lasted for 2 h. Samples were collected at indicated intervals with cell free supernatant samples used for standard plaque assays (27) and cell lysates used for quantitative PCR (qPCR). For the latter, a standard curve with primers targeting a region in the *US7* gene homology arm was created using the linearized donor plasmid used to create the FHV-1-gD-DsRed virus as template (Table 1). Efficiency of amplification was confirmed to be >98% with R^2= 0.998 and qPCR was performed, as previously described (28). For samples containing high amounts of virus, template DNA was first diluted 1:100 to keep the copy number within the copy number limits of the standard curve. The standard curve was used to interpolate the genome copies, which were expressed as genomes per cell based on the estimation that 5,000 cells contain approximately 30 ng DNA (40).

Cidofovir toxicity assays

The 3-(4,5-dimethylthiazol-2-yl)-2,5-diphenyltetrazolium bromide (MTT) assay was used to assess cidofovir toxicity, similar to as previous described (41, 42). Briefly, 20,000 cells were plated into duplicate wells of a 96-well plate. Cells were treated with 2-fold serial dilutions of cidofovir 24 hpp. At 5 days post treatment MTT, dissolved in DMEM, was added to cells for 1 hour. The resulting formazan crystals were dissolved in an equal volume of the solubilization

solution. The absorbance was then measured spectrophotometrically at 570 nm, was used to construct a dose response curve, and the CC_{50} was determined. Cidofovir toxicity was evaluated by ECIS similar to as previously described (43, 44). Briefly, 20,000 CRFK cells were plated and monitored for 24 hours, as described above. Cells were then treated with 2-fold serial dilutions of cidofovir. At 3 days post treatment, the CC_{50} was calculated based on the normalized impedance.

Statistical Analyses

Data were statistically evaluated by GraphPad Prism (Version 6.04 for Windows) and are expressed as the mean ± standard deviation. On all ECIS graphs, the mean is presented as a solid line and standard deviations are presented as dotted lines. For comparisons of the Z'_{50}, R'_{50}, and C'_{50} values across infection with different MOIs, one-way ANOVAs were performed, followed by a Tukey's honest significant difference (HSD) test to establish significance for the multiple comparisons. For the plaque size assays, normality was first assessed using the Shapiro-Wilks test and significance was then established using a Mann-Whitney U test. All other statistical analysis was performed with Student's T Tests. All experiments were performed 3 times. ECIS experiments were additionally performed with 3 technical replicates per sample. $P < 0.05$ was considered significant.

Acknowledgements

We would like to thank Adam Parks for his helpful discussions in designing the sgRNA and Donald Miller, Brian Wasik, and Lauren Tofano for their technical assistance. We also like to thank the staff of Applied BioPhysics, specifically Catherine Toniatti-Yanulavich, Charles Keese, and Christian Renken, for their support with the ECIS data analyses. This work was funded by a grant from the Cornell University Feline Health Center to G.R. Van de Walle. The

funding agency had no role in study design, data collection and interpretation, manuscript preparation, or the decision to submit the work for publication.

4.6. References

1. Giaever I, Keese CR. 1984. Monitoring fibroblast behavior in tissue culture with an applied electric field. Proc Natl Acad Sci U S A 81:3761–4.
2. Wegener J, Keese CR, Giaever I. 2000. Electric Cell–Substrate Impedance Sensing (ECIS) as a noninvasive means to monitor the kinetics of cell spreading to artificial surfaces. Exp Cell Res 259:158–166.
3. Xu Y, Xie X, Duan Y, Wang L, Cheng Z, Cheng J. 2016. A review of impedance measurements of whole cells. Biosens Bioelectron 77:824–836.
4. Harman RM, Curtis TM, Argyle DJ, Coonrod SA, Van de Walle GR. 2016. A comparative study on the in vitro effects of the DNA methyltransferase inhibitor 5-Azacytidine (5-AzaC) in breast/mammary cancer of different mammalian species. J Mammary Gland Biol Neoplasia 21:51–66.
5. Pennington MR, Curtis TM, Divers TJ, Wagner B, Ness SL, Tennant BC, Van de Walle GR. 2016. Equine mesenchymal stromal cells from different sources efficiently differentiate into hepatocyte-like cells. Tissue Eng Part C Methods 22:596–607.
6. Bussche L, Harman RM, Syracuse BA, Plante EL, Lu YC, Curtis TM, Ma M, Van de Walle GR. 2015. Microencapsulated equine mesenchymal stromal cells promote cutaneous wound healing in vitro. Stem Cell Res Ther 6:66.
7. Kilani MM, Mohammed KA, Nasreen N, Hardwick JA, Kaplan MH, Tepper RS, Antony VB. 2004. Respiratory syncytial virus causes increased bronchial epithelial permeability. Chest 126:186–191.
8. McCoy MH, Wang E. 2005. Use of electric cell-substrate impedance sensing as a tool for quantifying cytopathic effect in influenza A virus infected MDCK cells in real-timeJournal of Virological Methods.
9. Bondu V, Schrader R, Gawinowicz M, McGuire P, Lawrence D, Hjelle B, Buranda T. 2015. Elevated cytokines, thrombin and PAI-1 in severe HCPS patients due to sin nombre virus. Viruses 7:559–589.

10. Mansouri M, Rose PP, Moses A V, Früh K. 2008. Remodeling of endothelial adherens junctions by Kaposi's sarcoma-associated herpesvirus. J Virol 82:9615–28.
11. Gaskell R, Dawson S, Radford A, Thiry E. 2007. Feline herpesvirus. Vet Res 38:337–54.
12. Gould D. 2011. Feline Herpesvirus-1. Ocular manifestations, diagnosis and treatment options. J Feline Med Surg 13:333–346.
13. Stiles J. 2014. Ocular manifestations of feline viral diseases. Vet J 201:166–173.
14. Maes R. 2012. Felid herpesvirus type 1 infection in cats: a natural host model for alphaherpesvirus pathogenesis. ISRN Vet Sci 2012:495830.
15. Opp D, Wafula B, Lim J, Huang E, Lo J-C, Lo C-M. 2009. Use of electric cell-substrate impedance sensing to assess in vitro cytotoxicity. Biosens Bioelectron 24:2625–9.
16. Stolwijk JA, Matrougui K, Renken CW, Trebak M. 2015. Impedance analysis of GPCR-mediated changes in endothelial barrier function: overview and fundamental considerations for stable and reproducible measurements. Pflugers Arch 467:2193–218.
17. Musée J, Mbuy GNK, Woodruff RI. 2002. Antiviral agents alter ability of HSV-2 to disrupt gap junctional intercellular communication between mammalian cells in vitro. Antiviral Res 56:143–51.
18. Suenaga T, Kohyama M, Hirayasu K, Arase H. 2014. Engineering large viral DNA genomes using the CRISPR-Cas9 system. Microbiol Immunol 58:513–522.
19. Ran FA, Hsu PD, Wright J, Agarwala V, Scott DA, Zhang F. 2013. Genome engineering using the CRISPR-Cas9 system. Nat Protoc 8:2281–2308.
20. Russell TA, Stefanovic T, Tscharke DC. 2015. Engineering herpes simplex viruses by infection–transfection methods including recombination site targeting by CRISPR/Cas9 nucleases. J Virol Methods 213:18–25.
21. Arii J, Kato K, Kawaguchi Y, Tohya Y, Akashi H. 2009. Analysis of herpesvirus host specificity determinants using herpesvirus genomes as bacterial artificial chromosomes. Microbiol Immunol 53:433–441.
22. Baird GS, Zacharias DA, Tsien RY. 2000. Biochemistry, mutagenesis, and oligomerization of DsRed, a red fluorescent protein from coral. Proc Natl Acad Sci 97:11984–11989.
23. Vrzheshch P V, Akovbian NA, Varfolomeyev SD, Verkhusha V V. 2000. Denaturation and partial renaturation of a tightly tetramerized DsRed protein under mildly acidic

conditions. FEBS Lett 487:203–8.

24. Fontenelle JP, Powell CC, Veir JK, Radecki S, Lappin MR. 2008. Effect of topical ophthalmic application of cidofovir on experimentally induced primary ocular feline herpesvirus-1 infection in cats. Am J Vet Res 69:289–293.
25. Maggs DJ, Clarke HE. 2004. In vitro efficacy of ganciclovir, cidofovir, penciclovir, foscarnet, idoxuridine, and acyclovir against feline herpesvirus type-1. Am J Vet Res 65:399–403.
26. van der Meulen K, Garré B, Croubels S, Nauwynck H. 2006. In vitro comparison of antiviral drugs against feline herpesvirus 1. BMC Vet Res 2:13.
27. Pennington MR, Fort MW, Ledbetter EC, Van de Walle GR. 2016. A novel corneal explant model system to evaluate antiviral drugs against feline herpesvirus type 1 (FHV-1). J Gen Virol 97:1414–1425.
28. Marconi P, Manservigi R. 2014. Herpes simplex virus growth, preparation, and assay. Methods Mol Biol 1144:19–29.
29. Gröbner S, Lukowski R, Autenrieth IB, Ruth P. 2014. Lipopolysaccharide induces cell volume increase and migration of dendritic cells. Microbiol Immunol 58:61–67.
30. Motamedifar M, Noorafshan A. 2008. Cytopathic effect of the herpes simplex virus type 1 appears stereologically as early as 4h after infection of Vero cells. Micron 39:1331–1334.
31. Giaever I, Keese CR. 1991. Micromotion of mammalian cells measured electrically. Proc Natl Acad Sci U S A 88:7896–900.
32. Lo CM, Keese CR, Giaever I. 1995. Impedance analysis of MDCK cells measured by electric cell-substrate impedance sensing. Biophys J 69:2800–2807.
33. Lo C-M, Keese CR, Giaever I. 1999. Cell–substrate contact: another factor may influence transepithelial electrical resistance of cell layers cultured on permeable filters. Exp Cell Res 250:576–580.
34. Szulcek R, Bogaard HJ, van Nieuw Amerongen GP. 2014. Electric cell-substrate impedance sensing for the quantification of endothelial proliferation, barrier function, and motility. J Vis Exp.
35. Ledbetter EC. 2013. Canine herpesvirus-1 ocular diseases of mature dogs. N Z Vet J 61:193–201.
36. Lobner D. 2000. Comparison of the LDH and MTT assays for quantifying cell death:

validity for neuronal apoptosis? J Neurosci Methods 96:147–52.

37. Fotakis G, Timbrell JA. 2006. In vitro cytotoxicity assays: Comparison of LDH, neutral red, MTT and protein assay in hepatoma cell lines following exposure to cadmium chloride. Toxicol Lett 160:171–177.
38. Walton TE, Gillespie JH. 1970. Feline viruses. VII. Immunity to the feline herpesvirus in kittens inoculated experimentally by the aerosol method. Cornell Vet 60:232–9.
39. Tai S-HS, Holz C, Engstrom MD, Cheng HH, Maes RK. 2016. In vitro characterization of felid herpesvirus 1 (FHV-1) mutants generated by recombineering in a recombinant BAC vector. Virus Res 221:15–22.
40. Butler JM. 2001. Forensic DNA typing: biology & technology behind STR markers. Academic Press, London.
41. Murono S, Raab-Traub N, Pagano JS. 2001. Prevention and inhibition of nasopharyngeal carcinoma growth by antiviral phosphonated nucleoside analogs. Cancer Res 61:7875–7.
42. Wakisaka N, Yoshizaki T, Raab-Traub N, Pagano JS. 2005. Ribonucleotide reductase inhibitors enhance cidofovir-induced apoptosis in EBV-positive nasopharyngeal carcinoma xenografts. Int J Cancer 116:640–645.
43. Xie F, Xu Y, Wang L, Mitchelson K, Xing W, Cheng J. 2012. Use of cellular electrical impedance sensing to assess in vitro cytotoxicity of anticancer drugs in a human kidney cell nephrotoxicity model. Analyst 137:1343.
44. Bennet D, Kim S. 2013. Impedance-based cell culture platform to assess light-induced stress changes with antagonist drugs using retinal cells. Anal Chem 85:4902–4911.

CHAPTER FIVE

THE HIV INTEGRASE INHIBITOR RALTEGRAVIR INHIBITS FELID ALPHAHERPESVIRUS 1 (FHV-1) REPLICATION BY TARGETING BOTH DNA REPLICATION AND LATE GENE EXPRESSION

*Manuscript from: Matthew R. Pennington, Ian E. H. Voorhees, Heather M. Callaway, Shannon D. Dehghanpir, Joel D. Baines, Colin R. Parrish, and Gerlinde R. Van de Walle. 2018. The HIV integrase inhibitor raltegravir inhibits felid alphaherpesvirus 1 (FHV-1) replication by targeting both DNA replication and late gene expression. *Journal of Virology.* In Press.

5.1. Summary

Alphaherpesvirus-associated ocular infections in humans, caused by human alphaherpesvirus 1 (HHV-1), remain challenging to treat due to the frequency of drug application required and the potential for the selection of drug resistant viruses. Repurposing on-the-market drugs is a viable strategy to accelerate the pace of drug development. It has been reported that the human immunodeficiency virus (HIV) integrase inhibitor raltegravir inhibits HHV-1 replication by targeting the DNA polymerase accessory factor and limits terminase-mediated genome cleavage of the human betaherpesvirus 5 (HHV-5). We have previously shown, both *in vitro* and *in vivo*, that raltegravir can also inhibit the replication of felid alphaherpesvirus 1 (FHV-1), a common ocular pathogen of cats with a similar pathogenesis to HHV-1 ocular disease. In contrast to what was reported for HHV-1, we were unable to select for a raltegravir-resistant FHV-1 in order to define any basis for drug action. A candidate-based approach to explore the mode-of-action of raltegravir against FHV-1 showed that raltegravir did not impact FHV-1 terminase function, as described for HHV-5. Instead, raltegravir inhibited DNA replication, similar to HHV-1, but by targeting the initiation of viral DNA replication rather than elongation. In addition, we found that raltegravir specifically repressed late gene expression independent of DNA replication, and both activities are consistent with inhibition of ICP8. Taken together, these results suggest that raltegravir could be a valuable therapeutic agent against herpesviruses.

Importance: The rise of drug-resistant herpesviruses is a long-standing concern, particularly among immunocompromised patients. Therefore, therapies targeting viral proteins other than the DNA polymerase that may be less likely to lead to drug-resistant viruses are urgently needed. Using FHV-1, an alphaherpesvirus closely related to HHV-1 that similarly causes ocular herpes

in its natural host, we found that the HIV integrase inhibitor raltegravir targets different stages of the virus life cycle beyond DNA replication and that it does so without developing drug resistance under the conditions tested. This shows that this drug could prove a viable strategy for the treatment of herpesvirus infections.

Keywords: FHV-1, raltegravir, terminase, ICP8, late gene expression, DNA replication

5.2. Introduction

Alphaherpesviruses are large DNA viruses that cause acute infection of mucosal and epithelial surfaces and which typically establish lifelong latency in neurons. These ubiquitous viruses cause a variety of diseases in many species (1). Human alphaherpesvirus 1 (HHV-1, also known as herpes simplex virus 1) and human alphaherpesvirus 2 (HHV-2, also known as herpes simplex virus 2) are highly prevalent and are associated with cold sores and genital ulceration, respectively (2). In addition, HHV-1 is associated with chronic and recurrent ocular disease, characterized by conjunctivitis, corneal ulceration, and epithelial and stromal keratitis, often leading to corneal scarring and loss of transparency (3). All currently approved therapies for ophthalmologic alphaherpesvirus infection rely on nucleoside analogues that prevent base pairing when incorporated into the growing DNA polymer, thus inhibiting genome replication (4). However, and despite the proven value of these drugs in limiting HHV-1-associated corneal damage, effective treatment of this condition remains challenging due to toxicity concerns, frequency of treatment required, and the potential for selection of drug-resistant variants, especially in immunocompromised individuals (5–8). Furthermore, it has been noted that a small percentage of patients with recurrent ocular herpes do not respond to treatment for unknown reasons (9). These factors may lead to high recurrence rates, resulting in damage to the ocular tissues that may progress to blindness.

Compared with the challenges of bringing a new drug to market, repurposing approved drugs to treat new conditions can accelerate the drug development process and reduce associated costs since the safety and pharmacokinetic profiles of these drugs are already known (10, 11). This strategy has already been used to identify approved therapeutics that, in addition to their on-label use, inhibit viral infection caused by ebolavirus, coronaviruses, and chikungunya virus (12–14).

Raltegravir was approved by the United States Food and Drug Administration in 2007 for the treatment of human immunodeficiency virus (HIV) infection and functions as an integrase inhibitor (15). It specifically binds to an aspartic acid-aspartic acid- glutamic acid (DDE) motif located in the catalytic core domain of HIV integrase to prevent the strand transfer reaction that joins the 3'-processed viral cDNA ends to the host genomic DNA, thus preventing integration (16, 17). The region targeted is structurally homologous to the RNase H domain of eukaryotic recombinases and transposases.

Two studies have explored the potential of using raltegravir as a novel anti-herpesvirus therapy. The terminase protein (pUL89) of human betaherpesvirus 5 (HHV-5, also known as human cytomegalovirus) contains an RNase H-like fold that is structurally similar, including containing a homologous DDE domain, to that of HIV integrase (18). Terminase is highly conserved across the herpesviruses and is responsible for cleaving newly synthesized concatemeric DNA into individual genome segments so that it can be packaged into assembling nucleocapsids. Consequently, herpesviral terminase has been previously proposed as a target for rational drug design and the HHV-5 terminase inhibitor letermovir was recently approved by the United States Food and Drug Administration (19, 20). Raltegravir was shown to inhibit the nuclease function of HHV-5 pUL89 in an *in vitro* plasmid cleavage assay, suggesting it could function by preventing genome cleavage (18). Another group also showed that raltegravir could also inhibit replication of HHV-1, but they mapped its activity to UL42, the DNA polymerase accessory factor, by sequencing a raltegravir-resistant HHV-1 (21). This suggests that raltegravir might be a useful drug for treatment of herpesvirus infection, but that it may function differently depending on the *in vitro* assay used to evaluate functionality and/or the target herpesvirus family or species.

Felid alphaherpesvirus 1 (FHV-1) causes ocular infections in cats and due to the analogous presentation of the diseases in humans and cats, FHV-1 is increasingly being considered to be a useful natural host model of ocular alphaherpesvirus infection (22, 23). Like HHV-1, FHV-1 has similar challenges for successful treatment (24, 25). Our lab has shown previously that raltegravir can inhibit replication of FHV-1, both in cell culture and in an *ex vivo* corneal explant model, to levels comparable to the currently utilized antivirals (26). Furthermore, we recently demonstrated that raltegravir reduces FHV-1 shedding duration and improves clinical outcomes in experimentally infected cats (C.B. Spertus, M.R. Pennington, G.R. Van de Walle, Z.I. Badanes, B.E. Judd, H.O. Mohammed, E.C. Ledbetter, submitted for publication).

The goal of this study was to evaluate the mode-of-action of raltegravir against FHV-1. In contrast to HHV-1, we were unable to select for a raltegravir-resistant FHV-1 for sequencing purposes. We, therefore, used a candidate-based approach guided by the existing literature. We found that raltegravir did not impact FHV-1 terminase function, as described for HHV-5, but instead targeted both DNA replication initiation and late gene expression, a mechanism consistent with inhibition of the functions of the early protein ICP8. Together, this work demonstrates that raltegravir targets multiple stages of the FHV-1 life cycle and does so without developing drug resistance under the conditions tested.

5.3. Results

FHV-1 did not develop raltegravir resistance in vitro

A standard, unbiased approach to identify targets of antiviral drugs, and the one adopted by Zhou *et al.* (21) in the context of raltegravir and HHV-1, is to select for drug resistance, deep sequence the resultant virus, and then identify mutations associated with drug resistance. We

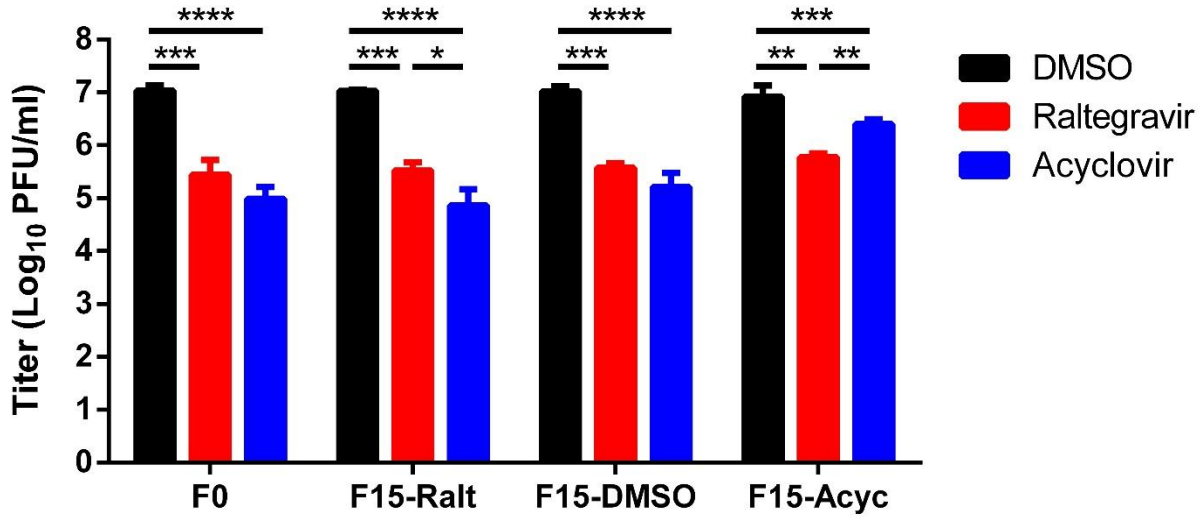

Figure 5.1: Generation of mutant felid alphaherpesvirus 1 (FHV-1) under continuous drug treatment. Wild type (F0) FHV-1 was passaged for 15 passages in the presence of increasing concentrations of raltegravir (F15-Ralt), DMSO (F15-DMSO), or acyclovir (F15-Acyc), and plaque purified. Drug susceptibility was assessed by infecting CRFKs with viruses at a multiplicity of infection (MOI) = 0.01 for 2 h. Inoculum was removed and cells were rinsed with low-pH citrate buffer. Growth media containing DMSO, 500 µM raltegravir, or 160 µM acyclovir was then added. Cells and supernatants were collected together at 48 h post infection (hpi) and viral titers were determined by plaque assay on CRFKs. Significance for each virus was assessed by One-Way ANOVA, with Tukey's HSD post-hoc test; *$p \leq 0.05$; **$p < 0.01$; ***$p < 0.001$, ****$p < 0.0001$.

used a similar methodology to select for a raltegravir-resistant FHV-1 by culturing the virus in increasing concentrations of raltegravir for 15 passages (F15-Ralt). The growth of both the original wild type FH2CS strain of FHV-1 (F0) and the F15-Ralt virus was reduced by approximately 1.5 $\log_{10}$ following raltegravir treatment (Fig. 5.1), indicating that no resistant virus was selected. As expected, we observed no loss of raltegravir susceptibility by repeated passage of the virus in DMSO (F15-DMSO) as a vehicle control (Fig. 5.1). To confirm that our methodology was appropriate, we selected for acyclovir resistance (F15-Acyc) as a positive control. We found that growth of the F0 virus was reduced by approximately 2.1 $\log_{10}$, while

growth of the F15-Acyc FHV-1 was reduced by only 3-fold (Fig. 5.1). Furthermore, no significant differences in the baseline growth between the F0, F15-DMSO, F15-Acyc, or F15-Ralt viruses were noted (One-Way ANOVA, P=0.65). Therefore, although our method was adequate to produce viruses resistant to nucleoside analogs, it did not to select for raltegravir resistance, which is in contrast to what was found for HHV-1 (21).

Nevertheless, we decided to sequence the F0, F15-Ralt, and F15-Acyc viruses, to determine if any single nucleotide polymorphisms (SNPs) resulted from extended passage in the presence of the antivirals. The F0 FH2CS strain exhibited 0.03% sequence divergence in protein coding genes with the C-27 reference strain available in the National Center for Biotechnology Information (NCBI) database (NC_013590.2), in close agreement with the observed low genetic diversity of FHV-1 isolates (27–29). Only 9 SNPs were detected in protein coding genes, 6 conferring synonymous (data not shown) and 3 conferring nonsynonymous mutations, all of which have been previously identified in other FHV-1 isolates (Table 5.1). Extended passage in the presence of raltegravir did not produce any non-synonymous mutations (Table 5.1), consistent with the absence of selection of a raltegravir-resistant virus. More specifically, no mutations were identified in UL42, as had been described previously for raltegravir-resistant HHV-1 (21), or in the FHV-1 terminase (UL15), as proposed for HHV-5 (18). In contrast, passage with acyclovir conferred a single amino acid mutation in UL30, the DNA polymerase (Table 5.1). While acyclovir resistance commonly maps to UL23, the viral thymidine kinase, HHV-1 acyclovir resistant mutants mapping to UL30 have also been well described (30–32). These results further indicate that our methodology was appropriate for identification of drug resistance-associated SNPs for alphaherpesviruses. However, a more targeted approach was necessary to identify the mechanism since FHV-1 did not develop resistance to raltegravir.

Table 5.1: Non-synonymous mutations in protein coding genes associated with drug selection of FHV-1. Wild type FH2CS strain FHV-1 (F0), raltegravir passaged (F15-Ralt), and acyclovir passaged (F15-Acyc) viruses were sequenced on the Illumina platform. F0 was aligned to the C-27 strain FHV-1 reference genome **(**NC_013590.2) and the drug-passaged viruses (F15) were aligned to F0, to identify amino acid changes in protein coding genes.

Gene	Protein	Nucleotide Mutation	Amino Acid Mutation
FH2CS Strain (F0) vs C-27 Reference Strain			
UL29	ICP8 (ssDNA binding protein)	T3265C	S1089P
UL35	Minor capsid protein	T9G	S3R
US7	Glycoprotein I	T494C	M165T
F0 vs F15-Ralt			
No mutations identified			
F0 vs F15-Acyc			
UL30	DNA polymerase	T2167C	F723L

Raltegravir partly inhibits viral DNA replication

As raltegravir had been described previously to target UL42, the DNA polymerase accessory factor, of HHV-1 (21), we decided to first explore the effects of raltegravir on FHV-1 DNA replication using both single- and multi-step growth kinetics. During single-step replication kinetics, we observed a ~1 $\log_{10}$ reduction in viral DNA replication with raltegravir therapy beginning as early as 4 hours post infection (hpi) (Fig. 5.2Ai). However, a slightly larger ~1.5 $\log_{10}$ reduction in the yield progeny virus production was found (Fig. 5.2Aii). Similarly, during multi-step replication, we only observed a ~0.5 $\log_{10}$ decrease in viral DNA replication following

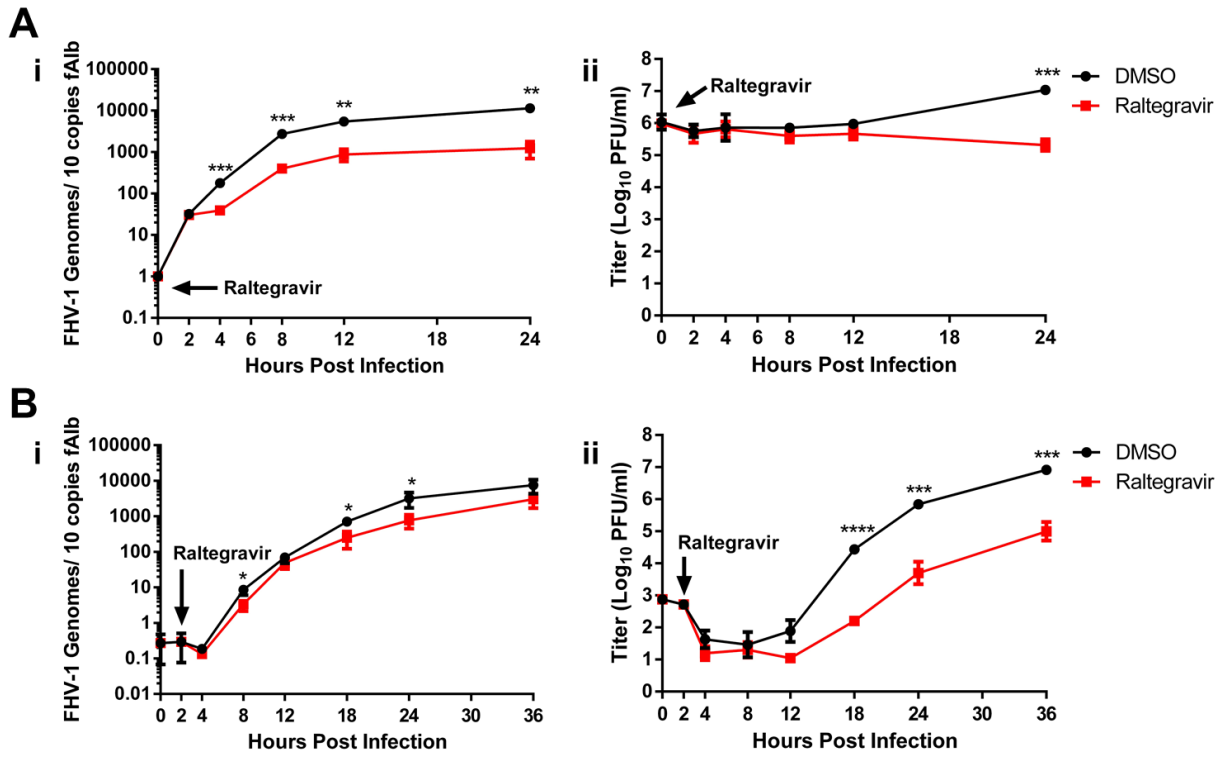

Figure 5.2: Growth kinetics of FHV-1 following raltegravir treatment. **(A)** Single-step growth kinetics. CRFKs were infected with FHV-1, MOI=10, and treated at the time of infection with DMSO or 500 µM raltegravir. **(B)** Multi-step growth kinetics. CRFKs were infected with FHV-1, MOI=0.01, for 2 h. Inoculum was removed, cells were rinsed with low-pH citrate buffer, and media containing DMSO or 500 µM raltegravir was added. Cells and supernatants were individually collected at indicated time points. Virus replication was assessed by qPCR of cellular samples (i) and titration of extracellular virus by plaque assay (ii). Student's T Test, *p≤0.05; **p<0.01; ***p<0.001, ****p<0.0001.

raltegravir treatment (Fig. 5.2Bi), but we observed a more substantial ~3 $\log_{10}$ reduction in the production of fully infectious virus (Fig. 5.2Bii). These results indicate that raltegravir does reduce viral DNA replication, similar to what was described for HHV-1 (21). However, the reduction in viral DNA synthesis was consistently smaller than the reduction in viral yields observed in both the single- and multi-step replication kinetics. We, therefore, hypothesized that raltegravir additionally targeted a second stage of the virus replication cycle, most likely downstream of viral DNA replication.

Raltegravir does not inhibit FHV-1 genome packaging or terminase activity

Based on what was described previously for HHV-5 (18), we next evaluated whether raltegravir could block FHV-1 terminase activity, using two experimental approaches. First, we performed electron microscopy to determine the effects of raltegravir on DNA packaging. This was based on a previous observation that inhibition of terminase activity with letermovir resulted in an accumulation of assembled HHV-5 capsids without DNA in infected cells, as observed by electron microscopy (33). Cells were infected with FHV-1, treated with raltegravir 1 h later, and processed for electron microscopy at 7 hpi. We observed no difference in the number of capsids with or without DNA (data not shown), indicating that viral terminase is most likely not affected. However, we did observe a statistically significant reduction in the total number of cells with viral capsids in raltegravir-treated infected cell cultures when compared to DMSO-treated infected cell cultures (Fisher's exact test, P=0.023, Fig. 5.3Ai) as well as in the average number of capsids per nuclei (Student's T Test, $p<0.01$, Fig. 5.3Aii), indicating that raltegravir likely inhibits a stage at or before capsid assembly.

Second, we biochemically assessed the impact of raltegravir on viral terminase-mediated DNA cleavage. We expressed and purified the C-terminal, nuclease containing, domain of the FHV-1 terminase protein UL15 (pUL15-C). We then performed an *in vitro* nuclease activity assay, using the same protocol as described to assess HHV-1 terminase activity (34), in the presence or absence of raltegravir. When pUL15-C was mixed with a DNA plasmid, cleavage was observed with the production of nicked and linearized products (Fig. 5.3B). When increasing concentrations of raltegravir were added, up to super-physiological concentrations of 10,000 µM, comparable amounts of DNA cleavage were still observed (Fig. 5.3B). As expected, (i) no cleaved DNA plasmid was observed in the absence of pUL15-C and (ii) plasmid DNA was fully

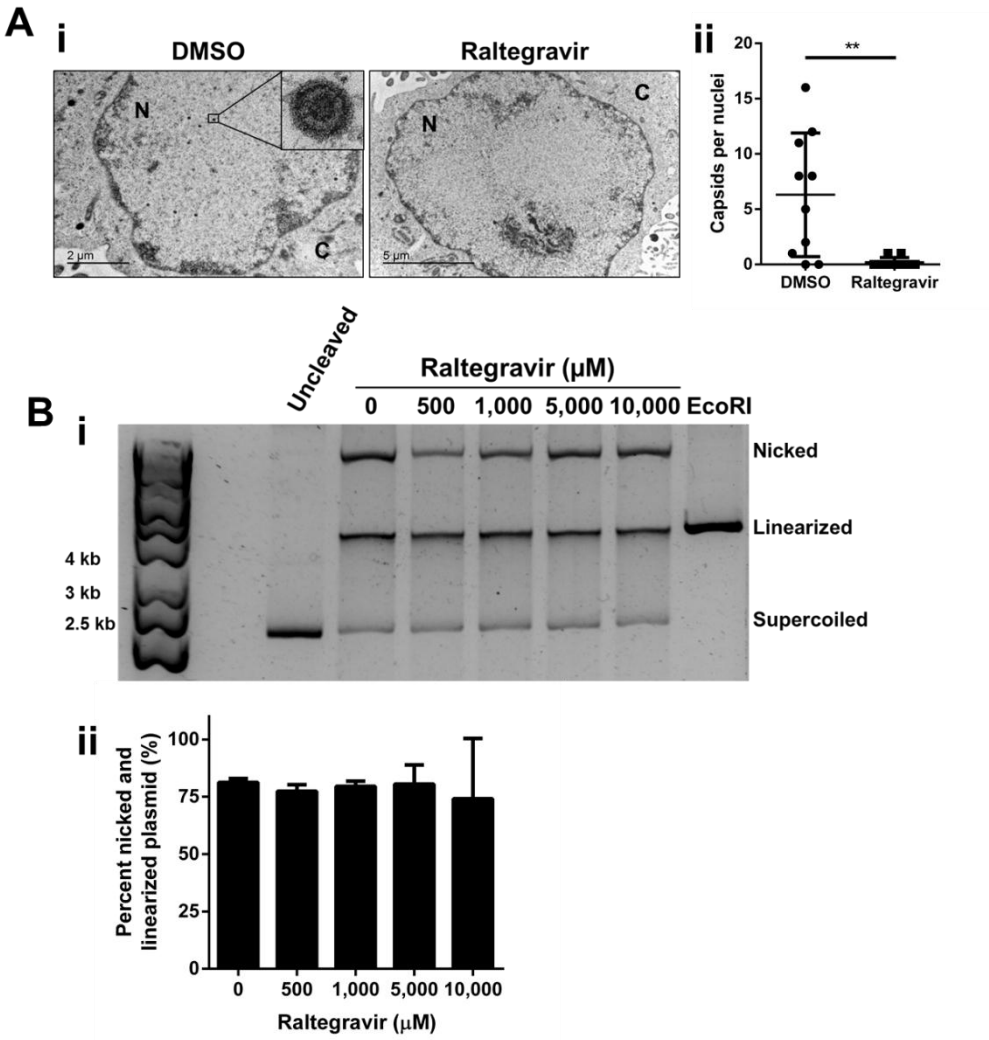

Figure 5.3: Raltegravir does not block terminase-mediated genome cleavage. (A) Electron microscopy. CRFKs were infected with FHV-1, MOI=3 for 1 h, treated with DMSO or 1000 µM raltegravir, and processed for imaging at 7 hpi. Representative electron microscopy images assessing FHV-1 capsid formation are shown. Red boxes indicate FHV-1 nucleocapsids. N, nucleus; C, cytoplasm (i). Quantification of the average number of capsids per nuclei (ii). Student's T Test, **$p<0.01$. **(B)** Biochemical assessment of terminase inhibition. Recombinant FHV-1 pUL15-C was mixed with the pET-20b(+) plasmid and increasing concentrations of raltegravir. Uncleaved and EcoRI cleaved plasmids were included as controls. Following digestion for 1 h at 37°C, products were separated by agarose gel electrophoresis to identify plasmid cleavage. Representative gel (i) and quantification of percentage of nicked and linearized plasmid (ii).

linearized when treated with EcoRI (Fig. 5.3B). These results indicate that raltegravir does not inhibit FHV-1 terminase-mediated genome cleavage, in contrast to what has been described for HHV-5 (18).

Raltegravir inhibits the early stages of DNA replication

It has previously been shown that XZ45, a hydrazide HIV-integrase inhibitor that also targets the RNase H-like fold of integrase, can inhibit the replication of alpha, beta, and gammaherpesviruses (35). For HHV-1, this compound was proposed to target the early protein ICP8. ICP8 is a multifunctional viral protein essential for viral replication. It is required for DNA replication as a single-stranded DNA (ssDNA) binding protein and, plays a role in the initiation of DNA replication in conjunction with the origin binding protein UL9 (36–40). It also has a separate role in the initiation of late gene expression (41, 42) and is thought to be important for viral recombination (43). Interestingly, ICP8 is also known to contain an RNase H-like domain homologous to that of HIV integrase (35). We therefore hypothesized that raltegravir could target FHV-1 ICP8.

However, we first needed to address the observed point mutation in ICP8 of FH2CS, the FHV-1 strain used in the present study, compared to the reference strain C-27 (Table 5.1). CRFK cells were infected with either virus strain, treated with raltegravir or DMSO control, and viral titers were determined by plaque assay. As determined by One-Way ANOVA with Tukey's HSD post-hoc test, no difference in the susceptibility to raltegravir was found between FH2CS and C-27. Furthermore, there were no differences in virus production at baseline levels between these strains, indicating that this mutation does not affect virus viability or drug susceptibility (Fig. 5.4).

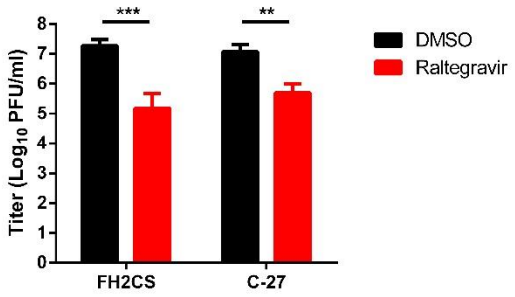

Figure 5.4: Raltegravir is similarly effective against the FHV-1 strains FH2CS and C-27. CRFKs were infected with the FHV-1 strain FH2CS or C-27, MOI=0.01, for 2 h. Inoculum was removed, cells were rinsed with low-pH citrate buffer, and media containing DMSO or 500 µM raltegravir was added. Cells and supernatants were collected together at 48 hpi and viral titers were determined by plaque assay on CRFK cells. Student's T test, **p<0.01; ***p<0.001.

Raltegravir could inhibit DNA replication via ICP8 by either interfering with its ability to bind ssDNA or to initiate DNA synthesis. In order to test the effects of raltegravir on ICP8 ssDNA binding, we recombinantly expressed FHV-1 ICP8. Utilizing an electromobility shift assay, we found that raltegravir did not interfere with ICP8's ability to bind ssDNA, except at high concentrations (Fig. 5.5A). We observed a similar reduction on ssDNA binding when a volume matched amount of DMSO was added, indicating that this reduction is likely due to the effects of the vehicle, rather than the drug itself (Fig. 5.5A). These results indicate that raltegravir likely does not affect ICP8 ssDNA binding, in line with what has been reported previously for the activity of XZ45 against HHV-1 (35).

Next, we sought to determine if raltegravir inhibits the initiation of DNA replication, which requires ICP8. Since ICP8 is essential for viral replication, it is not possible to create viable mutant viruses deficient of the complete protein. We, therefore, adapted a previously described polymerase pausing experiment (44) to address our question indirectly. Briefly, cells were infected and treated with a high dose of phosphonoacetic acid (PAA) for 12 h. Since PAA inhibits DNA replication via inhibition of the DNA polymerase, this results in the initiation of

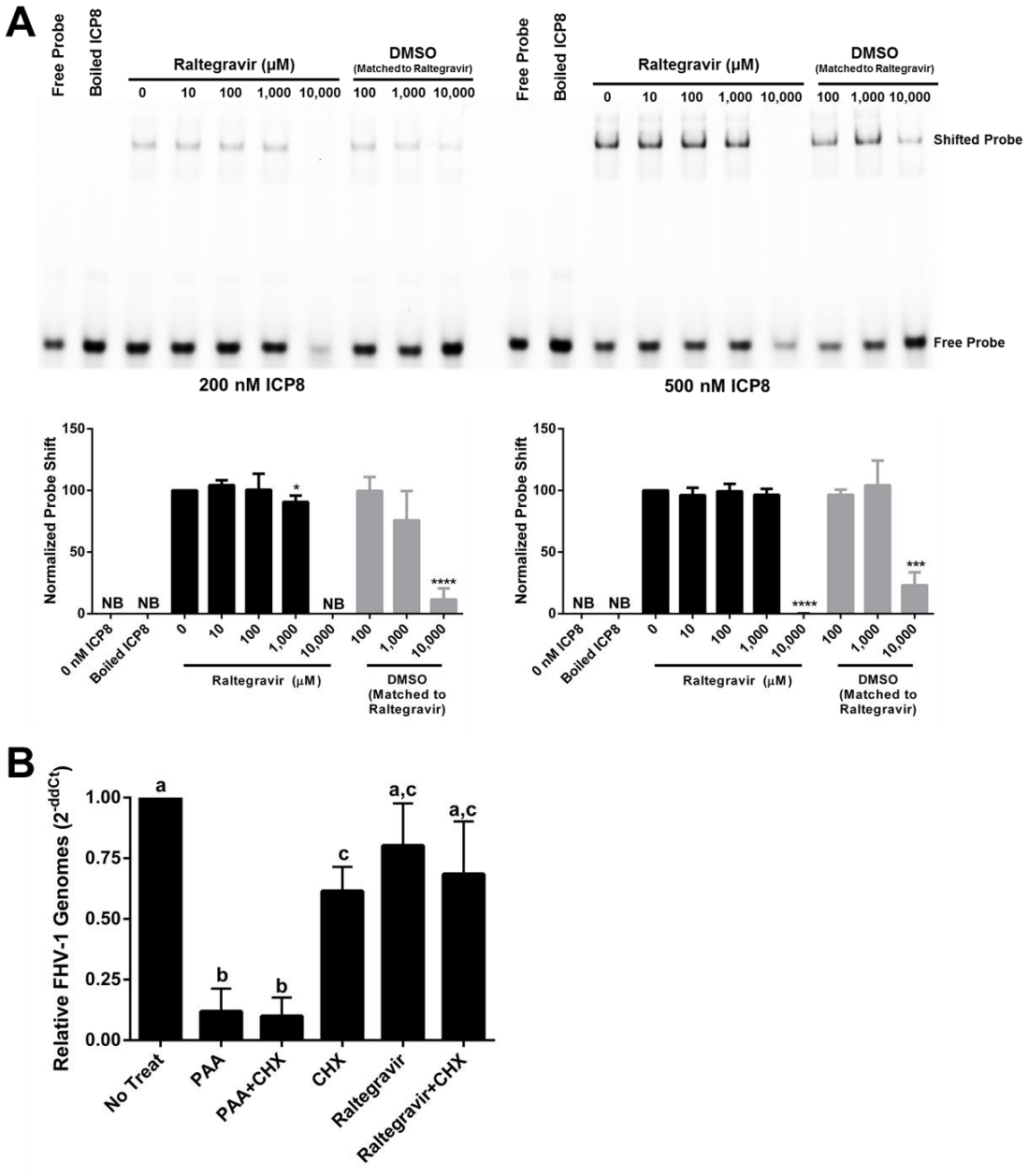

Figure 5.5: Raltegravir inhibits an early stage of DNA replication, consistent with ICP8 inhibition. **(A)** Raltegravir does not block ICP8 single stranded DNA binding activity. Recombinant FHV-1 ICP8 (200 or 500 nM) was mixed with a Cy3-labeled ssDNA probe and increasing concentrations of raltegravir or volume-matched amounts of DMSO for 1 h at 37°C. ICP8-bound and unbound probes were resolved by native PAGE electrophoresis and the percent of shifted probe, normalized to the 0 μM raltegravir samples, was calculated. Student's T test, comparing each concentration to 0 μM raltegravir; *p<0.05; ***p<0.001;

Figure 5.5 continued. ****p<0.0001. **(B)** Raltegravir inhibits an early stage of viral DNA replication. CRFKs were infected with FHV-1, MOI=2, for 12 h and treated at the time of infection with 100 µg/ml PAA to allow for the initiation of DNA replication, but not strand elongation. Inoculum and PAA were removed and replaced with cell line media containing no drugs, 100 µg/ml PAA, 100 µg/ml PAA with 50 µg/ml CHX, 50 µg/ml CHX, 500 µM raltegravir, or 500 µM raltegravir with 50 µg/ml CHX. Cells were cultured for an additional 16 h, at which point they were collected and processed for relative genome replication using qPCR. Significantly different groups ($p<0.05$), as determined by One-Way ANOVA with Tukey's HSD post-hoc test, are indicated using superscript letters.

DNA replication but not DNA elongation, thereby effectively "pausing" DNA synthesis at this stage (45). The PAA block was then released by washing away this drug. The following fresh drugs were then added: (i) PAA, to continue to inhibit DNA elongation, (ii) cycloheximide (CHX), to allow for DNA elongation but not cellular or viral protein translation, (iii) raltegravir, to determine its effects, or (iv) combinations of these drugs (Fig. 5.5B). Genome replication was assessed by qPCR for each of these conditions and normalized to cells that were left untreated after PAA removal in order to permit full viral replication. As expected, PAA continued to effectively inhibit genome synthesis, both when given alone and in combination with CHX (Fig. 5.5B). CHX, in contrast, only minimally affected genome synthesis when given after DNA replication was initiated (Fig. 5.5B). Similarly, we found that raltegravir, both alone and in combination with CHX, did not affect genome replication (Fig. 5.5B). As raltegravir no longer inhibited genome replication following release of the PAA block, this indicates that it must impact DNA replication at an early stage, prior to DNA elongation. This is consistent with an inhibition of ICP8 activity during the initiation of DNA synthesis and inconsistent with an effect on polymerase processivity, as was proposed previously for HHV-1.

Raltegravir specifically downregulates late gene expression, independent of DNA replication

In addition to its known roles in DNA replication, ICP8 also independently stimulates transcription of at least three late genes, gC, gD, and UL47 (41, 42). To determine the effects of raltegravir on FHV-1 gene expression, we adopted a similar methodology as was used to originally define the effects of ICP8 on late gene expression (41, 42). To this end, cells were infected at a high multiplicity of infection (MOI), treated with raltegravir, and collected at 6 hpi for qRT-PCR analysis. We observed a ~50% reduction in viral genome replication (Fig. 5.6A), which is similar to what we observed previously in the single-step growth kinetics (Fig. 5.2Bi). At this time point, we found that raltegravir had no effect, or drove a slight upregulation, of immediate early genes (Fig. 5.6B), consistent with inhibition of viral DNA replication. We also observed no effect, or only a slight downregulation, of the two early genes that we tested, including ICP8 itself. In contrast, we observed a significant downregulation of 7 out of the 9 late genes that we assessed, including gC and gD (Fig. 5.6B). To determine if the downregulation of late genes was (i) a direct consequence of the reduction in DNA replication, as expression of late genes is known to be partially dependent on DNA replication (46), or (ii) an independent effect on late gene expression specifically, we repeated this experiment using PAA instead of raltegravir, an approach which was used previously to define the roles of ICP8 during HVV-1 replication (41, 42). When treating infected cells with PAA, using a concentration that we previously determined resulted in a similar level of inhibition of FHV-1 genome replication compared to raltegravir (47), we did not observe a downregulation of any of the tested genes (Fig. 5.6C). Next, we wanted to confirm this downregulation of late gene expression in raltegravir-treated FHV-1-infected cells on a protein level. However, since monoclonal antibodies targeting single FHV-1 proteins are not commercially available, we utilized a

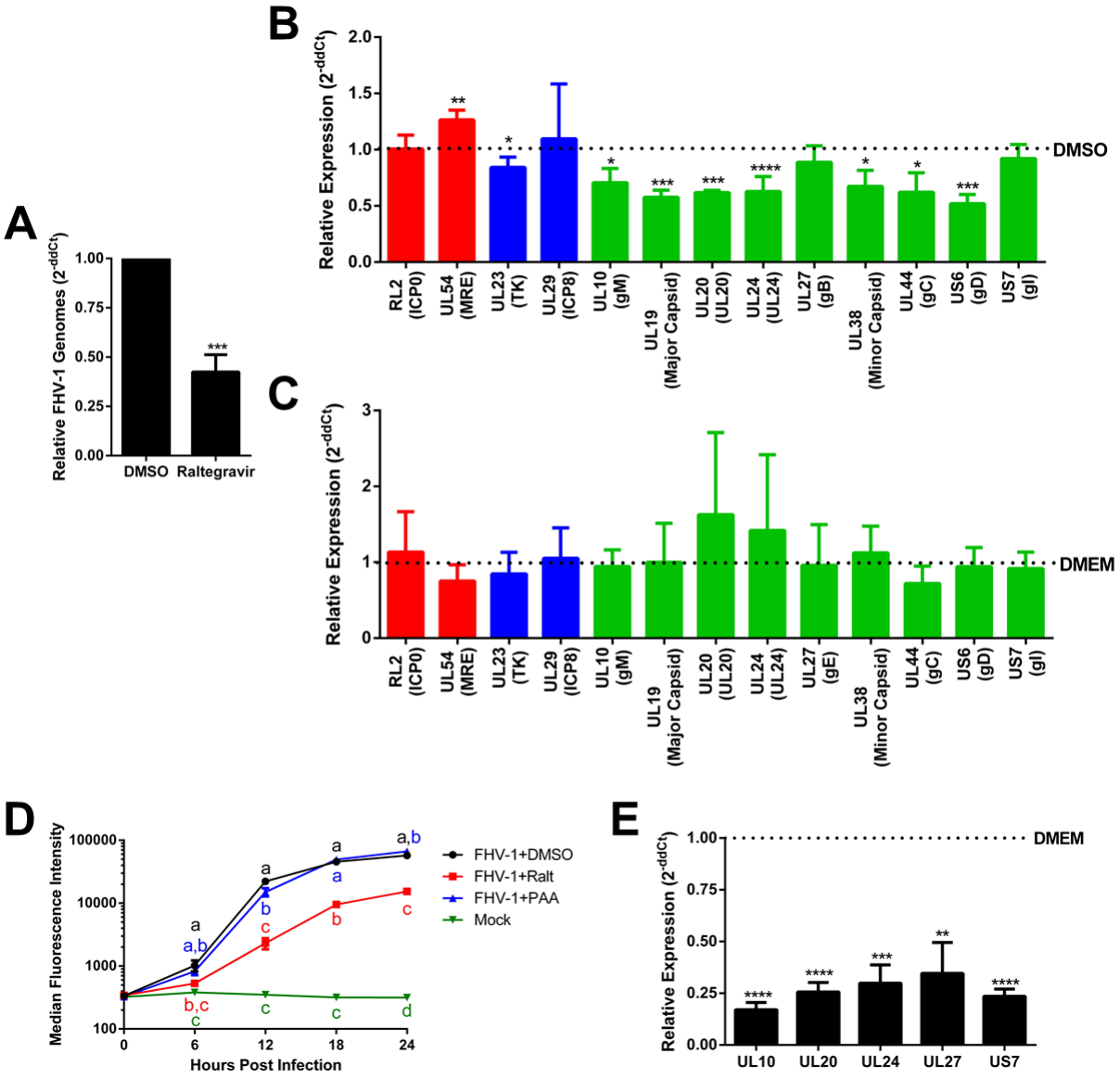

Figure 5.6: Raltegravir specifically inhibits late gene expression, consistent with ICP8 inhibition. Primary feline corneal epithelial cells (FCECs) were infected with FHV-1, MOI=10, and treated at infection with 500 µM raltegravir, 12.5 µg/ml PAA, or indicated vehicle control. Cells were collected at 6 hpi for analysis. **(A)** Relative viral genomic DNA replication following raltegravir treatment, as determined by qPCR. **(B-C)** Relative expression of immediate early (red), early (blue), and late (green) viral genes. Relative gene expression, as determined by qRT-PCR, following raltegravir (B) and PAA (C) treatment. Student's T Test. **(D)** Flow cytometric analysis of glycoprotein D (gD) protein expression. FCECs were infected with FHV-1-gD-DsRed, MOI=3, and treated at the time of infection

Figure 5.6 continued. with DMSO, 500 µM raltegravir, or 12.5 µg/ml PAA, or left uninfected. At indicated time points, cells were collected and analyzed by flow cytometry. Significantly different groups ($p<0.05$), as determined by One-Way ANOVA with Tukey's HSD post-hoc test, are indicated using superscript letters. **(E)** Treatment with phosphonoacetic acid (PAA) inhibits late gene expression. FCECs were infected with FHV-1, MOI=10, and treated at the time of infection with 200 µg/ml PAA. Cells were collected at 6 hpi, RNA was isolated, and expression of select late genes relative to DMEM treated controls was assessed by qRT-PCR. Student's T Test. *$p\leq0.05$; **$p<0.01$; ***$p<0.001$,

recombinant FHV-1 virus expressing the DsRed Express2 fluorophore fused to the C-terminus of glycoprotein D (FHV-1-gD-DsRed) (48). This virus was suitable for these experiments as gD expression was found to be downregulated by raltegravir, but not PAA, treatment (Fig. 5.6B-C). Similar to the mRNA expression results, we found gD protein expression to be reduced upon raltegravir treatment (Fig 5.6D). In contrast, gD protein was produced at approximately the same rate in PAA-treated infected cells compared to DMSO-treated control cells (Fig. 5.6D). To confirm that PAA (i) can indeed result in reduced late gene expression upon reducing DNA replication and (ii) was functioning properly in our hands, we treated FHV-1-infected cells with 200 µg/ml PAA, which previously was shown to inhibit FHV-1 DNA replication by over 99% (47), and defined the expression of a subset of late genes. Using this dose, FHV-1 late gene expression was decreased to approximately 25% of that of untreated controls (Fig. 5.6E), which is in close agreement to what has been described for HHV-1 treated with PAA (49). Collectively, while raltegravir also inhibited viral DNA replication, these results support a mechanism involving a further specific inhibition of late gene expression by raltegravir. This appeared to proceed through a mechanism independent of the observed direct effect on inhibiting DNA replication as treatment with a comparable dose of PAA did not inhibit late gene expression. This further supports a mechanism by which raltegravir inhibits known functions of ICP8.

5.4. Discussion

The goal of this present study was to evaluate the mode-of-action of the HIV integrase inhibitor raltegravir against FHV-1, an alphaherpesvirus closely related to HHV-1 that also causes severe ocular disease. In contrast to previous studies reporting that raltegravir inhibits terminase-mediated genome cleavage of HHV-5 (18) and DNA replication of HHV-1 via interference with the DNA polymerase accessory factor (21), we propose that raltegravir targets the ICP8 protein of FHV-1, similar to the hydrazide-based integrase inhibitor XZ45 (35). Both ICP8 and HIV integrase belong to the DDE recombinase class of enzymes that coordinate divalent metal cations in their active sites within an RNase H-like fold (18, 50). Their shared domains, therefore, suggests a structural basis for an interaction between raltegravir and ICP8.

Functionally, ICP8 is required for viral replication and has at least four well-defined roles in the life cycle of alphaherpesviruses. The centrality of this protein in viral replication may explain why we were unable to select for raltegravir resistance. Indeed, it may be difficult to introduce mutations in such a vital protein without loss of functionality. First, ICP8 was originally identified as the primary ssDNA binding protein, binding in a non-sequence-specific manner to stabilize the open replication forks during DNA replication (36, 51). Similar to XZ45, we found that raltegravir did not inhibit the ability of ICP8 to bind ssDNA. Second, ICP8 has been shown to interact with and stimulate the helicase activity of UL9, the origin binding protein, to mediate the initiation of DNA replication (52). These proteins accumulate at the origins of replication on the viral DNA (53), and it is thought that ICP8 binds to an inhibitory region of UL9, thereby acting as a positive regulator to neutralize this region and increase the efficiency of the UL9-mediated DNA opening (54). Using a DNA polymerase pausing assay (44), we observed that raltegravir specifically inhibited an early stage of DNA replication prior to processive DNA

elongation mediated by the DNA polymerase and its accessory factor. It is possible that this early stage inhibition is due to raltegravir blocking the ability of ICP8 to either bind to or activate UL9 helicase activity, although additional experiments are needed to study this. Moreover, this result does not exclude the possibility that ICP8 impacts other proteins necessary for DNA replication initiation, including UL9, the helicase and/or the primase. Third, it has been shown that ICP8 mediates the transcription of at least three late genes, gC, gD, and UL47, via a DNA replication-independent mechanism thought to involve interactions with other viral and host proteins (42). Consistent with this, we found that raltegravir treatment resulted in a reduction of many late genes, including both gC and gD gene transcripts, independent of DNA replication, and we confirmed this for gD on a protein level. Similar to our results, XZ45 was also shown to reduce gC protein expression in HHV-1-infected cells, consistent with inhibiting ICP8 function (35). Although it has not been determined which additional late genes may depend on ICP8, our results suggest that gM, UL19, UL20, UL24, and UL38 may also be transcriptionally regulated directly or indirectly by ICP8. Consistent with the known activity of ICP8 (42), raltegravir appeared to exhibit no preference towards ɣ1 or ɣ2 genes as both gD, a model ɣ1 (55), and gC, a model ɣ2 gene, were downregulated following treatment. Fourth, it has been shown that ICP8, either by itself or in combination with the UL12 exonuclease can mediate strand invasion to promote homologous recombination (56, 57). It has been suggested that alphaherpesvirus DNA replication may involve a recombination-dependent replication stage due to the presence of genome concatemers that form complex structures and inversion of the L and S genome segments (39). The precise mechanisms by which this relates to DNA replication remain poorly understood, although it has been proposed that the strand-invasion activity mediates the transition from theta form replication to rolling circle DNA synthesis (35, 58). While we did not

investigate the effects of raltegravir on viral recombination during FHV-1 infection, XZ45 was shown to inhibit HHV-1 recombination both *in vitro* and during viral co-infections (35). It is, therefore, tempting to speculate that raltegravir may also inhibit viral recombination, further leading to the observed inhibition of DNA replication.

For HHV-1, it was found that raltegravir resistance mapped to a V296I mutation in UL42, the DNA polymerase accessory factor (21). It was hypothesized that the drug might block the interaction of UL42 with other components of the replication complex (i.e. DNA polymerase, helicase, and primase) based on the position of this mutation in the protein. Raltegravir reduced the gDNA replication by ~50% of a recombinant HHV-1 bearing this UL42 mutation, compared to a ~80% reduction with wild-type HHV-1. Based on this, the authors concluded that they were unable to exclude the possibility that additional viral proteins were affected by the drug, leaving open the possibility that raltegravir may also affect HHV-1 ICP8 function. Likewise, we cannot rule out some interference of raltegravir with the functions of FHV-1 UL42, contributing in part to the observed inhibition of DNA replication in raltegravir-treated, FHV-1-infected cells.

A screen of HIV RNase and integrase inhibitors revealed that synthetic α-hydroxytropolones are also effective against HHV-1 and HHV-2, further highlighting the value of and interest in using HIV inhibitors against herpesviruses (59). These compounds were also initially hypothesized to inhibit either ICP8 or the nuclease function of HHV-1 terminase, based on the structural homology of these proteins with the RNase H-like folds in HIV proteins (60). The effects of these compounds on HHV-1 ICP8 function were not explored. However, when their effects on HHV-1 pUL15-C-mediate DNA cleavage were investigated, it was found that the compounds that strongly inhibited HHV-1 replication had little effect on pUL15-C activity *in vitro* (60). These results are consistent with our observation that raltegravir inhibited FHV-1

replication without apparent effects to pUL15-C activity. It was also recently reported that these α-hydroxytropolones could inhibit the replication a range of alphaherpesviruses, including FHV-1 (61). They demonstrated that these compounds inhibited HHV-1 DNA replication rather than genome cleavage, similar to our observations with raltegravir. Three proteins were noted to possess either RNase H-like domains or activity that the compounds could target to account for these effects: UL30, the DNA polymerase, UL12, the alkaline nuclease, and ICP8. However, neither the effect of these compounds specifically on these proteins nor their effects on FHV-1 DNA replication and protein expression were evaluated, leaving this an open question. Raltegravir, likewise, could have theoretically also impacted UL30 or UL12 function. However, our results from the DNA polymerase pausing experiment (Fig. 5.5B) and gene expression results (Fig. 5.6A-C) are inconsistent with raltegravir affecting only UL30 and/or UL12 and are consistent with inhibition of the multiple functions of ICP8. Nevertheless, effects on the RNase H activity of UL30 and/or UL12, in addition to the effects on ICP8, cannot be excluded.

Taken together, this study adds the body of literature that suggests that HIV integrase inhibitors can also be useful in the treatment of herpesvirus infections. More specifically, no approved inhibitors of ICP8 exist today and, to our knowledge, no inhibitors other than XZ45 are in development with experimentally-supported inhibitory activity against ICP8. As such, repurposing raltegravir to inhibit ICP8, either alone or in combination with traditional nucleoside analogues, may be a novel strategy to treat herpesvirus infections.

5.5. Methods

Cells, viruses, and drugs

Crandell Rees feline kidney cells (CRFKs) (American Type Culture Collection) were maintained in cell line medium consisting of Dulbecco's Modified Eagle Medium (DMEM) with 1 g/L glucose, L-glutamine, and sodium pyruvate, supplemented with 10% fetal bovine serum, and penicillin (200 U/ml)-streptomycin (200 µg/ml). Primary feline corneal epithelial cells (FCECs) were isolated from specific pathogen free cats euthanized for reasons unrelated to the current study and cultured as previously described (47, 62). Cell lines were maintained at 37°C and 5% CO_2. The FHV-1 strain FH2CS (63) was used for all experiments, and compared with the FHV-1 strain C-27 (64) for sequencing and drug susceptibility purposes. For flow cytometry, a recombinant FH2CS FHV-1 strain (FHV-1-gD-DsRed) was used, which we generated in house using CRISPR/Cas9 genome engineering to express DsRed Express 2 fused to the C-terminal end of glycoprotein D (48). All viral stocks were grown and titered on CRFKs, as previously described (26). Raltegravir (ChemieTek, Indianapolis, IN) and acyclovir (Sigma-Aldric, St. Louis, MO) were diluted in DMSO. Phosphonoacetic acid (PAA) and cycloheximide (CHX) (Sigma-Aldrich) were both diluted in DMEM. All drugs were stored at -20°C until use.

Generation, validation, and deep-sequencing of drug-resistant herpesviruses

Putative drug-resistant herpesviruses were generated as previously described for selection of a raltegravir-resistant HHV-1 (21). Briefly, confluent CRFKs in T25 flasks were infected with 300,000 plaque forming units of FHV-1 in the presence of 200 µM raltegravir, 80 µM acyclovir, or DMSO. Cells were collected by freeze/thawing three times and centrifuging at 300 ×g for 5 minutes (min) to remove cellular debris when robust cytopathic effect was apparent, typically 2 days post infection. Then, 2 µl of the passage was used to inoculate new CRFKs in the same

manner and 7 passages were performed with these drug concentrations. Three passages were then performed in 500 µM raltegravir, 160 µM acyclovir, or DMSO. Virus stocks were plaque purified, selected for an additional 5 passages in 500 µM raltegravir, 160 µM acyclovir, or DMSO, and stocks of the 15th passage (F15) were prepared.

Drug resistance was evaluated by infecting confluent CRFK cultures with the wild-type, designated F0, DMSO passaged (F15-DMSO), raltegravir passaged (F15-Ralt), or acyclovir passaged (F15-Acyc) FHV-1 at a multiplicity of infection (MOI) =0.01 for 2 h at 37°C. Cultures were then rinsed with ice cold, low pH citrate buffer to reduce cell-associated virus and growth media supplemented with DMSO, 500 µM raltegravir, or 160 µM acyclovir was added. Cells and supernatants were collected together at 48 h post infection (hpi) by freeze/thawing three times. Samples were titered on CRFKs, as previously described (26). Drug susceptibility of the FH2CS versus the C-27 strain to 500 µM raltegravir was determined using the same method.

Plaque purified herpesvirus isolates were deep sequenced, similar to as has been previously described (65). Briefly, confluent CRFKs were infected with 2 µl of the F0, F15-DMSO, F15-Ralt, or F15-Acyc FHV-1. Cells were collected via trypsinization when robust cytopathic effect was visible, approximately 2 days post infection. Genomic DNA was isolated using the Qiagen Blood and Tissue Kit (Qiagen, Valencia, CA). One nanogram of DNA, quantified using the Qubit DNA HS assay kit (Thermo-Fisher Scientific, Waltham, MA), was used for library preparation using the Nextera XT library prep kit (Illumina Inc, San Diego, CA) according to the manufacturer's protocol. Deep sequencing was performed on the MiSeq platform (Illumina, Inc) with 250 nt paired-end reads. Initial de novo assemblies, using SPAdes (Version 3.9.0), did not produce full length FHV-1 genome sequences and reads were subsequently mapped to the FHV-1 C-27 reference genome (NC_0.13590.2) with Geneious (Version 10.2.2, Biomatters Ltd,

Auckland, New Zealand) using the default medium-low sensitivity settings. Reference mapping revealed that our sequencing approach failed to generate reads over the intergenic palindromic repeats and G/C rich regions of the FHV-1 genome. As these regions are non-coding, and therefore were not expected to influence drug susceptibility phenotypes, they were excluded from our analysis. For each viral isolate, our sequencing completely captured all annotated protein coding regions in the FHV-1 genome with an average coverage of >125. Majority consensus sequences were determined for all protein coding regions and mutations differentiating the experimental treatment groups from control viruses were identified.

Accession Numbers

All reads from these experiments have been submitted to the National Center of Biotechnology Information (NCBI) as Sequence Read Archive datasets under the SRA study accession SRP148532.

Viral Growth Kinetics

Viral growth kinetics were assessed by single- and multi-step growth curves. For single-step kinetics, confluent CRFKs were infected with FHV-1 at MOI=10 and treated with DMSO or 500 µM raltegravir at the time of infection. At designated time points, media was removed and centrifuged at 1,000 ×g for 5 min to pellet cellular debris. Cells were collected via trypsinization and combined with the centrifuged cellular debris. Cell-free extracellular virus titers were determined using plaque assays (26). Genomic DNA was isolated from cellular samples using the Qiagen Blood and Tissue Kit. Viral genome replication was determined using absolute qPCR, as previously described (66). For multi-step kinetics, confluent CRFKs were infected with FHV-1 at MOI=0.01 for 2 h. Inoculum was then removed and residual extracellular virus was reduced by rinsing with low-pH citrate buffer. Growth media containing DMSO or 500 µM

raltegravir was added. Cells were collected at designated time points and processed as in the multi-step kinetics.

Electron Microscopy

Capsid formation was evaluated, similarly to as previously described (67). Confluent CRFKs were infected with FHV-1 at MOI=3 for 1 h. The inoculum was removed and replaced with cell line media containing DMSO or 1,000 µM raltegravir. At 7 hpi, cells were fixed in fixative solution consisting of 2% formaldehyde and 2.5% glutaraldehyde in 0.1 M sodium phosphate buffer, pH 7.4 for 10 min at room temperature (RT). Cells were harvested by scraping, pelleted by centrifugation, resuspended in fixative solution, and incubated for 2 h at RT while shaking. Cells were pelleted by centrifugation, resuspended in an equal amount of 3% agarose, and, when solidified, cut into 1-2 mm cubes. Cubes were then placed in a glass vial of 0.1 M sodium phosphate buffer, washed 5 times, for 15 min each, with 0.08 M glycine in 0.1 M sodium phosphate buffer, fixed in 2% OsO_4 in 0.1 M sodium phosphate buffer in the dark for 1 h, and then washed 3 times, 5 min each, in water. Cells were dehydrated through a series of increasing ethanol concentrations (50%, 70%, 80%, 90%, 15 min each, 100%, 20 min, 3 times). After dehydration, the cells were infiltrated with 1:1 Ethanol:LR white resin (Electron Microscopy Sciences, Hatfield, PA). One cell pellet was placed into the bottom of a Beem capsule, covered in resin, and incubated for 24 h at 65°C. Ultra-thin sections (90 nm) for transmission electron microscopy were cut on a Leica EM UC7 microtome. Sections were stained with 2% uranyl acetate for 5 min, followed by 2% lead citrate for 3 min, and 10 independent sections for each condition were photographed with a JEOL JEM-1400 transmission electron microscope.

FHV-1 terminase expression, purification, and activity assay

The C-terminal, nuclease containing domain of UL15 (pUL15-C), from amino acid 477 to 735, approximately corresponding to what has previously been described for HHV-5 pUL89-C (18), was expressed in *E. coli*. Briefly, this region of UL15 was cloned into the pET-His-TEV plasmid (a kind gift of Yuxin Mao, Cornell University) between the BamHI and XhoI restriction sites, which additionally encoded a 6× His epitope on the N-terminus. The resultant plasmid was transformed into Rosetta DE3 *E. coli* (also a kind gift of Yuxin Mao). Expression was induced by addition of 0.25 mM IPTG to a 500 ml culture of bacteria at OD_{600}= 0.6. Bacteria were cultured overnight (approximately 16 h) at 15°C. Bacteria were centrifuged at 5,800 ×g, 4°C for 30 min and resuspended in collection buffer, consisting of 20 mM Tris-HCl pH 8.8, 500 mM NaCl, and 10 mM 2-mercaptoethanol. Bacteria were lysed by sonication, and the lysate was clarified by centrifugation at 24,500 ×g, 4°C for 1 h. Proteins from the resulting supernatant were bound to equilibrated HisPur Ni-NTA Resin (Thermo-Fisher Scientific) for 1.25 h at 4°C. Resin was washed extensively with collection buffer and then protein was eluted in collection buffer with 400 mM imidazole. Protein was desalted and concentrated using a Centriprep centrifugal filter-10 kDa (EMD Millipore, Burlington, MA). Resultant protein was snap frozen in liquid nitrogen, stored at -80°C, and used in nuclease activity assays.

Nuclease activity was assessed as previously described for HHV-1 (34). Briefly, 25 µl reactions containing 20 mM Tris-HCl pH 7.6, 10 mM NaCl, 1 mM $MgCl_2$, 400 ng pET-20b(+) plasmid (EMD Millipore), 370 nM pUL15-C, and 0-10,000 µM raltegravir were incubated for 1 h at 37°C. Undigested and EcoRI digested pET-20b(+) plasmid were included as negative and positive controls. Nuclease activity was terminated by addition of EDTA to a final concentration of 40 mM. Samples were resolved by gel electrophoresis on a 1% agarose gel containing gel red.

The percent of plasmid that was nicked or linearized was determined using ImageJ (Version 1.51k).

FHV-1 ICP8 expression, purification, and activity assay

FHV-1 ICP8 was expressed using the Bac-to-Bac Baculovirus Expression System (Invitrogen, Carlsbad, CA) and purified, similarly to as described for HHV-1 (50). The full length FHV-1 FH2CS strain ICP8 gene was amplified. A 6× His tag was added to the ICP8 N-terminus, flanked by XbaI and EcoRI restriction enzyme sites (nucleotide sequence: TCTAGAATGGAGTTCCATCATCATCATCATCATGAATTC-FHV-1 FH2CS ICP8) and a KpnI site was added after the C-terminus. A pFastBac1 vector encoding canine parvovirus VP2 was digested with XbaI and KpnI to remove this gene and the plasmid backbone was then purified. The modified ICP8 fragment was then cloned into this pFastBac1 vector between the XbaI and KpnI sites (pFastBac1-FH2CS ICP8). Recombinant bacmids were generated by transforming chemically competent *E. coli* DH10Bac cells (Invitrogen) with pFastBac1-FH2CS ICP8, according to the manufacturer's instructions. Sf9 insect cells were transfected with recombinant bacmids by using TransIT-Insect Transfection Reagent (Mirus Bio, Madison, WI) according to the manufacturer's protocol. The supernatant from transfected cells was collected and designated as the P1 stock. This was used to infect new Sf9 cells to generate a P2 stock. The P2 stock was then used to infect High Five (Trichoplusia ni) cells (Boyce Thompson Institute, clone BTI-TN-551-4) for the expression of ICP8.

ICP8 was purified, similarly to as described for HHV-1 ICP8 (50). Briefly, cells were collected by centrifugation at 200 ×g for 15 min. The resultant cell pellet was resuspended in lysis buffer (20 mM Tris-HCl pH 7.5, 300 mM NaCl, 20% glycerol, and 0.5% NP-40) and cells were incubated on ice for 30 min to allow for lysis. Cell debris was pelleted at 12,000 ×g at 4°C

for 15 min. Proteins from the resulting supernatant were bound to equilibrated HisPur Ni-NTA Resin (Thermo-Fisher Scientific) at RT for 1 h. Bound protein was washed extensively with wash buffer consisting of 20 mM Tris-HCl pH 7.5, 300 mM NaCl, 5% glycerol, 20 mM imidazole and 0.1% NP-40, adjusted to pH 7.4. Protein was eluted with wash buffer containing 400 mM imidazole, buffer exchanged into water on a PD Minitrap G-25 column (GE Healthcare), rebound to beads as above, and washed with wash buffer containing increasing concentrations of imidazole (0-400 mM). Fractions containing ICP8, as determined by Coomassie gel, were combined and buffer exchanged on an Amicon Ultra-15 centrifugal filter (50 kDa) unit (EMD Millipore) into ICP8 storage buffer consisting of 50 mM Tris-HCl pH 7.5, 150 mM NaCl, 1 mM EDTA, and 1 mM DTT, adjusted to pH 7.4.

Single stranded DNA binding capacity was assessed similarly to a previously described protocol (68). 10 µL reaction mixtures containing 20 mM Tris-HCl pH 7.5, 4% glycerol, 0.1 mg/ml BSA, 0.5 mM DTT, 5 mM $MgCl_2$, and 100 nM 5'-Cy3 labeled 50-nucleotide ssDNA probe (5'Cy3, TGCGGATGGCTTAGAGCTTAATTGCTGAATCTGGTGCTGTAGCTCAACAT) (Sigma-Aldrich) were incubated with 200 or 500 nM FHV-1 ICP8 and increasing concentrations of raltegravir or volume-matched amounts of DMSO for 1 h at 37°C. Reactions were terminated by addition of 2 µl of a 6× loading buffer (187.5 mM Tris-HCl pH 6.8, 40% glycerol, 0.01% Bromophenol blue). Mixtures were separated on 5% nondenaturing PAGE gels and Cy3 fluorescent signals were visualized using a Bio-Rad ChemiDoc MP imaging system. The percent of probe that was shifted was determined using ImageJ (Version 1.51k) and normalized to untreated controls.

DNA polymerase pausing assay

Similar to previous studies (44), confluent CRFKs were infected with FHV-1 at MOI=2 for 12 h and treated at the time of infection with 100 µg/ml PAA, to inhibit DNA elongation by the viral DNA polymerase. Inoculum and PAA was removed to release cells from PAA block and replaced with cell line media containing no drugs, 100 µg/ml PAA, 100 µg/ml PAA with 50 µg/ml CHX, 50 µg/ml CHX, 500 µM raltegravir, or 500 µM raltegravir with 50 µg/ml CHX. Cells were cultured for an additional 16 h, at which point they were collected, and gDNA was isolated using the Qiagen Blood and Tissue Kit. Relative genome quantification was determined using SYBR green-based qPCR targeting viral ICP4 and the housekeeping gene feline ribosomal protein L17 (*RPL17*) (Table 5.2) using an Applied Biosystems 7500 Fast Real Time PCR instrument (Applied Biosystems, Carlsbad, CA) in triplicate, and expressed relative to DMSO-treated using the $2^{-\Delta\Delta Ct}$ method

Analysis of viral gene expression

To evaluate viral gene expression during a single-step infection, confluent FCEC cultures were infected with FHV-1 at MOI=10 and treated at the time of infection with DMSO, 500 µM raltegravir, 12.5 µg/ml PAA, or 200 µg/ml PAA for 6 h. Cells were lysed with a QIAshredder column (Qiagen), lysates were passed through a gDNA eliminator column to remove gDNA, and RNA was then isolated using the RNeasy Plus Mini Kit (Qiagen). cDNA was synthesized using M-MLV Reverse Transcriptase. Primers were designed using Primer3 (Version 0.4.0) (69), based on the C-27 FHV-1 reference strain or feline reference genome in the NCBI GenBank database (Table 5.2). SYBR green-based qRT-PCR assays were performed using an Applied Biosystems 7500 Fast Real Time PCR instrument (Applied Biosystems, Carlsbad, CA) and all

samples were run in triplicate. The comparative C_t method ($2^{-\Delta\Delta Ct}$) was used to calculate fold change relative to DMSO- or DMEM-treated samples.

Table 5.2: Primer sequences used for qRT-PCR in this study. All viral sequences were designed based on the C-27 FHV-1 strain. IE, immediate early gene; E, early gene; L, late gene; RPL17, Feline Ribosomal Protein L17 (housekeeping gene); NA, not applicable.

Gene	Viral gene classification	Viral Protein	Forward (5'-3')	Reverse (5'-3')
RL2	IE	ICP0	GTGTGACATCGCTCATCCAC	GGATCCCAATCGAGATACTCC
UL54	IE	ICP27	TCGTTACGTCCTCCAATTCC	AGCCGCTCCAAACATATCAC
UL24	E	TK	CAATCCAATCGAGAGTGGTG	GACATCGGTACGTGGTTCG
UL29	E	ICP8	AGACCAAACGACAACGAACC	CCTTGCTGCTCCATATCACC
UL10	L	Glycoprotein M	CGCCAGCCTTCTCAATTATC	CGCAACCTCGACGTAAAATC
UL19	L	Major capsid protein	GAACTGCCGATCAACTCCTC	CCCATACTATGCCCACCATC
UL20	L	UL20	CGTCTCATCATCGGATTCTC	CCACGGCGTCACATATAGC
UL24	L	UL24	CAATCCAATCGAGAGTGGTG	GACATCGGTACGTGGTTCG
UL27	L	Glycoprotein B	CAGACTGGAACCCTGGAGAC	ATCTACCGTGCGATTGGAAC
UL38	L	Minor capsid protein	CTATATGCGCCTCGGTATCC	CACGGGAACTTCAACACCTC
UL44	L	Glycoprotein C	TCTTGACGGGAAGCCAATAG	TGTCGGAATAGCCAACACAG
US6	L	Glycoprotein D	CAGACGATGAACTGGGTTTG	CAACATGGCGTTGGAGATAG
US7	L	Glycoprotein I	TAATGCTTTCCGGTCCTGTC	TACCCGCAGTGCGTAGATTC
RPL17	NA	NA	AAGAACACACGGGAAACTGC	CTGGGCACACCTACCAACTC

Flow cytometric evaluation of glycoprotein D (gD) expression

Flow cytometry was used to determine the kinetics of gD protein expression in drug-treated cells. Confluent FCECs were infected with FHV-1-gD-DsRed (48) at MOI=3 or mock infected and treated at the time of infection with DMSO, 500 µM raltegravir, or 12.5 µg/ml PAA. Cells were collected at 0, 6, 12, 18, and 24 hpi via trypsinization and rinsed once with PBS. After rinsing, 20,000 live cells were analyzed on a Gallios flow cytometer controlled by

Kaluza for Gallios software (Beckman Coulter, Indianapolis, IN). Data analysis was conducted using FlowJo Version 10.4.1 (FlowJo LLC, Ashland, OR).

Statistical analysis

Data were statistically evaluated using GraphPad Prism, Version 6.04 for Windows and are expressed as the mean ± standard deviation. Student's T tests were used to compare 2 groups and One-Way ANOVAs with a Tukey HSD post-hoc test were used where 3 or more groups were compared. Fisher's exact test was used to analyze results of the electron microscopy. All experiments, with exception of the electron microscopy, were performed at least three times. A P value of ≤ 0.05 was considered significant.

Acknowledgements

We thank Don Miller for his helpful advice with cloning, and Jon Wasilko and Roy Cohen for their assistance with protein expression and purification. We additionally thank Lauren Tofano, Brian Wasik, Rebecca Harman, and the Louisiana State University electron microscopy facility for excellent technical assistance. This work was funded by a Cornell University Feline Health Center grant to G. Van de Walle. The funders had no role in study design, data collection and interpretation, or the decision to submit the work for publication. The authors declare no conflicts of interest.

5.6. References

1. Davison AJ, Eberle R, Ehlers B, Hayward GS, McGeoch DJ, Minson AC, Pellett PE, Roizman B, Studdert MJ, Thiry E. 2009. The order Herpesvirales. Arch Virol 154:171–7.

2. Looker KJ, Magaret AS, May MT, Turner KME, Vickerman P, Gottlieb SL, Newman LM. 2015. Global and regional estimates of prevalent and incident herpes simplex virus type 1 infections in 2012. PLoS One 10:e0140765.

3. Rowe AM, St Leger AJ, Jeon S, Dhaliwal DK, Knickelbein JE, Hendricks RL. 2013. Herpes keratitis. Prog Retin Eye Res 32:88–101.

4. Austin A, Lietman T, Rose-Nussbaumer J. 2017. Update on the management of infectious keratitis. Ophthalmology 124:1678–1689.

5. Andrei G, Snoeck R. 2013. Herpes simplex virus drug-resistance. Curr Opin Infect Dis 26:551–560.

6. Tsatsos M, MacGregor C, Athanasiadis I, Moschos MM, Hossain P, Anderson D. 2016. Herpes simplex virus keratitis: an update of the pathogenesis and current treatment with oral and topical antiviral agents. Clin Experiment Ophthalmol 4:824–837.

7. Piret J, Boivin G. 2016. Antiviral resistance in herpes simplex virus and varicella-zoster virus infections. Curr Opin Infect Dis 29:654–662.

8. Azher TN, Yin X-T, Tajfirouz D, Huang AJ, Stuart PM. 2017. Herpes simplex keratitis: challenges in diagnosis and clinical management. Clin Ophthalmol 11:185–191.

9. Al-Dujaili LJ, Clerkin PP, Clement C, McFerrin HE, Bhattacharjee PS, Varnell ED, Kaufman HE, Hill JM. 2011. Ocular herpes simplex virus: how are latency, reactivation, recurrent disease and therapy interrelated? Future Microbiol 6:877–907.

10. Law GL, Tisoncik-Go J, Korth MJ, Katze MG. 2013. Drug repurposing: a better approach for infectious disease drug discovery? Curr Opin Immunol 25:588–592.

11. Mounce BC, Cesaro T, Moratorio G, Hooikaas PJ, Yakovleva A, Werneke SW, Smith EC, Poirier EZ, Simon-Loriere E, Prot M, Tamietti C, Vitry S, Volle R, Khou C, Frenkiel M-P, Sakuntabhai A, Delpeyroux F, Pardigon N, Flamand M, Barba-Spaeth G, Lafon M,

Denison MR, Albert ML, Vignuzzi M. 2016. Inhibition of polyamine biosynthesis is a broad-spectrum strategy against RNA viruses. J Virol 90:9683–9692.

12. Johansen LM, Brannan JM, Delos SE, Shoemaker CJ, Stossel A, Lear C, Hoffstrom BG, Dewald LE, Schornberg KL, Scully C, Lehár J, Hensley LE, White JM, Olinger GG. 2013. FDA-approved selective estrogen receptor modulators inhibit Ebola virus infection. Sci Transl Med 5:190ra79.

13. Dyall J, Coleman CM, Hart BJ, Venkataraman T, Holbrook MR, Kindrachuk J, Johnson RF, Olinger GG, Jahrling PB, Laidlaw M, Johansen LM, Lear-Rooney CM, Glass PJ, Hensley LE, Frieman MB. 2014. Repurposing of clinically developed drugs for treatment of Middle East respiratory syndrome coronavirus infection. Antimicrob Agents Chemother 58:4885–4893.

14. Albulescu IC, van Hoolwerff M, Wolters LA, Bottaro E, Nastruzzi C, Yang SC, Tsay S-C, Hwu JR, Snijder EJ, van Hemert MJ. 2015. Suramin inhibits chikungunya virus replication through multiple mechanisms. Antiviral Res 121:39–46.

15. Summa V, Petrocchi A, Bonelli F, Crescenzi B, Donghi M, Ferrara M, Fiore F, Gardelli C, Gonzalez Paz O, Hazuda DJ, Jones P, Kinzel O, Laufer R, Monteagudo E, Muraglia E, Nizi E, Orvieto F, Pace P, Pescatore G, Scarpelli R, Stillmock K, Witmer M V., Rowley M. 2008. Discovery of raltegravir, a potent, selective orally bioavailable HIV-integrase inhibitor for the treatment of HIV-AIDS infection. J Med Chem 51:5843–5855.

16. Mouscadet JF, Tchertanov L. 2009. Raltegravir: molecular basis of its mechanism of action. Eur J Med Res 14 Suppl 3:5–16.

17. McColl DJ, Chen X. 2010. Strand transfer inhibitors of HIV-1 integrase: Bringing IN a new era of antiretroviral therapy. Antiviral Res 85:101–118.

18. Nadal M, Mas PJ, Mas PJ, Blanco AG, Arnan C, Solà M, Hart DJ, Coll M. 2010. Structure and inhibition of herpesvirus DNA packaging terminase nuclease domain. Proc Natl Acad Sci U S A 107:16078–83.

19. Bogner E. 2002. Human cytomegalovirus terminase as a target for antiviral chemotherapy. Rev Med Virol 12:115–27.

20. Bowman LJ, Melaragno JI, Brennan DC. 2017. Letermovir for the management of cytomegalovirus infection. Expert Opin Investig Drugs 26:235–241.

21. Zhou B, Yang K, Wills E, Tang L, Baines JD. 2014. A mutation in the DNA polymerase accessory factor of herpes simplex virus 1 restores viral DNA replication in the presence of raltegravir. J Virol 88:11121–11129.

22. Maes R. 2012. Felid herpesvirus type 1 infection in cats: a natural host model for alphaherpesvirus pathogenesis. ISRN Vet Sci 2012:495830.

23. Pennington M, Ledbetter E, Van de Walle G. 2017. New paradigms for the study of ocular alphaherpesvirus infections: insights into the use of non-traditional host model systems. Viruses 9:349.

24. Gaskell R, Dawson S, Radford A, Thiry E. 2007. Feline herpesvirus. Vet Res 38:337–54.

25. Thomasy SM, Maggs DJ. 2016. A review of antiviral drugs and other compounds with activity against feline herpesvirus type 1. Vet Ophthalmol 19:119–130.

26. Pennington MR, Fort MW, Ledbetter EC, Van de Walle GR. 2016. A novel corneal explant model system to evaluate antiviral drugs against feline herpesvirus type 1 (FHV-1). J Gen Virol 97:1414–1425.

27. Vaz PK, Job N, Horsington J, Ficorilli N, Studdert MJ, Hartley CA, Gilkerson JR, Browning GF, Devlin JM. 2016. Low genetic diversity among historical and contemporary clinical isolates of felid herpesvirus 1. BMC Genomics 17:704.

28. Kolb AW, Lewin AC, Moeller Trane R, McLellan GJ, Brandt CR. 2017. Phylogenetic and recombination analysis of the herpesvirus genus varicellovirus. BMC Genomics 18:887.

29. Lewin AC, Kolb AW, McLellan GJ, Bentley E, Bernard KA, Newbury SP, Brandt CR. 2018. Genomic, recombinational and phylogenetic characterization of global feline herpesvirus 1 isolates. Virology 518:385–397.

30. Sauerbrei A, Bohn K, Heim A, Hofmann J, Weiβbrich B, Schnitzler P, Hoffmann D, Zell R, Jahn G, Wutzler P, Hamprecht K. 2011. Novel resistance-associated mutations of thymidine kinase and DNA polymerase genes of herpes simplex virus type 1 and type 2.

Antivir Ther 16:1297–1308.

31. Frobert E, Burrel S, Ducastelle-Lepretre S, Billaud G, Ader F, Casalegno JS, Nave V, Boutolleau D, Michallet M, Lina B, Morfin F. 2014. Resistance of herpes simplex viruses to acyclovir: An update from a ten-year survey in France. Antiviral Res 111:36–41.

32. Schmidt S, Bohn-Wippert K, Schlattmann P, Zell R, Sauerbrei A. 2015. Sequence analysis of herpes simplex virus 1 thymidine kinase and DNA polymerase genes from over 300 clinical isolates from 1973 to 2014 finds novel mutations that may be relevant for development of antiviral resistance. Antimicrob Agents Chemother 59:4938–4945.

33. Goldner T, Hewlett G, Ettischer N, Ruebsamen-Schaeff H, Zimmermann H, Lischka P. 2011. The novel anticytomegalovirus compound AIC246 (Letermovir) inhibits human cytomegalovirus replication through a specific antiviral mechanism that involves the viral terminase. J Virol 85:10884–93.

34. Selvarajan Sigamani S, Zhao H, Kamau YN, Baines JD, Tang L. 2013. The structure of the herpes simplex virus DNA-packaging terminase pUL15 nuclease domain suggests an evolutionary lineage among eukaryotic and prokaryotic viruses. J Virol 87:7140–8.

35. Yan Z, Bryant KF, Gregory SM, Angelova M, Dreyfus DH, Zhao XZ, Coen DM, Burke TR, Knipe DM. 2014. HIV integrase inhibitors block replication of alpha-, beta-, and gammaherpesviruses. MBio 5:e01318-14.

36. Ruyechan WT, Weir AC. 1984. Interaction with nucleic acids and stimulation of the viral DNA polymerase by the herpes simplex virus type 1 major DNA-binding protein. J Virol 52:727–33.

37. Leinbach SS, Heath LS. 1989. Characterization of the single-stranded DNA-binding domain of the herpes simplex virus protein ICP8. Biochim Biophys Acta - Gene Struct Expr 1008:281–286.

38. Nimonkar A V., Boehmer PE. 2002. In vitro strand exchange promoted by the herpes simplex virus type-1 single strand DNA-binding protein (ICP8) and DNA helicase-primase. J Biol Chem 277:15182–15189.

39. Reuven NB, Staire AE, Myers RS, Weller SK. 2003. The herpes simplex virus type 1

alkaline nuclease and single-stranded DNA binding protein mediate strand exchange in vitro. J Virol 77:7425–33.

40. Reuven NB, Willcox S, Griffith JD, Weller SK. 2004. Catalysis of strand exchange by the HSV-1 UL12 and ICP8 proteins: potent ICP8 recombinase activity is revealed upon resection of dsDNA substrate by nuclease. J Mol Biol 342:57–71.

41. Gao M, Knipe DM. 1991. Potential role for herpes simplex virus ICP8 DNA replication protein in stimulation of late gene expression. J Virol 65:2666–75.

42. Chen Y, Knipe D. 1996. A dominant mutant form of the herpes simplex virus ICP8 protein decreases viral late gene transcription. Virology 221:281–290.

43. Wilkinson D, Weller S. 2003. The role of DNA recombination in herpes simplex virus DNA replication. IUBMB Life 55:451–458.

44. Schang LM, Rosenberg A, Schaffer PA. 2000. Roscovitine, a specific inhibitor of cellular cyclin-dependent kinases, inhibits herpes simplex virus DNA synthesis in the presence of viral early proteins. J Virol 74:2107–20.

45. Becker Y, Asher Y, Cohen Y, Weinberg-Zahlering E, Shlomai J. 1977. Phosphonoacetic acid-resistant mutants of herpes simplex virus: effect of phosphonoacetic acid on virus replication and in vitro deoxyribonucleic acid synthesis in isolated nuclei 11:919–922.

46. Gruffat H, Marchione R, Manet E. 2016. Herpesvirus late gene expression: a viral-specific pre-initiation complex is key. Front Microbiol 7:869.

47. Pennington MR, Grenier JK, Van de Walle GR. 2018. Transcriptome profiling of alphaherpesvirus-infected cells treated with the HIV-integrase inhibitor raltegravir reveals profound and specific alterations in host transcription. J Gen Virol.

48. Pennington MR, Van de Walle GR. 2017. Electric cell-substrate impedance sensing to monitor viral growth and study cellular responses to infection with alphaherpesviruses in real time. mSphere 2:e00039-17.

49. Honess RW, Watson DH. 1977. Herpes simplex virus resistance and sensitivity to phosphonoacetic acid. J Virol 21:584–600.

50. Bryant KF, Yan Z, Dreyfus DH, Knipe DM. 2012. Identification of a divalent metal cation bindings site in herpes simplex virus 1 (HSV-1) ICP8 required for HSV replication. J Virol 86:6825–6834.

51. Leinbach SS, Casto JF. 1983. Identification and characterization of deoxyribonucleoprotein complexes containing the major DNA-binding protein of herpes simplex virus type 1. Virology 131:274–86.

52. Boehmer PE, Dodson MS, Lehman IR. 1993. The herpes simplex virus type-1 origin binding protein. DNA helicase activity. J Biol Chem 268:1220–5.

53. Makhov AM, Lee SSK, Lehman IR, Griffith JD. 2003. Origin-specific unwinding of herpes simplex virus 1 DNA by the viral UL9 and ICP8 proteins: visualization of a specific preunwinding complex. Proc Natl Acad Sci 100:898–903.

54. Arana ME, Haq B, Tanguy Le Gac N, Boehmer PE. 2001. Modulation of the herpes simplex virus type-1 UL9 DNA helicase by its cognate single-strand DNA-binding protein, ICP8. J Biol Chem 276:6840–6845.

55. Arsenakis M, Campadelli-Fiume G, Roizman B. 1988. Regulation of glycoprotein D synthesis: does alpha 4, the major regulatory protein of herpes simplex virus 1, regulate late genes both positively and negatively? J Virol 62:148–58.

56. Nimonkar A V, Boehmer PE. 2003. The herpes simplex virus type-1 single-strand DNA-binding protein (ICP8) promotes strand invasion. J Biol Chem 278:9678–82.

57. Reuven NB, Weller SK. 2005. Herpes simplex virus type 1 single-strand DNA binding protein ICP8 enhances the nuclease activity of the UL12 alkaline nuclease by increasing its processivity. J Virol 79:9356–9358.

58. Weller SK, Coen DM. 2012. Herpes simplex viruses: mechanisms of DNA replication. Cold Spring Harb Perspect Biol 4:a013011.

59. Ireland PJ, Tavis JE, D'Erasmo MP, Hirsch DR, Murelli RP, Cadiz MM, Patel BS, Gupta AK, Edwards TC, Korom M, Moran EA, Morrison LA. 2016. Synthetic α-hydroxytropolones inhibit replication of wild-type and acyclovir-resistant herpes simplex viruses. Antimicrob Agents Chemother 60:2140–9.

60. Masaoka T, Zhao H, Hirsch DR, D'Erasmo MP, Meck C, Varnado B, Gupta A, Meyers MJ, Baines J, Beutler JA, Murelli RP, Tang L, Le Grice SFJ. 2016. Characterization of the C-terminal nuclease domain of herpes simplex virus pUL15 as a target of nucleotidyltransferase inhibitors. Biochemistry 55:809–819.

61. Dehghanpir SD, Birkenheuer CH, Yang K, Murelli RP, Morrison LA, Le Grice SFJ, Baines JD. 2018. Broad anti-herpesviral activity of α-hydroxytropolones. Vet Microbiol 214:125–131.

62. Sandmeyer LS, Keller CB, Bienzle D. 2005. Culture of feline corneal epithelial cells and infection with feline herpesvirus-1 as an investigative tool. Am J Vet Res 66:205–9.

63. Walton TE, Gillespie JH. 1970. Feline viruses. VII. Immunity to the feline herpesvirus in kittens inoculated experimentally by the aerosol method. Cornell Vet 60:232–9.

64. Tai SHS, Niikura M, Cheng HH, Kruger JM, Wise AG, Maes RK. 2010. Complete genomic sequence and an infectious BAC clone of feline herpesvirus-1 (FHV-1). Virology 401:215–227.

65. Pizzurro F, Mangone I, Zaccaria G, De Luca E, Malatesta D, Innocenti M, Carmine I, Cito F, Marcacci M, Sabatino D Di, Lorusso A. 2016. Whole-genome sequence of a suid herpesvirus-1 strain isolated from the brain of a hunting dog in Italy. Genome Announc 4:1333–16.

66. Spertus CB, Pennington MR, Van de Walle GR, Badanes ZI, Judd BE, Mohammed HO, Ledbetter EC. 2018. Effects of oral raltegravir in cats with experimentally-induced ocular and respiratory feline herpesvirus-1 infection. Am J Vet Res.

67. Le Sage V, Jung M, Alter JD, Wills EG, Johnston SM, Kawaguchi Y, Baines JD, Banfield BW. 2013. The herpes simplex virus 2 UL21 protein is essential for virus propagation. J Virol 87:5904–15.

68. Darwish AS, Grady LM, Bai P, Weller SK. 2015. ICP8 filament formation is essential for replication compartment formation during herpes simplex virus infection. J Virol 90:2561–70.

69. Untergasser A, Cutcutache I, Koressaar T, Ye J, Faircloth BC, Remm M, Rozen SG. 2012.

Primer3--new capabilities and interfaces. Nucleic Acids Res 40:e115.

CHAPTER SIX

TRANSCRIPTOME PROFILING OF ALPHAHERPESVIRUS-INFECTED CELLS TREATED WITH THE HIV-INTEGRASE INHIBITOR RALTEGRAVIR REVEALS PROFOUND AND SPECIFIC ALTERATIONS IN HOST TRANSCRIPTION

*Manuscript from: Matthew R. Pennington, Jennifer K. Grenier, and Gerlinde R. Van de Walle 2018. Transcriptome profiling of alphaherpesvirus-infected cells treated with the HIV-integrase inhibitor raltegravir reveals profound and specific alterations in host transcription. *Journal of General Virology*. 29 June 2018, doi:10.1099/jgv.0.001090.

6.1. Summary

Anti-microbial compounds typically exert their action by directly interfering with one or more stages of the pathogen's life cycle. However, some compounds also have secondary effects on the host that aid in pathogen clearance. Raltegravir is a human immunodeficiency virus (HIV)-integrase inhibitor which has been shown to alter the host immune response to HIV, besides its direct antiviral effect. Interestingly, raltegravir can also directly inhibit the replication of various herpesviruses. However, the host-targeted effects of this drug in the context of a herpesvirus infection have gone unexplored. Here, we used felid alphaherpesvirus 1 (FHV-1), a close relative of human alphaherpesvirus 1 (HHV-1) that similarly causes ocular herpes, to characterize the host-targeted effects of raltegravir on corneal epithelial cells during an alphaherpesvirus infection. Using RNA deep sequencing, we found that raltegravir specifically boosts the expression of anti-angiogenic factors and promotes metabolic homeostasis in FHV-1-infected cells. In contrast, few changes in host gene transcription were found in uninfected cells. Importantly, we could demonstrate that these effects were specific to raltegravir and independent of the direct-acting antiviral effect of the drug, since treatment with the DNA polymerase inhibitor phosphonoacetic acid did not induce these host-targeted effects. Taken together, these results indicate that raltegravir has profound and specific effects on the host transcription profile of herpesvirus-infected cells that may contribute to the overall antiviral activity of the drug and could provide therapeutic benefits *in vivo*. Furthermore, this study provides a framework for future efforts evaluating host-targeted effects of anti-microbial compounds.

Keywords: transcriptome profiling, raltegravir, FHV-1, ocular herpesvirus, RNAseq

6.2. Introduction

Many compounds have been developed to specifically target viral proteins with the goal of interrupting the viral replication cycle (1, 2). The observation that several of these antivirals, in addition to their virus-specific inhibitory effects, possess immunomodulatory properties has led to a new research interest in their ability to modify the host's response to infection, thus enabling a more efficient antiviral immune response (3). However, and in contrast to antibacterial agents, studies on the possible immunomodulatory activities of direct-acting antivirals remain scarce. One study showed that several human immunodeficiency virus (HIV) protease inhibitors can inhibit tumor growth and alter angiogenesis and cytokine production *in vivo*, besides their direct antiviral effect on the viral protease itself (3). Another study demonstrated that Arbidol, a broad-spectrum antiviral compound that blocks viral fusion of influenza and hepatitis C virus (4), enhanced interleukin 6 and tumor necrosis factor alpha and reduced transforming growth factor beta expression when added to human alphaherpesvirus 1 (HHV-1)-infected keratinocytes *in vitro* (5). Perhaps the most researched example is lactoferrin, a glycoprotein of the transferrin family commonly found in milk, other exocrine secretions, and neutrophil granules. It exerts a direct-acting antiviral effect against a wide variety of viruses by binding directly to either the virus or cellular receptors, such as heparan sulfate, to prevent entry (6, 7). In the context of herpesvirus infections, lactoferrin increased interleukin 18 production in HHV-1-infected mice (8) and was shown to inhibit human gammaherpesvirus 4, also known as Epstein-Barr virus,-induced upregulation of monocyte chemoattractant protein-1 and interleukin 8 in macrophages *in vitro* (9).

Raltegravir was the first HIV integrase inhibitor approved by the United States Food and Drug Administration for therapeutic use (10–12). Interestingly, microarray-based transcriptomic

profiling of the CD8+ T cell compartment of HIV patients on antiretroviral therapy, based on either protease inhibitors or non-nucleoside reverse transcriptase inhibitors supplemented with (intensified) or not supplemented with (non-intensified) raltegravir, revealed significant effects of raltegravir-intensive antiretroviral therapy on host cell metabolism, immune regulation, and cell proliferation (13). These results indicate that raltegravir can have cellular effects in addition to its direct-acting antiviral effects in the context of a viral infection. More recently, raltegravir was shown to be effective at inhibiting a variety of human herpesviruses, including HHV-1 and human betaherpesvirus 5, also known as human cytomegalovirus (14, 15). Although the direct-acting antiviral mechanisms of raltegravir have been determined for these viruses (14, 15), the cellular effects of raltegravir in the context of herpesvirus infections have not been explored to date.

Our group works with felid alphaherpesvirus 1 (FHV-1), a close relative of HHV-1 and a common cause of corneal ulceration and stromal keratitis in cats (16, 17). We found raltegravir also to be effective in reducing FHV-1 replication, both in 2D cell culture and in a corneal explant model (18). The aim of the present study was to determine the cellular effects of raltegravir in FHV-1-infected feline corneal epithelial cells utilizing RNA deep sequencing (RNAseq). Significant host gene transcriptional changes were identified and subsequent studies showed that FHV-1-infected cells expressed higher levels of anti-angiogenic factors when treated with raltegravir. In addition, we found that raltegravir altered the metabolism of FHV-1-infected cells by promoting an aerobic, rather than glycolytic, phenotype. Importantly, we could demonstrate that these effects were specific to raltegravir and independent of the direct-acting antiviral effect of the drug, as treatment with the DNA polymerase inhibitor phosphonoacetic acid did not induce these effects. Collectively, these results indicate that raltegravir has cellular

host-targeted effects besides direct-acting antiviral effects in the context of a herpesvirus infection. In contrast, few host gene transcriptional changes were found in uninfected cells following raltegravir treatment, indicating that raltegravir is unlikely to affect the basal cellular activity of uninfected cells.

6.3. Results

Experimental approach for RNA deep sequencing

We used primary feline corneal epithelial cells (FCECs) to determine the effects of raltegravir on host gene transcription in the context of FHV-1 infection. FCECs were isolated from a clinically healthy cat, infected with FHV-1 at a multiplicity of infection (MOI) of 10 for 2 hours (h), treated with either raltegravir or dimethyl sulfoxide (DMSO, vehicle) for 2 h, and then processed for subsequent RNA deep sequencing (RNAseq). We had determined that an MOI=10

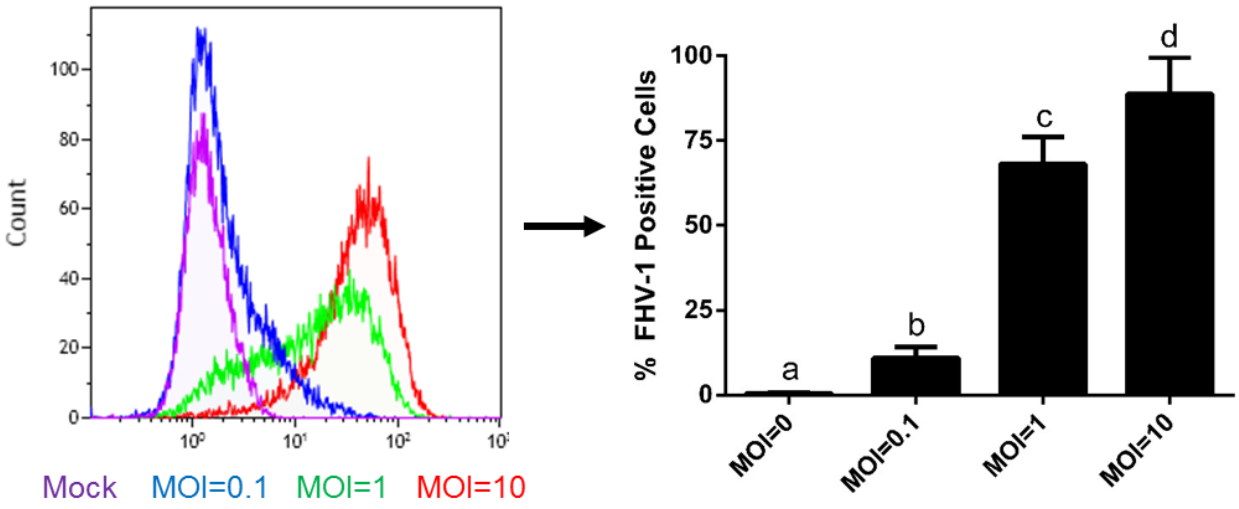

Figure 6.1: Selection of multiplicity of infection (MOI) for RNAseq of FHV-1-infected cells. CRFKs were infected for 2 h with FHV-1, at the indicated MOIs. Inoculum was removed at 2 h and replaced with fresh culture media. Virus replication at 6 hpi was determined by flow cytometry. One-Way ANOVA, with Tukey's HSD post-hoc test.

resulted in ~80% of FHV-1-infected cells, as quantified by flow cytometry (Fig. 6.1), and, therefore, was used to minimize the noise from transcriptional changes in non-infected cells. The 500 µM concentration of raltegravir was selected because we previously showed that this

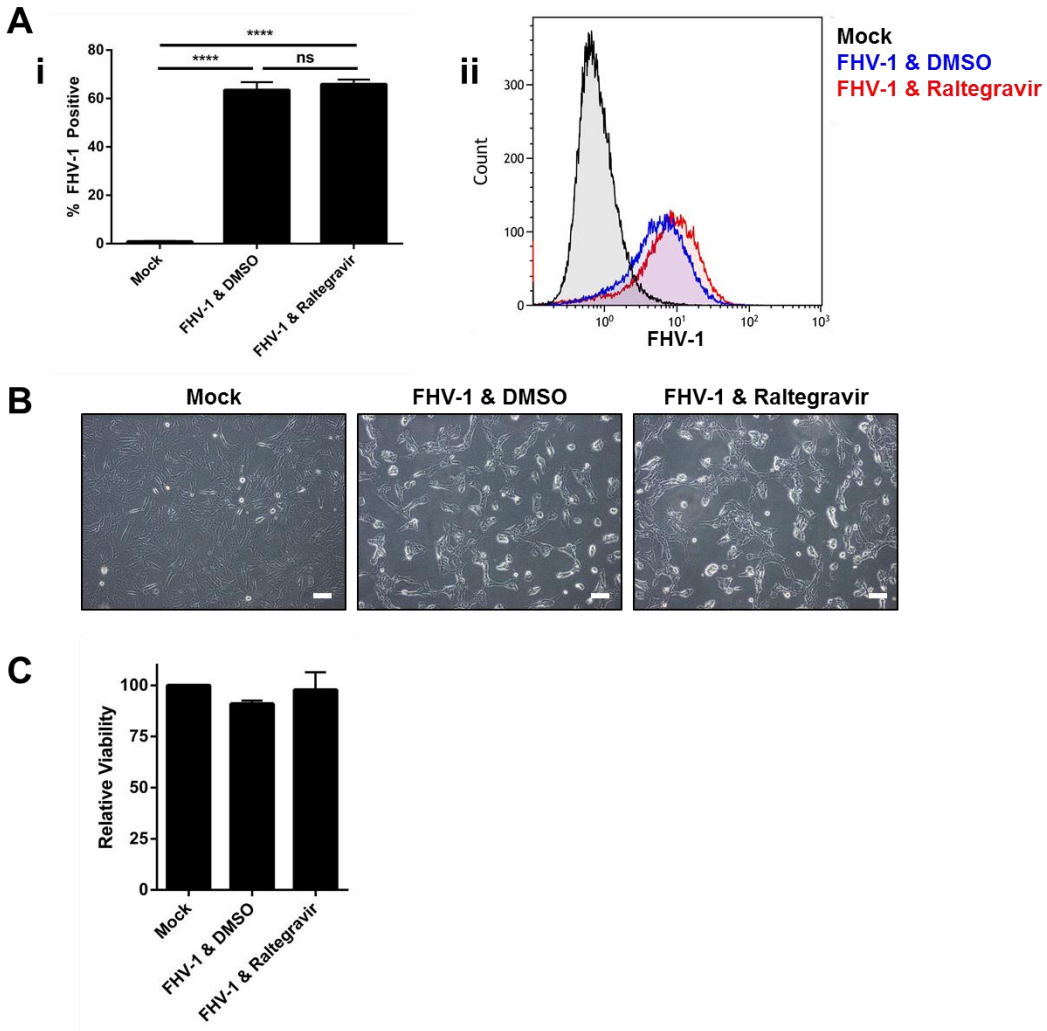

Figure 6.2: Validation of experimental conditions for RNAseq of FHV-1-infected cells. Primary FCECs were infected for 2 h with FHV-1, at an MOI of 10, treated with 500 µM raltegravir or DMSO for 2 h, and processed for subsequent analyses (4 hpi). **(A)** Quantification of percent FHV-1-positive cells as determined by flow cytometry (i) and representative histogram (ii) at 4 hpi. **(B)** Representative light micrographs of FHV-1-infected FCECs at 4 hpi. Scale bar, 100 µm. **(C)** Determination of cell viability by MTT assay at 6 hpi. ****, $p \leq 0.0001$.

significantly reduced viral replication both in cell culture and in a cornea explant model (18). The 4 h post infection (pi) time point was selected as it (i) resulted in infection of the majority of the FCECs, as quantified by flow cytometry (Fig. 6.2A), (ii) did not cause detachment of infected cells from the culture flask, as shown by light microscopy (Fig. 6.2B), and (iii) did not significantly affect cell viability, as determined by the 3-(4,5-dimethylthiazol-2-yl)-2,5-diphenyltetrazolium bromide (MTT) assay (Fig. 6.2C). Read count analysis for these samples is presented in Table 6.1.

Table 6.1: Numbers of Illumina sequencing reads per replicate sample in FHV-1-infected cells.

		Number of Reads			
Sample	**Description**	**Raw**	**Filtered**	**Mapping cat genome**	**Mapping FHV-1 genome**
1	DMSO	43,819,785	37,303,044	15,281,316	18,017,258
2	DMSO	37,047,036	32,568,788	13,442,786	15,930,750
3	DMSO	39,345,886	33,556,021	14,027,987	15,906,365
			Avg	14,250,696	16,618,124
			SD	939,280.4	1,211,746.6
4	Raltegravir	37,852,487	33,523,719	16,287,160	13,998,770
5	Raltegravir	36,696,822	32,244,468	15,464,572	13,800,705
6	Raltegravir	39,489,372	33,717,453	16,316,683	14,048,700
			Avg	16,022,805	13,949,392
			SD	483,669	131,164
		T-test DMSO vs Raltegravir		0.0478	0.0188

Raltegravir induces dramatic host gene transcriptional changes in FHV-1-infected cells

In general, in FHV-1-infected cells, over 19,500 genes were tested for differential expression by cuffdiff2 and 5,598 genes were initially identified as differentially expressed by raltegravir treatment. Following additional filtration for minimum expression level and fold-change between conditions and curation for protein coding genes (see methods), 401 genes were identified as stringently differentially expressed during FHV-1 infection, with 333 being upregulated and 68 downregulated by raltegravir treatment (Fig. 6.3A). The top 20 differentially expressed genes (DEGs) are presented in Table 6.2 and the complete list can be found in the appendix of this dissertation. As an initial literature search of the top 20 DEGs did not show a clear connection between these genes and herpesvirus infections, we analyzed the lists of up- and down-regulated DEGs using the PANTHER statistical overrepresentation test for Gene Ontology (GO) terms. Based on the PANTHER GO analysis, several pathways were differentially regulated in raltegravir-treated FHV-1-infected corneal cells compared to DMSO-treated FHV-1-infected cells (Fig. 6.3B). To be able to determine whether these changes were raltegravir-specific or merely a consequence of a reduced viral replication due to the direct-acting virus inhibition of this drug, we included, where relevant, FHV-1-infected cells treated with phosphonoacetic acid (PAA), a herpesvirus DNA polymerase inhibitor, as a control in our follow-up experiments. A concentration of 89.25 μM PAA was used for these experiments, based on a similar level of inhibition of viral replication compared to the 500 μM raltegravir concentration we used in our studies (Fig. 6.4).

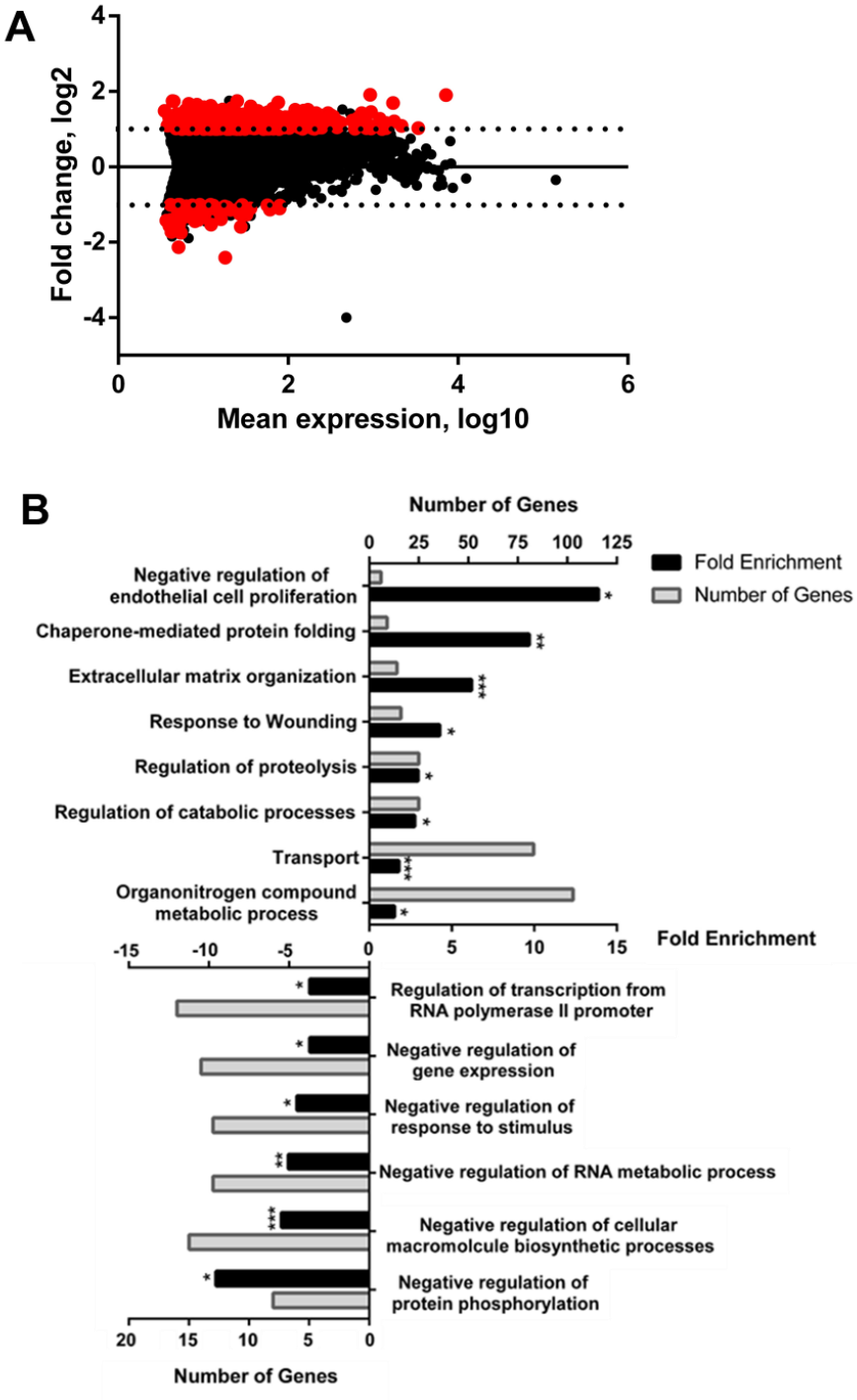

Figure 6.3: Raltegravir treatment of FHV-1-infected cells alters several related biological processes. (A) MA plot of gene expression in FHV-1-infected cells. Red, stringent-DEGs following raltegravir treatment; black, expressed genes. **(B)** PANTHER GO analysis of up- and downregulated genes following raltegravir treatment of FHV-1-infected FCECs.

Table 6.2: Top 20 protein-coding differentially expressed genes (DEGs) following raltegravir treatment of FHV-1-infected cells. Fold changes were calculated by comparison of the mean fragments per kilobase of transcript per million mapped reads (FPKM) values of DMSO vs raltegravir treated cells at 4 hours post infection (2 h post drug treatment). Genes were ranked according to fold change.

		Average FPKM values		
Gene symbol	**Fold change**	**DMSO**	**Raltegravir**	**Adjusted p-value**
TESK1	-5.32	30.62	5.76	0.00005
RGS16	-4.39	8.31	1.89	0.00005
TFL or *BAX*	3.77	387.78	1461.45	0.00005
FTH1	3.74	3037.38	11357.80	0.00005
LZTS3	3.36	2.00	6.72	0.00005
TMEM54	3.36	11.49	38.57	0.00005
CYB5R3	-3.36	8.38	2.50	0.01365
GCNT4A	3.33	2.07	6.90	0.00475
FAM46C	-3.30	6.46	1.96	0.00005
DYNLT1	3.27	35.56	116.40	0.00005
COL1A1	3.23	812.53	2624.05	0.00005
TIGD7	3.18	3.22	10.23	0.00220
SGCD	3.14	4.06	12.73	0.00005
CINP	3.08	6.01	18.49	0.00005
TGFBI	3.04	17.94	54.54	0.00005
ATF3	-3.02	41.65	13.80	0.00005
RNF26	3.00	5.10	15.28	0.00005
KIAA1217 or *ET14*	-2.96	5.97	2.02	0.01080
UROS	2.95	6.50	19.19	0.00120
LHFP	2.95	10.93	32.28	0.00005

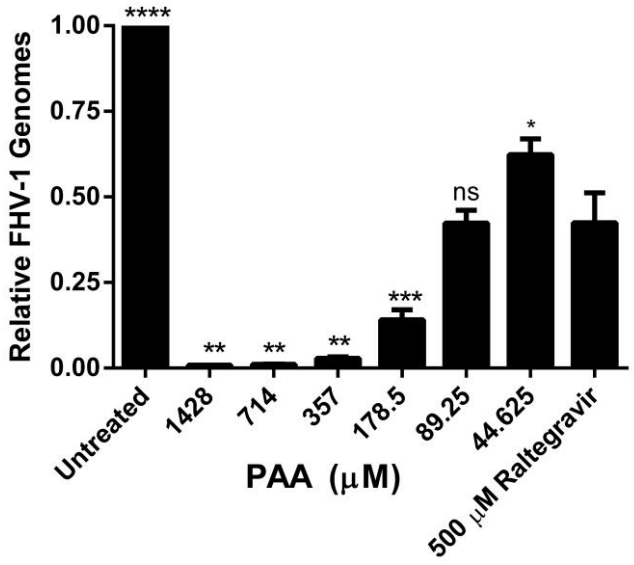

Figure 6.4: Determination of PAA dose. CRFKs were infected with FHV-1, at an MOI of 10, and treated at the time of infection with 500 μM raltegravir or various concentrations of PAA. Viral genome replication was determined at 6 hpi by absolute qPCR. Student's T test was used to compare each treatment to 500 μM raltegravir treatment. ****, p≤0.0001; ***, p≤0.001; **, p≤0.01, *, p≤0.05.

Raltegravir induces upregulation of anti-angiogenic genes and downregulation of repressive transcription factors

The most highly upregulated pathway consisted of 6 genes related to the negative regulation of endothelial cell proliferation (Fig. 6.3B & Fig. 6.5A). Neovascularization is common during ocular herpesvirus infection and is an important contributor to visual impairment (19). We first confirmed that raltegravir-treatment of FHV-1-infected cells indeed upregulated expression of these genes when compared to DMSO-treated infected cells, using qRT-PCR (Fig. 6.5B). Of specific note in this group was *THBS1*, a gene which encodes thrombospondin 1 (TSP-1) (Fig. 6.5A). It has been shown that HHV-1 can selectively suppress TSP-1 protein expression in human keratinocytes *in vitro*, suggesting that modulation of TSP-1 levels may be one of the mechanisms that HHV-1 utilizes to drive corneal neovascularization (20). An antiviral drug that

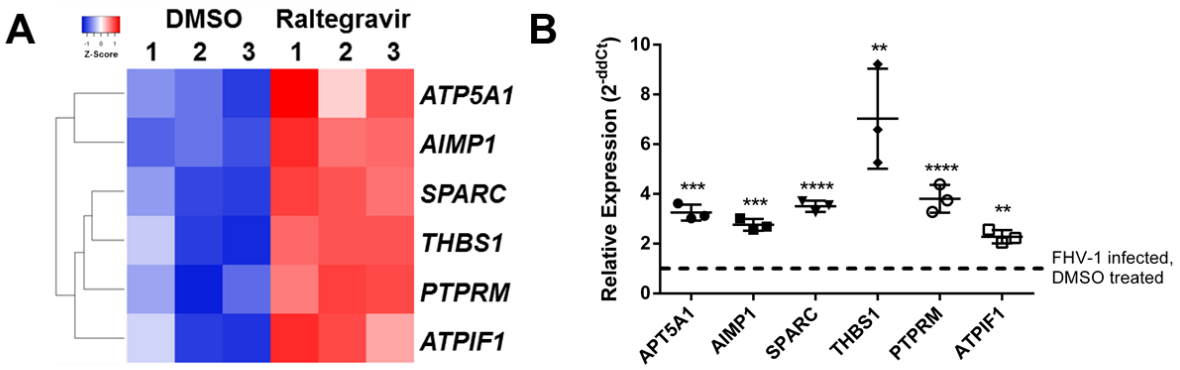

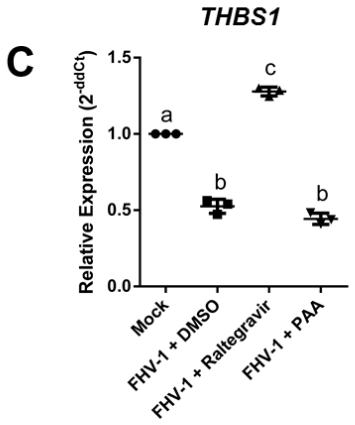

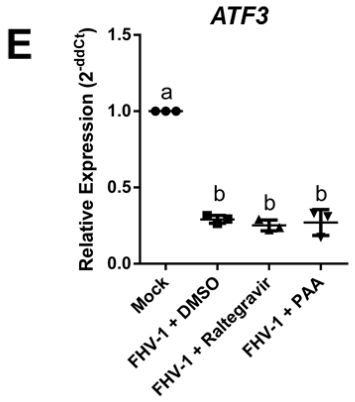

D

Gene	PANTHER GO Biological Process: Transcription from RNA Pol II Promoter	Neg. Reg. Gene Expression	Neg. Reg Response to stimulus	Neg. Reg. RNA Metabolic Proc.	Neg. Reg Macromolecule Biosynthesis	Neg. Reg. Protein Phosphorylation
ATF3	X	X	X	X	X	X
PPP1R15A	X	X	X	X	X	X
ZC3H12A	X	X	X	X	X	X
HDAC1	X	X	X	X	X	
KLF4	X	X	X	X	X	
PCGF2	X	X	X	X	X	
HIST1H1B	X	X		X	X	
HIST1H1E	X	X		X	X	
ID1	X	X		X	X	
IRF1	X	X		X	X	
REL	X	X		X	X	
GDNF	X		X	X		
ID2		X		X	X	

Figure 6.5: Raltegravir treatment of FHV-1-infected cells promotes the expression of anti-angiogenic genes and inhibits cell stress-associated gene expression. (A) Heatmap of expression of negative regulators of endothelial cell proliferation genes. **(B)** Gene expression profiling of negative regulators of endothelial cell proliferation by qRT-PCR, using the same RNA utilized in the RNAseq experiment. FHV-1-infected, raltegravir-treated expression was normalized against FHV-1-infected, DMSO-treated samples using the $2^{-\Delta\Delta Ct}$ method.

Figure 6.5 continued. **(C)** Expression of *THBS1* at 4 hpi, as determined by qRT-PCR, in a separate set of FHV-1-infected FCECs, at an MOI of 5 and treated with DMSO, 500 µM raltegravir, or 89.25 µM PAA at 2 hpi. Expression was normalized against mock-infected cells. **(D)** Downregulated genes categorized in three or more GO biological pathways. **(E)** Expression of *ATF3*, determined as in C. **, $p \leq 0.01$; ***, $p \leq 0.001$; ****, $p \leq 0.0001$.

stimulates the expression of *THBS1* in corneal cells during a herpesvirus infection might, therefore, be beneficial in controlling herpesvirus-induced neovascularization. Similar to what has been reported for HHV-1, we found that FHV-1 infection downregulated *THBS-1* expression relative to mock-infected cells (Fig. 6.5C). In the presence of raltegravir, however, infected cells expressed levels of *THBS-1* RNA that were higher compared to untreated infected cells and even exceeded the levels of *THBS-1* expression observed in mock-infected cells (Fig. 6.5C). This effect appeared to be specific for raltegravir, as treatment with the viral DNA replication inhibitor PAA had no effect on mitigating the reduction in *THBS-1* expression in infected cells (Fig. 6.5C). Two other pathways that were significantly upregulated in raltegravir-treated FHV-1-infected cells were those involved in extracellular matrix (ECM) organization and in driving wound healing (Fig. 6.3B & Fig. 6.6). It could be of interest to follow up in more detail on several genes, and their respective proteins, involved in these pathways to better understand the potential role of raltegravir in healing of corneas damaged by ocular herpesvirus infections.

Treatment with raltegravir also resulted in a significant downregulation of several biological pathways in FHV-1-infected cells, most notably those involved in negative regulation of gene expression, transcription, and RNA metabolism (Fig. 6.3B). Interestingly, thirteen out of the 26 genes in these downregulated processes were shared across three or more GO terms, with three genes being shared across all six pathways (Fig. 6.5D). Of these three genes, activating transcript factor 3 (*ATF3)*, a key stress response transcription factor (21), was of interest to us as

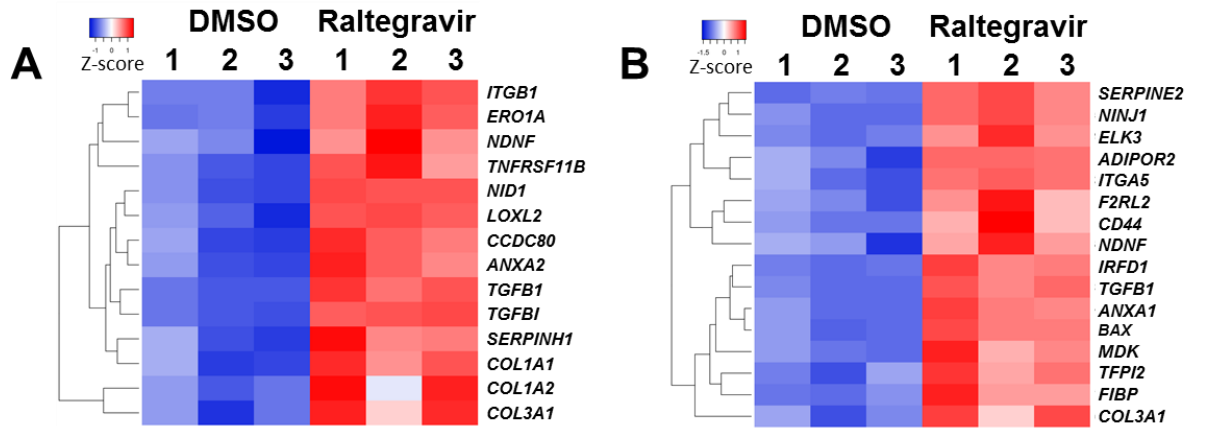

Figure 6.6: Heatmaps of additional functional families upregulated following raltegravir treatment of FHV-1-infected cells. (A) Genes involved in extracellular matrix organization. **(B)** Genes involved in wound healing.

(i) this gene was also present in the list of the top 20 DEGs (Table 6.2) and (ii) its expression has been shown to be increased in HHV-1-infected cells (22). Evaluation of *ATF3* gene expression showed that FHV-1 infection downregulated *ATF3* expression, which is in contrast to what has been described for HHV-1. Moreover, there was no difference in expression of *ATF3* between untreated and raltegravir (or PAA)-treated FHV-1-infected cells, which is in contrast to our RNAseq results where a significant downregulation of *ATF3* was identified (Fig. 6.5E). The latter could be explained by an animal-specific response instead of a general consequence of raltegravir treatment, since the FCEC cultures used for these follow-up experiments were derived from different donors than those used for RNAseq.

Raltegravir alters the cellular metabolism of FHV-1-infected cells

Besides analyzing our dataset using PANTHER, we also submitted the complete list of DEGs to the STRING database to identify potential functional protein-protein interactions. No additional gene enrichments or interactions of note beyond those discussed above were observed among the downregulated genes (data not shown). Among the upregulated genes, STRING identified a significant enrichment of 38 genes related to cellular metabolic pathways that were

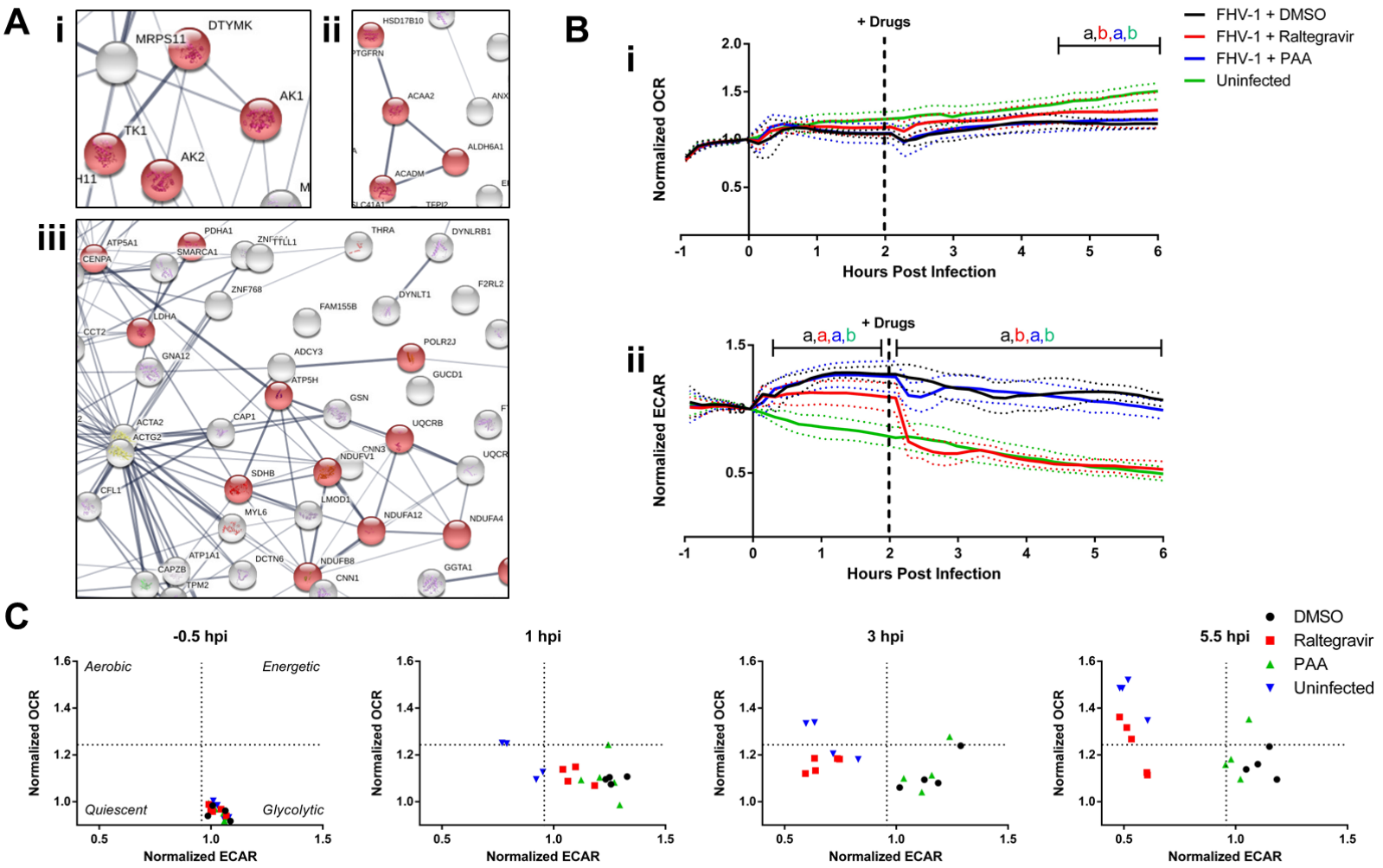

Figure 6.7: Raltegravir induces metabolic changes in FHV-1-infected FCECs. (A) STRING network analysis of upregulated genes related to metabolic processes following raltegravir treatment of FHV-1-infected cells. Three networks of genes were identified with functions in nucleotide triphosphate homeostasis (i), fatty acid catabolism and acetyl CoA production (ii), and

Figure. 6.7 continued. oxidative phosphorylation (iii). **(B)** Agilent Seahorse XF24 measurements of normalized OCR, a measure of oxidative phosphorylation, (i) and ECAR, a measure of glycolysis (ii). FCECs were infected with FHV-1, at an MOI of 3, and treated at 2 hpi with DMSO, 500 µM raltegravir, or 89.25 µM PAA. One-way ANOVA was used to determine significance at each time point. **(C)** Characterization of the metabolic phenotype of FHV-1-infected cells at indicated time points.

grouped into three distinct networks (Fig. 6.7A). Network 1 (Fig. 6.7Ai) consisted of the nucleotide kinases adenylate kinase 1 and adenylate kinase 2, which convert AMP to ATP, as well as thymidine kinase 1 and deoxythymidylate kinase, which together convert dTMP to dTTP (23–26). Network 2 (Fig. 6.7Aii) consisted of enzymes that metabolize fatty acids and other molecules, leading to the production of acetyl CoA, a key molecule in the citric acid cycle which delivers the acetyl group to be oxidized for energy production. Network 3 (Fig. 6.7Aiii) consisted of enzymes related to oxidative phosphorylation, primarily those involved in the mitochondrial electron transport chain and pyruvate conversion. Collectively, these enzymes play important roles in maintaining cellular homeostasis, especially in response to stress, and in the production of ATP. Therefore, we hypothesized that raltegravir treatment of FHV-1-infected cells would shift metabolism to more closely resemble the uninfected state. To test this, we decided to perform metabolic profiling of infected cells using a Seahorse XF24 analyzer. Baseline metabolism was recorded for 1 h, cells were infected with FHV-1, and then treated at 2 hpi with either DMSO, raltegravir, or PAA. No changes in the oxygen consumption rate (OCR), a measure of oxidative phosphorylation, were observed initially following infection with FHV-1 (Fig. 6.7Bi). However, treatment of these infected cells with raltegravir caused a moderate increase in the OCR late in the infection, while treatment with either DMSO (vehicle) or PAA had no effect (Fig. 6.7Bi). Furthermore, a significant increase in the extracellular acidification

rate (ECAR), a measure of glycolysis, was noted following infection with FHV-1, starting around 0.5 hpi (Fig. 6.7Bii). Treatment with raltegravir caused a dramatic and rapid drop in the ECAR to levels similar as observed in the uninfected cells. No such effect was observed following treatment of infected cells with either DMSO or PAA (Fig. 6.7Bii). In order to determine the metabolic phenotype of these cells at the different stages of infection, ECAR vs OCR data from selected time points were plotted. Prior to infection, all cells exhibited a glycolytic phenotype (Fig. 6.7C). Over time, both the uninfected cells and raltegravir-treated FHV-1-infected cells adopted an aerobic phenotype, while the FHV-1-infected control cells and PAA-treated FHV-1-infected cells maintained a glycolytic phenotype (Fig. 6.7C). These results indicate that raltegravir induces metabolic changes in FHV-1-infected cells, promoting a return to homeostasis in response to stress. Moreover, these results appear to be independent of the direct-acting antiviral effect of the drug, as no such effect was observed with PAA.

Raltegravir induces few transcriptional changes in uninfected cells

Since raltegravir induced dramatic changes in host gene transcription of FHV-1-infected cells, we wanted to investigate whether raltegravir also causes these changes in the absence of a herpesvirus infection. To this end, we performed RNAseq on uninfected FCECs that were either treated with 500 μM raltegravir or DMSO for 2 h, and used the same analysis pipeline as used for analyzing the FHV-1-infected FCECs. Read count analysis for these samples is presented in Table 6.3. In total, over 22,000 genes were tested for differential expression by cuffdiff2 and 895 were called differentially expressed between the two conditions. Following the addition of filters for minimum expression level and fold-change between conditions and curation for protein coding genes (see methods), 27 of these genes were considered differentially expressed (Fig. 6.8A), with 18 genes upregulated and 9 downregulated in raltegravir-treated cells compared to

Table 6.3: Numbers of Illumina sequencing reads per replicate sample in uninfected cells.

		Number of Reads		
Sample	**Description**	**Raw**	**Filtered**	**Mapping cat genome**
1	DMSO	31,441,286	28,185,206	24,390,039
2	DMSO	39,724,723	36,356,866	31,886,603
3	DMSO	35,953,076	32,476,236	28,022,864
			Avg	28,099,835
			SD	3,748,875
4	Raltegravir	37,329,225	33,472,797	28,952,259
5	Raltegravir	38,255,929	34,891,953	30,416,721
6	Raltegravir	33,998,470	30,799,813	26,628,178
			Avg	28,665,719
			SD	1,910,456
		T-test DMSO vs Raltegravir		0.827

control cells (Table 6.4). When comparing this list of DEGs in raltegravir-treated uninfected cells (Table 6.4) with the list of DEGs in raltegravir-treated FHV-1-infected cells (see appendix), no genes were found to be similarly downregulated in raltegravir-treated cells with or without infection. In contrast, two genes were found to be similarly upregulated in both lists: methionine adenosyltransferase 2A, which forms s-adenosylmetionine, the principle methyl donor in cells (27), and pleckstrin homology-like domain family A member 1, an apoptotic mediator in a variety of tissues (28). As, to our knowledge, no specific function of either of these genes has been demonstrated in the context of a herpesvirus infection or in relation to corneal cells, we

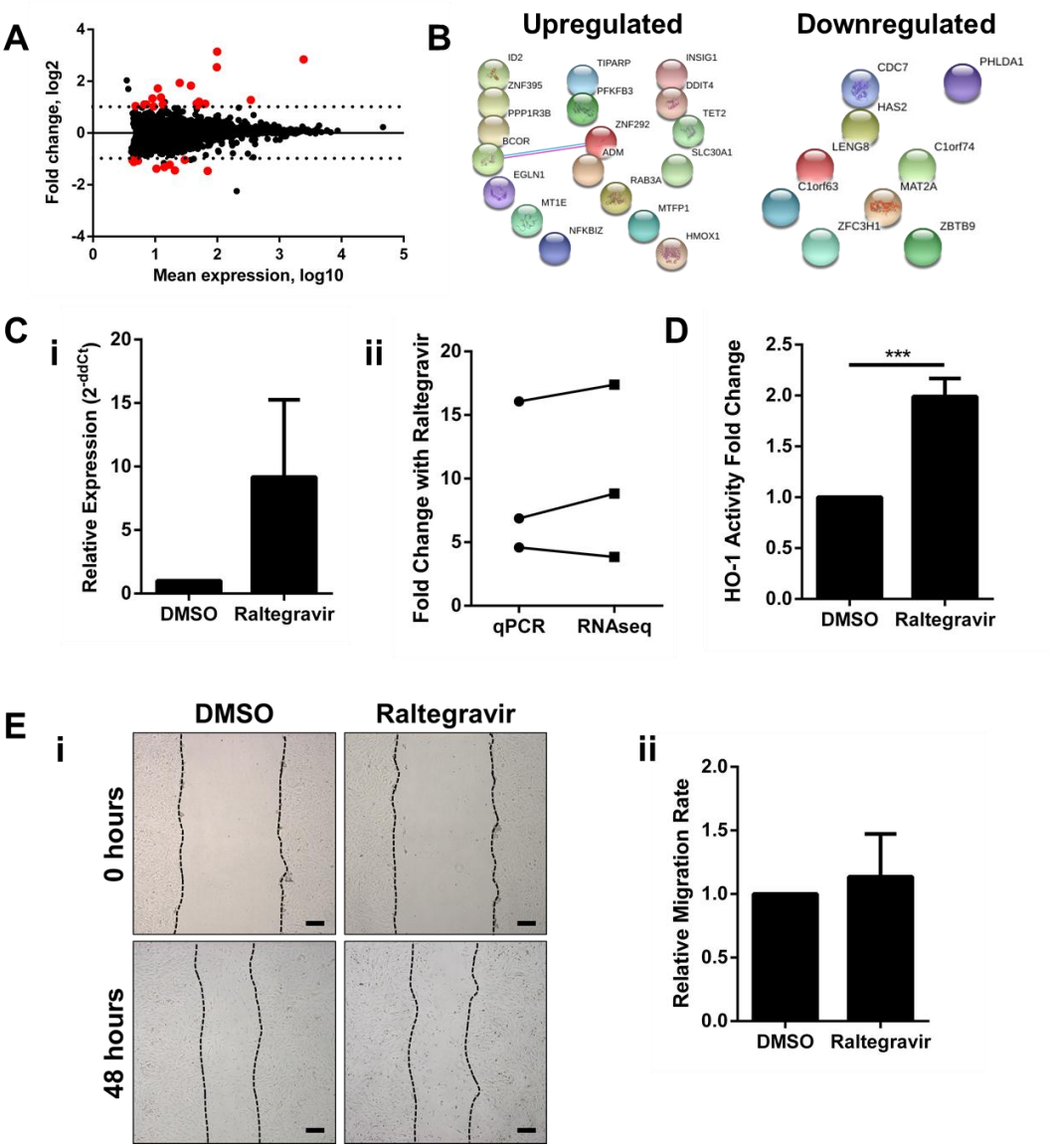

Figure 6.8: Raltegravir induces few transcriptional changes in uninfected FCECs. Uninfected FCECs were treated for 2 h with 500 µM raltegravir or DMSO, and processed for RNAseq analysis. **(A)** MA plot of gene expression in raltegravir treated, uninfected cells. Red, stringent- DEGs; black, expressed genes. **(B)** STRING pathway analysis of up and downregulated DEGs. **(C)** Assessment of *HO-1* expression in FCECs following 2 h of 500 µM raltegravir treatment by qPCR (i) and comparison of qPCR fold change to fold change as determined by RNA sequencing (ii). **(D)** Determination of HO-1 enzymatic activity in FCECs following 2 h of 500 µM raltegravir treatment. **(E)** Representative images (i) and quantification (ii) of FCEC migration rate over 48 h following monolayer wounding and 500 µM raltegravir treatment every 24 h. Scale bars, 200 µm. ***, $p \leq 0.001$.

Table 6.4: List of protein-coding differentially expressed genes (DEGs) following raltegravir treatment of uninfected cells. Fold changes were calculated by comparison of the mean FPKM values of DMSO vs raltegravir treated cells at 2 h post treatment. Genes were ranked according to fold change.

		Average FPKM values		
Gene symbol	**Fold change**	**DMSO**	**Raltegravir**	**Adjusted p-value**
HMOX1	8.83	20.27	178.92	0.00005
MT1E	7.18	600.69	4312.86	0.00005
SLC30A1	5.84	28.85	168.38	0.00005
ADM	3.84	10.29	39.46	0.00005
PFKFB3	3.55	16.61	58.97	0.00005
RAB3A	3.3	5.15	16.98	0.00005
MAT2A	-2.76	102.63	37.16	0.00005
HAS2	-2.72	30.32	11.16	0.00005
ZFC3H1	-2.6	15.16	5.83	0.00005
PPP1R3B	2.6	6.87	17.86	0.00005
MTFP1	2.52	5.14	12.98	0.00005
RSRP1	-2.49	20.09	8.07	0.00005
DDIT4	2.43	202.67	491.83	0.00005
LENG8	-2.33	23.97	10.27	0.00005
ID2	2.31	30.85	71.25	0.00005
EGLN1	2.2	29.14	64.07	0.00005
TIPARP	2.19	40.12	87.7	0.00005
ZBTB9	-2.17	6.2	2.86	0.00005
ZNF395	2.16	8.4	18.11	0.00005
INSIG1	2.15	4.6	9.89	0.00005
ZNF292	2.15	4.26	9.16	0.00005
NFKBIZ	2.1	31.45	66.14	0.00005
CDC7	-2.1	7.15	3.41	0.00005
C1orf74	-2.07	5.84	2.81	0.00005
TET2	2.06	3.17	6.54	0.00005
PHLDA1	-2.05	40.29	19.61	0.00005
BCOR	2.04	6.25	12.72	0.00005

decided to not follow up on these genes in the current study, although their potential role could be pursued in future studies.

When we analyzed the list of DEGs in raltegravir-treated uninfected cells for GO term enrichment, no shared biological processes or molecular functions were identified in either up- or downregulated genes, likely due to the low number of DEGs (data not shown). Likewise, no major gene interactions were identified by STRING (Fig. 6.8B). These results indicate that raltegravir has few effects in uninfected cells and that this drug modulates the expression of a handful of specific genes rather than stimulating specific pathways. We decided to focus on *HMOX-1*, which encodes heme oxygenase 1 (HO-1), for further evaluation. *HMOX*-1 was the most upregulated gene following raltegravir treatment (Table 6.4) and induction of HO-1 is known to contribute to corneal wound healing in mice models (29, 30). HO-1 is an inducible isozyme of HO that catalyzes the degradation of cellular heme into equimolar amounts of carbon monoxide, iron, and biliverdin in order to avoid the accumulation of free iron. However, the byproducts of this reaction also have useful biological functions. The biliverdin is converted to bilirubin, by the biliverdin reductases A and B, and exogenous application of bilirubin has been shown to have broad-spectrum antiviral properties (31, 32). Furthermore, carbon monoxide and iron have known anti-inflammatory effects (33, 34).

We first evaluated the upregulation of *HMOX-1* by qRT-PCR. While we observed an ~8 fold upregulation in raltegravir-treated FCECs compared to control cells, this result failed to reach statistical significance due to the high standard deviation between the samples (Student's T Test, p=0.08, Fig. 6.8Ci). Nevertheless, close agreement was noted in the fold change following raltegravir treatment in each individual sample when analyzed by qRT-PCR versus RNAseq (Fig. 6.8Cii). Using a previously described assay to assess the enzymatic activity of HO-1 (35),

we found that raltegravir treatment resulted in a 2-fold upregulation of relative HO-1 activity in FCECs compared to DMSO-treated control cells (Fig. 6.8D). Using scratch assays, an *in vitro* assay commonly used to assess wound healing (30), we observed no difference in migration rate between raltegravir-treated and DMSO-treated cells (Student's T Test, p=0.515, Fig. 6.8E). This indicates that the two-fold upregulation in HO-1 activity following raltegravir did not translate into a functional effect on wound healing. This lack of an effect on cell migration was further confirmed using electric cell-substrate impedance sensing (ECIS), an assay commonly used to

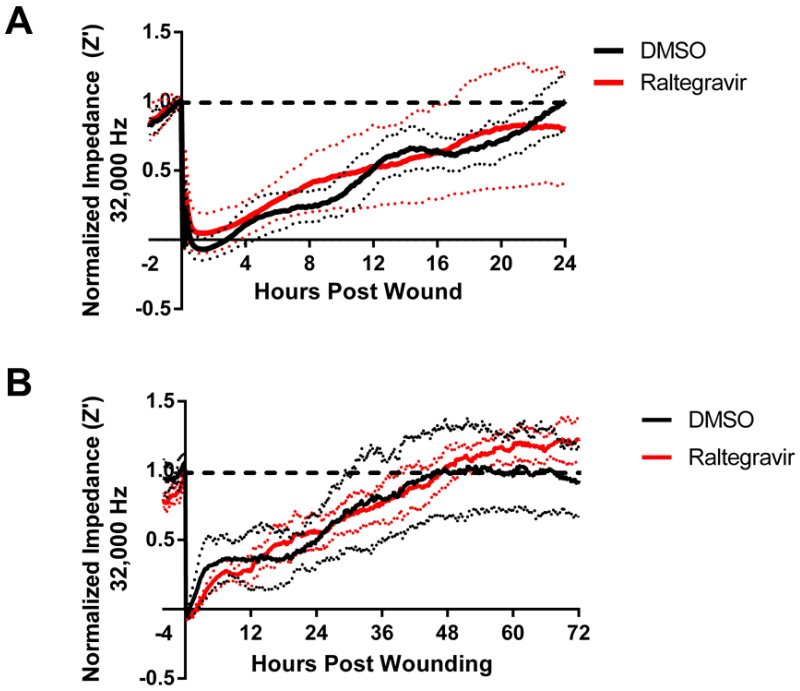

Figure 6.9: Electric cell-substrate impedance sensing to evaluate the effects of raltegravir treatment on migration rate of mock-infected cells. **(A)** FCECs were serum starved for 6 h, wounded, and then treated with 500 µM raltegravir or DMSO. **(B)** FCECs were serum starved and pretreated for 6 h with 500 µM raltegravir or DMSO, wounded, and drug treatment was continued. For both experiments, impedance (Z) was recorded at 32,000 Hz and normalized to the last time point prior to wounding. Solid lines, average of 4-6 technical replicates; dotted lines, standard deviation of 4-6 technical replicates. N=1 biological replicates.

measure *in vitro* wound closure rates (36), using cells treated with raltegravir immediately following wounding (Fig. 6.9A), as well as pre-treated with raltegravir (Fig. 6.9B).

6.4. Discussion

In this study, we utilized RNAseq to evaluate the transcriptome profile of alphaherpesvirus-infected cells treated with the HIV-integrase inhibitor raltegravir. We used FHV-1 to infect feline corneal epithelial cells as proof-of-concept, as it is a close relative of HHV-1 that similarly causes ocular herpes (37). We found that FHV-1-infected cells expressed higher levels of anti-angiogenic factors and showed an altered cellular metabolism when treated with raltegravir. These effects were specific to raltegravir and independent of the direct-acting antiviral effect of the drug, since treatment with the DNA polymerase inhibitor phosphonoacetic acid did not induce these effects.

The effects of raltegravir on host gene expression have previously been evaluated in the context of HIV infection (13). Both similar and contrasting observations were made between this study and ours, despite significant differences in methodology. First, the observed alterations in metabolic genes were similar, with a significant upregulation of genes related to glucose and carbohydrate metabolism, such as *PFKB2*. Interestingly, both HIV-1 and HHV-1 have been shown to induce metabolic changes, with a specific shift towards glycolysis, in infected cells (38–40). For HHV-1, multiple mechanisms are responsible for inducing a glycolysis shift, including the blockage of the electron transport chain between complexes II and III by the viral serine-threonine protein kinase US3 to inhibit mitochondrial respiration (39) and an increase in 6-phosphofructo-1-kinase activity, a rate-limiting enzyme in the glycolytic pathway (40). Since these mechanisms are required to promote replication, it suggests that a glycolytic profile is

beneficial for efficient alphaherpesvirus production. In our present study, we likewise observed an increase in glycolysis shortly after cells were infected with FHV-1 and a maintenance of the metabolic phenotype similar to that of uninfected cells with raltegravir. It has been shown previously that treatment with the drug 2-deoxy-glucose, which inhibits glycolysis by competitively inhibiting the conversion of glucose to glucose-6-phosphate by phosphoglucoisomerase, reduced the size of corneal lesions and the amounts of pro-inflammatory mediators in a murine corneal HHV-1 infection model (41). It will be interesting in future studies to determine the extent to which this inhibition of glycolysis contributes to the antiviral activity of raltegravir, as well as to explore the potential effects of raltegravir on host metabolism in the context of other infections for which raltegravir does not show direct-acting antiviral activity. Second, whereas we found that raltegravir enhanced the expression of a group of anti-angiogenic factors in corneal cells, the study of Ouyang *et al*. found an upregulation in CD8+ T cells of *AGGF1* and *ROBO4*, two genes which promote angiogenesis (42, 43). These results suggest that the effects of raltegravir on angiogenesis might, at least in part, depend on the target cell and infection context in which this drug is used. Finally, and again in contrast to the Ouyang study (13), we did not identify a substantial differential expression of clear mediators of innate immunity that would contribute to viral clearance. Although we identified an upregulation of the oncostatin M receptor, a member of the interleukin 6 group of cytokines, transforming growth factor beta 1, beta-2 microglobulin, interleukin 13 receptor alpha 1, *CD44*, *CXCL8*, and either *CXCL5* or *6*, immune genes that are critical in orchestrating the systemic immune responses to infection, we did not observe any alterations in modulators of local antiviral immunity, such as interferons. Collectively, these results appear to indicate that the main antiviral effects of raltegravir on alphaherpesviruses are due to the direct-acting nature of this

drug, rather than indirect manipulation of the local host immune responses, with the possible exception of the aforementioned metabolic manipulations that could make the host environment less hospitable to viral replication. It would be interesting in future studies to perform similar analysis in raltegravir-treated HHV-1-infected cells to determine if these effects are conserved between herpesviruses. Such studies may also provide more opportunities for functional characterization of the effects without the inherent limitations of working with cells of feline origin.

We also determined if raltegravir induced similarly dramatic effects in uninfected cells. However, we found that raltegravir treatment resulted in very few changes in host gene expression, suggesting that raltegravir is unlikely to have unintended side effects if delivered to healthy, non-infected target cells. One possible explanation for the lack of changes in host gene expression in non-infected cells could be that raltegravir interacts with the cellular stress response pathways, which would be activated during viral infection, but not at steady-state. Additional studies evaluating the effects of raltegravir in stressed cells, for example under hypoxic conditions, would be of interest to further determine the specificity of these effects. In uninfected cells, of the 27 DEGs, we followed up on *HMOX-1*. Although we could confirm a 2-fold increase in the activity of the HO-1 protein following raltegravir treatment, we did not observe a functional improvement in wound healing, as has been reported for other inducers of HO-1 activity (29, 30). We propose three possible reasons that could account for this lack of a functional effect on wound healing. First, it is possible that the increase in HO-1 activity upon raltegravir treatment was not sufficient to boost the endogenous levels of bilirubin, the molecule directly implicated in wound healing. We attempted to measure bilirubin production in corneal cells following raltegravir treatment, but the levels were below the detection limit (data not

shown). Second, the observed downregulation of hyaluronan synthase 2 (HAS2) (Table 6.4) may counteract any benefit of HO-1 induction, resulting in no change in wound healing. HAS2 catalyzes the production of hyaluronic acid, a main component of the extracellular matrix that is critical for efficient wound healing and cellular migration (44, 45). Third, since the context in which the drug is given seems to play a key role in which genes are induced, as demonstrated by the differences in genes affected by raltegravir in infected versus uninfected cells, it could be that wounding the corneal cells *in vitro* for the scratch assays sufficiently alters the baseline state of these cells, causing raltegravir to have different effects than those we measured in uninfected cells.

We were also interested in comparing host gene expression in uninfected vs FHV-1-infected FCECs in the absence of raltegravir treatment to better understand the types of host responses induced by infection. However, we found evidence of transcriptional alterations in response to FHV-1 infection that precluded a simple comparison of gene expression. When RNAseq reads were aligned to the reference genome, we noted that FHV-1-infection was associated with an increase in intronic reads, compared to uninfected cells (Fig. 6.10). Furthermore, we noted that many isoforms of genes detected in our analysis contained retained introns and alternative 3' ends. This indicates that FHV-1 infection significantly altered mRNA processing and/or stability in host cells. Such disruptions have been well described in the literature for other alphaherpesviruses and three mechanisms have been described to explain this effect in the context of HHV-1: (i) the tegument protein virion host shutoff (vhs) catalyzes the degradation of host mRNAs rapidly following infection, (ii) ICP27 interferes with splicing of unprocessed mRNAs into mature mRNAs, and (iii) infection has been shown to reduce recruitment of DNA polymerase II to host gene promoters to reduce transcriptional elongation

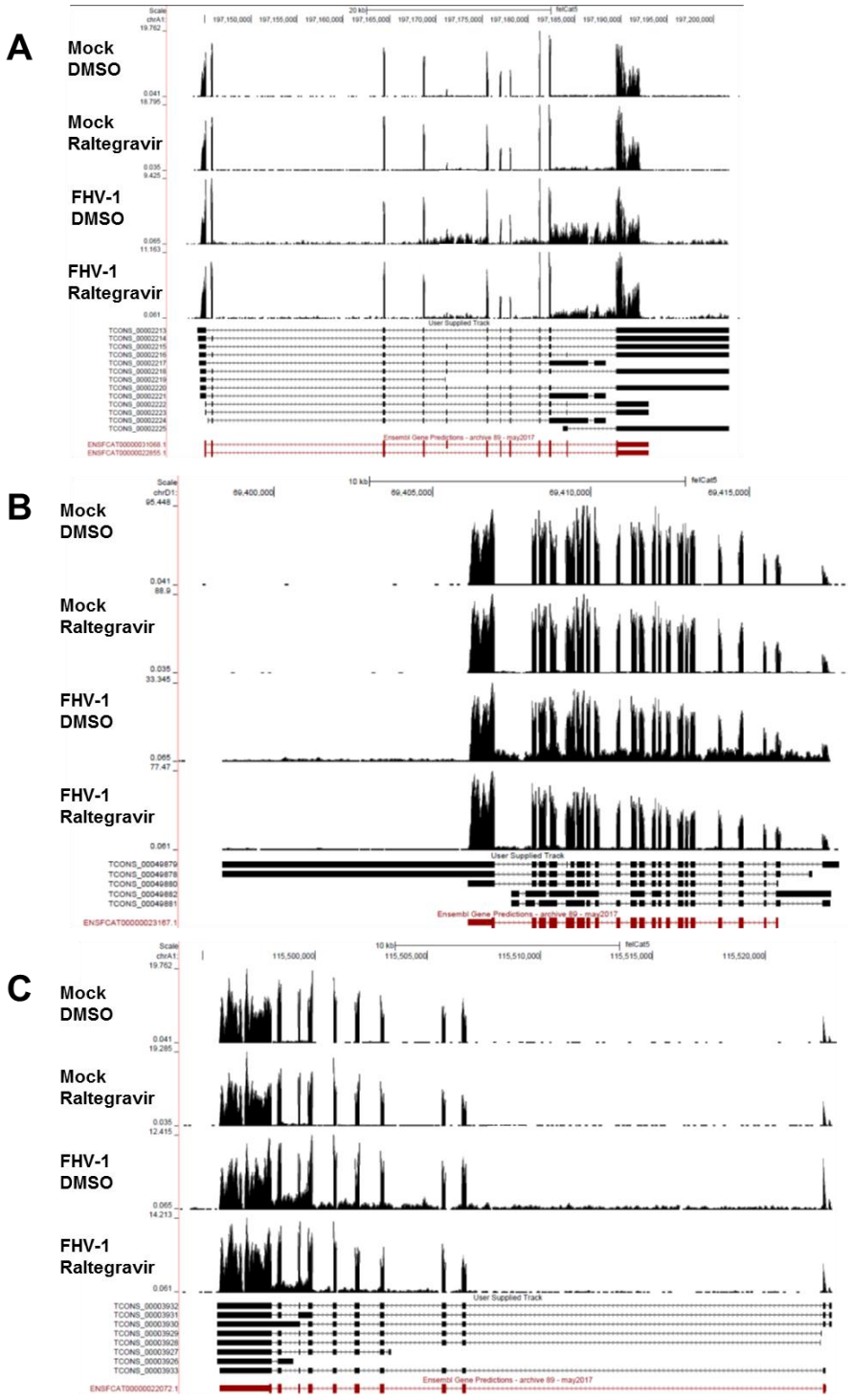

Figure 6.10: FHV-1 infection induces global disruption of host transcription. Alignment of RNAseq reads to the *Felis catus* genome reveals an increase in intronic reads and evidence for extended 3'UTRs in *CSNK1A1* **(A)**, *EIF4G2* **(B)**, and *ETF1* **(C)** following infection with FHV-1.

(46–48). Recently, it was also shown that HHV-1 triggers the disruption of transcriptional termination of host, but not viral genes, resulting in transcription of long 3' untranslated regions extending thousands of nucleotides into intergenic regions and downstream genes. The result of this is the transcription of cellular genes that are not translated (49). Because these changes to host mRNA isoforms in the context of FHV-1 infection significantly complicated gene-level analysis, a comparison of gene expression between uninfected vs FHV-1-infected FCECs was deemed beyond the scope of the current study.

Taken together, this is the first study, to our knowledge, to explore the host-targeted effects of an anti-alphaherpesvirus drug using an untargeted, deep sequencing approach, and it highlights the profound impacts antiviral therapies can have on host cell transcription. Additionally, this study provides a framework RNAseq approach that can be used to study the host-targeted effects of any antiviral compound in the context of any virus infection, providing additional insights into the host responses to virus infections.

6.5. Methods

Cells, virus, and drug

Primary FCECs were isolated in-house from the corneas of healthy specific pathogen free cats that were euthanized for reasons unrelated to the current study and cultured in supplemented hormonal epithelium medium (SHEM), as previously described (50). FCECs from one cat were used for the RNA deep sequencing, to reduce inter-animal variability and in line with previous studies performing RNAseq on microbe-infected cells (51–53), and FCECs from multiple different cats were used for follow-up experiments. The FH2CS strain of FHV-1, originally isolated from a litter of kittens presenting to Cornell University with upper respiratory disease in

1969 (54), was used in this study, and propagated and titered on Crandell Reese Feline Kidney cells (CRFKs), as previously described (18). Raltegravir (ChemieTek, Indianapolis, IN) and PAA (Sigma Aldrich, St. Louis, MO) were dissolved in DMSO and Dulbecco's Modified Eagle Medium (DMEM), respectively, and stored at -20°C.

Validation of RNAseq approach

For flow cytometry, confluent FCECs were serum starved with 2% fetal bovine serum (FBS) SHEM for 6 h and then either mock-infected or infected with FHV-1 at an MOI of 10. Media was removed 2 h later, cells were rinsed with phosphate buffered saline (PBS), and fresh 2% FBS SHEM was added containing either 500 µM raltegravir or DMSO as a vehicle control. Cells were collected 2 h later (4 hpi) using Accutase cell detachment solution (Innovative Cell Technologies, San Diego, CA). Cells were fixed for 15 min in 2% paraformaldehyde, blocked and permeabilized in 10% normal goat serum, 1% bovine serum albumin (BSA), and 0.1% Triton-X in PBS for 1 h at room temperature (RT), and stained using a mouse anti-FHV-1 monoclonal antibody which recognizes FHV-1 gB, gC, gD, and gI (Clone FHV7-7C, Bio-Rad, Hercules, CA) diluted 1:100 in 1% BSA in PBS for 1 h at RT. An Alexa Fluor 488 conjugated goat anti-mouse polyclonal antibody (Jackson ImmunoResearch, Inc, West Grove, PA, 115-545-166) diluted 1:100 in 1% BSA in PBS for 30 min at RT was used as a secondary antibody. 50,000 events were recorded on a Gallios flow cytometer (Beckman Coulter, Indianapolis, IN) equipped with a 488-nm laser. Data were analyzed using Kaluza Analysis (Version 1.3.14026.13330) software (Beckman Coulter, Brea, CA).

For cell viability, the MTT cell viability assay (Sigma Aldrich) was used, similarly to as previously described (55). Briefly, $1x10^4$ FCECs were plated into triplicate wells of a 96 well plate and grown overnight. Cells were serum starved for 6 h in 2% FBS SHEM and then mock-

infected or infected with FHV-1 at an MOI of 10 for 2 h. Cells were rinsed with PBS and then treated with either 500 µM raltegravir or DMSO for an additional 4 h. Media was removed from the wells and replaced with 2% FBS SHEM containing the MTT reagent. Cells were incubated for 45 min and then an equal volume of solubilization solution was added to dissolve the formazan crystals. The absorbance was measured spectrophotometrically at 570 nm and expressed relative to mock-infected, DMSO-treated cells.

RNA deep sequencing (RNAseq) and analysis

For analysis of drug effects on FHV-1 infected cells, three independent biological replicate cultures of $3x10^5$ FCECs per condition (FHV-1-infected, DMSO-treated, and FHV-1-infected, raltegravir-treated) were each plated into T25 flasks and cultured for 2 days until confluent. In order to minimize the effects of serum stimulation on transcription (56), cells were serum starved in 2% FBS SHEM for 6 h and then infected with FHV-1 at an MOI of 10 for 2 h. Media was removed, cells were rinsed with PBS to remove unattached virus, and 2% FBS SHEM containing either 500 µM raltegravir or DMSO as a vehicle control. Two h later (4 hpi), media was removed, cells were rinsed with PBS, and cells were lysed with 2 ml Trizol (ThermoFisher, Waltham, MA). Lysates were stored at -80°C for further processing. For analysis of drug effects on uninfected cells, three independent biological replicate cultures of $3x10^5$ FCECs per condition (Uninfected, DMSO-treated, and uninfected, raltegravir-treated) were plated into T25 flasks and cultured for 2 days until confluent. Cells were serum starved in SHEM containing 2% FBS for 6 h, treated for 2 h with either 500 µM raltegravir or DMSO, and collected as described above.

Total RNA was purified from Trizol-lysed cells according to the manufacturer's protocol, with the following additions: after the first phase separation, an additional chloroform extraction step of the aqueous layer in Phase-lock gel heavy tubes (Quanta Biosciences, Beverly, MA),

addition of 1 µl Glyco-blue (ThermoFisher) immediately prior to isopropanol precipitation, and two washes of the RNA pellet with 75% ethanol. Additionally, cell lysates were spiked with a 1:4.65 ratio of *Drosophila* S2 cells to feline cells prior to RNA isolation in the event that this exogenous RNA spike would be useful for normalization. However, it was determined that these reads were not useful for normalization and were filtered out in subsequent analysis, described below. RNA sample quality was initially confirmed by spectrophotometry and then using a Fragment Analyzer (Advanced Analytical, Ankeny, IA) to determine RNA integrity. PolyA+ RNA was isolated from 1 µg total RNA per sample with the NEBNext Poly(A) mRNA Magnetic Isolation Module (New England Biolabs, Ipswich, MA). TruSeq-barcoded RNAseq libraries were generated with the NEBNext Ultra Directional RNA Library Prep Kit (New England Biolabs) and libraries were sequenced on the HiSeq2500 instrument (Illumina, San Diego, CA) to generate 100 nt single-end reads. Reads were trimmed to remove low quality and adaptor sequences with cutadapt v1.8 (-m 20 -q 20 -a AGATCGGAAGAGCACACGTCTGAAC-TCCAGTC --match-read-wildcards) (57). Reads that mapped to the FHV-1 (NC_013590.2) and *Drosophila melanogaster* (UCSC Dm3) reference genome were removed using bowtie2 (-un-gz [nonmatching_reads.fastq.gz]; default bowtie2 mapping parameters) (58). The resultant non-FHV-1, non-*Drosophila*, reads were mapped to the *Felis catus* genome (GCA_000181335.2, Version 6.2), guided by the annotated Ensembl transcriptome with tophat2 v2.0.13 (59). The common transcriptome was called with cufflinks/cuffmerge and was used to analyze differential gene expression (60). Cuffdiff2 v2.2 was used to generate fragments per kilobase of transcript per million mapped reads (FPKM) values and perform statistical analysis of differential gene expression (61). An adjusted p-value <0.05 was considered to be statistically significant as determined by cuffdiff2.

To more stringently define differentially expressed gene, the following filters were implemented: (i) Genes were only considered to be robustly expressed if the average FPKM values were greater than 5 in at least one of the two conditions being compared. (ii) Genes were only considered to be robustly detected if the counts per million mapped reads (CPM) were greater than 10 in at least one of the two conditions. (iii) Genes were only considered to be differentially expressed if log2 fold change was greater than 1 (or less than -1 for downregulated genes). DEGs that passed these filters were curated to filter out false-positive genes called by Cufflinks that are not well-quantified with polyA+ RNAseq. The identity of certain DEGs was assigned based on homology to other mammalian genes where the feline genome was not annotated. In the few cases where the identity of a gene could not be conclusively identified as one specific gene, but rather narrowed down to two or three genes, all possible homologous genes were included in the gene ontology analysis. Lists of protein-coding DEGs were submitted to both the PANTHER Classification Systems (Version 12.0) for GO enrichment analysis (62) and the STRING database (Version 10.5) (63) to identify direct and indirect protein associations.

Phosphonoacetic acid (PAA) dose determination

To determine the dose of PAA that inhibited viral DNA replication to the same level as 500 µM raltegravir, $2x10^5$ CRFKs were plated in 6 well plates and grown overnight in cell line media consisting of DMEM, 10% FBS, and 100 U/ml penicillin/100 µg/ml streptomycin. Cells were infected with FHV-1 at an MOI of 10 and treated at the time of infection with increasing concentrations of PAA, 500 µM raltegravir, or left untreated. Cells were collected at 6 hpi and genomic DNA was isolated using a Blood and Tissue Kit (Qiagen, Frederick, MD). Viral genome replication relative to untreated, FHV-1 infected control cells was determined using SYBR green-based qPCR using primers against *US7* (55) and feline albumin as a housekeeping

gene (Table 6.5). Amplification was performed using an Applied Biosystems 7500 Fast Real Time PCR instrument (Applied Biosystems, Carlsbad, CA) and all samples were run in triplicate. The comparative C_t method ($2^{-\Delta\Delta Ct}$) was used to calculate fold change.

Gene expression analyses by qPCR

For evaluation of anti-angiogenic factors and *HMOX-1* gene expression, RNA was isolated from the same Trizol-lysed cells utilized for the RNAseq experiment, treated with DNase, and cDNA was synthesized using M-MLV Reverse Transcriptase (RT) (ThermoFisher Scientific, Waltham, MA). For evaluation of *THBS1* and *ATF3* expression in relation to uninfected cells, a separate set of FCECs were infected and treated with DMSO, 500 µM raltegravir, or 89.25 µM PAA, exactly as above for the RNAseq infections, except cells were infected with FHV-1 at an MOI of 5. These cells were lysed with a QIAshredder column (Qiagen), lysates were passed through the gDNA eliminator column to remove gDNA, and RNA was then isolated using the RNeasy Plus Mini Kit (Qiagen). cDNA was synthesized using M-MLV RT. Primers were designed using Primer3 (Version 0.4.0) (64), based on sequences found in the National Center of Biotechnology Information (NCBI) GenBank database and, where possible, were designed to bridge an intronic gap (Table 6.5). Feline ribosomal protein L17 (RPL17) was used as a reference gene. SYBR green-based qRT-PCR assays were performed using an Applied Biosystems 7500 Fast Real Time PCR instrument (Applied Biosystems, Carlsbad, CA) and all samples were run in triplicate. The comparative C_t method ($2^{-\Delta\Delta Ct}$) was used to calculate fold change.

Table 6.5: Primers targeting *Felis catus* genes utilized in this study for quantitative RT-PCR.

Gene	Forward	Reverse
ALB	TTCTGCTCTGCAAGTCGATG	TCTCAGCCTCAGGAAGTGTG
AIMP1	CAGGCAATGGTAATGTGTGC	CTCCTTGTCAGGCTCTCCAG
ATF3	CACTGGAGTCGGTCACTGTC	CTTCTTGTTGCGGCACTTG
ATPIF1	GAGAACAAGCTGAAGAGGAACG	CATGGTGTTTCTTCAAGGCTGC
APT5A1	ATCTGCTGCTCAAACCAGGG	CTCAAGAGTTGTTGCGTGGC
HMOX1	CACGTCCAGGCAGAGAATG	GCCATCACCAGCTTAAATCC
PTPRM	TGAAGTGTGCCGAGGGTTAC	CTTAGCGGAGTCCCATGGTG
RPL17	AAGAACACACGGGAAACTGC	CTGGGCACACCTACCAACTC
THBS1	TGCTGCAGAATGTGAGGTTC	GAGGGTGAGAAGAACGTTGG
US7 (FHV-1)	CTTTCCGGTCCTGTCTCCAC	GGTTAAATCTTACCCGCAGTGC

Metabolic Characterization of Infected Cells

A Seahorse XF24 analyzer (Agilent, Santa Clara, CA) was used to monitor the baseline rates of extracellular acidification (ECAR) and oxygen consumption (OCR), similar to previous studies (65). Briefly, $5.5x10^4$ FCECs were plated onto Seahorse plates and cultured overnight. Culture medium was replaced with SHEM made with modified Eagle's medium (MEM) without L-glutamine or sodium bicarbonate. Cells were then incubated at 37°C for 1 h in a non-CO_2 incubator. OCR and ECAR were monitored for 1 h. FHV-1 at an MOI of 3 was then injected into the wells and metabolism was monitored for an additional 2 h. DMSO, raltegravir to a final concentration of 500 µM, or PAA to a final concentration of 89.25 µM was injected. Metabolism

was then monitored for an additional 4 h. Data were normalized to the rate at the time of virus infection. For these experiments 4-6 biological replicates, with 2 technical replicates, were included, spread across 2 Seahorse plates.

Heme oxygenase functional assays

HO-1 activity assays were conducted, as previously described, to determine the rate of bilirubin production (35). Briefly, uninfected FCECs were treated with DMSO or 500 µM raltegravir for 2 h. After treatment, cells were collected and $1x10^6$ cells were resuspended in 1 ml of $MgCl_2$-PBS (100 mM KH_2PO_4 and 2 mM $MgCl_2$). Cells were frozen and thawed three times to lyse cells. 600 µl of cell lysates were added to a reaction mixture containing 0.8 mM NADPH, 2 mM glucose-6-phosphate, 0.2 U glucose-6-phosphate dehydrogenase type XV, 20 µM hemin, and 3 mg rat liver cytosol (used as a source of biliverdin reductase) in $MgCl_2$-PBS (1 ml total volume). Blank reactions consisted of reaction reagents without cell lysates. The mixtures were incubated at 37°C in the dark for 60 min. One volume of chloroform was added to terminate the reaction. Mixtures were vortexed for 30 sec and centrifuged at 15,000 xg for 10 min at RT. The lower chloroform phase was collected. Bilirubin concentration was determined by calculating the differences between the absorbance at 464 nm and 530 nm, measured on a Tecan Infinite 200 PRO (extinction coefficient for bilirubin: 53/mM/cm). Total protein content of cell lysates was determined by bicinchoninic acid (BCA) assay at 562 nm utilizing an albumin standard according to manufacturer's protocol (ThermoFisher). HO-1 activity was calculated as pmol of bilirubin formed per h per mg of total protein and expressed relative to activity in the DMSO control.

Wound healing assays

In vitro scratch assays were performed, as described previously (66). Briefly, $2x10^5$ FCECs per well were seeded in 12-well plates and grown overnight to confluency (3 wells per condition). Cells were washed twice with PBS and serum-starved (2% FBS) overnight. Reference marks were made on the bottoms of wells using a marker. A linear scratch was made on the monolayer using a 200-µl pipette tip. Culture media was removed to remove dislodged cells and replaced with fresh 2% FBS SHEM containing either DMSO or 500 µM raltegravir. Photographs of scratches were taken at 0 and 48 h after scratching using an Olympus CKX41 microscope (Olympus, Center Valley, PA) controlled with Infinity Analyze (Version 6.4) software (Lumenera Corporation, Ottawa, Ontario, Canada). Fresh media and drugs were added at 24 h post scratch. The widths of the scratches were measured in 3 places on each side of the reference line for each well in a blinded-manner using ImageJ. Migration rate were calculated by subtracting the scratch width at 48 h from the scratch width at 0 h and dividing by 48 h. Migration rates were then expressed relative to the DMSO control.

ECIS wound healing assays were performed similarly to as previously described (66). Briefly, wells of ECIS 96W1E+PET plates (Applied BioPhysics Inc, Troy, NY) were rinsed with 10 mM L-cysteine and then pretreated overnight with 10% FBS SHEM at 37°C. $2x10^4$ FCECs were plated into each well and cultured on the ECIS system for 6 h. Impedance was measured in a series RC circuit at 32,000 Hz. Two experimental protocols were utilized. First, cells were treated after wounding. Cells serum starved in 2% FBS SHEM for 6 h. Monolayers were wounded with an electrical current delivered at 1400 µA, 40,000 Hz, for 20 sec. Media was then removed and replaced with fresh 2% FBS SHEM containing either DMSO or 500 µM raltegravir, and impedance was monitored until monolayers recovered. Second, cells were

pretreated prior to wounding. Following the 6 h plating period, cells were serum starved in 2% FBS SHEM and pretreated with either DMSO or 500 µM raltegravir for 6 h. Wounds were performed as above and impedance was monitored until monolayers recovered, without an additional media change. Unwounded wells and wells without cells were included as controls. All conditions were performed with at least 4 technical replicates. These experiments were performed one time each.

Accession Numbers

GEO (NCBI) Series GSE109806

Statistical analysis

All statistical analyses, with exception of the RNAseq analysis (see above), were conducted in GraphPad Prism (Version 6.04 for Windows) and are expressed as the mean ± standard deviation. Significance was evaluated using the Student's T test or ANOVA when more than two groups were compared. All experiments were performed at least three times, except where otherwise noted. A P value of ≤ 0.05 was considered significant.

Acknowledgements

This work was funded by a Cornell University Feline Health Center grant to G. Van de Walle (grant #: NA). The funders had no role in study design, data collection and interpretation, or the decision to submit the work for publication. We would like to thank Lauren Tofano and Cybelle Tabilas for their excellent technical assistance. The authors declare no financial conflicts of interest.

6.6. References

1. Razonable RR. 2011. Antiviral drugs for viruses other than human immunodeficiency virus. Mayo Clin Proc 86:1009–26.

2. De Clercq E, Li G. 2016. Approved antiviral drugs over the past 50 years. Clin Microbiol Rev 29:695–747.

3. Labro MT. 2012. Immunomodulatory effects of antimicrobial agents. Part I: antibacterial and antiviral agents. Expert Rev Anti Infect Ther 10:319–340.

4. Boriskin YS, Leneva IA, Pécheur EI, Polyak SJ. 2008. Arbidol: a broad-spectrum antiviral compound that blocks viral fusion. Curr Med Chem 15:997–1005.

5. Perfetto B, Filosa R, De Gregorio V, Peduto A, La Gatta A, de Caprariis P, Tufano MA, Donnarumma G. 2014. In vitro antiviral and immunomodulatory activity of arbidol and structurally related derivatives in herpes simplex virus type 1-infected human keratinocytes (HaCat). J Med Microbiol 63:1474–1483.

6. Redwan EM, Uversky VN, El-Fakharany EM, Al-Mehdar H. 2014. Potential lactoferrin activity against pathogenic viruses. C R Biol 337:581–595.

7. Wakabayashi H, Oda H, Yamauchi K, Abe F. 2014. Lactoferrin for prevention of common viral infections. J Infect Chemother 20:666–671.

8. Wakabayashi, H, Kurokawa, M, Shin, K, Teraguchi, S, Tamura, Y, Shiraki K. 2004. Oral lactoferrin prevents body weight loss and increases cytokine responses during herpes simplex virus type 1 infection of mice. Biosci Biotechnol Biochem 68:537–544.

9. Zheng Y, Qin Z, Ye Q, Chen P, Wang Z, Yan Q, Luo Z, Liu X, Zhou Y, Xiong W, Ma J, Li G. 2014. Lactoferrin suppresses the Epstein–Barr virus-induced inflammatory response by interfering with pattern recognition of TLR2 and TLR9. Lab Investig 94:1188–1199.

10. Summa V, Petrocchi A, Bonelli F, Crescenzi B, Donghi M, Ferrara M, Fiore F, Gardelli C, Gonzalez Paz O, Hazuda DJ, Jones P, Kinzel O, Laufer R, Monteagudo E, Muraglia E, Nizi E, Orvieto F, Pace P, Pescatore G, Scarpelli R, Stillmock K, Witmer M V., Rowley M. 2008. Discovery of raltegravir, a potent, selective orally bioavailable HIV-integrase

inhibitor for the treatment of HIV-AIDS infection. J Med Chem 51:5843–5855.

11. Ingale KB, Bhatia MS. 2011. HIV-1 integrase inhibitors: a review of their chemical development. Antivir Chem Chemother 22:95–105.

12. Mouscadet JF, Tchertanov L. 2009. Raltegravir: molecular basis of its mechanism of action. Eur J Med Res 14 Suppl 3:5–16.

13. Ouyang Z, Buzon MJ, Zheng L, Sun H, Yu XG, Bosch RJ, Mellors JW, Eron JJ, Gandhi RT, Lichterfeld M. 2015. Transcriptional changes in CD8+ T cells during antiretroviral therapy intensified with raltegravir. Open Forum Infect Dis 2:ofv045.

14. Nadal M, Mas PJ, Mas PJ, Blanco AG, Arnan C, Solà M, Hart DJ, Coll M. 2010. Structure and inhibition of herpesvirus DNA packaging terminase nuclease domain. Proc Natl Acad Sci U S A 107:16078–83.

15. Zhou B, Yang K, Wills E, Tang L, Baines JD. 2014. A mutation in the DNA polymerase accessory factor of herpes simplex virus 1 restores viral DNA replication in the presence of raltegravir. J Virol 88:11121–11129.

16. Maes R. 2012. Felid herpesvirus type 1 infection in cats: a natural host model for alphaherpesvirus pathogenesis. ISRN Vet Sci 2012:495830.

17. Gaskell R, Dawson S, Radford A, Thiry E. 2007. Feline herpesvirus. Vet Res 38:337–54.

18. Pennington MR, Fort MW, Ledbetter EC, Van de Walle GR. 2016. A novel corneal explant model system to evaluate antiviral drugs against feline herpesvirus type 1 (FHV-1). J Gen Virol 97:1414–1425.

19. Giménez F, Suryawanshi A, Rouse BT. 2013. Pathogenesis of herpes stromal keratitis--a focus on corneal neovascularization. Prog Retin Eye Res 33:1–9.

20. Kaye S, Choudhary A. 2006. Herpes simplex keratitis. Prog Retin Eye Res 25:355–380.

21. Thompson MR, Xu D, Williams BRG. 2009. ATF3 transcription factor and its emerging roles in immunity and cancer. J Mol Med 87:1053–1060.

22. Shu M, Du T, Zhou G, Roizman B. 2015. Role of activating transcription factor 3 in the synthesis of latency-associated transcript and maintenance of herpes simplex virus 1 in

latent state in ganglia. Proc Natl Acad Sci U S A 112:E5420–E5426.

23. Shirwany NA, Zou MH. 2014. AMPK: a cellular metabolic and redox sensor. A minireview. Front Biosci (Landmark Ed) 19:447–74.

24. Panayiotou C, Solaroli N, Karlsson A. 2014. The many isoforms of human adenylate kinases. Int J Biochem Cell Biol 49:75–83.

25. Huang SH, Tang A, Drisco B, Zhang SQ, Seeger R, Li C, Jong A. 1994. Human dTMP kinase: gene expression and enzymatic activity coinciding with cell cycle progression and cell growth. DNA Cell Biol 13:461–471.

26. Munch-Petersen B. 2010. Enzymatic regulation of cytosolic thymidine kinase 1 and mitochondrial thymidine iinase 2: a mini review. Nucleosides, Nucleotides and Nucleic Acids 29:363–369.

27. Lu SC, Mato JM. 2008. S-Adenosylmethionine in cell growth, apoptosis and liver cancer. J Gastroenterol Hepatol 23 Suppl 1:S73-7.

28. Nagai MA. 2016. Pleckstrin homology-like domain, family A, member 1 (PHLDA1) and cancer. Biomed Reports 4:275–281.

29. Patil K, Bellner L, Cullaro G, Gotlinger KH, Dunn MW, Schwartzman ML. 2008. Heme oxygenase-1 induction attenuates corneal inflammation and accelerates wound healing after epithelial injury. Investig Opthalmology Vis Sci 49:3379.

30. Halilovic A, Patil KA, Bellner L, Marrazzo G, Castellano K, Cullaro G, Dunn MW, Schwartzman ML. 2011. Knockdown of heme oxygenase-2 impairs corneal epithelial cell wound healing. J Cell Physiol 226:1732–1740.

31. Santangelo R, Mancuso C, Marchetti S, Di Stasio E, Pani G, Fadda G. 2012. Bilirubin: an endogenous molecule with antiviral activity in vitro. Front Pharmacol 3:36.

32. Espinoza JA, González PA, Kalergis AM. 2017. Modulation of antiviral immunity by heme oxygenase-1. Am J Pathol 187:487–493.

33. Soares MP, Bach FH. 2009. Heme oxygenase-1: from biology to therapeutic potential. Trends Mol Med 15:50–58.

34. Zhao J, Tan S, Liu F, Zhang Y, Su M, Sun D. 2012. Heme oxygenase and ocular disease: a review of the literature. Curr Eye Res 37:955–960.

35. Castilho ÁF, Aveleira CA, Leal EC, Simões NF, Fernandes CR, Meirinhos RI, Baptista FI, Ambrósio AF. 2012. Heme oxygenase-1 protects retinal endothelial cells against high glucose- and oxidative/nitrosative stress-induced toxicity. PLoS One 7:e42428.

36. Keese CR, Wegener J, Walker SR, Giaever I. 2004. Electrical wound-healing assay for cells in vitro. Proc Natl Acad Sci U S A 101:1554–9.

37. Pennington M, Ledbetter E, Van de Walle G. 2017. New paradigms for the study of ocular alphaherpesvirus infections: insights into the use of non-traditional host model systems. Viruses 9:349.

38. Gutierrez AD, Balasubramanyam A. 2012. Dysregulation of glucose metabolism in HIV patients: epidemiology, mechanisms, and management. Endocrine 41:1–10.

39. Derakhshan M, Willcocks MM, Salako MA, Kass GEN, Carter MJ. 2006. Human herpesvirus 1 protein US3 induces an inhibition of mitochondrial electron transport. J Gen Virol 87:2155–2159.

40. Abrantes JL, Alves CM, Costa J, Almeida FCL, Sola-Penna M, Fontes CFL, Souza TML. 2012. Herpes simplex type 1 activates glycolysis through engagement of the enzyme 6-phosphofructo-1-kinase (PFK-1). Biochim Biophys Acta 1822:1198–1206.

41. Varanasi SK, Donohoe D, Jaggi U, Rouse BT. 2017. Manipulating glucose metabolism during different stages of viral pathogenesis can have either detrimental or beneficial effects. J Immunol 199:1748–1761.

42. Yadav SS, Narayan G. 2014. Role of ROBO4 signalling in developmental and pathological angiogenesis. Biomed Res Int 2014:1–9.

43. Wang W, Li GY, Zhu JY, Huang DB, Zhou HC, Zhong W, Ji CS. 2015. Overexpression of AGGF1 is correlated with angiogenesis and poor prognosis of hepatocellular carcinoma. Med Oncol 32:131.

44. Stiebel-Kalish H, Gaton DD, Weinberger D, Loya N, Schwartz-Ventik M, Solomon A.

1998. A comparison of the effect of hyaluronic acid versus gentamicin on corneal epithelial healing. Eye 12:829–833.

45. Gomes JAP, Amankwah R, Powell-Richards A, Dua HS. 2004. Sodium hyaluronate (hyaluronic acid) promotes migration of human corneal epithelial cells in vitro. Br J Ophthalmol 88:821–5.

46. Sandri-Goldin RM. 2008. The many roles of the regulatory protein ICP27 during herpes simplex virus infection. Front Biosci 13:5241–56.

47. Sandri-Goldin RM. 2011. The many roles of the highly interactive HSV protein ICP27, a key regulator of infection. Future Microbiol 6:1261–1277.

48. Rivas HG, Schmaling SK, Gaglia MM. 2016. Shutoff of host gene expression in influenza A virus and herpesviruses: similar mechanisms and common themes. Viruses 8:102.

49. Rutkowski AJ, Erhard F, L'Hernault A, Bonfert T, Schilhabel M, Crump C, Rosenstiel P, Efstathiou S, Zimmer R, Friedel CC, Dölken L. 2015. Widespread disruption of host transcription termination in HSV-1 infection. Nat Commun 6:7126.

50. Sandmeyer LS, Keller CB, Bienzle D. 2005. Culture of feline corneal epithelial cells and infection with feline herpesvirus-1 as an investigative tool. Am J Vet Res 66:205–9.

51. Baddal B, Muzzi A, Censini S, Calogero RA, Torricelli G, Guidotti S, Taddei AR, Covacci A, Pizza M, Rappuoli R, Soriani M, Pezzicoli A. 2015. Dual RNA-seq of Nontypeable Haemophilus influenzae and Host Cell Transcriptomes Reveals Novel Insights into Host-Pathogen Cross Talk. MBio 6:e01765-15.

52. Jeffers V, Gao H, Checkley LA, Liu Y, Ferdig MT, Sullivan WJ, Jr. 2016. Garcinol Inhibits GCN5-Mediated Lysine Acetyltransferase Activity and Prevents Replication of the Parasite Toxoplasma gondii. Antimicrob Agents Chemother 60:2164–70.

53. Baer A, Lundberg L, Swales D, Waybright N, Pinkham C, Dinman JD, Jacobs JL, Kehn-Hall K. 2016. Venezuelan Equine Encephalitis Virus Induces Apoptosis through the Unfolded Protein Response Activation of EGR1. J Virol 90:3558–72.

54. Walton TE, Gillespie JH. 1970. Feline viruses. VII. Immunity to the feline herpesvirus in

kittens inoculated experimentally by the aerosol method. Cornell Vet 60:232–9.

55. Pennington MR, Van de Walle GR. 2017. Electric cell-substrate impedance sensing to monitor viral growth and study cellular responses to infection with alphaherpesviruses in real time. mSphere 2:e00039-17.

56. Kirkconnell KS, Paulsen MT, Magnuson B, Bedi K, Ljungman M. 2016. Capturing the dynamic nascent transcriptome during acute cellular responses: the serum response. Biol Open 5:837–47.

57. Martin M. 2011. Cutadapt removes adapter sequences from high-througput sequencing reads. EMBnet.journal 17:10–12.

58. Langmead B, Salzberg SL. 2012. Fast gapped-read alignment with Bowtie 2. Nat Methods 9:357–359.

59. Kim D, Pertea G, Trapnell C, Pimentel H, Kelley R, Salzberg SL. 2013. TopHat2: accurate alignment of transcriptomes in the presence of insertions, deletions and gene fusions. Genome Biol 14:R36.

60. Trapnell C, Williams BA, Pertea G, Mortazavi A, Kwan G, van Baren MJ, Salzberg SL, Wold BJ, Pachter L. 2010. Transcript assembly and quantification by RNA-Seq reveals unannotated transcripts and isoform switching during cell differentiation. Nat Biotechnol 28:511–515.

61. Trapnell C, Hendrickson DG, Sauvageau M, Goff L, Rinn JL, Pachter L. 2012. Differential analysis of gene regulation at transcript resolution with RNA-seq. Nat Biotechnol 31:46–53.

62. Mi H, Muruganujan A, Thomas PD. 2012. PANTHER in 2013: modeling the evolution of gene function, and other gene attributes, in the context of phylogenetic trees. Nucleic Acids Res 41:D377–D386.

63. Szklarczyk D, Morris JH, Cook H, Kuhn M, Wyder S, Simonovic M, Santos A, Doncheva NT, Roth A, Bork P, Jensen LJ, von Mering C. 2017. The STRING database in 2017: quality-controlled protein–protein association networks, made broadly accessible. Nucleic Acids Res 45:D362–D368.

64. Untergasser A, Cutcutache I, Koressaar T, Ye J, Faircloth BC, Remm M, Rozen SG. 2012. Primer3--new capabilities and interfaces. Nucleic Acids Res 40:e115.

65. Hübner D, Jahn K, Pinkert S, Böhnke J, Jung M, Fechner H, Rujescu D, Liebert UG, Claus C. 2017. Infection of iPSC lines with miscarriage-associated coxsackievirus and measles virus and teratogenic rubella virus as a model for viral impairment of early human embryogenesis. ACS Infect Dis 3:886–897.

66. Bussche L, Harman RM, Syracuse BA, Plante EL, Lu YC, Curtis TM, Ma M, Van de Walle GR. 2015. Microencapsulated equine mesenchymal stromal cells promote cutaneous wound healing in vitro. Stem Cell Res Ther 6:66.

CHAPTER SEVEN

DISCUSSION- SUMMARY AND IMPLICATIONS FOR FUTURE ANTIVIRAL DEVELOPMENT

7.1. Summary of Findings

Treating ocular herpesvirus infection remains an ongoing challenge in both human and veterinary medicine, as many current therapies are not satisfactory. Moreover, the experimental systems available to evaluate novel therapies are sub-optimal (**Chapter 1-2**). One key limitation in developing antivirals is that many drugs are effective *in vitro*, but not *in vivo*. New tools and technologies, particularly those that bridge this gap, are needed to aid in the identification of the next generation of anti-herpesviral therapies. Repurposing existing drugs may also be a faster and more cost-effective strategy than *de novo* drug development. The anti-retroviral integrase drug raltegravir is one such candidate as it has been shown to inhibit the DNA cleavage function of the human betaherpesvirus 5 (HHV-5) terminase protein (1) and the replication of HHV-5, human alphaherpesvirus 1 (HHV-1), and human alphaherpesvirus 2 (HHV-2) *in vitro* (2). Therefore, the primary goal of this dissertation was to evaluate raltegravir as a therapy for felid alphaherpesvirus 1 (FHV-1)-associated ocular disease. The secondary goal was to develop novel technologies, tools, and assays to aid in the discovery of antiviral therapies.

To meet these goals, a feline cornea explant model of FHV-1 infection was first developed and validated as a bridge between *in vitro* and *in vivo* work. This model was used to demonstrate that raltegravir could effectively inhibit FHV-1 growth in the cornea (**Chapter 3**). Next, electric cell-substrate impedance sensing (ECIS), was evaluated for its utility in studying both the effects of antivirals and the replication kinetics of viruses, using cidofovir and a recombinant fluorescent FHV-1 virus as examples, respectively (**Chapter 4**). The observed efficacy of raltegravir against FHV-1 raised the question of how an anti-retroviral could inhibit herpesvirus replication. Raltegravir was shown to inhibit both genome replication initiation and late gene expression as two separate events, consistent with a mechanism involving inhibition of

the viral protein ICP8 (**Chapter 5**). Beside the direct antiviral effects of this drug, potential host-targeted effects of raltegravir treatment, both in the presence or absence of an FHV-1 infection, were defined by performing RNA sequencing (RNAseq) on feline primary corneal cells. It was found that raltegravir both boosted the expression of anti-angiogenic factors and maintained metabolic homeostasis in infected cells, potentially contributing to the therapeutic value and antiviral effects of this drug. In contrast, only minimal alterations were found in gene expression profiles in non-infected cells (**Chapter 6**).

Collectively, these studies demonstrate the antiviral efficacy of raltegravir *in vitro,* and have led to the development of several new tools that can aid in future antiviral evaluation. The following sections will discuss how this work addresses the goals of the dissertation and examine the broader applicability of both raltegravir and the technologies developed.

7.2. Prospects for raltegravir as a therapy for ocular herpesvirus infections

7.2.1 Evaluation of raltegravir in vivo

In this dissertation, raltegravir was shown to inhibit FHV-1 replication *in vitro,* using the CRFK immortalized cell culture line, primary feline corneal epithelial cells (FCECs), and a feline cornea explant model. These results recently enabled the evaluation of raltegravir *in vivo,* in close collaboration with Dr. Eric Ledbetter and Dr. Chloe Spertus (3). Fourteen nonvaccinated, specific pathogen free (SPF) cats were experimentally infected with 10^6 PFU FHV-1 per eye, similar to what has been described previously for *in vivo* antiviral studies (4–7). Cats received oral raltegravir (80 mg) or vehicle (lactulose) capsules by mouth, twice daily, for 14 days. This dose of oral therapy was chosen because it has previously been shown to be well tolerated by cats (8), and because the safety of topical raltegravir has not yet been demonstrated

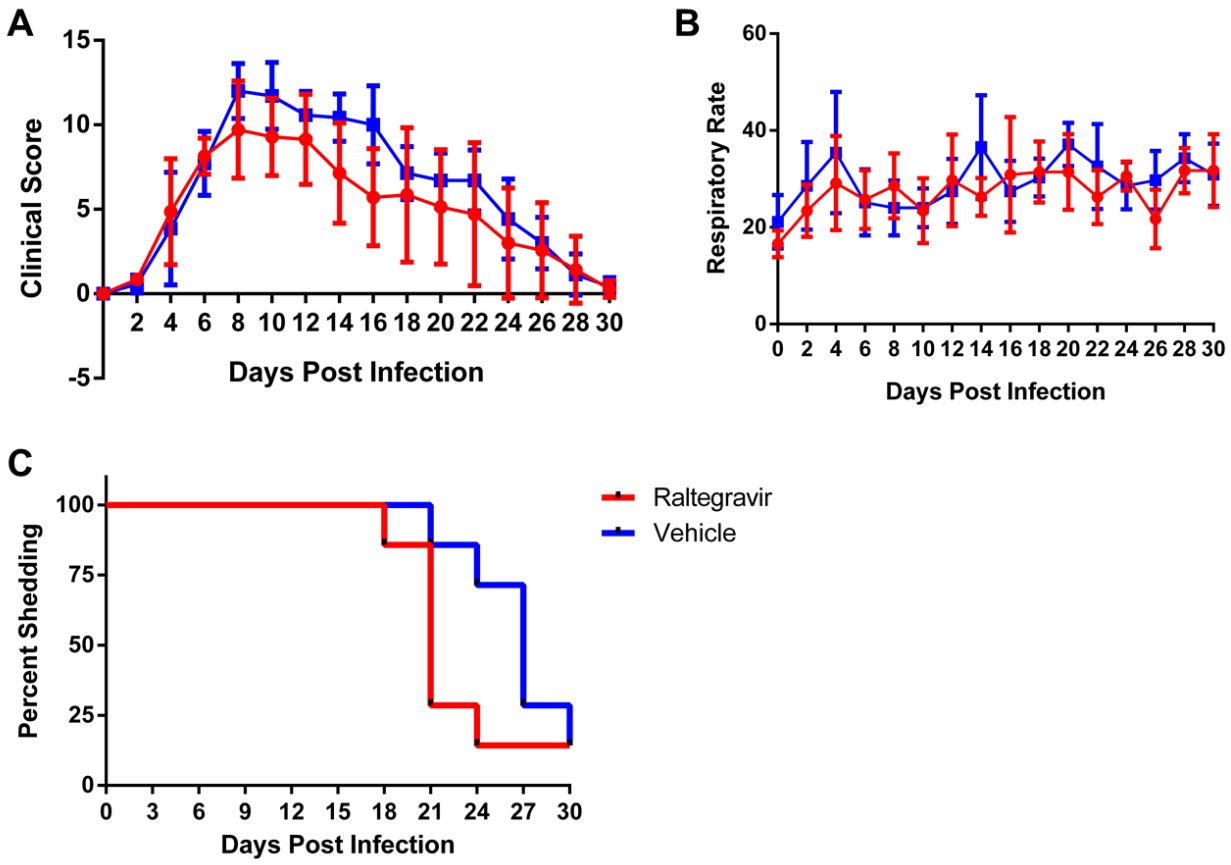

Figure 7.1: Evaluation of raltegravir in experimentally FHV-1-infected cats. SPF cats (N=7 per group) were infected ocularly with 10^6 PFU FHV-1 per eye and treated twice daily for 14 days with 80 mg oral raltegravir or vehicle (lactulose). Cats were evaluated every 2 days by veterinary ophthalmologists for **(A)** combined clinical and respiratory scores (P=0.039) and **(B)** respiratory rates (P= 0.007). Mean ± standard deviation, least squares linear regression analysis using the general linear method. **(C)** Virus was isolated and quantified by plaque assay from ocular swabs collected every 3 days. Kaplan-Meier curve of duration to undetectable virus shedding. Gehan-Breslow-Wilcoxon test, P= 0.0509. Adapted from Spertus, *et al.* 2018 (3).

in any species. Ophthalmic examinations were performed every two days and ocular samples for FHV-1 virus isolation were collected every three days for 30 days. While all cats developed ocular and respiratory disease typical of primary FHV-1 infection, including conjunctivitis and ulcerative keratitis, the raltegravir-treated group had significantly lower ocular disease scores and respiratory rates compared to the vehicle group (Fig. 7.1A-B). The median duration of ocular

viral shedding was also significantly shorter in the raltegravir group compared to the control group (Fig. 7.1C). Furthermore, no leukocyte inflammation was noted, as was observed previously with cidofovir treatment of canid alphaherpesvirus 1 (CHV-1)-infected dogs (9), and no differences in hemogram and serum biochemistry panels were detectable (data not shown). Overall, these results demonstrate that twice daily oral raltegravir is a safe and viable treatment option to reduce the ocular and respiratory clinical signs associated with FHV-1 infection in cats (3).

7.2.2. Comparison of raltegravir to current FHV-1 therapies

Oral raltegravir treatment is in line with what has been described for some of the current therapies to treat ocular FHV-1 infection in cats, with several advantages. Cidofovir and famciclovir have both been evaluated in masked, placebo-controlled clinical trials with an experimental design similar to our own and are widely used clinically (6, 7). It was shown that a topical 0.5% cidofovir ophthalmic solution, given twice per day starting at day 4 post infection and continuing for 10 days, was effective at moderately reducing clinical disease scores. However, they noted no reduction in viral shedding, as determined by qPCR, associated with cidofovir treatment (6). We observed a comparable reduction in clinical disease scores (Fig. 7.1A-B) and also noted no difference in viral shedding as determined by either plaque assays or qPCR (data not shown) with raltegravir treatment. Topical cidofovir lead to a resolution of viral shedding between 7-9 days post infection compared to 12-18 days without treatment (i.e. 5-9 days faster), as determined by qPCR (6). We noted shedding of infectious virus, as determined by plaque assays, for a longer duration of time in both groups, likely due to the higher infectious dose used to inoculate the cats and the development of more severe clinical disease in our study. However, we likewise noted a ~6 day faster cessation of viral shedding (Fig. 7C). Systemic

administration of raltegravir may be advantageous compared to topical cidofovir as the former could be useful for both ophthalmic and respiratory disease, and potentially other FHV-1-associated conditions. Cidofovir is only used for ophthalmic disease due to the poor oral bioavailability of this compound (10). Oral famciclovir, in comparison, given 3 times daily at a 90 mg/kg dose for 21 days starting at infection, significantly reduced clinical disease over a two week period. However, like raltegravir and cidofovir, famciclovir only head a minimal impacted viral shedding, as determined by qPCR, with a significant reduction only being detectable on day 4 post infection (7). It has been anecdotally reported by clinicians that lower concentrations of famciclovir may be sufficient to achieve the same effects, but, due to famciclovir's complex and non-linear pharmacokinetics in cats, this still has to be experimentally determined (11).

Compared to the topical therapies of acyclovir, idoxuridine, vidarabine, and trifluridine, oral raltegravir's twice daily dosage schedule is superior. For example, a 0.5% acyclovir ophthalmic ointment was used in a preliminary, non-blinded study of naturally infected cats, but required 5 times per day therapy (12). However, the use of acyclovir in cats is generally discouraged due to its poor inhibition of FHV-1 *in vitro*, poor bioavailability, and the toxicity of its oral prodrug (see Chapter 1). The other therapies suffer from similar dosage frequencies. Topical idoxuridine, vidarabine, and trifluridine are all recommended to be given every 4-6 hours for 21 days, which is a schedule owners may struggle to adhere to (13). Anecdotally, some owners report that oral treatment is easier to give to their cat compared to eye drops. Oral therapies that have to be given less frequently, such as raltegravir or famciclovir, may, therefore, increase owner compliance and thus treatment efficacy. Finally, only a handful of retrospective case series have evaluated the use of these compounds in cats (11), and so masked, placebo-controlled studies are still needed to evaluate all 4 of these topical therapies.

All of the traditional FHV-1 drugs described above are nucleoside analogues that inhibit viral DNA elongation. The finding that raltegravir inhibits both DNA replication initiation and late gene expression, a mechanism consistent with inhibition of ICP8, raises the possibility that raltegravir could also be compounded with these existing drugs to target multiple stages of the viral life cycle. Additionally, the upregulation of anti-angiogenic compounds following raltegravir treatment may have therapeutic benefits *in vivo* by preventing corneal neovascularity, similar to what was recently demonstrated for ophthalmic metronidazole solutions in rats with experimentally-induced chemical burns (14). However, before such conclusion can be made, it will be important to evaluate raltegravir' anti-angiogenic potential *in vivo*.

7.2.3. Considerations for the practical implementation of oral and topical raltegravir therapy

It has been argued that systemic antiviral medications may generally not be well suited for FHV-1 infection, despite their advantages (7). This is primarily due to the systemic toxicity and poor bioavailability of many of these compounds, as previously discussed. It is a common occurrence that many drugs that are useful in other companion animal species are toxic to cats. The reasons for this are not well understood, but potentially are due to deficiencies in several key conjugation enzymes, such as the major phenol UDP-glucuronosyltransferase enzymes, N-acetyltransferase 2, and thiopurine methyltransferase (15). It is, therefore, important to experimentally confirm the safety of oral drugs to be given to cats, as evidenced by the renal and hepatic toxicity associated with valacyclovir, a common oral anti-herpesviral drug (4). Toxicity does not seem likely to be a major issue in the case of raltegravir. Oral raltegravir has previously been shown to be non-toxic to cats when given for up to 9 weeks (8) and, likewise, we found no evidence of drug toxicity (3).

It is plausible that low oral bioavailability of raltegravir accounts, at least in part, for the relatively modest, though statistically significant, effects on clinical scores we observed. Not taking into account owner compliance, it could be anticipated that topical raltegravir treatment would be more effective than oral treatment, as higher concentrations of drug at the site of infection would be achieved. Indeed, a recent study evaluating the ocular penetration of several anti-retrovirals revealed that a 20 mg dose of raltegravir given orally to a 3-4 kg rabbit only resulted in 0.8±0.69 ng/ml drug detectable in the aqueous humor and 1.99±0.27 ng/ml in the vitreous humor (16). Neither that study nor our study (3) determined the corneal concentration of raltegravir, and it is difficult to extrapolate from the rabbit study to a cat. Still, it is likely that while raltegravir can penetrate ocular tissue when given orally, the 80 mg dose likely results in concentrations well below the drug's EC_{50} against FHV-1. In order to evaluate topical raltegravir therapy against FHV-1, first an ophthalmologic formulation would need to be developed by a compounding pharmacy, either alone or in combination with a polymer to increase contact time (17) and/or a substance to increase tissue penetration of the drug (18). Furthermore, an appropriate ophthalmologic concentration and dosing schedule of such a compound would need to be evaluated for toxicity, preferably first in the cornea explant model and then *in vivo*, before an efficacy study in FHV-1-infected cats could be undertaken.

7.2.4. Intellectual property and cost considerations

Finally, one needs to also consider the intellectual property rights and costs associated with this drug. The inventors, Merck & Company, have protected raltegravir (sold under the brand name Isentress®) as a treatment for HIV infection with two primary patents (U.S. Patent No. 7,169,780 and U.S. Patent No. 7,754,731), which do not expire until 2023 and 2029, respectively. However, at least 50 other U.S.-based patents and dozens of international patents,

some of which do not expire until 2031, further protect the intellectual property of this drug. This has direct consequences for the cost for treatment as long as this drug is under patent protection. Although estimating the cost of raltegravir treatment for ocular herpesvirus treatment is difficult, a treatment cost of approximately $250 per cat was calculated for the duration of our study (3). In comparison, a typical topical cidofovir treatment regimen costs about $70 per cat. However, it has to be noted that when famciclovir was first adopted in cats, it was approximately equal to the current cost of raltegravir and, despite this, was widely used (Eric Ledbetter, *personal communication*). Recently, Merck did license a low-cost, generic raltegravir to the United Nations-supported Medicines Patent Pool. However, this generic is only available in 92 low- and middle-income nations, primarily in sub-Saharan Africa, and is exclusively available for pediatric HIV treatment (19). It is currently not clear if a low-cost generic would be made available for veterinary use or if owners would be willing to pay a premium, compared to other treatment options, for raltegravir.

Overall, raltegravir has clear promise as an anti-herpesviral therapy. Further optimization to develop a more effective topical formulation of the drug and investigations into its viability as a treatment for human ocular herpesvirus infections are required. However, intellectual property issues and licensing issues may need to be resolved to enable the use of raltegravir clinically at a reasonable price. More broadly, these results demonstrate that repurposing FDA-approved drugs can be a good strategy for the identification of new antiviral therapies and highlight the role HIV integrase inhibitors can play in combating herpesvirus infections.

7.3. Application of new techniques in the evaluation of antiviral drugs

Through this thesis, four tools were developed that may have broader applicability in the assessment of antiviral drugs.

The first was the development of the feline cornea explant model that supports FHV-1 replication and can be used to study antiviral drug efficacy. The advantages of this model and its validation were presented in Chapters 2 and 3, respectively. We have already begun to apply this model to test other drugs. For example, povidone-iodine (PVP-I) based compounds are gaining interest as broad-spectrum therapies against ocular infections (20–22). Though it is rarely used therapeutically, ophthalmologic PVP-I has been in use since 1951, primarily as a pre- and post-operative disinfectant, due to its bactericidal, viricidal, antifungal, and antimycotic effects. PVP-I is particularly attractive as it is readily available worldwide, is inexpensive, and ophthalmic use is not known to cause microbial resistance (23). The efficacy of PVP-I in non-ophthalmologic settings has been extensively studied against HHV-1, HHV-2, and human alphaherpesvirus 3 (HHV-3, also known as varicella-zoster virus, VZV) *in vitro*, in mouse models, as well as in clinical trials using human patients (24–28). We, therefore, recently evaluated PVP-I, both alone and compounded with hydroxyethyl cellulose (HEC), as a prophylactic and therapy against FHV-1 infection (29). HEC was used as a viscosity-enhancing agent in ophthalmic formulations to prolong corneal contact time and increase intraocular drug levels (30). We first evaluated toxicity and efficacy of a compound of PVP-I+HEC in CRFK cells, demonstrating that this compound had a synergistic inhibitory effect on virus replication compared to its individual components (Fig. 7.2A-B). Encouraged by these results, we next tested the efficacy of this compound in the cornea explant model. However, we found that the PVP-I+HEC formulation was toxic to the cornea, resulting in the stripping of the epithelial layer off of the underlying

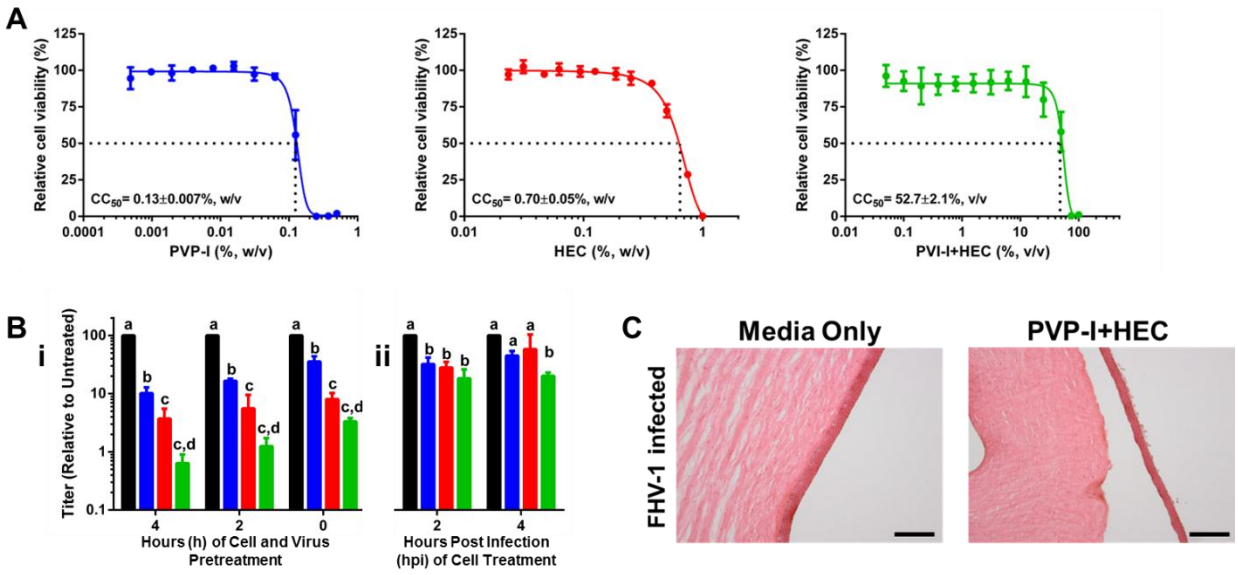

Figure 7.2: Evaluation of PVP-I based compounds against FHV-1. (A). Evaluation of compound toxicity. Confluent CRFKs were treated with various dilutions of PVP-I (%, w/v, aqueous), HEC, (%, w/v, aqueous), or PVP-I+HEC (%, v/v, aqueous, 100%= 0.5% w/v PVP-I+1% w/v HEC), as indicated, for 48 h. Cellular toxicity was evaluated using an MTT-based cell viability assay (Sigma-Aldrich) and normalized to untreated controls. CC_{50}, half maximal cellular cytotoxicity. **(B).** Evaluation of compound efficacy against the FeHV-1 strain FH2CS. **(i)** To evaluate effects of compound pretreatment, both CRFK cells and virus were pre-treated for 4, 2, or 0 h with a 25% v/v dilution of PVP-I+HEC (corresponding to 0.125% w/v PVP-I and 0.25% w/v HEC), 25% v/v dilutions of 0.5% w/v PVP-I (corresponding to 0.125% w/v PVP-I), 1% w/v HEC (corresponding to 0.25% w/v HEC), or left untreated. Cells and virus, at an MOI=0.01, were then incubated in the presence of media containing the compounds for 2 h. **(ii)** To evaluate effects when cells were treated after infection, CRFK cells were infected with FeHV-1 at MOI=0.01 in media for 2h in the same experiment. Media was then replaced at 2 or 4hpi with fresh media containing the compounds. Untreated virus and cells were included as controls. At 48 hpi, all wells were frozen, viral titers were determined by plaque forming assay, and expressed relative to untreated controls. One-Way ANOVA at each time point, $P<0.05$. Average ± SD, n=3. From Pennington, *et al.* 2018 (29) **(C).** Corneas were infected with $3x10^5$ PFU/eye FHV-1, strain FH2CS, for 2 h. Corneas were then cultured in media only or 25% PVP-I+HEC, diluted in media. At 24 hpi, corneas were collected, fixed overnight in 4% PFA, sucrose invaded, sectioned, and stained with hematoxylin and eosin. Scale bars, 200 µm.

stroma layer in both FHV-1-infected (Fig. 7.2C) and uninfected (data not shown) corneas. These results demonstrate that our current formulation is likely to be toxic to the cornea *in vivo* and additional modifications are necessary. This was only revealed when tested *ex vivo,* and thus highlights the importance of testing compounds in such intermediary models before immediately moving *in vivo*. In addition, it would be interesting to (i) adapt the current cornea explant and (ii) develop a new conjunctival explant that could support the replication of other common ocular feline pathogens, such as feline calicivirus, *Mycoplasma felis*, and *Chlamydophila felis*.

The second tool was electric cell-substrate impedance sensing (ECIS), which was used to evaluate the toxicity and efficacy of compounds against FHV-1 as a model for alphaherpesviruses, as described in Chapter 4. Up to 45 compounds, including appropriate controls and replicates, can be tested simultaneously with this system, making it a valuable medium-throughput screening method for the evaluation of drug toxicity and antiviral efficacy (31). As it measures morphological changes in the cells on a nanoscale range (32), it can also be used to quantify changes in cellular behavior in real time in response to drug treatment, which may provide useful information to supplement or replace traditional end-point assays.

Third, CRISPR/Cas9 genome engineering was used to successfully insert a DsRed Express2 fluorophore onto the C-terminal end of glycoprotein D in the FHV-1 strain FH2CS. In combination with the existing literature (33–36), this provides further evidence that CRISPR/Cas9 can be used to quickly edit and create recombinant herpesviruses. The primary reason for creating this virus was to have a fluorescent virus that can be used to readily identify infected cells, or evaluate the expression levels of glycoprotein D, as antibodies against FHV-1 are not widely commercially available. Indeed, it was found that this virus is readily and easily detectable in live cells by flow cytometry, as shown in Chapter 5.

Finally, two recombinant FHV-1 protein, terminase (UL15C) and ICP8, were successfully expressed and purified. These proteins, as well as the previously expressed HHV-1 homologs (37, 38), could be used for screening of inhibitors that specifically target these proteins. Both terminase and ICP8 are attractive drug targets due to their high conservation among the herpesviruses and their central role in the life cycle of these viruses (39). Indeed, the HHV-5 terminase inhibitor letermovir was approved in November 2017 by the FDA, highlighting its value as a drug target. However, letermovir does not cross react with alphaherpesviruses, human betaherpesvirus 6 (HHV-6), or human gammaherpesvirus 4 (HHV-4, also known as Epstein-Barr virus, EBV) (40). Therefore, the search for broad spectrum terminase inhibitors is still ongoing.

Figure 7.3 gives a schematic overview of how the tools developed in this thesis could collectively be used in antiviral drug discovery. First, compounds could be tested for direct inhibition of either terminase-mediated DNA cleavage (Fig. 7.3Ai) or ICP8-mediated ssDNA binding or strand invasion (Fig. 7.3Aii). Drugs could then be validated in cell culture using ECIS to confirm activity during an infection (Fig. 7.3Bi) and to assess cell toxicity. Reduction in viral replication can simultaneously be quantified using flow cytometric analysis of FHV-1-gD-DsRed-infected cells (Fig. 7.3Bii). Finally, promising drugs can then be evaluated in the cornea explant model. Safety can be verified and anti-FHV-1 activity can be assessed by qPCR analysis of the corneas and titration of the culture supernatant (Fig. 7.3Ci). Corneal morphology can be assessed by hematoxylin and eosin staining of cross sections (Fig. 7.3Cii). Upon completion of this pipeline, promising compounds could then proceed to *in vivo* trials in cats. A similar pipeline could be run concurrently to evaluate the efficacy of the compounds against HHV-1 as well, using HHV-1 recombinant viruses and proteins developed by other research groups.

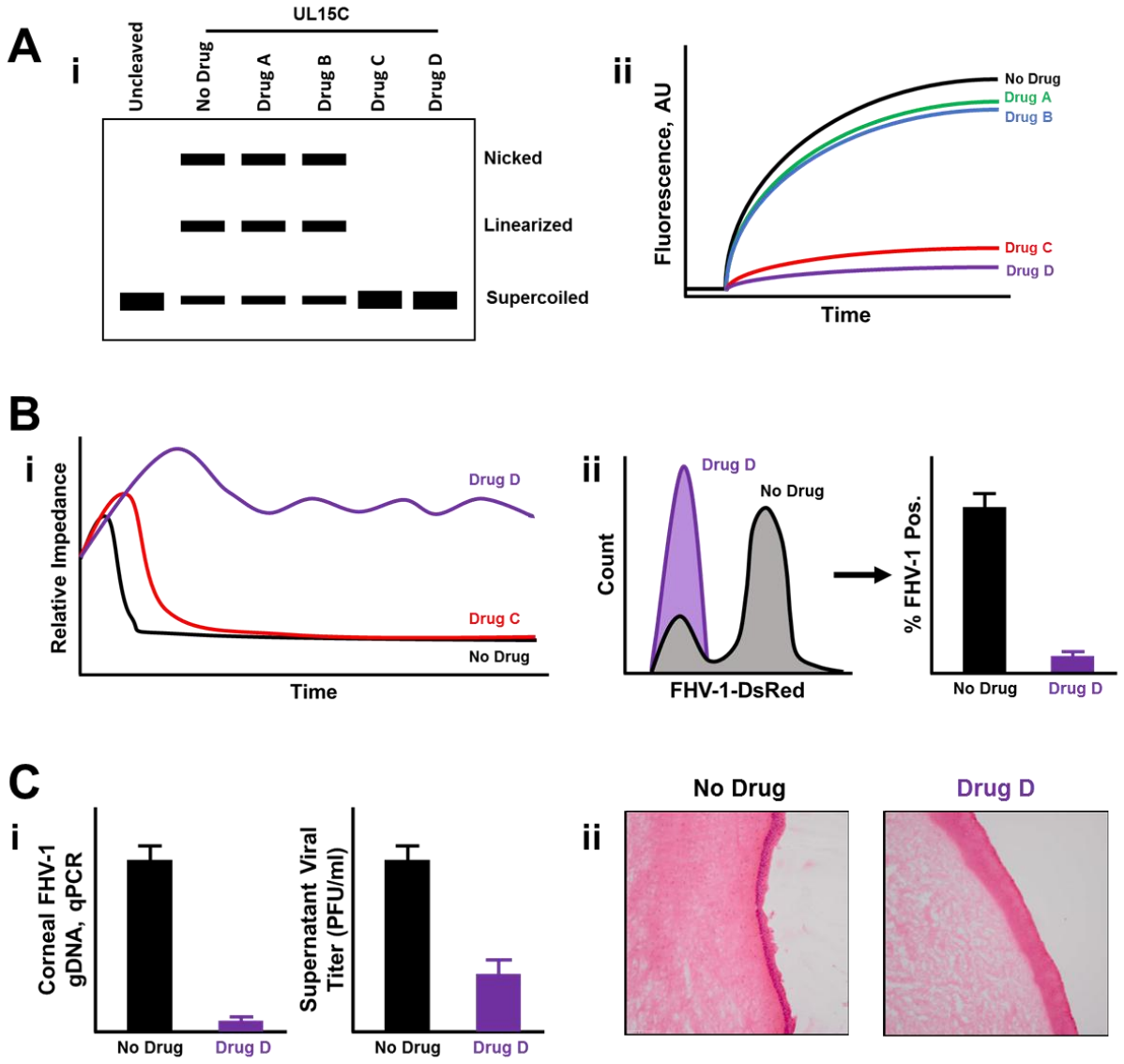

Figure 7.3: Pipeline for antiviral drug discovery and validation using the tools developed in this thesis. (A) Libraries of drugs can first be screened to identify inhibitors of terminase using the DNA cleavage assay (i) or ICP8 using the strand invasion assay (ii) or single stranded DNA binding assay (not depicted) to identify inhibitors of these specific enzymes. **(B)** Hits from enzymatic screen can be evaluated by electric cell-substrate impedance sensing for antiviral-efficacy (i) and toxicity (not depicted). Additionally, or alternatively, inhibition of viral growth can be evaluated by flow cytometric quantification of FHV-1-gD-DsRed infected cells (ii). **(C)** Compounds showing antiviral efficacy can then be evaluated for efficacy by qPCR and titration of the culture supernatant (i) and effects on corneal morphology (ii) using the feline cornea explant model.

7.4. The cat as a natural host model of ocular herpesvirus disease

This thesis raises the possibility of using the cat as a natural host model to study ocular herpesvirus pathogenesis, the merits of which were reviewed in Chapter 2 and are well recognized for many viruses. As herpesviruses closely co-evolved with and are exquisitely adapted to their hosts (41–43), one should not expect HHV-1 infection of a mouse or rabbit to accurately recapitulate the disease as it appears in humans. Indeed, HHV-1 infection in these species differs from human infection in the disease presentation, reactivation mechanics, and recurrent disease (44). In contrast, infection of cats and dogs with their respective herpesviruses closely recapitulates the pathogenesis as seen in humans (45). Still, mice and rabbits remain widely used due to their low-cost, the wide availability of transgenic animals, and the relative ease of working with these species. It is for this reason that nearly all of our mechanistic knowledge on the immune response and pathogenesis comes from experimental infection of these species. Therefore, it is likely that these species will continue to be the workhorses of ocular herpesvirology, despite their limitations.

The cat has the potential to supplement studies done in these species in a more relevant system. However, optimization of this model is still needed. Almost all work thus far, including our work, has utilized primary infections of herpesvirus-naïve animals to evaluate antivirals. This system has proven to be quite reproducible and results in lytic replication of the virus, development of ocular and respiratory signs by 3-6 days post infection, and clearance of clinical signs by about 30 days post infection (3–7). However, and as previously mentioned, much of the severe immunopathology that leads to blindness in humans develops following reactivation of latent virus and is driven by a strong pro-inflammatory immune response (46, 47). To date, no group has described a robust and repeatable infection-latency-reactivation model in the cat,

similar to the reactivation model described for the dog (45). As it is difficult to induce virus reactivation in mice, and to a lesser extent rabbits, such a model could prove a valuable advantage in this regard over these other species.

In general, the immune response to FHV-1 infection has not been well defined. The mechanisms of stromal keratitis disease manifestations are not known in the cat, but are understood to be responses to viral antigens in the stroma, unrelated to virus replication (48). It is also known that these responses are mediated by corneal antigen-presenting cells (APCs) that infiltrate the cornea after an inflammatory stimulus, as well as resident APCs (49). Neither the populations and distributions of APCs and other immune cells resident in the feline cornea nor their responses to FHV-1 infection have been defined. The feline cornea explant could help to elucidate this as it would contain all cornea resident immune cells. Uninfected and FHV-1-infected (potentially using the FHV-1-gD-DsRed virus) corneas can be collected at various time points, sectioned, and stained with antibodies recognizing different immune cell markers to identify the cell types, number, localization, and infection status of cornea-resident immune cells, similar to what was previously done with equid alphaherpesvirus 1 (EHV-1)-infected equine nasal mucosal explants (50). A current potential limitation is the lack of antibodies that cross react with feline markers. However, a sufficient variety of antibodies have been reported by their manufacturer to detect the feline version of these markers (Table 7.1), though cross reactivity would first need to be verified.

While the resident and recruited APCs are essential for stimulating the damaging immune response, they themselves are not thought to be directly responsible for the immunopathology. It has been demonstrated that neutrophils are first recruited to the eye following FHV-1 infection, followed by both T and B lymphocytes (51), but the contribution of these cells to FHV-1-

Table 7.1: Antigens and cross-reacting antibodies currently available to identify feline immune cells. All antibodies below, except CD40, are either reported by the manufacturer or demonstrated in published studies to cross react with feline antigen, allowing for phenotyping of feline corneal resident immune cells.

Antigen	Cellular Expression	Antibody	Clone	Company
CD3	T cells	Mouse anti-cat	Vpg34	AbD Serotec
CD11b	Mϕ , not on DCs	Mouse anti-dog	CA16.3E10	AbD Serotec
CD11c	DCs & neutrophils, but not on ocular Mϕ in mouse	Mouse anti-cat	Fe5.5C1	P.M. Moore, UC Davis
CD14	Monocytes, Mϕ; 10-fold less on neutrophils	Mouse anti-human	TÜK4	AbD Serotec
CD16	NK cells, neutrophils	Mouse anti-human	YFC120-5	AbD Serotec
CD21	B cells	Mouse anti-dog	CA2.1D6	AbD Serotec
CD24	B cells, neutrophils	Mouse anti-human	M1/69	Santa Cruz
CD40	DCs, B cells, Mϕ	*None Validated for Cat*		
CD45	All leukocytes	Mouse anti-dog	T29/33	Dako
CD56	NK cells	Rabbit anti-human	3H15L12	ThermoFisher Scientific
CD80	Mature DCs	Rabbit anti-feline	Polyclonal	W. Thompkins, NC State
CD86	Mature DCs	Rabbit anti-feline	Polyclonal	W. Thompkins, NC State
CD172a	Myeloid cells	Mouse anti-bovine	DH59B	Washington State University
MHC II	Antigen presenting cells	Mouse anti-cat	42.3	AbD Serotec

associated ocular disease is not known. Based on studies using HHV-1 in mice, it is assumed that neutrophils produce a variety of pro-inflammatory cytokines, leading to a Th1 skewed, proinflammatory cytokine response, resulting in tissue damage (49). There is no direct evidence for this in the cat and understanding this response would contribute to our understanding of the clinical disease. Peripheral blood mononuclear cells (PBMCs) can be isolated from cats (52), enabling a number of standard stimulation assays to be performed *in vitro* to define cytokine expression in response to FHV-1 antigen. For example, enzyme-linked immunosorbent assays (ELISAs) have been used to measure feline cytokine production, including IFNɣ, GM-CSF, IL-

4, IL-10, and IL-12, by PBMCs isolated from clinically healthy cats that were stimulated with several chemical compounds (53). Furthermore, a multiplex microsphere-based assay was described as an alternative to ELISAs to detect feline IFNɣ, IL-10, and IL-12/23p40 (54). In the context of FHV-1, Vermeulen, *et al*. isolated PBMCs from cats that were vaccinated with the Nobivac vaccine and measured the proliferation of specific lymphocyte sub-populations by 5-bromo-2'-deoxyuridine (BrdU) labeling and flow cytometry (55) in response to re-stimulation with FHV-1 antigens. Such techniques could be used to look at the cytokine responses of specific immune cell populations in the cat to FHV-1. Additionally, during *in vivo* infection studies, tear fluid could be collected and evaluated for cytokine expression ELISAs. These experiments would allow for a rigorous examination of the ocular immune responses in cats and enable a direct comparison to the responses in mice and humans.

7.5. Conclusions

Raltegravir appears to be a promising antiviral for the treatment of ocular herpesvirus infection in cats, and is the first FDA-approved drug identified to act in a manner consistent with targeting the viral protein ICP8. As such, raltegravir provides exciting opportunities to develop new treatment modalities for this disease. It also raises the possibility of using raltegravir to treat a wider range of herpesviruses due to the highly conserved nature of ICP8. Taken together, the tools and techniques developed in this thesis can be useful in the discovery of novel anti-herpesviral therapies and this thesis highlights the value of FHV-1 infection in cats as a natural host model for ocular herpesvirus infections.

7.6. References

1. Nadal M, Mas PJ, Mas PJ, Blanco AG, Arnan C, Solà M, Hart DJ, Coll M. 2010. Structure and inhibition of herpesvirus DNA packaging terminase nuclease domain. Proc Natl Acad Sci U S A 107:16078–83.
2. Zhou B, Yang K, Wills E, Tang L, Baines JD. 2014. A mutation in the DNA polymerase accessory factor of herpes simplex virus 1 restores viral DNA replication in the presence of raltegravir. J Virol 88:11121–11129.
3. Spertus CB, Pennington MR, Van de Walle GR, Badanes ZI, Judd BE, Mohammed HO, Ledbetter EC. 2018. Effects of oral raltegravir in cats with experimentally-induced ocular and respiratory feline herpesvirus-1 infection. Am J Vet Res. Under Review.
4. Nasisse MP, Dorman DC, Jamison KC, Weigler BJ, Hawkins EC, Stevens JB. 1997. Effects of valacyclovir in cats infected with feline herpesvirus 1. Am J Vet Res 58:1141–4.
5. Haid C, Kaps S, Gönczi E, Hässig M, Metzler A, Spiess BM, Richter M. 2007. Pretreatment with feline interferon omega and the course of subsequent infection with feline herpesvirus in cats. Vet Ophthalmol 10:278–284.
6. Fontenelle JP, Powell CC, Veir JK, Radecki S, Lappin MR. 2008. Effect of topical ophthalmic application of cidofovir on experimentally induced primary ocular feline herpesvirus-1 infection in cats. Am J Vet Res 69:289–293.
7. Thomasy SM, Lim CC, Reilly CM, Kass PH, Lappin MR, Maggs DJ. 2011. Evaluation of orally administered famciclovir in cats experimentally infected with feline herpesvirus type-1. Am J Vet Res 72:85–95.
8. Boesch A, Cattori V, Riond B, Willi B, Meli ML, Rentsch KM, Hosie MJ, Hofmann-Lehmann R, Lutz H. 2015. Evaluation of the effect of short-term treatment with the integrase inhibitor raltegravir (Isentress^{TM}) on the course of progressive feline leukemia virus infection. Vet Microbiol 175:167–178.
9. Ledbetter EC, Spertus CB, Pennington MR, Van de Walle GR, Judd BE, Mohammed HO. 2015. In vitro and in vivo evaluation of cidofovir as a topical ophthalmic antiviral for ocular canine herpesvirus-1 infections in dogs. J Ocul Pharmacol Ther 31:642–649.
10. Sykes JE, Papich MG. 2014. Antiviral and Immunomodulatory Drugs, p. 54–65. *In* Sykes, JE (ed.), Canine and Feline Infectious Diseases. Elsevier, St. Louis.

11. Thomasy SM, Maggs DJ. 2016. A review of antiviral drugs and other compounds with activity against feline herpesvirus type 1. Vet Ophthalmol 19:119–130.
12. Williams DL, Robinson JC, Lay E, Field H. 2005. Efficacy of topical aciclovir for the treatment of feline herpetic keratitis: results of a prospective clinical trial and data from in vitro investigations. Vet Rec 157:254–7.
13. Gould D. 2011. Feline Herpesvirus-1. Ocular manifestations, diagnosis and treatment options. J Feline Med Surg 13:333–346.
14. Claros-Chacaltana FDY, Aldrovani M, Kobashigawa KK, Padua IRM, Valdetaro GP, de Barros Sobrinho AAF, Abreu TGM, Laus JL. 2018. Effect of metronidazole ophthalmic solution on corneal neovascularization in a rat model. Int Ophthalmol.
15. Court MH. 2013. Feline drug metabolism and disposition: pharmacokinetic evidence for species differences and molecular mechanisms. Vet Clin North Am Small Anim Pract 43:1039–54.
16. Gerber W-M, Meyer D, Smit DP. 2016. Ocular and cerebrospinal fluid penetration of antiretroviral agents. J Ocul Pharmacol Ther 32:476–481.
17. Chou TY, Hong BY. 2014. Ganciclovir ophthalmic gel 0.15% for the treatment of acute herpetic keratitis: background, effectiveness, tolerability, safety, and future applications. Ther Clin Risk Manag 10:665–81.
18. Furrer P, Mayer JM, Plazonnet B, Gurny R. 2002. Ocular tolerance of absorption enhancers in ophthalmic preparations. AAPS PharmSci 4:E2.
19. Moore K. 2015. The medicines patent pool signs licensing agreement with MSD for paediatric formulations of raltegravir. <https://medicinespatentpool.org/mpp-media-post/the-medicines-patent-pool-signs-licensing-agreement-with-msd-for-paediatric-formulations-of-raltegravir/>.
20. Pelletier JS, Miller D, Liang B, Capriotti JA. 2011. In vitro efficacy of a povidone–iodine 0.4% and dexamethasone 0.1% suspension against ocular pathogens. J Cataract Refract Surg 37:763–766.
21. Clement C, Capriotti JA, Kumar M, Hobden JA, Foster TP, Bhattacharjee PS, Thompson HW, Mahmud R, Liang B, Hill JM. 2011. Clinical and Antiviral Efficacy of an Ophthalmic Formulation of Dexamethasone Povidone-Iodine in a Rabbit Model of Adenoviral Keratoconjunctivitis. Investig Opthalmology Vis Sci 52:339.

22. Pelletier JS, Stewart KP, Capriotti K, Capriotti JA. 2015. Rosacea Blepharoconjunctivitis Treated with a Novel Preparation of Dilute Povidone Iodine and Dimethylsulfoxide: a Case Report and Review of the Literature. Ophthalmol Ther 4:143–150.
23. Isenberg SJ. 2003. The ocular application of povidone-iodine. Community eye Heal 16:30–1.
24. Woodbridge P. 1977. The use of betadine antiseptic paint in the treatment of herpes simplex and herpes zoster. J Int Med Res 5:378–381.
25. Kawana R, Kitamura T, Nakagomi O, Matsumoto I, Arita M, Yoshihara N, Yanagi K, Yamada A, Morita O, Yoshida Y, Furuya Y, Chiba S. 1997. Inactivation of human viruses by povidone-iodine in comparison with other antiseptics. Dermatology 195:29–35.
26. Zeitlin L, Whaley KJ, Hegarty TA, Moench TR, Cone RA. 1997. Tests of vaginal microbicides in the mouse genital herpes model. Contraception 56:329–35.
27. Wutzler P, Sauerbrei A, Klöcking R, Burkhardt J, Schacke M, Thust R, Fleischer W, Reimer K. 2000. Virucidal and chlamydicidal activities of eye drops with povidone-iodine liposome complex. Ophthalmic Res 32:118–125.
28. Wutzler P, Sauerbrei A, Klöcking R, Brögmann B, Reimer K. 2002. Virucidal activity and cytotoxicity of the liposomal formulation of povidone-iodine. Antiviral Res 54:89–97.
29. Pennington MR, Capriotti JA, Van de Walle GR. 2018. Povidone iodine (PVP-I) compounds effectively inhibit several common feline ocular pathogens in vitro. Vet J. Under Review.
30. Durand-Cavagna G, Delort P, Duprat P, Bailly Y, Plazonnet B, Gordon LR. 1989. Corneal toxicity studies in rabbits and dogs with hydroxyethyl cellulose and benzalkonium chloride. Fundam Appl Toxicol 13:500–8.
31. Pennington MR, Van de Walle GR. 2017. Electric cell-substrate impedance sensing to monitor viral growth and study cellular responses to infection with alphaherpesviruses in real time. mSphere 2:e00039-17.
32. Giaever I, Keese CR. 1984. Monitoring fibroblast behavior in tissue culture with an applied electric field. Proc Natl Acad Sci U S A 81:3761–4.
33. Suenaga T, Kohyama M, Hirayasu K, Arase H. 2014. Engineering large viral DNA genomes using the CRISPR-Cas9 system. Microbiol Immunol 58:513–522.
34. Russell TA, Stefanovic T, Tscharke DC. 2015. Engineering herpes simplex viruses by

infection–transfection methods including recombination site targeting by CRISPR/Cas9 nucleases. J Virol Methods 213:18–25.

35. van Diemen FR, Kruse EM, Hooykaas MJG, Bruggeling CE, Schürch AC, van Ham PM, Imhof SM, Nijhuis M, Wiertz EJHJ, Lebbink RJ. 2016. CRISPR/Cas9-mediated genome editing of herpesviruses limits productive and latent infections. PLOS Pathog 12:e1005701.
36. Yuan M, Webb E, Lemoine N, Wang Y. 2016. CRISPR-Cas9 as a powerful tool for efficient creation of oncolytic viruses. Viruses 8:72.
37. Selvarajan Sigamani S, Zhao H, Kamau YN, Baines JD, Tang L. 2013. The structure of the herpes simplex virus DNA-packaging terminase pUL15 nuclease domain suggests an evolutionary lineage among eukaryotic and prokaryotic viruses. J Virol 87:7140–8.
38. Bryant KF, Yan Z, Dreyfus DH, Knipe DM. 2012. Identification of a divalent metal cation bindings site in herpes simplex virus 1 (HSV-1) ICP8 required for HSV replication. J Virol 86:6825–6834.
39. Melendez DP, Razonable RR. 2015. Letermovir and inhibitors of the terminase complex: a promising new class of investigational antiviral drugs against human cytomegalovirus. Infect Drug Resist 8:269–77.
40. Marschall M, Stamminger T, Urban A, Wildum S, Ruebsamen-Schaeff H, Zimmermann H, Lischka P. 2012. In vitro evaluation of the activities of the novel anticytomegalovirus compound AIC246 (letermovir) against herpesviruses and other human pathogenic viruses. Antimicrob Agents Chemother 56:1135–7.
41. Domingo E, Parrish CR, Holland JJ. 2008. Origin and evolution of viruses. Elsevier Academic Press.
42. White DW, Suzanne Beard R, Barton ES. 2012. Immune modulation during latent herpesvirus infection. Immunol Rev 245:189–208.
43. Wertheim JO, Smith MD, Smith DM, Scheffler K, Kosakovsky Pond SL. 2014. Evolutionary origins of human herpes simplex viruses 1 and 2. Mol Biol Evol 31:2356–2364.
44. Webre JM, Hill JM, Nolan NM, Clement C, McFerrin HE, Bhattacharjee PS, Hsia V, Neumann DM, Foster TP, Lukiw WJ, Thompson HW. 2012. Rabbit and mouse models of HSV-1 latency, reactivation, and recurrent eye diseases. J Biomed Biotechnol

2012:612316.

45. Pennington M, Ledbetter E, Van de Walle G. 2017. New paradigms for the study of ocular alphaherpesvirus infections: insights into the use of non-traditional host model systems. Viruses 9:349.
46. Al-Dujaili LJ, Clerkin PP, Clement C, McFerrin HE, Bhattacharjee PS, Varnell ED, Kaufman HE, Hill JM. 2011. Ocular herpes simplex virus: how are latency, reactivation, recurrent disease and therapy interrelated? Future Microbiol 6:877–907.
47. Rowe AM, St Leger AJ, Jeon S, Dhaliwal DK, Knickelbein JE, Hendricks RL. 2013. Herpes keratitis. Prog Retin Eye Res 32:88–101.
48. Andrew SE. 2001. Ocular manifestations of feline herpesvirus. J Feline Med Surg 3:9–16.
49. Andrew SE. 2008. Immune-mediated canine and feline keratitis. Vet Clin North Am Small Anim Pract 38:269–290.
50. Vandekerckhove AP, Glorieux S, Gryspeerdt AC, Steukers L, Duchateau L, Osterrieder N, Van de Walle GR, Nauwynck HJ. 2010. Replication kinetics of neurovirulent versus non-neurovirulent equine herpesvirus type 1 strains in equine nasal mucosal explants. J Gen Virol 91:2019–28.
51. Nasisse MP, English R V, Tompkins MB, Guy JS, Sussman W. 1995. Immunologic, histologic, and virologic features of herpesvirus-induced stromal keratitis in cats. Am J Vet Res 56:51–5.
52. Toth TE, Smith B, Pyle H. 1992. Simultaneous separation and purification of mononuclear and polymorphonuclear cells from the peripheral blood of cats. J Virol Methods 36:185–195.
53. Aronson LR, Stumhofer JS, Drobatz KJ, Hunter CA. 2011. Effect of cyclosporine, dexamethasone, and human CTLA4-Ig on production of cytokines in lymphocytes of clinically normal cats and cats undergoing renal transplantation. Am J Vet Res 72:541–549.
54. Wood BA, O'Halloran KP, VandeWoude S. 2011. Development and Validation of a Multiplex Microsphere-Based Assay for Detection of Domestic Cat (Felis catus) Cytokines. Clin Vaccine Immunol 18:387–392.
55. Vermeulen BL, Gleich SE, Dedeurwaerder A, Olyslaegers DA, Desmarets LM, Dewerchin HL, Nauwynck HJ. 2012. In vitro assessment of the feline cell-mediated

immune response against feline panleukopeniavirus, calicivirus and felid herpesvirus 1 using 5-bromo-2′-deoxyuridine labeling. Vet Immunol Immunopathol 146:177–184.

APPENDIX

List of all protein-coding stringent-DEGs following raltegravir treatment of FHV-1-infected cells. Fold changes were calculated by comparison of the mean read per kilobase of transcripts per million mapped reads (FPKM) values of DMSO vs raltegravir treated cells at 4 hpi (2 h post drug treatment. Genes were ranked according to the absolute value of fold change.

			Average FPKM Value		
gene_id	**Gene Symbol**	**Fold Change**	**DMSO**	**Raltegravir**	**p_value**
XLOC_025005	*TESK1*	-5.32130	30.62	5.76	0.00005
XLOC_031100	*RGS16*	-4.39048	8.31	1.89	0.00005
XLOC_029085	*TFL* or *BAX*	3.76881	387.78	1461.45	0.00005
XLOC_022030	*FTH1*	3.73933	3037.38	11357.80	0.00005
XLOC_005354	*LZTS3*	3.35893	2.00	6.72	0.00005
XLOC_017247	*TMEM54*	3.35746	11.49	38.57	0.00005
XLOC_014020	*CYB5R3*	-3.35532	8.38	2.50	0.01365
XLOC_000723	*GCNT4A*	3.33078	2.07	6.90	0.00475
XLOC_016217	*FAM46C*	-3.30177	6.46	1.96	0.00005
XLOC_010669	*DYNLT1*	3.27381	35.56	116.40	0.00005
XLOC_026618	*COL1A1*	3.22950	812.53	2624.05	0.00005
XLOC_030231	*TIGD7*	3.17794	3.22	10.23	0.00220
XLOC_000895	*SGCD*	3.13599	4.06	12.73	0.00005
XLOC_012938	*CINP*	3.07650	6.01	18.49	0.00005
XLOC_000499	*TGFBI*	3.03947	17.94	54.54	0.00005
XLOC_031705	*ATF3*	-3.01885	41.65	13.80	0.00005
XLOC_020308	*RNF26*	2.99700	5.10	15.28	0.00005
XLOC_013131	*KIAA1217* or *ET14*	-2.95992	5.97	2.02	0.01080
XLOC_023383	*UROS*	2.95316	6.50	19.19	0.00120
XLOC_001285	*LHFP*	2.95289	10.93	32.28	0.00005
XLOC_029516	*AKTIP*	2.93040	4.15	12.15	0.00010
XLOC_002203	*OSMR*	2.91109	33.73	98.19	0.00005
XLOC_010979	*CYP1A1*	2.89997	5.74	16.64	0.00005
XLOC_008914	*HIST1H1B*	-2.89421	18.33	6.33	0.00005
XLOC_006128	*L3MBTL1*	-2.88630	7.71	2.67	0.00005
XLOC_013807	*TMTC2*	2.86970	8.77	25.17	0.00010
XLOC_014739	*ITGA5*	2.86160	62.71	179.45	0.00005
XLOC_009601	*SMPDL3A*	2.85013	88.82	253.15	0.00005
XLOC_007182	*SCARA3*	2.83029	3.20	9.05	0.00005
XLOC_006170	*RPN2*	2.81421	79.74	224.39	0.00005
XLOC_029520	*CRNDE*	2.79973	22.98	64.33	0.00005

XLOC_031864	*SLC41A1*	2.79295	1.85	5.17	0.00005
XLOC_019146	*UBE2E2*	2.76807	7.45	20.61	0.00005
XLOC_034151	*RPL36AL*	2.73929	505.33	1384.25	0.00005
XLOC_026762	*GRN*	2.72319	30.69	83.57	0.00005
XLOC_017239	*HDAC1*	-2.71652	11.68	4.30	0.00005
XLOC_020817	*TSPAN18*	2.69691	6.22	16.78	0.00005
XLOC_022043	*LRRN4CL*	2.69387	3.36	9.05	0.00005
XLOC_028823	*CENPBD1*	-2.68630	5.35	1.99	0.00835
XLOC_011089	*ANXA2*	2.68565	397.59	1067.79	0.00005
XLOC_028305	*PLAUR*	2.68537	115.93	311.32	0.00005
XLOC_013889	*HSP90B1*	2.68035	160.03	428.93	0.00005
XLOC_015004	*NDUFA12*	2.67578	25.32	67.76	0.00005
XLOC_011741	*SERPINA3*	2.67395	11.26	30.10	0.00005
XLOC_028333	*TGFB1*	2.66565	13.66	36.42	0.00005
XLOC_021044	*ARL2*	2.66366	3.56	9.47	0.00005
XLOC_026002	*ZNF79*	-2.65700	11.53	4.34	0.00005
XLOC_018564	*RUNX1*	-2.65643	6.00	2.26	0.01355
XLOC_015061	*LARGE*	2.65562	7.58	20.12	0.00005
XLOC_010050	*PPR1R10*	-2.64165	12.74	4.82	0.00980
XLOC_002288	*SRD5A1*	2.63801	2.69	7.10	0.00005
XLOC_031585	*PIGC*	2.62393	16.53	43.38	0.00005
XLOC_013930	*HMOX1*	-2.61803	23.96	9.15	0.00005
XLOC_008940	*HIST1H2BJ* or *HIST1H2BK*	-2.61436	23.29	8.91	0.00025
XLOC_002565	*SLC44A2*	2.60256	24.96	64.96	0.00005
XLOC_001741	*SPRY4*	-2.59919	6.57	2.53	0.00220
XLOC_029915	*ORAI2*	2.59235	2.73	7.07	0.00005
XLOC_025660	*ZDHHC21*	2.59230	2.57	6.66	0.00210
XLOC_009843	*H2BFS*	-2.59138	8.03	3.10	0.00005
XLOC_024829	*ANXA1*	2.58480	162.62	420.33	0.00005
XLOC_013682	*TMEM5*	2.58102	3.33	8.59	0.00005
XLOC_002582	*CNN1*	2.58087	176.70	456.04	0.00005
XLOC_032643	*UQCRB*	2.58007	134.91	348.08	0.00005
XLOC_014464	*RECQL*	2.57766	4.45	11.47	0.00005
XLOC_015189	*TTLL1*	2.57325	7.13	18.35	0.00005
XLOC_020696	*NCR3LG1*	2.56691	9.81	25.19	0.00005
XLOC_019823	*SERPINI1*	2.55939	3.52	9.01	0.00005
XLOC_011390	*SNX6*	-2.55724	12.67	4.96	0.00005
XLOC_024870	*C9orf3*	2.55135	8.92	22.76	0.00005
XLOC_007108	*LOXL2*	2.53840	172.03	436.67	0.00005
XLOC_032701	*ZNF706*	2.53100	83.62	211.64	0.00520

XLOC_029102	*EHD2*	2.52853	43.22	109.30	0.00005
XLOC_035055	*SLC10A3* or *UBL4A*	2.52569	15.50	39.15	0.00005
XLOC_031882	*RGS2*	-2.52557	10.26	4.06	0.00005
XLOC_012686	*TIMM9*	2.52550	60.99	154.04	0.00570
XLOC_021365	*THY1*	2.52356	24.15	60.96	0.00005
XLOC_003393	*CALU*	2.51947	192.98	486.20	0.00005
XLOC_000947	*ATOX1*	2.51818	180.71	455.05	0.00005
XLOC_015965	*NEXN*	2.51704	6.91	17.38	0.00045
XLOC_004619	*SRI*	2.51352	11.47	28.84	0.00005
XLOC_025472	*NINJ1*	2.51174	14.86	37.32	0.00005
XLOC_025998	*ANGPTL2*	2.50378	42.51	106.43	0.00005
XLOC_023841	*RBBP8*	2.49659	2.31	5.77	0.00005
XLOC_014757	*SARNP* or *ORMD12* or *DNAJC14*	2.48825	53.38	132.82	0.00070
XLOC_016557	*COL3A1*	2.47823	186.07	461.12	0.00005
XLOC_021838	*DCTN6*	2.47197	13.50	33.38	0.00005
XLOC_027411	*NXPH3*	2.46868	4.88	12.06	0.00005
XLOC_027450	*PGAP3*	2.46541	2.29	5.65	0.00005
XLOC_008688	*PCDH7*	2.45659	15.28	37.54	0.00005
XLOC_023335	*FAM204A*	2.45151	11.14	27.30	0.00005
XLOC_018447	*DTYMK*	2.44910	24.09	58.99	0.00005
XLOC_034062	*PIN4*	2.44796	21.06	51.54	0.00005
XLOC_033998	*UBQLN2*	2.44535	2.53	6.18	0.00005
XLOC_007132	*NAT1* or *NAT2*	2.43863	6.05	14.76	0.00010
XLOC_017852	*FCGR1A* or *FCGR1B*	-2.43033	9.41	3.87	0.00005
XLOC_009054	*TBC1D7*	2.42767	13.47	32.69	0.00005
XLOC_025794	*TPM2*	2.42437	382.30	926.85	0.00005
XLOC_012001	*MRPS11*	2.42420	12.90	31.27	0.00100
XLOC_006845	*KCNS3*	2.42167	3.54	8.57	0.00005
XLOC_003053	*PPIA*	2.42115	697.88	1689.66	0.00005
XLOC_004656	*SGCE*	2.41990	8.52	20.62	0.00005
XLOC_014845	*LLPH*	-2.41710	14.67	6.07	0.00995
XLOC_012310	*B2M*	2.41391	194.18	468.72	0.00005
XLOC_015527	*RCAN3*	2.41135	3.58	8.63	0.00015
XLOC_008472	*SPP1*	2.40606	82.35	198.15	0.00005
XLOC_017404	*POMGNT1*	2.40426	12.54	30.15	0.00005
XLOC_010583	*SGK1*	-2.40416	45.37	18.87	0.00005
XLOC_025988	*HSPA5*	2.40249	184.22	442.60	0.00005
XLOC_007032	*DCTN6*	2.39984	20.46	49.10	0.00005

XLOC_021834	*CD59*	2.39888	42.34	101.57	0.00005
XLOC_034928	*ZDHHC9*	2.39517	4.23	10.14	0.00005
XLOC_020098	*CTNNB1*	2.38896	152.37	364.01	0.00005
XLOC_034240	*IL13RA1*	2.38846	76.97	183.83	0.00005
XLOC_008763	*TMEM129*	2.37384	6.74	16.00	0.00005
XLOC_022742	*DUSP5*	-2.37357	37.63	15.85	0.00005
XLOC_029682	*MPHOSPH6*	2.36766	12.14	28.74	0.00005
XLOC_021776	*SAA*	2.36656	5.32	12.59	0.00005
XLOC_008186	*CLU*	2.36380	8.81	20.83	0.00005
XLOC_025852	*ERP44*	2.35643	41.78	98.45	0.00005
XLOC_021566	*SPCS2*	2.35194	29.97	70.49	0.00005
XLOC_016544	*DNAJC10*	2.34728	6.35	14.89	0.00005
XLOC_029088	*NUCB1*	2.34414	33.07	77.52	0.00005
XLOC_011486	*LGALS3*	2.34297	340.28	797.28	0.00005
XLOC_019885	*MME*	2.34218	19.36	45.35	0.00005
XLOC_008557	*CXCL8*	2.34203	148.00	346.62	0.00005
XLOC_016752	*MFF*	2.34143	40.80	95.54	0.00005
XLOC_012868	*NDUFB1*	2.33861	59.57	139.30	0.00005
XLOC_021559	*SERPINH1*	2.33707	223.83	523.12	0.00005
XLOC_022114	*FIBP*	2.33381	22.74	53.07	0.00005
XLOC_000366	*MAPK9*	2.33218	3.23	7.53	0.00005
XLOC_001617	*TMED9*	2.32729	77.18	179.62	0.00005
XLOC_030478	*POLR2J*	2.31927	35.54	82.43	0.00520
XLOC_026479	*IFT20*	2.31684	20.44	47.37	0.00715
XLOC_005682	*TGOLN2*	2.31426	19.14	44.29	0.00005
XLOC_002270	*CCT5*	2.31206	80.91	187.08	0.00005
XLOC_020704	*LDHA*	2.31009	1071.71	2475.76	0.00005
XLOC_004923	*DENND2A*	2.30873	2.83	6.52	0.00005
XLOC_000240	*MBNL2*	2.30422	5.33	12.28	0.00005
XLOC_011765	*PAPOLA*	2.29905	20.29	46.66	0.00005
XLOC_005641	*ACTG2*	2.29525	43.13	99.00	0.00005
XLOC_027815	*TK1*	2.29188	16.18	37.08	0.00005
XLOC_026843	*C17orf58*	2.29097	10.93	25.05	0.00305
XLOC_002923	*PTPRG*	2.28631	5.53	12.64	0.00005
XLOC_029996	*ZNF768*	2.28534	5.72	13.07	0.00005
XLOC_020502	*LRRC32*	2.28379	2.65	6.06	0.00005
XLOC_017932	*S100A10*	2.28211	390.08	890.21	0.00005
XLOC_006270	*ID1*	-2.28050	21.27	9.33	0.00005
XLOC_016960	*ERRFI1*	-2.27914	40.52	17.78	0.00005
XLOC_007408	*NDNF*	2.27774	13.40	30.52	0.00005
XLOC_000991	*EMB*	2.27633	4.78	10.88	0.00005

XLOC_014624	*RND1*	-2.27488	21.29	9.36	0.00005
XLOC_013851	*ELK3*	2.27461	12.54	28.52	0.00005
XLOC_011494	*KTN1*	2.27343	23.67	53.82	0.00005
XLOC_012373	*THBS1*	2.27228	212.85	483.66	0.00005
XLOC_005685	*MAT2A*	-2.26783	44.71	19.71	0.00230
XLOC_030358	*GNA12*	2.26759	4.74	10.75	0.00005
XLOC_001238	*UBL3*	2.26632	5.66	12.83	0.00005
XLOC_006097	*PIGT*	2.26324	25.87	58.55	0.00005
XLOC_015739	*CAP1*	2.26261	138.36	313.05	0.00005
XLOC_003031	*RPN1*	2.26003	116.59	263.50	0.00005
XLOC_002674	*AP1M1* or *FAM32A*	2.25893	60.95	137.68	0.00005
XLOC_001721	*PFDN1*	2.25794	63.85	144.18	0.00005
XLOC_008790	*LRPAP1*	2.25427	32.95	74.27	0.00005
XLOC_012870	*ITPK1*	2.25427	4.12	9.28	0.00035
XLOC_004325	*EOGT*	2.25040	5.08	11.42	0.00005
XLOC_021726	*EIF4G2*	2.24966	254.76	573.13	0.00005
XLOC_031689	*QSOX1*	2.24684	51.77	116.32	0.00005
XLOC_014425	*MANSC1*	2.23887	15.60	34.93	0.00005
XLOC_006211	*DYNLRB1*	2.23665	160.77	359.58	0.00005
XLOC_006027	*RTFDC1*	2.23419	28.57	63.84	0.00005
XLOC_007506	*ADH5*	2.23395	16.64	37.16	0.00035
XLOC_032112	*UBE2V2*	2.23327	47.25	105.53	0.00005
XLOC_013640	*MYL6*	2.23253	887.75	1981.92	0.00005
XLOC_032262	*FAM92A1*	2.23191	12.09	26.99	0.00245
XLOC_018999	*SSR3*	2.22999	80.39	179.28	0.00005
XLOC_030164	*EMP2*	2.22743	23.79	53.00	0.00005
XLOC_020771	*CD44*	2.22606	106.85	237.85	0.00005
XLOC_027206	*SERPINF1*	2.22336	7.26	16.14	0.00005
XLOC_012501	*PSME2*	2.22257	41.60	92.46	0.00010
XLOC_019191	*CMTM7*	2.22008	523.56	1162.34	0.00005
XLOC_032066	*FDPS*	2.21988	22.85	50.72	0.00005
XLOC_012317	*HYPK*	2.21971	70.61	156.74	0.00005
XLOC_034020	*FAM155B*	2.21826	6.78	15.04	0.00005
XLOC_011379	*SCFD1*	2.21617	11.76	26.07	0.00005
XLOC_008291	*TLR2*	2.21473	3.11	6.90	0.00030
XLOC_013118	*PLXDC2*	2.21450	16.11	35.67	0.00005
XLOC_020839	*MDK*	2.21425	5.40	11.96	0.00005
XLOC_021028	*FKBP2*	2.21293	69.22	153.18	0.00005
XLOC_024643	*LMAN1*	2.21284	39.45	87.31	0.00005
XLOC_005909	*PDIA6*	2.21033	247.27	546.54	0.00005
XLOC_031197	*BTG2*	-2.21019	34.34	15.54	0.00005

XLOC_026034	*DOLK*	2.20707	6.46	14.26	0.00005
XLOC_026356	*RASD1*	-2.20457	28.69	13.01	0.00005
XLOC_034244	*LONRF3*	-2.20318	13.17	5.98	0.00005
XLOC_025871	*KLF4*	-2.20164	9.28	4.21	0.00005
XLOC_008556	*CXCL5* or *CXCL6*	2.20056	211.41	465.22	0.00005
XLOC_021148	*CTTN*	2.19791	85.35	187.59	0.00005
XLOC_001812	*ADAMTS6*	-2.19536	83.79	38.17	0.00235
XLOC_019033	*TM4SF1*	2.19121	11.97	26.22	0.00005
XLOC_002924	*C3orf14*	2.19083	6.99	15.32	0.00005
XLOC_003472	*AGK*	2.19068	3.18	6.96	0.00005
XLOC_023634	*UQCR10*	2.18872	242.74	531.29	0.00010
XLOC_017411	*EFCAB14*	2.18819	15.39	33.68	0.00005
XLOC_016941	*ICMT*	2.18575	30.65	66.99	0.00005
XLOC_004651	*TFPI2*	2.18120	37.48	81.75	0.00005
XLOC_029866	*COPS6*	2.17757	55.68	121.26	0.00005
XLOC_009122	*TCF19*	2.17639	3.48	7.58	0.00005
XLOC_020175	*ANO10*	2.17410	27.88	60.61	0.00005
XLOC_006997	*ASAH1*	2.17213	4.20	9.12	0.00005
XLOC_029183	*PVR*	2.17005	21.74	47.17	0.00005
XLOC_002925	*SYNPR*	2.16880	9.46	20.52	0.00005
XLOC_003759	*MYDGF*	2.16856	62.59	135.74	0.00005
XLOC_023220	*NDUFB8*	2.16837	53.61	116.25	0.00005
XLOC_029856	*ZSCAN25*	-2.16819	8.15	3.76	0.00795
XLOC_024119	*ZNF664*	2.16714	8.04	17.42	0.00005
XLOC_030612	*BOLA2*	2.16589	64.00	138.62	0.00005
XLOC_020163	*GLB1*	2.16586	27.98	60.61	0.00005
XLOC_010842	*FURIN*	2.16442	29.26	63.33	0.00005
XLOC_031642	*ABL2*	-2.16355	18.01	8.32	0.00005
XLOC_001836	*ENC1*	-2.16061	9.79	4.53	0.00005
XLOC_016199	*OLFML3*	2.15998	55.91	120.75	0.00005
XLOC_030648	*UBFD1*	2.15980	8.79	18.97	0.00005
XLOC_002852	*RAD54L2*	-2.15641	8.16	3.78	0.00005
XLOC_008136	*ADAM9*	2.15609	250.23	539.52	0.00005
XLOC_005635	*SPR*	2.15460	10.85	23.37	0.00030
XLOC_034859	*PSMD10*	2.15457	11.14	24.01	0.00005
XLOC_011661	*GPATCH2L*	-2.15200	8.76	4.07	0.00005
XLOC_019808	*SEC62*	2.15199	33.35	71.77	0.00005
XLOC_026725	*FKBP10*	2.15144	67.04	144.24	0.00005
XLOC_006884	*ID2*	-2.15075	108.05	50.24	0.00005
XLOC_017055	*CAPZB*	2.14922	60.31	129.61	0.00005
XLOC_024153	*PSMD9*	2.14765	10.77	23.13	0.00005

XLOC_009899	*HIST1H1E* or *HIST1H2BD*	-2.14706	17.91	8.34	0.00005
XLOC_025248	*SLC2A8*	-2.14624	10.58	4.93	0.00005
XLOC_015591	*ATPIF1*	2.14594	145.56	312.35	0.00005
XLOC_000878	*DUSP1*	-2.14465	48.97	22.83	0.00005
XLOC_032482	*C8orf33*	2.14430	6.45	13.83	0.00005
XLOC_006582	*TPRKB*	2.14420	9.91	21.25	0.00005
XLOC_031924	*AIDA*	2.14346	33.99	72.85	0.00005
XLOC_006836	*UBXN2A*	2.14225	11.95	25.59	0.00005
XLOC_009612	*HINT3*	2.14159	2.69	5.77	0.00165
XLOC_006802	*CENPA*	2.14056	7.57	16.21	0.00500
XLOC_023379	*FAM53B* or *METTL10*	2.14044	15.09	32.30	0.00005
XLOC_013567	*MFSD5*	2.13871	7.49	16.03	0.00005
XLOC_026644	*SNF8*	2.13678	39.65	84.72	0.00105
XLOC_017231	*PTP4A2*	2.13390	38.44	82.03	0.00005
XLOC_010918	*SNURF* or *SNURN*	2.13378	54.21	115.67	0.00035
XLOC_008754	*CTBP1*	2.13289	21.33	45.49	0.00005
XLOC_021441	*NFRKB*	-2.13098	7.62	3.57	0.00005
XLOC_026701	*THRA*	2.13095	2.42	5.16	0.00005
XLOC_005237	*FITM2*	2.13090	3.97	8.46	0.00005
XLOC_013182	*MICAL3*	-2.13063	17.43	8.18	0.00125
XLOC_034016	*YIPF6*	2.13019	5.14	10.96	0.00235
XLOC_013978	*MIEF1*	-2.13016	8.11	3.81	0.01230
XLOC_012638	*ERO1A*	2.12985	55.52	118.25	0.00005
XLOC_006086	*CTSA*	2.12834	35.39	75.32	0.00005
XLOC_014217	*ITGB1*	2.12676	399.61	849.87	0.00005
XLOC_018491	*CSTB*	2.12635	676.06	1437.54	0.00005
XLOC_022920	*ACTA2*	2.12612	1386.51	2947.89	0.00005
XLOC_021089	*RAB1B*	2.12168	29.34	62.25	0.00005
XLOC_029285	*ACTN4*	2.12095	98.22	208.33	0.00005
XLOC_029421	*PDCD5*	2.12043	55.88	118.50	0.00005
XLOC_034924	*SMARCA1*	2.12010	4.11	8.71	0.00005
XLOC_016707	*ARPC2*	2.11982	253.03	536.38	0.00005
XLOC_012742	*ATP6V1D*	2.11259	21.80	46.06	0.00005
XLOC_032255	*DECR1*	2.11191	19.83	41.89	0.00005
XLOC_015956	*ACADM*	2.11169	24.27	51.25	0.00005
XLOC_011503	*NAA30*	-2.10820	9.60	4.55	0.00070
XLOC_024614	*ACAA2*	2.10704	19.47	41.03	0.00005
XLOC_017046	*SDHB*	2.10636	49.19	103.61	0.00005
XLOC_008416	*AIMP1*	2.10625	13.56	28.56	0.00005

XLOC_009509	*AIM1*	2.10539	6.52	13.72	0.00005
XLOC_017255	*AK2*	2.10487	56.29	118.48	0.00005
XLOC_026752	*ARL4D*	-2.10469	25.95	12.33	0.00005
XLOC_034663	*HSD17B10*	2.10184	28.04	58.93	0.00005
XLOC_001134	*CCDC115*	2.10172	3.86	8.12	0.00005
XLOC_029558	*CDH11*	2.10083	52.94	111.22	0.00005
XLOC_010367	*HTR1B*	2.09936	3.44	7.22	0.00005
XLOC_027773	*ATP5H*	2.09908	106.51	223.58	0.00005
XLOC_023599	*RNF10*	2.09743	52.28	109.66	0.00005
XLOC_005259	*TGM2*	2.09730	638.60	1339.34	0.00005
XLOC_016875	*PPP1R7*	2.09615	26.31	55.16	0.00005
XLOC_009373	*BEND6*	2.09519	5.40	11.31	0.00005
XLOC_012793	*NPC2*	2.09424	84.93	177.87	0.00005
XLOC_011654	*FOS*	-2.09204	37.05	17.71	0.00005
XLOC_000088	*B3GLCT*	2.09171	19.86	41.53	0.00010
XLOC_027374	*SCPEP1*	2.08713	13.36	27.88	0.00005
XLOC_027945	*ZNF550*	-2.08690	8.08	3.87	0.00005
XLOC_030692	*NOMO3*	2.08664	32.69	68.22	0.00005
XLOC_021015	*C11orf84*	-2.08440	10.86	5.21	0.00005
XLOC_025946	*GGTA1*	2.08432	9.51	19.82	0.00005
XLOC_028964	*ZNF331*	-2.08398	13.42	6.44	0.00005
XLOC_017680	*CNN3*	2.08229	139.07	289.59	0.00005
XLOC_029437	*VPS35*	2.08041	18.91	39.34	0.00005
XLOC_011341	*LRP10*	2.08020	13.71	28.51	0.00005
XLOC_022127	*B4GAT1*	2.07654	6.34	13.16	0.00005
XLOC_022516	*ZMIZ1*	-2.07618	15.15	7.30	0.00005
XLOC_018717	*NIT2*	2.07494	3.96	8.22	0.00005
XLOC_006793	*ATRAID*	2.07311	16.55	34.31	0.00020
XLOC_006144	*FAM83D*	-2.07212	11.27	5.44	0.00040
XLOC_022698	*DPCD*	2.07197	23.02	47.69	0.00005
XLOC_029263	*PSMC4*	2.07174	25.46	52.75	0.00005
XLOC_034253	*SLC25A5*	2.06957	99.14	205.18	0.00005
XLOC_000685	*MAST4*	-2.06912	24.10	11.65	0.00005
XLOC_005664	*MRPL19*	2.06892	6.95	14.37	0.00005
XLOC_004381	*EMC3*	2.06864	16.80	34.76	0.00005
XLOC_014877	*PHLDA1*	-2.06825	12.34	5.96	0.00005
XLOC_016203	*ATP1A1*	2.06812	103.59	214.24	0.00005
XLOC_021901	*PSMC3*	2.06700	44.03	91.00	0.00005
XLOC_024130	*TMED2*	2.06650	245.89	508.13	0.00005
XLOC_004644	*SAMD9L*	2.06331	17.75	36.62	0.00005
XLOC_027862	*FAM195B*	2.06314	58.10	119.88	0.00120

XLOC_024596	*ATP5A1*	2.06249	147.82	304.87	0.00005
XLOC_003287	*SNX10*	2.06144	3.47	7.15	0.00005
XLOC_003501	*EPHB6*	2.06078	3.54	7.30	0.00005
XLOC_019572	*CCDC80*	2.06031	89.80	185.02	0.00005
XLOC_028343	*SERTAD3*	-2.06022	8.50	4.12	0.00105
XLOC_031805	*LMOD1*	2.05999	3.73	7.68	0.00005
XLOC_002510	*CD320*	2.05959	10.97	22.60	0.00005
XLOC_026166	*EDF1*	2.05825	124.71	256.69	0.00005
XLOC_005372	*FKBP1A*	2.05674	160.75	330.63	0.00005
XLOC_032778	*TNFRSF11B*	2.05616	4.29	8.83	0.00005
XLOC_001037	*GDNF*	-2.05573	6.07	2.95	0.00005
XLOC_001863	*F2RL2*	2.05553	41.48	85.26	0.00005
XLOC_011769	*VRK1*	2.05513	6.83	14.05	0.00005
XLOC_016821	*COPS8*	2.05435	35.91	73.77	0.00005
XLOC_028607	*PLA2G15*	2.05356	3.60	7.40	0.00005
XLOC_025930	*FBXW2*	2.05149	11.71	24.02	0.00005
XLOC_029135	*QPCTL*	2.05102	5.30	10.88	0.00005
XLOC_022319	*NID1*	2.05028	67.12	137.62	0.00005
XLOC_003337	*IFRD1*	2.04897	22.82	46.77	0.00030
XLOC_017502	*WLS*	2.04873	45.79	93.81	0.00005
XLOC_009633	*TMEM200A*	2.04742	9.38	19.21	0.00005
XLOC_001056	*C1QTNF3*	2.04606	6.77	13.84	0.00055
XLOC_028504	*FTO*	2.04568	4.91	10.05	0.00005
XLOC_012790	*ALDH6A1*	2.04523	19.75	40.40	0.00005
XLOC_027128	*TTC19*	2.04378	8.99	18.38	0.00080
XLOC_001654	*IRF1*	-2.04360	17.63	8.63	0.00005
XLOC_033799	*PDHA1*	2.04269	25.90	52.90	0.00005
XLOC_003224	*COL1A2*	2.04187	934.36	1907.83	0.00005
XLOC_006571	*TEX261*	2.04166	27.39	55.92	0.00005
XLOC_000949	*SPARC*	2.04069	2240.24	4571.63	0.00005
XLOC_017353	*P3H1*	2.03949	32.89	67.08	0.00005
XLOC_006745	*QPCT*	2.03856	12.59	25.66	0.00005
XLOC_025678	*HACD4*	2.03791	7.17	14.61	0.00005
XLOC_034057	*OGT*	-2.03661	106.72	52.40	0.00005
XLOC_001987	*TSPAN17*	2.03647	20.44	41.62	0.00005
XLOC_016209	*PTGFRN*	2.03596	11.25	22.90	0.00010
XLOC_012880	*SERPINA1*	2.03571	7.29	14.83	0.00005
XLOC_008522	*MRPL1*	2.03550	6.94	14.13	0.00005
XLOC_002044	*NPM1*	2.03521	551.86	1123.15	0.00005
XLOC_021132	*NDUFV1*	2.03462	25.08	51.03	0.00005
XLOC_004263	*SELK*	2.03363	18.81	38.24	0.00005

XLOC_024929	*ACER2*	-2.03321	7.29	3.59	0.00005
XLOC_005567	*REL*	-2.03282	6.01	2.96	0.00005
XLOC_002410	*GADD45B*	-2.03232	76.17	37.48	0.00005
XLOC_008514	*ANXA3*	2.03145	47.69	96.87	0.00005
XLOC_006337	*MKKS*	2.03056	26.38	53.57	0.00005
XLOC_033761	*TMSB4X*	2.03023	623.14	1265.12	0.00005
XLOC_005862	*ADCY3*	2.03003	3.14	6.37	0.00005
XLOC_031528	*DESI2*	2.02980	16.87	34.24	0.00005
XLOC_015035	*C12orf73*	2.02838	129.20	262.07	0.00245
XLOC_009579	*RWDD1*	2.02709	18.21	36.91	0.00005
XLOC_008724	*ZBTB49*	-2.02562	9.86	4.87	0.00005
XLOC_025325	*TOR1B*	2.02519	12.39	25.10	0.00005
XLOC_029089	*PPP1R15A*	-2.02387	38.52	19.03	0.00005
XLOC_006510	*CCDC88A*	2.02111	4.10	8.29	0.00050
XLOC_024508	*PTPRM*	2.02107	9.31	18.81	0.00005
XLOC_000216	*CLN5*	2.02086	8.35	16.87	0.00005
XLOC_013760	*CCT2*	2.01998	39.48	79.75	0.00005
XLOC_024373	*GUCD1*	2.01890	10.36	20.92	0.00320
XLOC_018361	*SERPINE2*	2.01858	97.28	196.37	0.00005
XLOC_004672	*NDUFA4*	2.01792	38.26	77.22	0.00005
XLOC_009296	*HSP90AB1*	2.01760	134.74	271.84	0.00020
XLOC_000640	*GPX8*	2.01746	36.49	73.62	0.00005
XLOC_016701	*RPL37A*	2.01677	403.38	813.53	0.00005
XLOC_032270	*PTDSS1*	2.01548	7.57	15.26	0.00005
XLOC_032763	*EXT1*	2.01520	44.40	89.47	0.00005
XLOC_023212	*ERLIN1*	2.01433	7.19	14.49	0.00005
XLOC_016215	*MAN1A2*	2.01430	8.78	17.68	0.00005
XLOC_000661	*ZSWIM6*	-2.01319	16.31	8.10	0.00005
XLOC_006655	*KRCC1*	2.01291	15.33	30.85	0.00005
XLOC_000413	*COMMD10*	2.01213	5.45	10.96	0.00005
XLOC_005352	*DDRGK1*	2.01027	8.04	16.15	0.00005
XLOC_008807	*KIAA0232*	-2.00988	7.05	3.51	0.00005
XLOC_018638	*ADAMTS1*	-2.00974	5.50	2.74	0.00005
XLOC_022109	*CFL1*	2.00834	847.64	1702.35	0.00005
XLOC_024424	*MRPL40*	2.00832	13.48	27.08	0.00005
XLOC_015719	*ZC3H12A*	-2.00828	12.16	6.05	0.00005
XLOC_022693	*SFXN3*	2.00733	6.75	13.55	0.00005
XLOC_005482	*CHST10*	2.00692	16.51	33.12	0.00005
XLOC_004660	*PON2*	2.00628	17.98	36.07	0.00005
XLOC_025152	*GSN*	2.00526	34.07	68.32	0.00005
XLOC_014257	*ADIPOR2*	2.00415	20.47	41.03	0.00005

XLOC_025271	*URM1*	2.00414	51.71	103.64	0.01240
XLOC_026010	*AK1*	2.00398	3.74	7.49	0.00005
XLOC_031667	*TSEN15*	2.00372	9.28	18.60	0.00005
XLOC_005622	*SNRNP27*	2.00361	12.77	25.58	0.00005
XLOC_018602	*TMEM50B*	2.00347	4.55	9.12	0.00005
XLOC_027437	*PCGF2*	-2.00347	6.74	3.37	0.00390
XLOC_002922	*PTPRG*	2.00128	9.62	19.25	0.00005